Alma Mater Studiorum - Università di Bologna

DOTTORATO DI RICERCA IN

INGEGNERIA CIVILE, AMBIENTALE E DEI MATERIALI

Ciclo XXX

Settore Concorsuale: 08/B3 – TECNICA DELLE COSTRUZIONI

Settore Scientifico Disciplinare: ICAR/09 – TECNICA DELLE COSTRUZIONI

SEISMIC FRAGILITY AND DYNAMIC BEHAVIOR OF ATMOSPHERIC CYLINDRICAL STEEL TANKS

Candidato: Marta D'Amico

Coordinatore Dottorato

Prof. Ing. Luca Vittuari

Supervisore

Prof. Ing. Claudio Mazzotti

Co- supervisore

Dott. Ing. Nicola Buratti

Esame finale anno 2018

Abstract

The main purpose of the research carried out in the aim of this PhD dissertation has been the analysis of the dynamic behavior of on-grade cylindrical steel storage tanks. This has been done through two main research fields: the evaluation of tank seismic fragility and the analytical modeling of the tank dynamics when subjected to the ground acceleration.

In the first part of the PhD study, new fragility models have been proposed with the aim to overcome limits and week points of past researches. For this purpose, a large dataset of information on failures of atmospheric tanks during past earthquakes has been collected. Two sets of Damage States have then been used in order to characterize the severity of damage and the intensity of liquid releases. Empirical fragility curves have been fitted by using Bayesian regression. Different generalized linear models have been employed in order to investigate the effects of tank aspect ratio, filling level and base anchorage. Moreover, the effects of the interaction between these critical aspects is included in fragility analysis. The hazard parameter used is the Peak Ground Acceleration. Seismic fragility curves obtained from the described procedure are compared to those available in the technical literature.

The second section of the present PhD study has focused on the mechanical modeling of unanchored tanks dynamic. These structures are known to show a complex behavior under seismic action, since their response involves the combination of vibrating and bouncing phenomena. Past researches provided simple tools for the seismic analysis of tank-fluid system, but they neglected the effects of the tank rocking-bulging motion interaction. However, as the comparison between analytical and experimental results corroborates in the present work, the rocking-bulging interaction is governed by rotational inertia, centrifugal and Coriolis forces that play a leading role in the dynamic response of the tank. Then, the current study proposes an investigation on inertial and centrifugal forces in the context of the interaction between rocking and translational motions. The simultaneous dynamic equations of a 2DOF model have been solved through a numerical software and results have been compared with those of experimental tests. Moreover, employing the dynamic properties governing the tank rocking-bulging motion into the 2DOF model equations, a simplified method to determine the tank bulging response and the measure in which it is reduced by the rocking appearance is provided. Validation of the proposed analysis is conducted comparing its results with those computed through an Explicit Finite Element Analysis on a sample tank.

Contents

INTRODUCTION 7

1. Dynamic behavior of tank-fluid systems 11

1.1. Introduction 11

1.2. Analytical formulation of the tank-fluid system in case of rigid tank 12

1.2.1. The exact solution 12

1.2.2. Mechanical models of tank-fluid system assuming rigid wall 20

1.3. Analytical formulation of tank-fluid system in case of flexible tank 22

1.3.1. Fluid-tank interaction under assumed mode 22

1.3.2. Mechanical models of tank-fluid system considering the effects of wall flexibility 27

1.4. Unanchored tanks and uplift – general remarks 28

2. Critical review of seismic codes provisions 30

2.1. European and international codes and standards 30

2.2. Critical comparison of the main design codes 33

2.2.1. Design seismic force: provisions from codes 33

2.2.2. Analysis of tank-fluid system: provisions from codes 35

2.3. Seismic design of on-grade steel tanks 38

2.3.1. Seismic design of on-grade steel tanks according to EC8-4 38

2.3.2. Seismic design of on-grade steel tanks according to NZSEE 53

2.3.3. Seismic design of on-grade steel tanks according to AWWA D100-05 71

2.3.4. Comparison between design procedures in terms of pressures 75

2.4. Conclusion 84

3. Definition of a new tank damage database 87

3.1. Introduction 87
3.2. Effects of seismic loading on liquid storage tanks 87
3.2.1. Review of the main tank failures caused by earthquake 87
3.2.2. Empirical performance of on-grade steel tanks under seismic action 90
3.3. Data sources and seismic events considered 106
3.4. Undamaged tanks 109
3.5. Recent earthquakes 110
3.6. Information collected 110
3.7. Criteria used for defining PGA values 111
3.7.1. ShakeMap 114
3.7.2. Attenuation model 116
4. Seismic fragility formulations 120
4.1. Introduction 120
4.2. Statistical procedures for developing seismic fragility curves 121
4.3. Critical analysis of fragility models available in literature 122
4.4. Characterization of tank damage 130
4.4.1. Definition of damage states 130
4.4.2. Definition of risk levels 132
4.5. Parametric fragility curves 133
4.5.1. General approach 133
4.5.2. Fragility curves based on individual damage states 134
4.6. Results 139
4.6.1. Fragility curves for damage states 139

4.6.2. Fragility curves for risk levels 142
4.7. Conclusion 156
5. Simplified analysis of the tank rocking motion 157
5.1. Introduction 157
5.2. Rocking-bulging motion in literature 159
5.3. Technical background on tank rocking-bulging motion 160
5.4. The two degrees of freedom model 174
5.4.1. Geometry, masses and degrees of freedom 174
5.4.2. Derivation of equation of motion for the 2DOF model 175
5.5. Experimental test 181
5.5.1. Steel model 181
5.5.2. Test instrumentation and set-up 183
5.5.3. Coordinates reference systems 185
5.5.4. Outputs and analysis of results 185
5.6. Numerical simulation 188
5.7. Comparison between experimental and numerical results 189
5.8. The tank model 192
5.9. Equation of motion for the tank model 194
5.10. Simplified analysis of the tank model 197
5.11. Numerical analysis on a sample tank 203
5.12. Conclusions 210
6. Concluding remarks 212
7. References 215

8. Appendix A 228

INTRODUCTION

Industrial plants are often located in highly seismic areas, such as the case of oil storage facilities placed along the coasts of countries like Japan, California, Peru, Alaska and Turkey. The twentieth century, characterized by the overall diffusion of chemical and power installations, has also been the century of many disasters related to the catastrophic failure of plants, often triggered by earthquakes, which caused serious economic and environmental consequences. Therefore, the evaluation of the seismic vulnerability of the different components of a plant is a fundamental task.

Official post-earthquake reports and technical article revealed that areas assigned to storage are among the most dangerous, because of the presence of huge volumes of dangerous substances. They are characterized by a widespread variety of containment structures, the features of which depend on pressure and temperature conditions in which substances are to be stored and on the state of matter. Failure of these structures could limit the operation of the entire plants and in addition represent a serious safety hazard due to the properties of toxicity and flammability of their contents. Often earthquakes lead to "NaTech" (Natural-Technological) accidents, i.e. technological disasters caused by natural phenomena of particular intensity in industrial sites already recognized as risk source. The 1964 Niigata earthquake (M_w=7.5) caused the collapse of a number of tanks at a local oil refinery. A resulting fire caused extensive damage to the plant [1,2]. During the Kern County earthquake in 1952 (M_w=7.5) severe damage occurred at the Paloma Gasoline Plant because of failure of two butane storage spheres which rolled off their supports and broke the piping systems. The escaping butane caught fire and destroyed the entire facility [2–4]. The 1999 Kocaeli earthquake (M_w=7.4) was one of the most severe natural disaster of Turkey. It caused significant structural damage and losses in industrial facilities. The earthquake sparked a disastrous fire at the Tupras petroleum refinery. The fire began at six naphtha cylindrical tanks having floating roof and it was completely extinguished four days after the earthquake. Moreover, at the AKSA acrylic fiber production plant, the earthquake damaged three storage tanks and caused 6,400 tons of acetonitrile, which is highly flammable, toxic and carcinogenic, to be released into air, sea and groundwater [5]. Another remarkable event is the 2011 Tohoku earthquake (M_w=9) that caused fires and explosion in Cosmo oil refinery located in Chiba. A butane tank, damaged by earthquake, caught fire and because of the occurrence of several Boiling Liquid Expanding Vapor Explosions (BLEVE) other sixteen tanks were burned [6].

A typical kind of containment used for storing liquids is represented by atmospheric on-grade steel tanks. In the last century, many studies have been conducted with the aim to understand

the behaviour of these structures under seismic action, focusing on analytical simplified models of tank-fluid systems or developing tank fragility functions. However, many aspects of the dynamic response of this structural typology have not been clarified yet.

In the context of the earthquake vulnerability assessment of industrial plants, a fundamental role is played by the seismic fragilities of main components, whose evaluation involves some critical features. One of these consists in the definition of different damage levels. In case of building-type structures, increasing damage levels also relate to increasing severity of mechanical damage, loss of functionality and associated repair costs. For atmospheric on-grade steel tanks, as well as many other plant critical components, this relation is not valid because of different dynamic mechanisms associated with the tank-fluid system. At the date, tank fragility functions based on empirical damage data adapted the HAZUS criteria [7], born for building-type structure, to the tank failure classification [8–10]. However, this can lead to a not consistent evaluation of the probability of damage occurrence.

The number of samples plays a key role in the reliability of fragility estimation. In case of empirical data, this issue is much more emphasized because of measurement errors, indirect nature of observations and different uncertainties affecting information. Due to the difficulties in obtaining damage information for less recent earthquakes, past researchers developed fragility curves using relatively small collections of data.

A further critical point of the fragility evaluation is the choice of a proper method of analysis. In this framework, some questionable decisions have been taken by past researchers, as it will be explained in Chapter 5.

In this light, one of the main purpose of this PhD research is to try to overcome the aforementioned limits by providing empirical fragility curves based on Bayesian approach. More than one model has been employed and the effects of three critical aspect on the tank fragility, i.e. the tank aspect ratio, the filling level of content, and the presence of anchorage system, have been investigated. For this purpose, a tank damage dataset larger than that used by previous researches has been assembled. A critical comparison between fragility curves obtained herein and those available in literature is proposed to the readers.

A further main topic of the present PhD dissertation is the mechanical modeling of the tank rocking motion. As confirmed by results from fragility analyses carried out in this work, unanchored tanks are more vulnerable than the corresponding anchored ones. The seismic response of cylindrical steel tanks fixed at the base has been widely investigated in the past. On the other hand, simply supported tanks are known to show a very complex dynamic behavior governed by the interaction between translational and rotational motions. For this reason, despite many researches on this topic, the mechanics of the tank uplift induced by the ground

acceleration has not been fully understood. Therefore, an analytical treatment of the rocking motion of unanchored cylindrical tanks focusing on the role of dynamic forces involved in rocking-bulging interaction is presented as well.

The subject matter is covered in five chapters, the scope of which is described in the following.

Chapter 1 deals with the methods of analysis of liquid storage tanks under seismic action. The analytical formulation of the tank-fluid system available in technical literature is provided for rigid and flexible tanks fixed at the base. The main mechanical models used by the various international codes are introduced. Some general remarks on unanchored tanks are given as well.

Chapter 2 provides a critical review of the seismic codes on liquid storage tanks, focusing on the different provisions adopted to deal with the low energy-dissipating capacity of liquid-containing tanks and proper modeling of hydrodynamic forces in analysis. The main differences among the codes are discussed. Furthermore, a detailed analysis of the seismic design procedures of on-grade cylindrical steel storage tanks subjected to horizontal and vertical ground accelerations, according to the UNI EN 1998-4:2006, NZSEE and AWWA D100-05 is presented. Finally, a comparison in terms of pressures distributions between the three codes examined is carried out as well. Analogies and differences between them are highlighted.

Chapter 3 presents a new database collecting damage data for on-grade cylindrical steel storage tanks involved in twenty-four seismic events. The number of tanks collected is much higher with respect to previous datasets available in literature. A detailed description of data sources, information collected and seismic events considered is provided. The different criteria used for defining for each database tank a reliable PGA value are explained. The main novels introduced by the current collection are presented and discussed. The entire tank database is attached in Appendix A.

Chapter 4 describes the analytical procedure used to develop empirical seismic fragility formulation for on-grade cylindrical steel storage tanks. In a first section, a critical analysis of fragility models available in literature is presented. The characterization of tank damage is given in terms of structural failure and content release intensity. A description of general approach and different models employed for deriving fragility curves is provided. Finally, results are shown and discussed.

Chapter 5 proposes an analytical treatment of tank rocking motion. First, the technical background on which the current study has been founded is presented. Starting from a mechanical model describing the simultaneous translational-rotational motion of a 2 degrees of freedom system, a simplified procedure to calculate the main response of unanchored tanks has

been developed, focusing on the fundamental role played the rotational and translational inertia forces in the framework of the tank rocking-bulging interaction. Experimental test and numerical simulations have been employed in order to corroborate the reliability of the analytical procedure.

1. Dynamic behavior of tank-fluid systems

1.1. Introduction

The objective of the present discussion is to provide a detailed description of the dynamic behavior of liquid-filled containers subjected to dynamic excitations, in particular earthquakes.

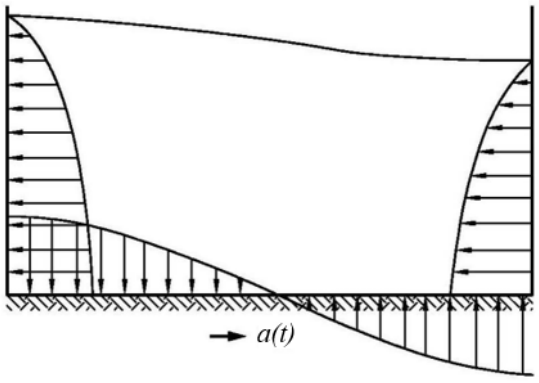

Figure 1-1. Distribution of dynamic pressures in a liquid storage tank subjected to the ground acceleration

Because of the horizontal acceleration *a(t)*, the liquid mass closed to the free liquid surface does not rigidly translate in unison with the tank. Therefore, the liquid portion in contact with the tank wall is forced to move in vertical direction, causing convective waves. Periods of this sloshing motion are typically high, 2 to 6-10 s [11] and depend on the tank shape and properties of the dynamic excitation. Figure 1-1 shows an antisymmetric wave corresponding to the lowest natural frequency; higher frequencies correspond to the formation of more complex waves, with a bigger number of null points. In proximity of the bottom, the liquid contained moves in unison with the shell, increasing the inertia of the structure. The percentage of the liquid mass involved in the convective motion depends on the ratio of the free surface height H over the tank diameter D [12]: the lower the aspect ratio H/D the bigger the convective mass. For very low values of H/D, only the 30% of the liquid moves in unison with walls, while the remaining part is involved in sloshing.

The present chapter analyzes in detail the dynamic response of cylindrical rigid and deformable tanks fixed at the base, considering impulsive and convective effects. Some general remarks on unanchored tanks are given as well.

1.2. Analytical formulation of the tank-fluid system in case of rigid tank

1.2.1. The exact solution

In the present section, the main steps of the procedure developed by Yang in 1976 [13] will be presented. The author calculated the exact solution for the dynamic problem of the tank-fluid system.

The solution of the equations governing the motion of a fluid contained in a rigid cylindrical tank can be expressed as the summation of the rigid-impulsive and convective contributes [14,15]. The rigid-impulsive component satisfies exactly the boundary conditions along the walls and the tank bottom, but it returns zero value at the free surface, (which is not true because of the presence of waves). Therefore, the convective term is added to the rigid-impulsive solution in order to restore the equilibrium conditions on the free surface.

System and assumptions

The system considered is shown in Figure 1-2. It is a rigid circular cylinder tank of radius a fixed to a rigid base.

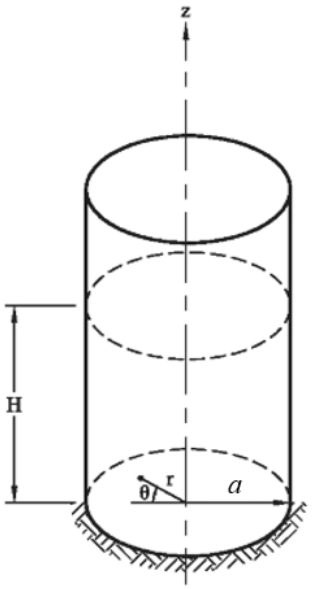

Figure 1-2. Rigid tank anchored to the foundation. Cilindrical coordinates

The cylindrical coordinate system (r, z, ϑ), depicted in Figure 1-2, has the origin at the center of the tank bottom; z is the vertical axis, whereas x is the direction of the horizontal ground acceleration $\ddot{x}(t)$ that excites the tank-fluid system.

Fundamental equations and boundary conditions

The equation of motion for the fluid, referred to the cylindrical coordinate system (r, z, ϑ) is

$$\frac{\partial^2\phi}{\partial r^2}+\frac{1}{r}\frac{\partial\phi}{\partial r}+\frac{1}{r^2}\frac{\partial^2\phi}{\partial\theta^2}+\frac{\partial^2\phi}{\partial z^2}=0 \tag{1.1}$$

In which ϕ is the potential velocity function. The velocity components of the fluid in the radial, tangential and vertical directions are

$$\begin{aligned} v_r &= -\frac{\partial\phi}{\partial r} \\ v_\theta &= -\frac{1}{r}\frac{\partial\phi}{\partial\theta} \\ v_z &= -\frac{\partial\phi}{\partial z} \end{aligned} \tag{1.2}$$

and the hydrodynamic pressure p is related to the potential velocity function ϕ by the equation:

$$p=\rho_l\frac{\partial\phi}{\partial t} \tag{1.3}$$

The boundary conditions of the problem are given as

- At $z=0$, the vertical velocity component of the fluid v_z must be zero, therefore

$$\left.\frac{\partial\phi}{\partial z}\right|_{z=0}=0 \tag{1.4}$$

- At $r=a$, the radial velocity component of the fluid must be equal to the corresponding component of the ground motion, therefore

$$-\left.\frac{\partial\phi}{\partial r}\right|_{r=a}=\dot{x}(t)\cos\theta \tag{1.5}$$

- If $d(t)$ is the instantaneous value of the vertical displacement of the fluid at the surface, the pressure at $z=H$ is given approximately by

$$p=\rho_l g\, d(t) \tag{1.6}$$

Considering the equivalence between Eqs. (1.6) and (1.3) and differentiating with respect to time, the following differential equation is obtained

$$\frac{\partial^2 \phi}{\partial t^2} + g\frac{\partial \phi}{\partial z} = 0 \tag{1.7}$$

The solution of Eq. (1.7) can be expressed as the sum of two partial solutions

$$\phi = \phi_1 + \phi_2 \tag{1.8}$$

in which the function Φ_1 satisfies the following boundary conditions:

$$\begin{aligned} &\text{at } z = 0 && \frac{\partial \phi_1}{\partial z} = 0 \\ &\text{at } r = a && \frac{\partial \phi_1}{\partial r} = -\dot{x}(t)\cos\theta \\ &\text{at } z = H && \frac{\partial \phi_1}{\partial t} = 0 \end{aligned} \tag{1.9}$$

and Φ_2 is subjected to the following boundary conditions:

$$\begin{aligned} &\text{at } z = 0 && \frac{\partial \phi_2}{\partial z} = 0 \\ &\text{at } r = a && \frac{\partial \phi_2}{\partial r} = 0 \\ &\text{at } z = H && \frac{\partial^2 \phi_2}{\partial t^2} + g\frac{\partial \phi_2}{\partial z} = -g\frac{\partial \phi_1}{\partial z} \end{aligned} \tag{1.10}$$

It should be noted that the third of Eqs. (1.9) imposes that the pressure at $z = H$ is zero. Hence, Φ_1 represents the solution for the impulsive effects. The partial solution Φ_2, which corrects for the difference between the correct boundary conditions and the one defined by the third of Eqs. (1.9), represents the solution for the convective effects.

Impulsive solution Φ_1

The solution for the impulsive effects is given as

$$\phi_1 = -\dot{x}(t)H\cos\theta \sum_{n=1}^{\infty} \frac{8(-1)^{n+1}}{\left[(2n-1)\pi\right]^2} \frac{I_1\left[(2n-1)\frac{\pi}{2}\frac{r}{H}\right]}{I_1'\left[(2n-1)\frac{\pi}{2}\frac{a}{H}\right]} \cos\left[(2n-1)\frac{\pi}{2}\frac{z}{H}\right] \tag{1.11}$$

in which I_1 and I_1' are respectively the modified Bessel function of the first kind and its derivative. The pressure induced by the impulsive motion is obtained by introducing Eq. (1.11) into Eq. (1.3):

$$p = -\ddot{x}(t)\rho_l H \cos\theta \sum_{n=1}^{\infty} \frac{8(-1)^{n+1}}{\left[(2n-1)\pi\right]^2} \frac{I_1\left[(2n-1)\frac{\pi}{2}\frac{r}{H}\right]}{I_1'\left[(2n-1)\frac{\pi}{2}\frac{a}{H}\right]} \cos\left[(2n-1)\frac{\pi}{2}\frac{z}{H}\right] \tag{1.12}$$

The total hydrodynamic force due to the liquid pressure exerted on the tank walls is equal to the total base shear, and it is obtained from the integral

$$Q_{0,l} = \int_0^H \int_0^{2\pi} p\Big|_{r=a} \cos\theta \, a \, d\theta dz \tag{1.13}$$

that provides the following result

$$Q_{0,l} = -\ddot{x}(t) m_l \frac{H}{a} \sum_{n=1}^{\infty} \frac{16}{\left[(2n-1)\pi\right]^3} \frac{I_1\left[(2n-1)\frac{\pi}{2}\frac{a}{H}\right]}{I_1'\left[(2n-1)\frac{\pi}{2}\frac{a}{H}\right]} \tag{1.14}$$

The overturning moment corresponding about the tank base is given by

$$M_{0,l} = \int_0^H \int_0^{2\pi} p\big|_{r=a} \cos\theta \, z \, a \; d\theta dz \tag{1.15}$$

that the following results

$$M_{0,l} = -\ddot{x}(t) m_l H \frac{H}{a} \sum_{n=1}^{\infty} \frac{16}{\left[(2n-1)\pi\right]^3} \frac{I_1\left[(2n-1)\frac{\pi}{2}\frac{a}{H}\right]}{I_1'\left[(2n-1)\frac{\pi}{2}\frac{a}{H}\right]} \left[1 - \frac{2(-1)^{n+1}}{(2n-1)\pi}\right] \tag{1.16}$$

By setting z=0, Eq. (1.12) provides the hydrodynamic pressure on the tank base, whereas the corresponding overturning moment is obtained as follows

$$M'_{0,l} = \int_0^{2\pi} \int_0^a p\big|_{z=0} \cos\theta \; r^2 \, dr d\theta \tag{1.17}$$

Providing the following result

$$M'_{0,l} = -\ddot{x}(t)\, m_l H \sum_{n=1}^{\infty} \frac{16(-1)^{n+1}}{\left[(2n-1)\pi\right]^3} \frac{I_1\left[(2n-1)\frac{\pi}{2}\frac{a}{H}\right]}{I_1'\left[(2n-1)\frac{\pi}{2}\frac{a}{H}\right]} \tag{1.18}$$

Convective solution Φ_2

In order to obtain the convective solution for an arbitrary ground motion, the first step is the evaluation of the solution for a harmonic ground acceleration.

Let consider the ground harmonic acceleration $\ddot{x} = \ddot{x}e^{i\omega t}$, the function Φ_2 satisfying Eq. (1.1) and the boundary conditions defined by Eq. (1.10) is given by

$$\phi_2 = -\frac{1}{i\omega}\ddot{x}_0 e^{i\omega t} H \frac{a}{H}\cos\theta \sum_{n=1}^{\infty} \frac{1}{1-\left(\frac{\omega}{\omega_n}\right)^2} \frac{2}{\lambda^2{}_n - 1} \frac{J_1\left(\lambda_n \frac{r}{a}\right)}{J_1(\lambda_n)} \frac{\cosh\left(\lambda_n \frac{z}{a}\right)}{\cosh\left(\lambda_n \frac{H}{a}\right)} \tag{1.19}$$

where λ_n are the zeros of the Bessel function of first order $J_1(x) = 0$ and ω_n are the natural frequency of sloshing motion, provided by

$$\omega^2{}_n = \frac{\lambda_n g}{a}\tanh\left(\lambda_n \frac{H}{a}\right) \tag{1.20}$$

Substituting Eq. (1.19) into Eq. (1.3) the harmonic convective pressure for the tank is obtained

$$p = \ddot{x}_0\, e^{i\omega t} \rho_l H \frac{a}{H}\cos\theta \sum_{n=1}^{\infty} \frac{1}{1-\left(\frac{\omega}{\omega_n}\right)^2} \frac{2}{\lambda^2{}_n - 1} \frac{J_1\left(\lambda_n \frac{r}{a}\right)}{J_1(\lambda_n)} \frac{\cosh\left(\lambda_n \frac{z}{a}\right)}{\cosh\left(\lambda_n \frac{H}{a}\right)} \tag{1.21}$$

Once the harmonic response of the system is determined, the response to an arbitrary excitation $\ddot{x}(t)$ is obtained by applying the inverse Fourier Transform and the Duhamel's integral.

The frequency response function for the harmonic convective pressure defined by Eq. (1.21) has the form

$$p(\omega) = \sum_{n=1}^{\infty} \frac{f(r,\theta,z)}{1-\left(\frac{\omega}{\omega_n}\right)^2} \tag{1.22}$$

The pressure, $h_p(t)$, induced by a unit impulsive acceleration, $\ddot{x}(t) = \delta(t)$ can be expressed by the inverse Fourier Transform of the Eq. (1.22) as

$$h_p(t) = \frac{1}{2\pi} \sum_{n=1}^{\infty} f(r,\theta,z) \int_{-\infty}^{\infty} \frac{1}{1-\left(\frac{\omega}{\omega_n}\right)^2} e^{i\omega t} d\omega \tag{1.23}$$

Hence, the pressure, $p(t)$, induced by an arbitrary acceleration, $\ddot{x}(t)$, is given by

$$p(t) = \sum_{n=1}^{\infty} f(r,\theta,z) \int_{0}^{t} \omega_n \ddot{x}(t) \sin[\omega_n (t-\tau)] d\tau \tag{1.24}$$

In which the convolution integral represents the instantaneous value of the pseudo-acceleration, $A_n(t)$, of a single-degree-of-freedom system having a natural frequency ω_n and subjected to the ground acceleration $\ddot{x}(t)$. Thus, the transient convective pressure for the tank is given as

$$p(t) = \rho_l H \cos\theta \sum_{n=1}^{\infty} \frac{2}{\lambda^2{}_n - 1} \frac{a}{H} \frac{J_1\left(\lambda_n \frac{r}{a}\right)}{J_1(\lambda_n)} \frac{\cosh\left(\lambda_n \frac{z}{a}\right)}{\cosh\left(\lambda_n \frac{H}{a}\right)} A_n(t) \tag{1.25}$$

Following the same criteria, one finds the expression for the other response quantities:

- the convective base shear

$$Q_{0,l} = m_l \sum_{n=1}^{\infty} \frac{2}{\lambda_n\left(\lambda^2{}_n - 1\right)} \frac{a}{H} \tanh\left(\lambda_n \frac{H}{a}\right) A_n(t) \tag{1.26}$$

- the overturning moment induced by the hydrodynamic pressure on the tank wall

$$M_{0,l} = m_l H \sum_{n=1}^{\infty} \frac{2}{\lambda_n(\lambda^2{}_n - 1)} \frac{a}{H} \tanh\left(\lambda_n \frac{H}{a}\right) \left[1 - \frac{a}{\lambda_n H} \tanh\left(\frac{\lambda_n H}{2a}\right)\right] A_n(t) \tag{1.27}$$

- the overturning moment induced by the hydrodynamic pressure on the tank bottom

$$M'_{0,l} = m_l H \sum_{n=1}^{\infty} \frac{2}{\lambda_n (\lambda^2{}_n - 1)} \left(\frac{a}{H}\right)^2 \frac{J_2(\lambda_n)}{J_1(\lambda_n)} \frac{1}{\cosh\left(\lambda_n \frac{H}{A}\right)} A_n(t) \tag{1.28}$$

Recast expressions

The hydrodynamic pressure exerted on the tank wall can be conveniently expressed as the sum of infinite terms as follows

$$p(z,\theta,t) = \sum_{n=0}^{\infty} C_n{}^p \rho_l H \cos\theta A_n(t) \tag{1.29}$$

For $n = 0$, the impulsive component of pressure is obtained (for $n = 0$, $A_n = \ddot{x}(t)$), whereas $n = 1, 2, 3$ ... correspond to the convective solution. C_n^p is a dimensionless function of z depending on the ratio H/a and it has been plotted in Figure 1-3 for $n = 0$ and $n = 1, 2$ for several values of H/a.

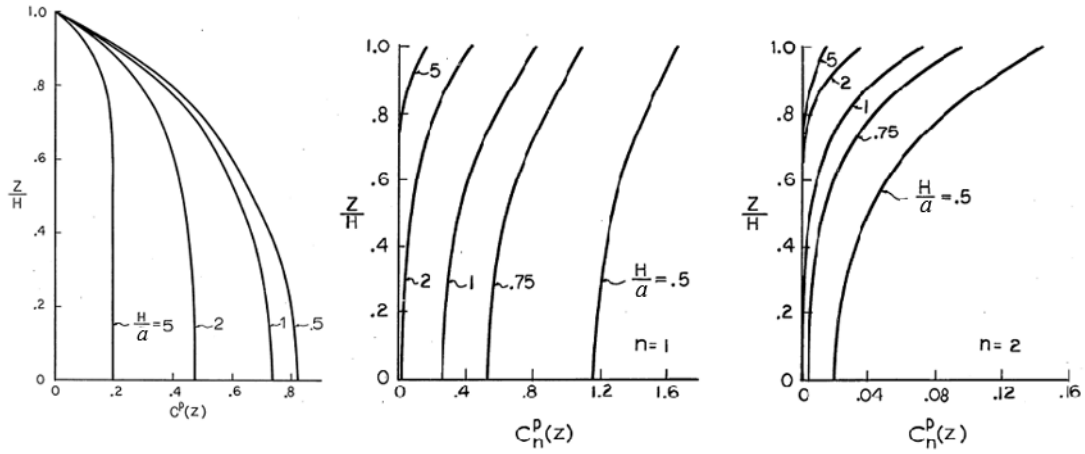

Figure 1-3. Distribution of hydrodynamic pressures on tank wall (a) impulsive pressure component, (b) 1st convective pressure component, (c) 2nd convective pressure component [13]

It should be noted that for low values of H/a, the impulsive pressure distribution is close to a cosine curve and the convective one is large and penetrates to the base of the tank; for large values of the H/a the impulsive pressure coefficient is almost uniformly distributed and the convective one is small and localized near the surface. It must be considered, however, that pressure is also function of $A_n(t)$ which depends on the natural frequency of sloshing motion of the liquid, so a large value of C_n^p does not necessarily imply a large pressure.

The hydrodynamic pressure on the tank base can be expressed in an analogous convenient form as

$$p(r,\theta,t)=\sum_{n=0}^{\infty} C_n^{\ p}(r)\rho_l H\cos\theta A_n(t) \tag{1.30}$$

The function $C_n^p(r)$ is plotted in Figure 1-4 respectively for $n=0$ and $n=1,2$ for the same range of H/a values.

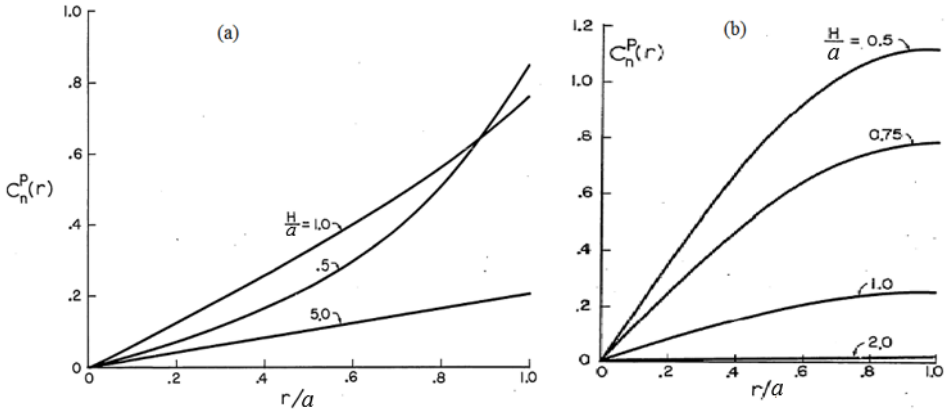

Figure 1-4. Distribution of hydrodynamic pressures on tank base (a) impulsive pressure component, (b) 1st convective pressure component [13]

It is noted that for values of H/a greater than 1, the distribution of the impulsive pressure on the tank base is linear.

The base shear induced by the hydrodynamic pressures can be expressed in the form:

$$Q_{0,l}=\sum_{n=0}^{\infty} C_n^{\ P} m_l A_n(t) \tag{1.31}$$

where C_n^p is a dimensionless coefficient equal to m_n/m_l, plotted in Figure 1-5 (a) for or $n=0$ and $n=1,2$ as a function of H/a. It should be noted that the coefficient related to the impulsive mass $(n=0)$ increases as the H/a value increases, while the coefficients related to the convective mass $(n=1,2)$ decreases as the ratio increases. Moreover, C_1^p is generally bigger than C_2^p. However, the second convective term may not be negligible since the maximum value of $A_2(t)$ can be larger than $A_1(t)$.

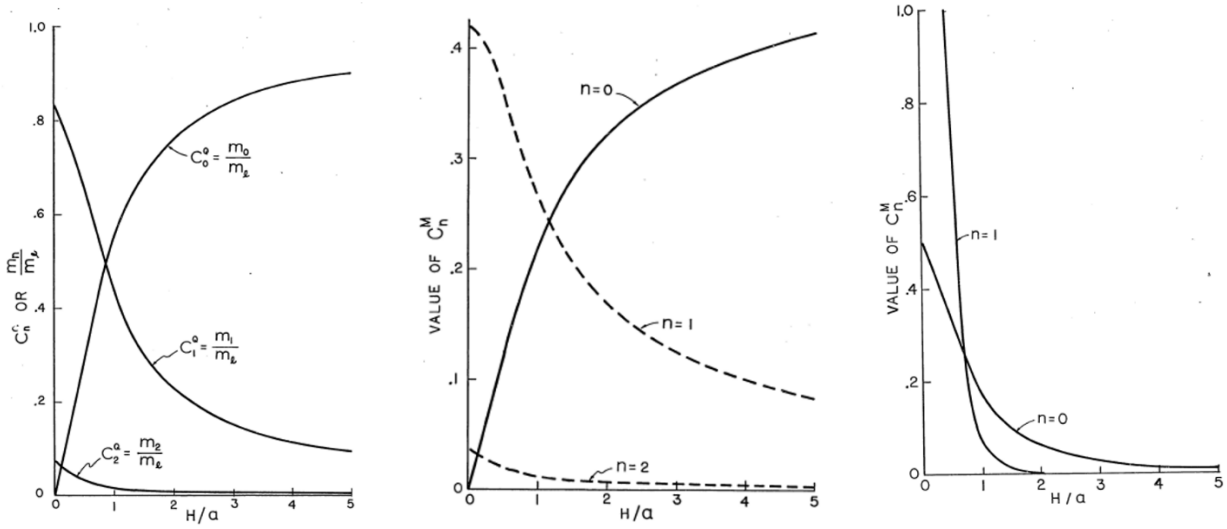

Figure 1-5. Equivalent masses (a), coefficients in expression of impulsive and convective moments at base of tank wall (b), at tank base (c) [13]

The overturning base moment induced by the pressure exerted on the wall can be expressed as

$$M_{0,l} = \sum_{n=0}^{\infty} C_n^{M} m_l H A_n(t) \tag{1.32}$$

where C_n^M are dimensionless coefficient plotted in Figure 1-5 (b) as a function of H/a.

The overturning moment induced by the pressure on the tank base can conveniently be expressed in the form

$$M'_{0,l} = \sum_{n=0}^{\infty} C_n^{M'} m_l H A_n(t) \tag{1.33}$$

where the dimensionless coefficient $C_n^{M\prime}$ is depicted in Figure 1-5 for different values of H/a.

1.2.2. Mechanical models of tank-fluid system assuming rigid wall

Housner in [16–18] proposed the mechanical model of the tank-fluid system under the assumption of rigid tank wall (Figure 1-6). His approach evaluates independently the effects of the two components of motion. Indeed, the aim of the model is to calculate the seismic responses of the SDOF systems separately and then combine them in order to obtain the total tank base shear and overturning moment. The mechanical model (Figure 1-6) consists of

different masses rigidly or elastically attached to the tank wall. The mass m_0, called impulsive mass, is rigidly attached to the wall and represents the effect of the portion of liquid which moves in unison with the tank. The masses m_1, m_2,...,m_n take into account the effects of the different convective modes; each mass is connected to the tank wall through a spring whose elastic constant is a function of the natural frequency of the convective mode considered: $K_i = 4\pi^2 \, m_i/{T_i}^2$, where T_i is the natural period of the i-th mass ($i = 1, 2$.. first, second.. convective periods). Other quantities associated with this mechanical model are the heights of each mass: h_0 is the height of the impulsive mass, whereas $h_{1,2,..}$ are the heights of the convective masses. It may be noted that heights h_0 and $h_{1,2,..}$ are used when hydrodynamic pressure exerted on the base plate is not considered. At the contrary, if base pressure is included, then the corresponding heights are denoted by h'_0 and $h'_{1,2,...}$. Therefore, the global overturning moment above the base plate is different from that below, since different pressures are taken into account. The overturning moment above the base plate is used to design the tank walls, whereas the overturning moment below the base plate is used to design the foundation (this is also called "foundation moment"). The sum of the impulsive and all convective masses provides the total liquid mass; however, Malhotra [19,20] later confirmed that the hydrodynamic forces can be calculated with sufficient accuracy by considering only m_0 and m_1, since the higher convective modes give a contribution of maximum 5% of the total action. On the contrary, when the liquid displacement has to be determined, these higher sloshing modes must be taken into account. ACI 350.3 and API 650 use mechanical model of Housner (1963) with modifications of Wozniak and Mitchell (1978). It is interesting to note that API 650 deal with circular steel tanks, which are flexible tanks. However, since there is no appreciable difference in the parameters of mechanical models of rigid and flexible tank models, this code evaluates parameters of impulsive and convective modes from rigid tank models.

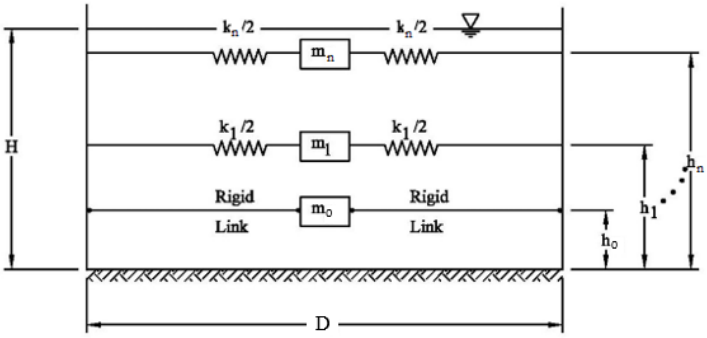

Figure 1-6. Mechanical model of tank with rigid wall [16–18]

1.3. Analytical formulation of tank-fluid system in case of flexible tank

In the previous section, the tank-fluid system has been analyzed under the assumption of rigid tank. However, the wall flexibility plays and important role on the evaluation of the seismic response and in some cases neglecting it can lead to erroneous results. One of the fundamental hypotheses of modeling rigid wall tanks is that the impulsive liquid mass experiences the same acceleration as the ground. Some researches carried out later, such as those of Veletsos and Yang [13,21–23] and Housner and Haroun [24–26], demonstrated that the tank wall flexibility may lead the impulsive mass to experience acceleration higher than the peak ground acceleration. Thus, the impulsive component of the tank seismic response calculated under the hypothesis of rigid wall may result non-conservative. On the other hand, the convective component is not sensitive to the wall flexibility due to its longer natural period, and then its effects may be evaluated by the procedure applicable to rigid tanks and added to the impulsive solution.

One of the first studies including the effects of wall flexibility has been provided by Yang in 1976 [13]. In the context of this analytical procedure, the tank flexibility is taken into consideration by assuming that the tank-fluid system behaves as a beam undergoing given shape modes. The following paragraph provides a description of the main steps of the Yang's method.

1.3.1. Fluid-tank interaction under assumed mode

This approach assumes that the tank-fluid system behaves as a beam, and the dynamic of the model is analyzed under the hypothesis that during the vibration, the tank cross section remains circular and the height-wise distribution of the deflection follows a given shape. Only the effects of impulsive motion are considered since it is presumed that the convective effects are not influenced by tank flexibility and then, they can be evaluated by the procedure described in the previous section for rigid tank and superimposed on the impulsive effects evaluated herein. The same method was used by Veletsos in [21], but in his work he assumed that the hydrodynamic pressure at $\vartheta = 0$ is equal to the pressure induced against a straight wall storing a reservoir, that is reasonable only for tank with H/a less than about 1.2.

The tank-fluid system considered is depicted in Figure 1-7. The cylindrical wall has an arbitrary thickness, radius a, height H_s and the level of fluid contained is H. The plane $\vartheta = 0$ is taken parallel to the direction of ground acceleration. It should be emphasized that the entire system represents a single-degree-of-freedom model, since the cross section cannot change its shape, and the deflection configuration at any time is of a prescribed term.

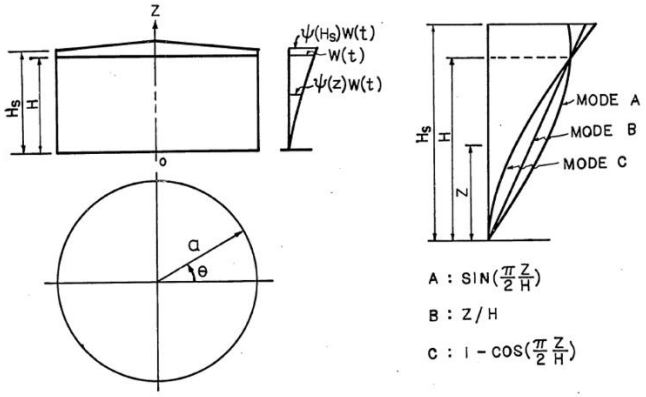

Figure 1-7. Mechanical model of tank-fluid system undergoing beam modes [13]

Let consider the dimensionless function $\psi(z)$ describing the heightwise distribution of the vibration mode and the acceleration of the tank wall at the free surface of the liquid, $\ddot{w}(t)$. Accordingly, the acceleration of the tank at a generic height z is given as $\ddot{w}(t)\psi(z)$, and the corresponding velocity as $\dot{w}(t)\psi(z)$. Since the fluid is assumed to be imcompressible and nonviscous, the velocity potential function of fluid ϕ must satisfy Laplace's equation, Eq. (1.1) at paragraph 1.2.1, and the following boundary conditions:

$$\frac{\partial \phi}{\partial r} = -\dot{w}(t)\psi(z)\cos\theta \qquad \text{at} \quad r = a \tag{1.34}$$

$$\frac{\partial \phi}{\partial z} = 0 \qquad \text{at} \quad z = 0 \tag{1.35}$$

$$\rho_l \frac{\partial \phi}{\partial t} = 0 \qquad \text{at} \quad z = H \tag{1.36}$$

The solution of the Eq. (1.1) is given as

$$\phi = -\dot{w}(t)\cos\theta \sum_{n=1}^{\infty} \frac{4H}{(2n-1)\pi} \frac{I_1}{I'_1} \frac{\left[(2n-1)\frac{\pi}{2}\frac{r}{H}\right]}{\left[(2n-1)\frac{\pi}{2}\frac{a}{H}\right]} \alpha_n \cos\left[(2n-1)\frac{\pi}{2}\frac{z}{H}\right] \tag{1.37}$$

where

$$\alpha_n = \frac{1}{H}\int_0^H \psi(z)\cos\left[(2n-1)\frac{\pi}{2}\frac{z}{H}\right]dz \tag{1.38}$$

In this study, three different functions $\psi(z)$ are used, depicted in Figure 1-7. The values of α_n for each of these functions and for $\psi(z) = 1$ are given as follows

$$For \quad \psi(z) = \sin\left(\frac{\pi}{2}\frac{z}{H}\right) \quad \alpha_n = 2/[(2n-1)(-1)^{n+1}+1]\pi$$

$$For \quad \psi(z) = \frac{z}{H} \quad \alpha_n = \frac{2}{(2n-1)\pi}\left[(-1)^{n+1} - \frac{2}{(2n-1)\pi}\right]$$

$$For \quad \psi(z) = 1-\cos\left(\frac{\pi}{2}\frac{z}{H}\right) \quad \alpha_n = \frac{2}{\pi} - \frac{1}{2} \quad for \;\; n=1 \qquad (1.39)$$

$$\alpha_n = (-1)^{n+1}\frac{2}{(2n-1)\pi} \quad for \;\; n>1$$

$$For \quad \psi(z) = 1 \quad \alpha_n = \frac{2(-1)^{n+1}}{(2n-1)\pi}$$

The hydrodynamic pressure exerted on the wall is obtained by applying Eq. (1.3) at paragraph 1.2.1, and given in the form

$$p(z,t) = \ddot{w}(t)\rho_l H\cos\theta\sum_{n=1}^{\theta}\frac{4\alpha_n}{(2n-1)\pi}\frac{I_1\left[(2n-1)\frac{\pi}{2}\frac{a}{H}\right]}{I_1'\left[(2n-1)\frac{\pi}{2}\frac{a}{H}\right]}\cos\left[(2n-1)\frac{\pi}{2}\frac{z}{H}\right] \qquad (1.40)$$

Once the hydrodynamic and inertia forces are identified, the equation of motion for the tank-fluid system are determined by application of the virtual work principle

$$[m_{w,s}^* + m_{w,l}^*]\ddot{w} + c^*\dot{w} + k^*\dot{w} = -[m_{x,s}^* + m_{x,l}^*]\ddot{x}(t) \qquad (1.41)$$

where $m_{X,s}^* + m_{X,l}^* = m_X^*$ represents the effective mass of the system for the rigid body component of motion, and $m_{X,s}^*$ and $m_{X,l}^*$ represent the contributions of the structural mass and liquid mass, respectively. In an analogous manner, $m_{w,s}^* + m_{w,l}^* = m_w^*$ represents the effective mass of the system for the motion specified by $\psi(z)$, and $m_{w,s}^*$ and $m_{w,l}^*$ represent the contribution of the structural mass and liquid mass. The quantities c^* and k^* are the effective damping and the effective stiffness of the system. The solution of equation of motion is obtained by analogy to that governing the motion of a single mass-spring-dashpot oscillator. This procedure provides the analytical function for the maximum hydrodynamic pressure on the tank

wall, the maximum value of the base shear and overturning moment due to the hydrodynamic pressure. It is worth to point out that the configuration of the assumed mode $\psi(z)$ depends on the relative magnitudes of flexural and shearing deformation of the filled-fluid tank during free vibration. These magnitudes, in turn, depend on the dimension of the tank, such as H/a and h/a, and on the relative weights of the roof system m_r to the virtual mass of contained fluid. In particular, for large values of H/a and h/a and m_r, the mode $\psi(z)$ will be more like a flexural type, while for small values of these functions, the mode $\psi(z)$ will be more like a shear beam type.

Veletsos in [21] proposed the following procedure for selecting a reasonable vibration mode $\psi(z)$.

1. Assume a trial configuration $\psi(z)$; for convenience it can be taken equal to one of those proposed in Eqs. (1.39) and depicted in Figure 1-7.
2. Compute the resulting inertia and hydrodynamic forces which are given in Eq. (1.40).
3. Compute the deflection of the tank due to the forces determined in step 2, considering the effects of both flexural and shearing deformations.
4. The deflection determined in step 3, normalized with respect to the deflection value computed at $z = H$ is the desired $\psi(z)$.

Once the vibration mode is selected, the circular natural frequency of the fluid-tank system, ω, is easily computed by Raileigh's quotient $\omega = \sqrt{V_0/T_0}$, where V_0 is the maximum potential energy of the system, obtained by integrating the product of forces, T_0 is the pseudo-kinetic energy of the system.

Figure 1-8 and Figure 1-9 show the hightwise variation of the impulsive pressure on the tank wall along $\vartheta = 0$ and the corresponding variation of the impulsive pressure on the base, respectively. Results are plotted for two H/a values corresponding, respectively, to a squat tank and a slender tank. Plots are in terms of $\rho_l HCA$, in which C and A are the participation factor and the pseudo-acceleration defined by the procedure. Results demonstrate as pressure for flexible tank is materially different from those from the rigid tank. Moreover, for flexible tank results are influenced by the assumed vibration mode.

Figure 1-10 depicts the virtual masses $m^*_{w,l}$ and $m^*_{X,l}$ appearing on Eq. (1.41). These are plotted as a function of H/a for each of the three modes of vibration considered herein. In Figure 1-11, values of base shear and moment for rigid tank are compared with those obtained for flexible tank for each of the three vibration modes.

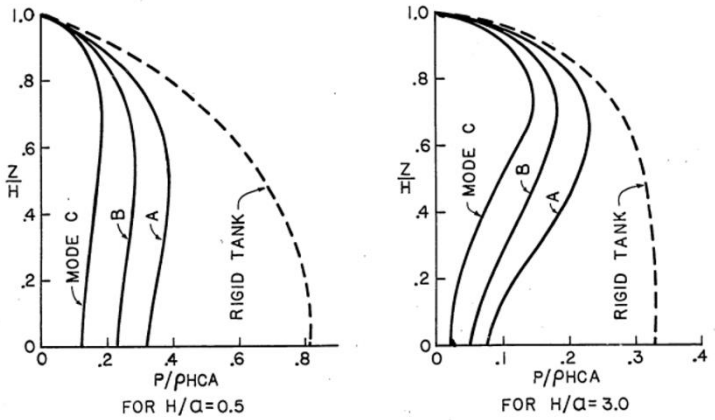

Figure 1-8. Distribution of the impulsive pressure on the tank wall [13]

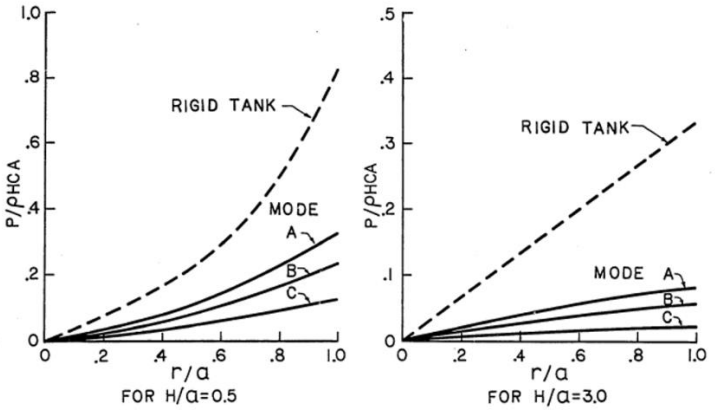

Figure 1-9. Distribution of the impulsive pressure on the tank base [13]

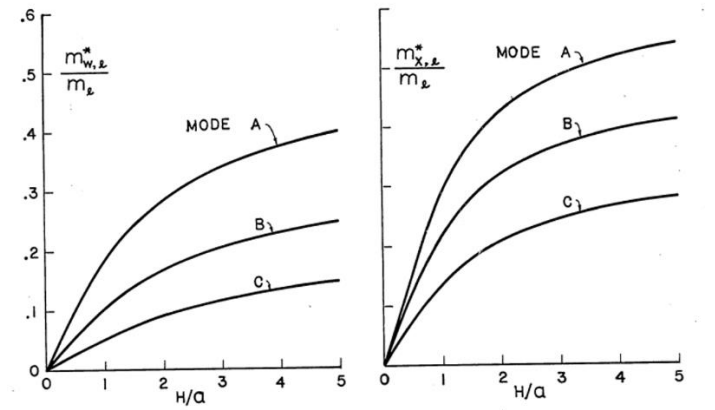

Figure 1-10. Virtual masses of the fluid [13]

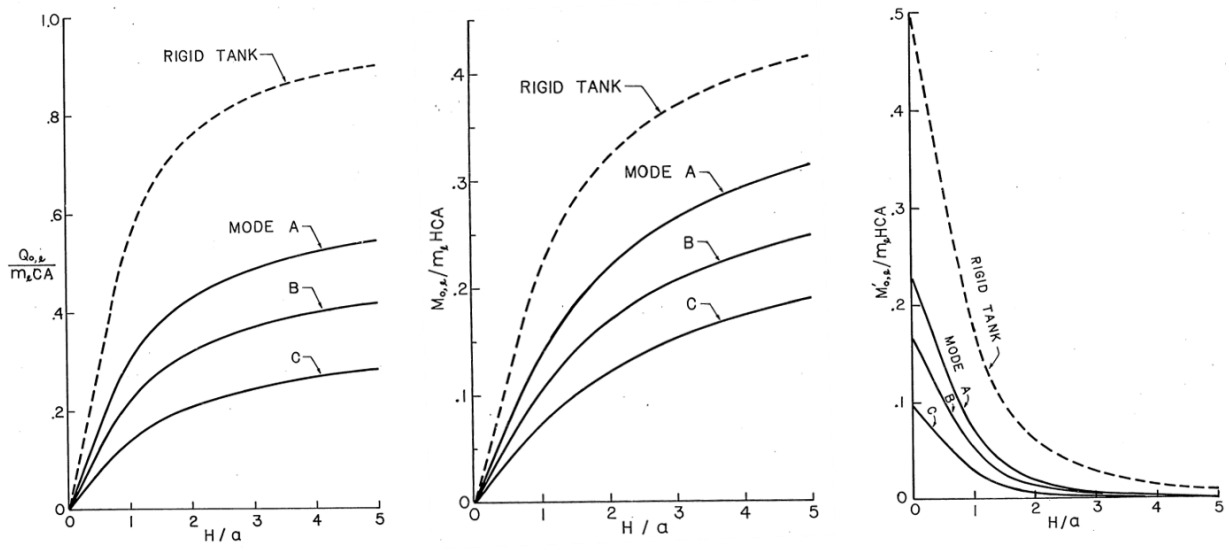

Figure 1-11. Impulsive shear forces a the tank base (a), overturning moment due to wall pressure (b), overturning moment due to base pressure (c) [13]

1.3.2. Mechanical models of tank-fluid system considering the effects of wall flexibility

The procedure proposed by Haroun, Housner and Ellaithy in [24–26], for the evaluation of the seismic response of the tank-fluid system considering the effects of wall flexibility, was based on the mechanical model depicted in Figure 1-12. With respect to the model proposed by Haroun for rigid wall, it maintains the concept of generalized single-degree-of-freedom (SDOF) systems. However, in this model the impulsive mass has two contributes: the rigid contribute, depicted in figure as m_d, rigidly attached to the tank wall, and the flexible contribute, m_f, attached to the wall through a spring whose elastic constant, k_f, is calculated as a function of H, a, m_f and m_l. The contribution of m_f to the overturning moment is determined by the height h_f', that takes into account the effects of pressure on the tank base.

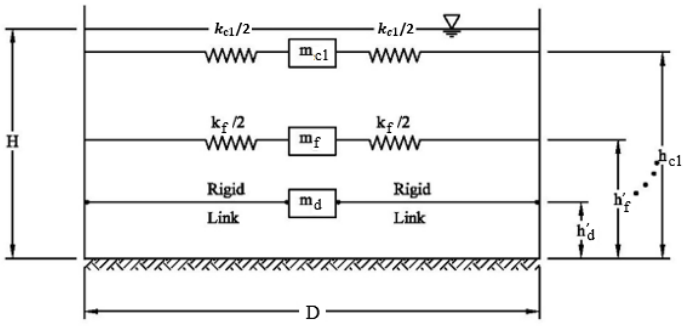

Figure 1-12. Mechanical model for tank with flexible wall [24–26]

A further mechanical model has been proposed by Malhotra in his simplified procedure for the seismic analysis of liquid-storage tanks [19] (Figure 1-13) adopted in Eurocode 8. This method takes into account impulsive and convective actions of the liquid in flexible steel or concrete tanks fixed to rigid foundations. Impulsive and convective masses, m_i and m_c, as well as their corresponding heights and natural periods, are obtained by the method described in [22,23,26–28]. Malhotra confirmed that for tanks with $0.3 < H/a < 3$, where H is the height of liquid, the first impulsive and first convective modes together account for 85-98% of the total liquid mass in the tank. The remaining mass of liquid vibrates primarily in higher impulsive modes for tall tanks ($H/a > 1$) and higher convective modes for broad tanks ($H/a \leq 1$). The seismic response (base shear, overturning moment and sloshing wave height) obtained involving the first impulsive mode and first convective mode is considered satisfactory in most cases. Thus in his simplified procedure, the author takes into account these modes only.

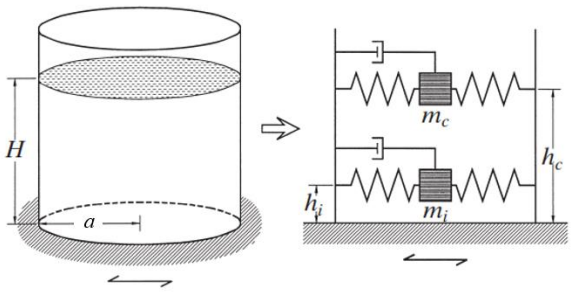

Figure 1-13. Malhotra's simplified tank model [19]

1.4. Unanchored tanks and uplift – general remarks

In the context of the tank seismic design, anchorage system should be provided when the tank overturning moment due to the horizontal ground acceleration, overcomes the restoring moments. In practice, a complete base anchorage is not always a feasible or economical solution. As a result, many tanks are unanchored or partially anchored to the base.

The base uplift has been found to reduce the hydrodynamic forces in the tank-fluid system; however, it leads to an increase of the axial compressive stress in the tank wall. Further studies showed that in the case of tank supported directly on flexible soil foundations, the base uplift does not cause a significant increase in the axial compressive stress in the tank wall, but it may lead to large foundation penetrations and large plastic rotations at the plate boundary. Therefore, flexibly supported unanchored tanks are susceptible to irregular settlement of the foundation

and fatigue rupture at the plate-shell junction, whereas they are less prone to elephant foot buckling.

The dynamic behavior of anchored tanks has been widely analyzed through analytical and numerical studies. For such kind of structures, the bottom plate is prevented from vertically displacing, and therefore, the seismic response can be evaluated by calculating the natural modes of vibration of the tank-fluid system and superimposing them properly. On the contrary, few approximate methods have been developed for the estimation of internal stresses at the bottom plate in case of unanchored tanks. Reports on damages caused by past earthquakes reveal that unanchored tanks have been subjected to extensive failures such as buckling of the lower part of shell wall, due to large compressive stresses, rupture at the bottom-wall junction, caused by excessive plastic yielding, and failure at pipes and fittings, that are not able to absorb large displacements [2]. Past theoretical studies conducted with the aim to clarify the uplift problem use static and dynamic models:

- static models have the main purpose to study the effects of uplift displacement on the stresses in the tank;
- dynamic models have been proposed to calculate the amplitude dependent natural frequencies, mode shapes and the dynamic pressures.

Dynamical investigation of unanchored tanks excited by earthquakes can be performed through the finite element method. The advance of using such a method is that the whole fluid-shell-foundation system can be modeled and different type of non-linearity can be taken into account. However, in case in which nonlinear effects such as yielding and partial uplift of the bottom plate are included in the analyses, the computational effort increases dramatically.

A critical overview on previous researches on unanchored tanks has been presented in Chapter 5, whereas analytical methods used by codes for the design are given in Chapter 2.

2. Critical review of seismic codes provisions

2.1. European and international codes and standards

Liquid storage tanks are widely used in industries for the containment of toxic and flammable liquids and in water distribution systems. The most common typologies are principally ground supported and elevated tanks, made of steel, ordinary or pre-stressed reinforced concrete. Past seismic events have highlighted the most serious deficiencies and weaknesses of these structures and helped codes in improving their dynamic performances. It should be pointed out that seismic analysis of liquid storage tanks presents some differences compared to the building-type structures. Indeed, liquid storage tanks are less ductile then buildings and they are subjected to fragile mechanisms (piping sheared, anchorage pull out or breakage, sliding of the bottom plate on the foundation, roof collapse, etc.). Moreover, the contained liquid excited by dynamic action causes hydrodynamic pressure on the tank wall and base. Due to low ductility, the design of liquid storage tank uses lateral seismic forces higher than that for building-type structures having equivalent dynamic properties. In addition, since the storage area usually represents one of the most dangerous of industrial plants, codes and standards further increase seismic design forces providing high values of the importance factor of tanks. A critical comparison between the main standards involved in design of storage tanks is provided by Jaiswal *et al.* in [15]. Some of the concepts developed in that previous study are reported in the present section, at Paragraph 2.2, in order to review codes provisions, common features and differences among them. The abovementioned considerations constitute the major principles common to all the main standards and codes for the seismic design of liquid storage tanks. However, the way to transpose these criteria in practice can vary from a code to another and lead to significant differences in the definition of seismic design force. Paragraph 2.3 provides a detailed description of the seismic design procedures of on-grade cylindrical steel storage tanks subjected to horizontal and vertical ground accelerations, according to the UNI EN 1998-4:2006, NZSEE and AWWA D100-05 is presented. Rigid and deformable tanks are considered in case of rigid or flexible foundation and in case of base perfectly or partially anchored to the foundation. Moreover, a comparison between the three codes examined is carried out as well.

The European and international codes and standards dealing with analysis, design and verification of storage tanks made of steel, pre-stressed or ordinary reinforced concrete located in areas of seismic activity are listed as follows:

- UNI EN 1998-4:2006 *Design of structures for earthquake resistance - Part 4: Silos, tanks and pipelines,* hereafter called EC8-4. This code provides rules and provisions for the

seismic design of piping system, steel, pre-stressed and ordinary reinforced concrete tanks and silos used for storage of liquid or granular substances. The code analyzed different types of tanks: (a)circular and rectangular, (b) rigid and flexible wall; (c) anchored and unanchored. Some considerations are made on elevated tanks and on the soil-structure interaction;

- BS EN 14015:2004 *Specification for the design and manufacture of site built, vertical, cylindrical, flat-bottomed, above ground, welded, steel tanks for the storage of liquids at ambient temperature and above*. This European Standard specifies the requirements for the materials, design, fabrication, erection, testing and inspection of tanks and the technical agreements that need to be reached. It is concerned with the structural integrity of the basic tank structure and does not provide requirements for considering process design, operational issues, safety, inspection, maintenance or repair. It deals extensively with the static behavior of the tank-fluid system, more briefly with the seismic one;

- *Seismic Design of Storage Tanks, Recommendations of a Study Group of the New Zealand National Society for Earthquake Engineering*. The first issue of this code dates back to 1986, while in 2009, M.J.N. Priestley published the last edition (the acronym NZSEE refers to this latter version). It incorporates provisions for the definition of the design loads given in NZS 4203 [29], Code of practice for general structural design and design loading for building (1992). The standard reflects the same tank typologies treated by EC8-4, however further information about buried and elevated tanks, and soil-structure interaction are given;

- ACI 350.3-06 *Seismic Design of Liquid-Containing Concrete Structures and Commentary* and ACI 371R-98 *Guide for the Analysis, Design and Construction of Concrete-Pedestal Water Towers*. These two codes provide provisions uniquely for reinforced concrete tanks;

- AWWA D100-05, 2005: *Welded carbon steel tanks for water storage* and AWWA D103-97 *Factory-coated bolted steel tanks for water storage*, American Water Works Association, Colorado. These standards specify rules and provisions for the design and construction of welded and bolted steel tanks for water storage but they are considered suitable also for the storage of fuel oils. Paragraph 13 of AWWA D100-05 deals with the seismic design of anchored, unanchored and elevated cylindrical tanks made of steel; AWWA D110-04 and D115-06 treat pre-stressed reinforced concrete tanks. At paragraph 4 they define horizontal and vertical seismic forces and design requirement under operating conditions;

- API 650, 2005: *Welded steel tanks for oil storage*, American Petroleum Institute Standards, Washington DC. These standards constitute the main world reference for the design of oil tanks. Appendix E analyses the seismic design of anchored and unanchored steel cylindrical tanks. Elevated tanks are not covered;

- Uniform Building Code, Vol. 2, *Structural Engineering Design Provisions* 1997 (Paragraph 1634) and ASCE 7 2005 (Paragraphs 15 and C15). For liquid storage tanks, the 2006 IBC refers to ASCE 7 2005, which contains two series of provisions: the first follows its own criterion in definition of design forces and in analysis; the second adopts modified expression of the seismic design forces provided in AWWA, API and ACI [15]. These codes analyses anchored, unanchored and elevated tanks made of steel, ordinary and pre-stressed reinforced concrete;

- IITK.GSDMA (2005) *Guidelines for Seismic Design of Liquid Storage Tanks, Previsions with Commentary and Explanatory Examples*, provided by NICEE, National Information Center of Earthquake Engineering. The guidelines include the documents: "Review of Code Provisions on Design Seismic Forces for Liquid Storage Tanks" and "Review of Code Provisions on Seismic Analysis of Liquid Storage Tanks" that provide a comparison on the international codes for the seismic design of liquid storage tanks. IITK.GSDMA 2005 receives principles and provisions from ACI 350.3-06;

The aforementioned and others codes are synthetically presented in Table 2.1 [15], in which details about type of tanks considered, seismic force level and provisions on convective mode are given. In particular, some of these standards specify the design seismic force at strength design level; in this case, loads are factored and lead to the ultimate state. On the other hand, some codes use working stress design level.

Table 2.1.Details of codes and standards [16]

Code/Standard	Type of tanks considered[1]	Seismic force level[2]	Provisions on convective mode
2006 IBC & ASCE 7	1,2,3,4	SD	Yes
Eurocode 8 (1998)	1,2,3,4	SD	Yes
NZSEE	1,2,3,4	SD	Yes
ACI 350.3 (2001)	1,3	ASD	Yes
ACI 371 (1998)	3	SD	No
AWWA D-100 (2005)	2,3,4	ASD	Yes[3]
AWWA D-110 (1995)	1	ASD	Yes
AWWA D-115 (1995)	1	ASD	Yes
API 650 (2005)	2	ASD	Yes

[1] 1=Ground-supported RC/PSC tanks; 2=ground-supported steel tanks; 3=elevated tanks on shaft-type tower 4=elevated tanks on frame-type tower
[2] SD=strength design level; ASD=allowable stress design level
[3] Provisions on convective mode are given for ground-supported tanks only.

2.2. Critical comparison of the main design codes

2.2.1. Design seismic force: provisions from codes

Design seismic force and reduction factor

The elastic design force is reduced by codes in order to take into account ductility and plastic resources of the structure. In this regard, each code gives different principles and provisions for the practical use of reduction factor. ASCE 7 specifies different values of the so called response modification factor R for two types of on-grade RC and PSC tanks and two types of on-grade steel tanks (see Table 2.2). NZSEE uses the correction factor C_f which is a function of the ductility factor μ and the damping ratio ξ. Moreover, it suggests different values of C_f, μ and ξ for different types of tanks. Table 2.3 specifies the classification of tanks used in NZSEE, very detailed for steel tanks, and the corresponding values of the aforementioned quantities. Eurocode 8 uses the behavior factor q and it assigns q=1 (the elastic design forces) for all on-grade tanks unless proper analysis demonstrates a substantial energy-dissipating capacity. Table 2.2 contains values of the response modification factor also for codes as ACI 350.3, D-110, D-115 and API 650. ASCE 7 defines the seismic design forces at the strength design level, whereas ACI 350.3, D-110 and API 650 are at the allowable stress design level. This is the reason for

the bigger values of response modification factor in ACI 350.3, D-110 and API 650. Code D-100 as well defines design forces at the allowable stress design level. However, values of response modification factor are the same as those in ASCE 7, because a factor of 1.4 is used to convert design forces from strength design level to allowable stress design level. Another subject of discussion in the context of ground-supported tanks is the usage of the response modification factor for the convective forces. Eurocode 8, ACI 350.3 and D-110 do not provide any reduction for convective modes. ASCE 7, D-100 and API 650 allow small reduction of the convective forces by providing values of the response modification factor lower than those specified for impulsive mode. On the contrary, D-115 and NZSEE use same values of the modification factor for impulsive and convective modes.

Table 2.2. Type of tanks and response modification factor from American standards [15]

Type of base	Response modification factor							
	Ground-supported RC/PSC tanks							
	ASCE 7		ACI 350.3		D-110		D-115	
	Impl.	Conv.	Impl.	Conv.	Impl.	Conv.	Impl.	Conv.
Anchored flexible	3.0	1.5	4.5	1.0	4.5	1.0	2.5	2.5
Reinforced nonsliding	2.0	1.5	2.75	1.0	2.75	1.0	3.0	3.0
Unanchored and contained flexible	—	—	2.0	1.0	—	—	3.0	3.0
Unanchored and uncontained flexible	1.5	1.5	2.0	1.0	2.0	1.0	1.0	1.0
	Ground-supported steel tanks							
	ASCE 7		D-100		API 650			
Mechanically anchored	3.0	1.5	3.0	1.5	4.0	2.0		
Self anchored	2.5	1.5	2.5	1.5	3.5	2.0		
	Elevated tanks							
	ASCE 7		ACI 350.3		ACI 371		D-100	
RC pedestal	2.0	1.5	3.0	1.0	2.0	*a*	3.0[1]	1.5[1]
Braced/ unbraced legs	3.0	1.5	—	—	—	—	3.0	1.5

a = No provision
[1] For steel pedestal

Table 2.3. Types of tanks, ductility factor, damping ratio and correction factor from NZSEE [15]

Type of Tank	μ	ξ(%)		C_f	
Steel Tanks on Grade		Impl.**	Conv.	Impl.	Conv.
Elastically supported	1.25	2	0.5	0.83	0.92
Unanchored tank designed for uplift (elephant foot shell buckling may occur under seismic overload)	2.0[a]	2	0.5	0.54	0.58
Unanchored tank designed for uplift and elastic (diamond shaped) shell buckling mode	1.25	2	0.5	0.83	0.92
Anchored with nonductile hold-down bolts	1.25	2	0.5	0.83	0.92
Anchored with ductile tension yielding hold-down bolts	3.0[b]	2	0.5	0.41	0.43
Ductile skirt pedestal	3.0[b]	2	0.5	0.41	0.43
On concrete base pad designed for rocking	2.0[b]	2	0.5	0.54	0.58
Concrete Tanks on Grade					
Reinforced concrete	1.25	5	0.5	0.72	0.92
Prestressed concrete	1.0	5	0.5	1.0	1.75
Elevated Tanks	*		0.5		

[a] Check that elastic buckling does not occur before elephant foot.
[b] Capacity design check required to protect against other forms of failure.
* As appropriate for support structure. Capacity design approach shall be used to protect elevated tanks against

Damping for impulsive and convective motions

For convective mode, all codes and standard specify 0.5% damping, whereas for impulsive mode they provide different values basing on tank type, material, foundation etc. In particular: ASCE 7 uses 5% damping for all tanks; Eurocode 8 uses 5% damping for RC and PSC tanks and 2% for steel tanks; NZSEE specifies values depending on tank geometry, aspect ratio, construction material, foundation soil shear velocity; ACI 350.3, which deals with RC and PSC tanks, API 650 and D-100, which deal with steel tanks, use 5% damping.

2.2.2. Analysis of tank-fluid system: provisions from codes

The present section has the aim to discuss on the different ways adopted by codes for modeling the tank-fluid system and the soil-structure interaction, combining impulsive and convective effects, evaluating the hydrodynamic pressure on wall and base and the sloshing wave height.

Mechanical model of tank-fluid system

As already explained in Chapter 1 of the present work, the liquid mass contained in a storage tank subjected to seismic action can be seen as the coexistence of two components undergoing different motions: the lower part of the liquid mass vibrates in unison with tank wall, whereas

the upper liquid mass vibrates relatively to the tank wall and with longer period. In technical literature, impulsive and convective motions have been studied using different mechanical models. Researchers as Housner in 1963 [16] , Veletsos and Yang in 1977 [22] studied the tank-fluid system through a two-masses model. In this model, the tank wall is considered to be rigid. Later, Housner and Haroun in 1981 [30] and Veletsos in 1984 [23] introduced included effects of the wall flexibility. All codes for seismic design of storage tanks use a tank model with rigid wall, except for EC8-4 and NZSSE. In particular EC8-4 introduces an impulsive component of pressure related to the wall flexibility; NZSEE uses a rigid tank model for reinforced concrete tanks and a flexible tank model for steel tanks. However, codes that use the rigid tank model take into account the wall flexibility in the evaluation of the natural period of impulsive and convective motions. Therefore, tank flexibility is not included only in case of masses evaluation.

Once the seismic responses has been calculated for impulsive and convective components of motion, the overall tank behavior is obtained by properly combining them. Codes give provisions for the combination rules. In particular, ASCE 7 and Eurocode 8 use the absolute summation rule, suggested by Malhotra in [19], whereas ACI 350.3, AWWA D-110, D-115, D-100, API 650 and NZSEE use the SRSS rule.

Hydrodynamic pressure on tank wall and base

Housner in 1963 [16] provides the analytical formulation for distribution of the impulsive and convective hydrodynamic pressure on the tank wall. It was adopted by NZSEE and Eurocode 8. In addition, NZSEE and ACI 350.3 described a simplified linear distribution of the hydrodynamic pressure. All codes take into account the effect of hydrodynamic pressure on the tank base for calculation of tank overturning moment, but only NZSEE provides the expression for its distribution along the base. Formulations of hydrodynamic pressure on tank wall and base is omitted in ASCE 7, but it suggests using provisions given from other standards.

Convective wave height

The convective motion of liquid contained causes the appearance of waves in the upper part of the tank. Depending on the tank size and aspect ratio, the effect of these waves can be relevant and their impact on tank wall and roof can cause damage to shell and junctions. It is important to provide a freeboard to prevent these kinds of damage and loss of content from the top. All codes and standards except AWWA D-115 and ACI 371 provide expressions for the calculation

of the maximum sloshing wave height. Table 2.4 shows a comparison between sloshing wave heights from different codes and standards. It should be noted that ACI 350.3 overestimates the maximum height of sloshing wave. Furthermore, NZSEE presents different values of the sloshing wave height for the different type of tank investigated. This comes from the usage of different values of the response modification factor employed in the formulation of the convective base shear coefficient. In particular, NZSEE distinguishes tanks into: 1) reinforced concrete and unanchored steel tanks, 2) pre-stressed concrete tanks, 3) anchored steel tanks with ductile bolts. On the contrary, all other codes propose a single value of height for all types of tanks.

Based on the sloshing wave height, Malhotra in 2005 [11] provided a simplified method for the estimation of the additional forces on the roof and tank wall resulting from the absence of a sufficient freeboard.

Table 2.4. Comparison of sloshing wave height form various codes and standards

T(s)	Sloshing wave height/radius of tank								
	ASCE 7	Eurocode 8	NZSEE[1]	NZSEE[2]	NZSEE[3]	ACI 350.3	D-110	D-100	API 650
2	0.56	0.38	0.46	0.87	0.21	0.88	0.75	0.56	0.56
4	0.28	0.14	0.23	0.43	0.107	0.28	0.19	0.28	0.28
6	0.125	0.063	—	—	—	0.125	0.083	0.125	0.125
8	0.07	0.035	—	—	—	0.07	0.047	0.07	0.07

[1] RC tanks and unanchored steel tanks
[2] PSC tanks
[3] Anchored steel tanks with ductile bolts

Soil structure interaction

It is known that soil flexibility enhances the impulsive time period, and radiation damping of the soil increases the total damping of the structure. Provisions for soil-structure interaction are given in ASCE 7, NZSEE and Eurocode 8. These codes provide expressions governing that interaction, as well as expressions of the equivalent damping of tanks that includes the effect of the soil radial damping, studied by Veletsos 1984 [23]. The other codes do not consider the soil effects on the tank seismic response.

2.3. Seismic design of on-grade steel tanks

The present section introduces the seismic analysis procedures for on grade cylindrical tanks subjected to horizontal and vertical ground accelerations according to EC8-4, NZSEE and AWWA D100-05 provisions (some prescriptions are given also for other codes). Rigid and deformable tanks will be considered in case of rigid or flexible foundation and in case of base perfectly or partially anchored to the foundation. Further details on the seismic design of tanks can be found in Calvi and Nascimbene [31].

2.3.1. Seismic design of on-grade steel tanks according to EC8-4

Rigid tanks perfectly anchored to the foundation

For rigid tanks, the instantaneous value of the hydrodynamic pressure at an arbitrary point, $p(\xi, \varsigma, \vartheta, t)$, is defined by the superposition of the impulsive component $p_i(\xi, \varsigma, \vartheta, t)$ and the convective component $p_c(\xi, \varsigma, \vartheta, t)$.

The system considered is a rigid circular cylinder tank of radius R fixed to a rigid base. The cylindrical coordinate system has the origin at the center of the tank bottom; z is the vertical axis, whereas x is the direction of the horizontal ground acceleration $\ddot{x}(t)$ that excites the tank-fluid system. H is the level of the fluid inside the tank (see Figure 1-2 in which the radius R is indicated with the letter a). The fluid density is ρ $[kg/m^3]$. It should be noted that the procedure adopted by EC8-4 has been developed by Yang in [13] explained in Chapter 1 of the current work at paragraph 1.2.1. However, for the sake of clarity, all the main equations have been reported also in this section.

Impulsive pressure

The spatial-temporal variation of the impulsive pressure is given in section A.2.1.2 of EC8-4 and determined by Yang in [13] (see Chapter 1of the current work, paragraph 1.2.1):

$$p_i(\xi, \varsigma, \theta, t) = C_i(\xi, \varsigma)\, \rho H \cos\theta\, a(t) \tag{2.1}$$

where $a(t)$ represents the ground acceleration time-history in the free field (with peak value denoted by a_g), while C_i has the following expression:

$$C_i(\xi,\varsigma) = 2\sum_{n=0}^{\infty} \frac{(-1)^n}{I'_1\left(\frac{\upsilon_n}{\gamma}\right)\upsilon_n^2} \cos(\upsilon_n \varsigma) I_1\left(\frac{\upsilon_n}{\gamma}\xi\right) \tag{2.2a}$$

$$\upsilon_n = \frac{2n+1}{2}\pi \tag{2.2b}$$

$$\gamma = \frac{H}{R} \tag{2.2c}$$

$I_1(\cdot)$ and $I_1'(\cdot)$ denotes the modified Bessel function of order 1 and its derivative.

The dimensionless function C_i represents the distribution of p_i normalized among the height; in Figure 2-1 (a) it is shown for $\xi = 1$, (i.e. at the wall of the tank) and $\cos\vartheta = 1$ (i.e. in the plane of the horizontal seismic action). Moreover, the impulsive pressure p_i is normalized with respect to $\rho R a(t)$. Figure 2-1 (b) shows the radial variation of p_i on the tank bottom ($z = 0$) for three different values of the slenderness parameter $\gamma = H/D$. Note that for large values of γ (i.e. for slender tanks) the pressure distribution on the tank bottom becomes linear.

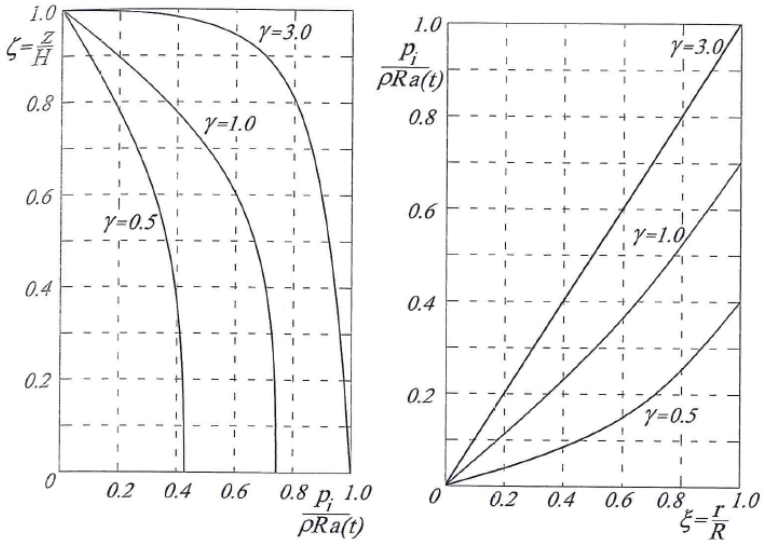

Figure 2-1. Distribution of the impulsive pressure normalized with respect to $\rho R a(t)$; (a) distribution among the height, (b) radial distribution among the tank bottom [31]

Pressure resultants

The horizontal resultant of the rigid impulsive pressure at the base of the wall is obtained from Eq. (2.1) and it represents the impulsive base shear

$$Q_i(t) = m_i a(t) \tag{2.3}$$

where m_i, named impulsive mass, denotes the mass of the contained fluid which moves together with the wall. The total impulsive moment with respect to an axis orthogonal to the direction of the seismic action, M_i', immediately below the tank bottom, includes the contributions of the pressures on the walls (Eq. (2.1)) and those of the pressure on the tank bottom plate:

$$M_i'(t) = m_i h_i' a(t) \tag{2.4}$$

where h_i' is the height of the centroid of the impulsive pressure measured from the tank bottom that takes into account the hydrodynamic pressure on the bottom [13,23]. The total impulsive moment M_i immediately above the tank bottom plate includes only the contributions of pressures on the walls:

$$M_i(t) = m_i h_i a(t) \tag{2.5}$$

The quantities m_i, h_i' and h_i are plotted in dimensionless form as functions of the slenderness ratio γ in Figure 2-2.

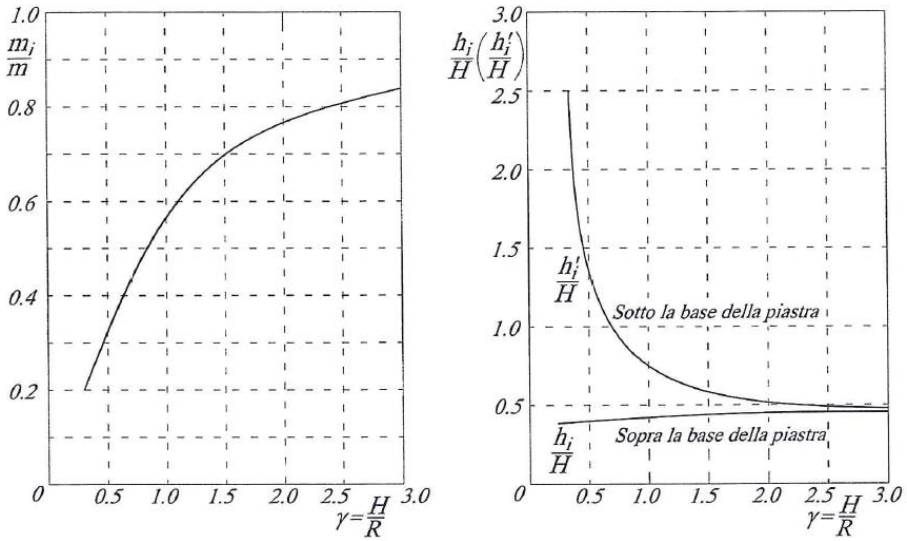

Figure 2-2. Ratios m_i/m, h_i/H and h_i'/H as functions of the tank aspect ratio [31]

Convective pressure

The spatial-temporal variation of the convective pressure is given in section A.2.1.2 of EC8-4 and determined by Yang in [13] (see Chapter 1of the current work, paragraph 1.2.1):

$$p_c(\xi,\varsigma,\theta,t)=\rho\sum_{n=1}^{\infty}\psi_n\cosh(\lambda_n\gamma\zeta)J_1(\lambda_n\xi)\cos\theta\, a_{cn}(t) \tag{2.6}$$

where the summation provides the contributes of all *n* sloshing modes, ρ (kg/m^3) is the fluid specific weight, $\gamma = H/R$ is tank aspect ratio, J_1 is the Bessel function of the 1^{st} order, λ_n stands for the n^{th} root of the 1^{st} derivative of the Bessel function of the 1^{st} kind and 1^{st} order; the first of these three roots are: $\lambda_1 = 1.8412$, $\lambda_2 = 5.3114$, $\lambda_3 = 8.5363$, $\lambda_4 = 11.0760$. The function ψ_n has the following expression:

$$\psi_n = \frac{2R}{(\lambda_n^2-1)J_1(\lambda_n)\cosh(\lambda_n\gamma)} \tag{2.7}$$

The anti-symmetric modal shapes of the first four sloshing modes is depicted in Figure 2-3 [32].

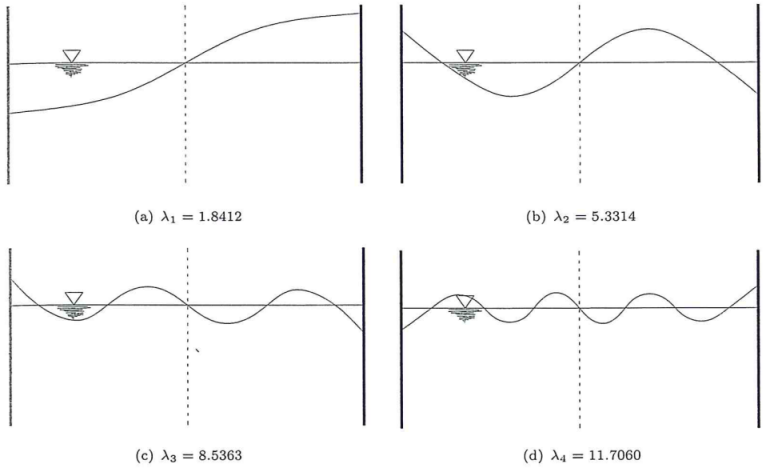

Figure 2-3. Antisymmetric modal shapes of the free liquid surface [31]

$a_{cn}(t)$ is the absolute acceleration time-history of the response of a single degrees of freedom oscillator having a circular frequency ω_{cn} given by the expression:

$$\omega_{cn} = \sqrt{g \frac{\lambda_n}{R} \tanh(\lambda_n \gamma)} \tag{2.8}$$

Only the first sloshing mode and the corresponding natural frequency ($n = 1$) needs to be considered in Eq. (2.6) for design purpose.

The vertical distribution of the sloshing pressures for the first two modes is shown in Figure 2-4 (a) (for $\vartheta = 0$ and $\xi = 1$), while Figure 2-4 (b) shows values of the first two frequencies as function of the aspect ratio H/R. In squat tanks ($\gamma = 0.5$) the sloshing pressures maintain relatively high values down to the bottom, while in slender tanks ($\gamma = 3$) the sloshing effect is limited to the vicinity of the liquid surface. The sloshing frequencies become independent from the parameter γ when it is greater than 1. For $\gamma > 1$, the frequency ω_{c1} is approximated by the expression (R in meters):

$$\omega_{c1} = \frac{4.2}{\sqrt{R}} \tag{2.9}$$

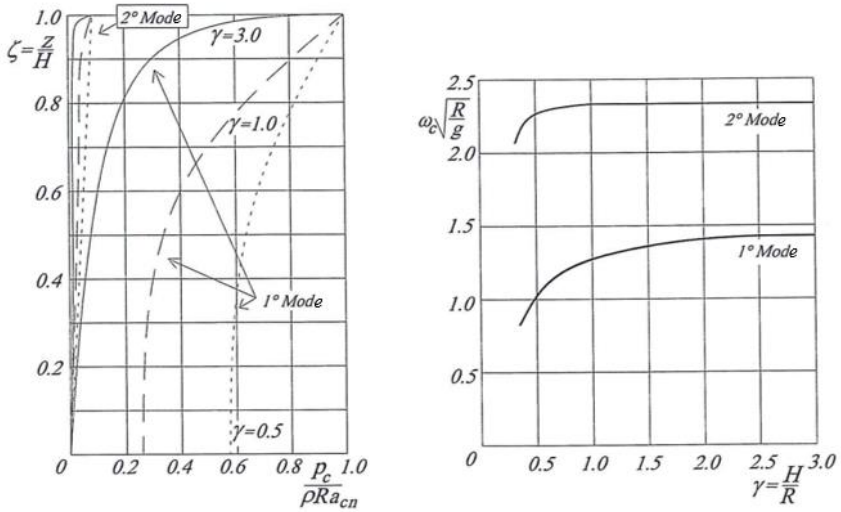

Figure 2-4. Distribution of pressure associated with the first and the second convective modes (n=1,2) among the tank height (a) and natural frequencies of the first and second modes as function of the tank slenderness [31].

Pressure resultants

The convective base shear is given as

$$Q_c(t) = \sum_{n=1}^{\infty} m_{cn} a_{cn}(t) \tag{2.10}$$

where m_{cn} is the n^{th} convective modal mass. The convective base moment immediately below the tank bottom plate is

$$M_c^{'}(t)=\sum_{n=1}^{\infty}(m_{cn}a_{cn}(t))h_{cn}^{'}=\sum_{n=1}^{\infty}Q_{cn}(t)h_{cn}^{'} \tag{2.11}$$

where h'_{cn} is the height of the centroid of pressure associated with the n^{th} convective mode that considers the hydrodynamic pressure on the bottom. Values of m_{c1} and m_{c2} [23] for the first two sloshing modes and values of their corresponding heights h'_{c1} and h'_{c2} are shown in Figure 2-5 as function of the slenderness ratio. The convective base moment immediately above the tank bottom plate is

$$M_c(t)=\sum_{n=1}^{\infty}(m_{cn}a_{cn}(t))h_{cn}=\sum_{n=1}^{\infty}Q_{cn}(t)h_{cn} \tag{2.12}$$

where the height of the centroid of pressure h_{cn} does not takes into account the hydrodynamic pressure on the bottom. Values of the heights h_{c1} and h_{c2} for the first two sloshing modes are shown in Figure 2-5 (b) as function of the slenderness ratio.

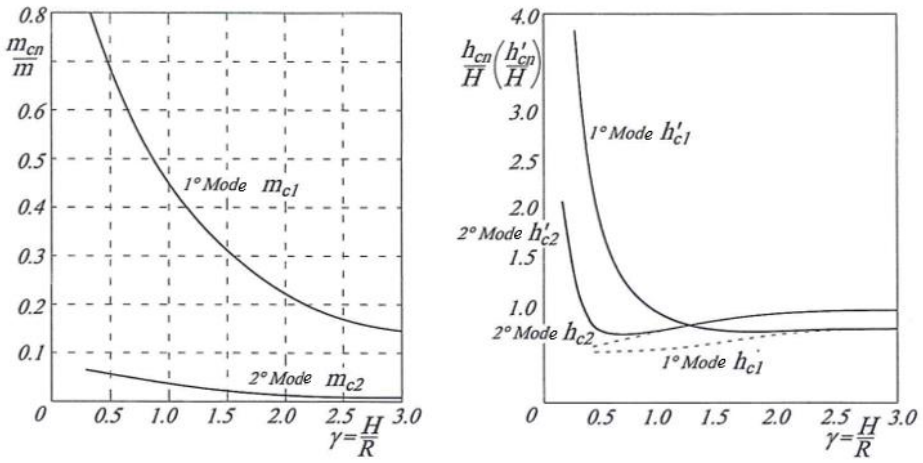

Figure 2-5. Masses m_{c1} and m_{c2} of the first two convective modes (a) and corresponding heights (b) as function of the tank slenderness [31]

The convective component of the response may be obtained from that of an oscillator having mass m_{cn} attached to the rigid tank through springs with stiffness $K_{cn}=\omega_{cn}^2 m_{cn}$. An oscillator for each significant mode is considered; normally the first mode is enough. The tank is subjected

to the ground acceleration time history $a(t)$ and the masses respond with acceleration $a_{cn}(t)$. Quantities h_{cn} and h'_{cn} represent the level at which the masses and the relative springs needs to be applied in order to provide the correct value respectively of M_{cn} and M'_{cn}.

Vertical pressure

The spatial-temporal variation of the axisymmetric hydrodynamic pressure on the wall of a rigid tank caused by a vertical acceleration $a_v(t)$ is given in EC8-4 at paragraph A.2.2:

$$p_{\upsilon r}(\zeta,t) = \rho H(1-\zeta)a_{\upsilon}(t) \tag{2.13}$$

where ρ is the density of the fluid (kg/m^3) and H is the tank height. In case of rigid support, $a_v(t) = a_{vg}(t)$, where $a_{vg}(t)$ is the vertical ground acceleration in the free field. In case of soil-structure interaction, $a_v(t)$ represents the variation in time of the acceleration response of a single degree of freedom with natural frequency subjected to $a_{vg}(t)$ at its base, ω_V obtained from Eq. (2.50). It should be noted that Eq. (2.13) is independent from ξ and ϑ since vertical pressure is axial symmetric and then it does not produce base shear and moment.

Natural period of the tank-fluid system

The natural period of the first convective motion of the fluid contained can be obtained from the expression of ω_{cn}, given in Eq. 2.8 of the current work, for $n = 1$ (Eq. (C3.24) Paragraph C3.6 NZSEE and Eq. (A.9) Paragraph A.2.1.3 EC8-4):

$$T_1 = \frac{2\pi}{\omega_{c1}} = \frac{2\pi\sqrt{\frac{R}{g}}}{\sqrt{\lambda_1 \tanh\left(\frac{\lambda_1 H}{R}\right)}} \tag{2.14}$$

where $\lambda_1 = 1.8412$ that is the root of the 1^{st} derivative of the Bessel function of the 1^{st} kind and the 1^{st} order.

Combination of pressures and behavior factor

The total pressure acting on the tank wall consists of three contributions (paragraph A.2.1.6 of EC8-4):

- the impulsive pressure p_i, governed by $a(t)$ (Eq. (2.1));
- the convective pressure p_c, governed by $a_{c1}(t)$ (Eq. (2.6);
- the vertical pressure p_{vr} (Eq. (2.13)).

Criteria and provisions used for combining horizontal and vertical pressures are discussed in the following.

In case in which the maxima values of the horizontal response are obtained from dynamic analyses that involves the elastic spectrum, they must be properly combined. Since the distance between the dominant frequencies of the convective and impulsive motion is usually large, the EC8-4 at the paragraph A.2.1.6 and the ASCE 7 at the paragraph 15.7.6.1 recommend summing the maxima absolute values of impulsive and convective modes.

The peak value of the pressure due to the combination of horizontal and vertical excitation is determined according to the paragraph 4.3.3.5.2 (4) of the UNI EN 1998-1:2004 as follows:

$E_h(+)0.30 \cdot E_V$
$0.30 \cdot E_h(+)0.30 \cdot E_V$
$0.30 \cdot E_h(+)E_V$

where E_h and E_v represent respectively the effects of the application of the horizontal and vertical components of the seismic action; symbol $(+)$ has the meaning "is combined with" and it is taken as the most unfavorable for the effect under consideration (paragraph 3.2 (3)P of the EC8-4). Then, the final combined pressure should be added to the hydrostatic pressure on the wall at the one side of the tank (where the wall accelerates into the liquid) and subtracted as suction at the opposite.

The impulsive and convective responses are characterized by different mechanisms of energy dissipation [15]. The EC8-4 at paragraph A.2.1.6 assumes a behavior factor $q = 1$ (no energy dissipation) for the convective response, and $q = 1.5$ for the impulsive response.

Flexible tanks

The evaluation of the tank stresses in the context of the seismic design can be un-conservative if shell wall is assumed to be rigid, especially in case of steel tanks. The fluid pressure in a flexible wall tank consists of four contributes:

- impulsive pressure for rigid tank $p_i(\xi, \varsigma, \vartheta, t)$ determined from Eq. (2.1);
- convective pressure $p_c(\xi, \varsigma, \vartheta, t)$ determined for the first n sloshing modes from the expression (2.6);
- impulsive pressure for flexible tank $p_f(\xi, \varsigma, \vartheta, t)$ determined from (2.16);
- vertical pressure $p_v(\varsigma, t)$ obtained from combination of the vertical pressure for rigid tank $p_{vr}(\varsigma, t)$ (Eq. (2.13)) and that for flexible tank $p_{vf}(\varsigma, t)$ (Eq. (2.27)).

The reference spring mass model is the one in Figure 1-12 at the paragraph 1.3.2

Impulsive pressure

The component $p_f(\xi, \varsigma, \vartheta, t)$ must satisfy the following boundary conditions: (1) the radial velocity of the fluid among the wall equals the strain rate of the tank wall; (2) the vertical velocity at the tank bottom is zero; (3) the pressure at the free surface of the fluid is zero. The dynamic coupling between the sloshing and the flexible components is very week, due to the significant differences between the natural frequency of the sloshing motion and that of the fundamental vibration mode of the tank-fluid system. This aspect allows determining the component $p_f(\xi, \varsigma, \vartheta, t)$ independently of the others. The rigid impulsive and the convective components determined in previous sections remain therefore unaffected.

However, the procedure suggested by Eurocode for flexible tanks requires a very high computational effort, since the flexible pressure distribution p_f (Eq. A.19 of the EC8-4, Appendix A) depends on the modes of vibration of the tank-fluid system, among which only those with one circumferential wave (n=1) are of interest:

$$f(\zeta)\cos\theta \tag{2.15}$$

Assuming to know function (2.15), the spatial-temporal variation $(\varsigma, \vartheta, t)$ of the impulsive component associated with the wall flexibility is given by the expression:

$$p_f(\zeta,\theta,t) = \rho H \psi \cos\theta \sum_{n=0}^{\infty} d_n \cos(v_n \zeta) a_{fn}(t) \tag{2.16}$$

where:

$$\psi = \frac{\int_0^1 f(\varsigma)\left[\frac{\rho_s}{\rho}\frac{s(\varsigma)}{H} + \sum_{n=0}^{\infty} b'_n \cos(v_n \varsigma)\right] d\varsigma}{\int_0^1 f(\varsigma)\left[\frac{\rho_s}{\rho}\frac{s(\varsigma)}{H} f(\varsigma) + \sum_{n=0}^{\infty} d_n \cos(v_n \varsigma)\right] d\varsigma} \tag{2.17a}$$

$$b'_n = 2\frac{(-1)^n I_1(v_n/\gamma)}{v_n^2 I'_1(v_n/\gamma)} \tag{2.17b}$$

$$d_n = 2\frac{\int_0^1 f(\varsigma)\cos(v_n \varsigma) d\varsigma I_1(v_n/\gamma) d\varsigma}{v_n I'_1(v_n/\gamma)} \tag{2.17c}$$

$$v_n = \frac{2n+1}{2}\pi \tag{2.17d}$$

In Eqs. (2.17a) - (2.17b) ρ_s is the mass density of the construction material of the tank wall (kg/m^3) of thickness $s(\varsigma)$; $a_{fn}(t)$ is the time history of the response acceleration (relative to the base) of a single degree of freedom system subjected to $a(t)$ having period $T_f = 2\pi/\omega_f$ and a damping ratio equal to 2% [26,33] or 1% [34]; ψ given from the expression (2.17a) can be considered as a modal participation factor. The fundamental mode, corresponding to $n = 0$ is generally sufficient. Equations (2.16) - (2.17) depend on the function $f(\varsigma)$ that can be determined through an iterative procedure suggested by Fischer et al. in [35], and reported in the EC8-4. It consists in a numerical algorithm based on the "added mass concept". Starting with a trial vibration mode $f_i(\varsigma)$, where i corresponds to the i^{th} iteration, the associated flexible pressure distribution $p_f^i(\varsigma)$ is obtained from Eq. (2.16) by imposing $\psi a_f(t) = g$. Following the added mass concept, an effective mass density $\rho^i(\varsigma)$ of the shell can be calculated from $p_f^i(\varsigma)$. Then, this effective mass density may be used in a structural analysis of the tank in order to evaluate the mode shape in the $(i+1)^{th}$ iteration, and so forth until convergence. The convergence criterion is defined by Fischer and Rammerstorfer in [36].

The fundamental frequency of the first impulsive mode for flexible tank, can be evaluated through the following expressions (neglecting the soil-structure interaction):

- the relation obtained by Rammerstorfer et al. in [33]:

$$\omega_f = \frac{\pi}{R} \frac{\sqrt{\frac{Es(\varsigma)}{\rho H}}}{(0.157\gamma^2 + \gamma + 1.49)} \tag{2.18}$$

  valid for ratios $\varsigma = z/H = 1/3$; E is the elastic modulus of the tank wall material, ρ is the density of the fluid (kg/m^3) and $\gamma = H/R$.

- the relation provided at Point 4.3.1.1 of the ITK-GSDMA (2005) and at Point A.3.1 of the Eurocode 8, Edition 2003:

$$\omega_f = \frac{\pi}{R} \sqrt{\frac{Es(\varsigma)}{\rho H}} (0.01675\gamma^2 - 0.15\gamma + 0.46) \tag{2.19}$$

The resultant tank base shear is given by the expression

$$Q_f(t) = m_f a_f(t) \tag{2.20}$$

where:

$$m_f = m\psi\gamma \sum_{n=0}^{\infty} \frac{(-1)^n}{\nu_n} d_n \tag{2.21}$$

The overturning moment immediately above the tank bottom plate is

$$M_f(t) = m_f h_f a_f(t) \tag{2.22}$$

where:

$$h_f = H \frac{\left[\gamma \sum_{n=0}^{\infty} d_n \frac{(-1)^n \nu_n - 1}{\nu_n^2}\right]}{\gamma \sum_{n=0}^{\infty} d_n \frac{(-1)^n}{\nu_n}} \tag{2.23}$$

while the overturning moment immediately below the tank bottom plate is

$$M_f^{'}(t) = m_f \; h_f^{'} a_f(t) \tag{2.24}$$

where:

$$h_f^{'} = H \frac{\gamma \sum_{n=0}^{\infty} d_n \frac{(-1)^n \nu_n - 1}{\nu_n^2} + \sum_{n=0}^{\infty} \frac{d_n}{\nu_n} \frac{I_2(\nu_n/\gamma)}{I_1(\nu_n/\gamma)}}{\gamma \sum_{n=0}^{\infty} d_n \frac{(-1)^n}{\nu_n^2}} \tag{2.25}$$

Vertical pressure

The total vertical pressure $p_v(\varsigma, t)$ is obtained by applying the rule of the square root of sum of squares (paragraph A.3.3 and A.8 of the EC8-4):

$$p_v(\varsigma,t) = \sqrt{\left[p_{vr}(\varsigma,t)\right]^2 + \left[p_{vf}(\varsigma,t)\right]^2} \tag{2.26}$$

where $p_{vr}(\varsigma, t)$ is the pressure on the wall of a rigid tank obtained from Eq. (2.13). The contribution $p_{vf}(\varsigma, t)$ associated with the wall flexibility may be calculated by using the expression proposed by by Veletsos and Tang [37]:

$$p_{vf}(\varsigma,t) = 0.8\rho H \cos\left(\frac{\pi}{2}\varsigma\right) a_{vf}(t) \tag{2.27}$$

where $a_{vf}(t)$ is the time history of the response acceleration of a single degree of freedom system subjected to a vertical acceleration $a_{vg}(t)$ at the base and having natural frequency ω'_{vf} (Eqs. (2.28)). The fundamental frequency of the first impulsive mode for flexible tank (neglecting the soil-structure interaction) can be evaluated through the equation proposed by Haroun et al. in [38] and by Rammerstorfer et al. in [33] (paragraph A.3.3 EC8-4):

$$\omega'_{vf} = \frac{1}{2R}\sqrt{\frac{2\pi E I_1(\gamma_1) s(\varsigma)}{\rho H (1-\upsilon^2) I_0(\gamma_1)}} \tag{2.28}$$

where $\varsigma = 1/3$, $\gamma_1 = \pi R/2H$, E and ν are the elastic modulus and the Poisson ratio of the construction material of the wall. The relation (2.28) is calculated by assuming the fundamental vibration mode $f(\varsigma) = \cos(\frac{\pi\varsigma}{2})$.

Combination of pressures

The total pressure acting on the flexible tank wall consists of the following contributes:

- the impulsive pressure in case of rigid wall p_i, governed by $a(t)$ (Eq. (2.1));
- the convective pressure p_c, governed by $a_{c1}(t)$ (Eq. (2.6);
- the impulsive pressure in case of flexible wall p_f (2.16) governed by $a_f(t)$;
- the total vertical pressure p_v, (Eq. (2.26)).

The resultant horizontal pressure p_h is obtained from combination of p_i, p_f and p_c whereas the total pressure is the sum of horizontal p_h and vertical p_v pressures in the following manners:

- employing the sum of the absolute values of maxima (p_i, p_f, p_c) as discussed in Haroun and Housner [24,26];
- using the peak value of pressure due to the combination of horizontal and vertical pressures:

  $E_h(+)0.30 \cdot E_V$
  $0.30 \cdot E_h(+)0.30 \cdot E_V$
  $0.30 \cdot E_h(+)E_V$

The achievement of the limit state of instability is one of the main cause of collapse during a seismic event [33,34]. The three possible combinations for the pressure components are defined by Rammerstorfer et al. in [33]:

$$\bar{p}_1 = p_{hs} + p_h + p_v$$
$$\bar{p}_2 = p_{hs} + p_h - p_v$$
$$\bar{p}_3 = p_{hs} - p_h - p_v$$

where p_{hs} represents the hydrostatic pressure, p_v the vertical pressure and p_h the combination between p_i, p_c and p_f. The first equation corresponds to the maximum value of circumferential tensile stress and determine the elastic-plastic instability of the shell ("elephant foot buckling"). The second expression is associated to the elastic buckling ("diamond buckling") and the third one to the occurring of suction in the upper part of the tank and consequent instability of the wall.

Convective wave height and pressure on the roof

The most significant contribution to the wave height is given by the first mode. In the light of this, EC8-4 at paragraph A.2.1.4 provides the following approximate expression:

$$d_{\max} = 0.84R\frac{S_e(T_1)}{g} \tag{2.29}$$

In case in which the tank has not a sufficient freeboard, the impact of the convective waves generates a pressure p_{max} on the wet surface of the roof and an increment of the impulsive mass m_i. For the evaluation of p_{max} and m_i, the simplified procedure provided by Malhotra in [11,39] is adopted.

Simplified procedure

The EC8-4 at the paragraph A.3.2.2 introduces a simplified procedure for cylindrical tank fixed at the base to rigid foundation. The method was developed by Malhotra in [20]. The tank-fluid system is described as a two degree of freedom system, as depicted in Figure 1-13 at the paragraph 1.3.2, Chapter 1 of the current work: the first degree of freedom corresponds to the impulsive component m_i, moving with the flexible tank wall, whereas the second one is given by the convective component m_c. The natural period of the impulsive and convective responses are:

$$T_{imp} = C_i\frac{H\sqrt{\rho}}{\sqrt{s/R}\sqrt{E}} \tag{2.30}$$

$$T_{con} = C_c\sqrt{R} \tag{2.31}$$

where H is the design fluid height, R is the tank radius, s is the equivalent uniform thickness of the tank wall, ρ is the density of the fluid and E is the elastic modulus of the material of which the tank wall is made. The coefficients C_i and C_c are obtained from Table 2.5 (paragraph A.3.2.2.1 of the EC8-4): C_i is dimensionless, while C_c is in $(sec\cdot\sqrt{m})$ if R is in (m). The values of impulsive and convective masses are given in Table 2.5, as fractions of the total liquid mass m_l, as well as the heights h_i and h_c of the centroid of the impulsive and convective pressures, measured from the tank bottom.

The total tank base shear is given as:

$$Q=(m_i+m_w+m_r)S_e(T_{imp})+m_cS_e(T_{con}) \quad (2.32)$$

where m_w is the mass of the tank wall and m_r is the mass of the roof; $S_e(T_{imp})$ is the impulsive spectral acceleration obtained from an elastic response spectrum with damping ratio equal to 2% for steel and pre-cast concrete tanks and 5% for ordinary concrete (according to provisions from EN 1998-2:2005 at point A.1.3 (1) and API 650 (2005) at point E.1); $S_e(T_{con})$ is the convective spectral acceleration obtained from an elastic spectrum damped of 0.5% (API 650 (2005) at point E.1). The overturning moment immediately above the tank bottom plate is:

$$M=(m_ih_i+m_wh_w+m_rh_r)S_e(T_{imp})+m_ch_cS_e(T_{con}) \quad (2.33)$$

where h_w and h_r are respectively the heights of the centers of gravity of the tank wall and roof. The overturning moment immediately below the tank bottom plate is given by the expression:

$$M'=(m_ih_i'+m_wh_w+m_rh_r)S_e(T_{imp})+m_ch_c'S_e(T_{con}) \quad (2.34)$$

where h_i' and h_c' are the heights of the centroids of the impulsive and convective pressures adjusted to take into account the effect of pressure acting on the bottom plate. These heights, as well as h_i and h_c are obtained from Table 2.5. The height of the sloshing wave is given by Eq. (2.29). When the tank set on an annular ring foundation (Figure 2-6 (a)), the overturning moment M is used for the design of wall, anchorage system and foundation; if the tank is set on a circular base plate (Figure 2-6 (b)), M is employed for designing the wall and the anchorage system and M' for the foundation.

Table 2.5. Recommended design values for the first impulsive and convective modes of vibration as a function of the tank height-to-radius ratio (H/r) [20]

H/r	C_i	C_c [s/√m]	m_i/m_l	m_c/m_l	h_i/H	h_c/H	h_i'/H	h_c'/H
0.3	9.28	2.09	0.176	0.824	0.400	0.521	2.640	3.414
0.5	7.74	1.74	0.300	0.700	0.400	0.543	1.460	1.517
0.7	6.97	1.60	0.414	0.586	0.401	0.571	1.009	1.011
1.0	6.36	1.52	0.548	0.452	0.419	0.616	0.721	0.785
1.5	6.06	1.48	0.686	0.314	0.439	0.690	0.555	0.734
2.0	6.21	1.48	0.763	0.237	0.448	0.751	0.500	0.764
2.5	6.56	1.48	0.810	0.190	0.452	0.794	0.480	0.796
3.0	7.03	1.48	0.842	0.158	0.453	0.825	0.472	0.825

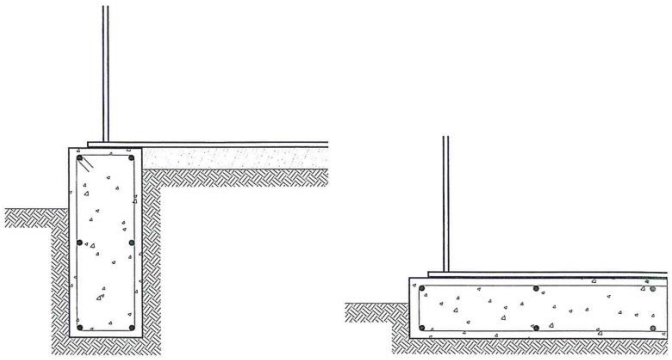

Figure 2-6. Foundation types for cylindrical steel tank: (a) ring foundation, (b) circular base plate

2.3.2. Seismic design of on-grade steel tanks according to NZSEE

In the context of NZSEE guidelines, the fluid pressure on the tank wall caused by the seismic action is the summation of three contributes:

- impulsive pressure $p_i(z,\vartheta)$ determined from Eq. (2.35) or $p_f(z,\vartheta)$ Eq. (2.60);
- convective pressure $p_{c1}(z,\vartheta)$ determined from Eq. (2.40);
- vertical pressure $p_V(z,\vartheta)$ determined from Eq. (2.44) or $p_{vf}(z,\vartheta)$ from Eq. (2.61).

The tanks properties and geometry should be analyzed in order to distinguish cases of rigid or deformable walls. In particular, in case of steel tanks, the flexibility of the tank wall may cause the impulsive liquid to experience accelerations that are several times greater than the peak ground acceleration. Thus, the base shear and overturning moment calculated by assuming the tank to be rigid can be non-conservative.

Rigid tanks perfectly anchored to the foundation

Impulsive pressure

According to the NZSEE, the maximum spatial-temporal value (z,ϑ,t) of the impulsive rigid component is given by the expression (Eq. (C3.3) - (C3.4) Paragraph C3.3.1 NZSEE):

$$p_i(z,\theta) = q_0(z)\frac{S_e(T_0)}{g}\gamma_w R\cos\theta \tag{2.35}$$

or similarly:

$$p_i(z,\theta) = q'_0(z)\frac{S_e(T_0)}{g}\gamma_w H\cos\theta \tag{2.36}$$

that represents the analogous of the relations (2.1) in EC8-4. In Eqs. (2.35) and (2.36), γ_w represents the specific weight of the liquid stored (in kN/m^3), $S_e(T_0)$ is the elastic spectrum in terms of acceleration corresponding to the natural period of the impulsive motion, $q_0(z)$ or $q'_0(z) = q_0(z)R/H$ are dimensionless functions providing the distribution of the impulsive pressure among the tank height. The usage of Eqs. (2.35) or (2.36) provides the same result. The maximum value of $q_0(z)$ and $q'_0(z)$ is found at the tank base (for $z = 0$) and Figure 2-7 (a) shows the dependency of $q_0(0)$ and $q'_0(0)$ on the slenderness ratio (H/R), in which H is the fluid level. Figure 2-7 (b) shows the ratio $q_0(z)/q_0(0)$ among the tank height for certain value of H/R. The analytical expression of $q_0(z)$ is provided by Yang in [13]:

$$q_0(z) = \frac{H}{R}\sum_{n=1}^{\infty}\frac{8(-1)^{n+1}}{[(2n-1)\pi]^2}\frac{I_1\left[(2n-1)\frac{\pi}{2}\frac{R}{H}\right]}{I'_1\left[(2n-1)\frac{\pi}{2}\frac{R}{H}\right]}\cos\left[(2n-1)\frac{\pi}{2}\frac{z}{H}\right] \tag{2.37}$$

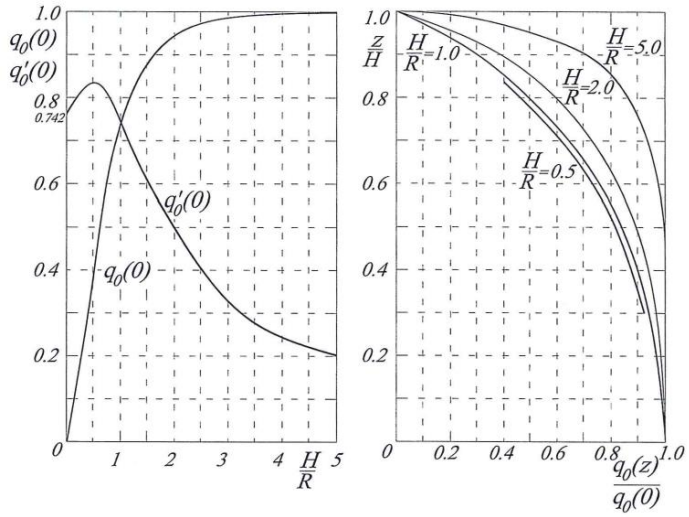

Figure 2-7. (a) Maximum values of the impulsive pressure coefficients at the tank base (z=0) as function of the aspect ratio; (b) vertical distribution of $q_0(z)/q_0(0)$ [31]

Pressure resultants

Eq. (C3.9) - (C3.10) at the paragraph C3.3.1 (NZSEE) provide the impulsive base shear Q_0 and moment M_0 immediately above the tank bottom plate including only the contributes if the pressures on the walls:

$$Q_0 = S_e(T_0)m_0 \tag{2.38a}$$

$$M_0 = Q_0 h_0 \tag{2.38b}$$

where m_0 and h_0 are obtained from graphs in Figure 2-8 and period T_0 from Eq. (2.48) of this paragraph. The moment M_0' immediately below the tank bottom plate includes the contributes of liquid pressure on the tank bottom:

$$M'_0 = Q_0 h'_0 \tag{2.39}$$

where h_0' is plotted in Figure 2-8 (b).

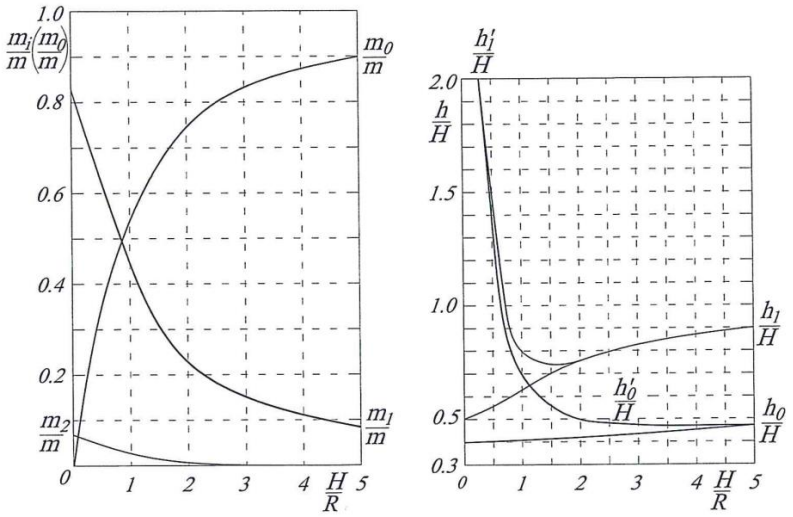

Figure 2-8. NZSEE code: (a) impulsive and convective masses; (b) heights of the centroids of impulsive and convective pressures [31]

Convective pressure

According to the NZSEE, the maximum spatial-temporal value of the convective component of the hydrodynamic pressure considering only the first sloshing motion ($n = 1$) is obtained from the expression C3.6 at paragraph C3.3.1 of NZSEE, reported herein:

$$p_{c1}(z,\theta) = q_1(z)\frac{S_e(T_1)}{g}\gamma_w R\cos\theta \tag{2.40}$$

That is the analogous of the Eq. (2.6) provided by EC8-4; γ_w represents the specific weight of the liquid stored (in kN/m^3), $S_e(T_0)$ is the elastic spectrum in terms of acceleration corresponding to the natural period of the first convective mode, $q_1(z)$ represents the dimensionless function providing the distribution of the convective pressure among the tank height. Figure 2-9 shows the dimensionless function $q_1(z)$ for the first convective mode and $q_2(z)$ for the second mode for different values of aspect ratio. For the j^{th} mode, the dimensionless function is given as [13,23]:

$$q_j(z) = \frac{2}{\lambda_j^2 - 1}\frac{\cosh\left(\lambda_j \frac{z}{R}\right)}{\cosh\left(\lambda_j \frac{H}{R}\right)} \tag{2.41}$$

It should be noted that, unlike the impulsive component (Figure 2-7), the function $q_1(z)$ is strictly dependent on the aspect ratio, excepted its maximum value which occurs at the free liquid surface.

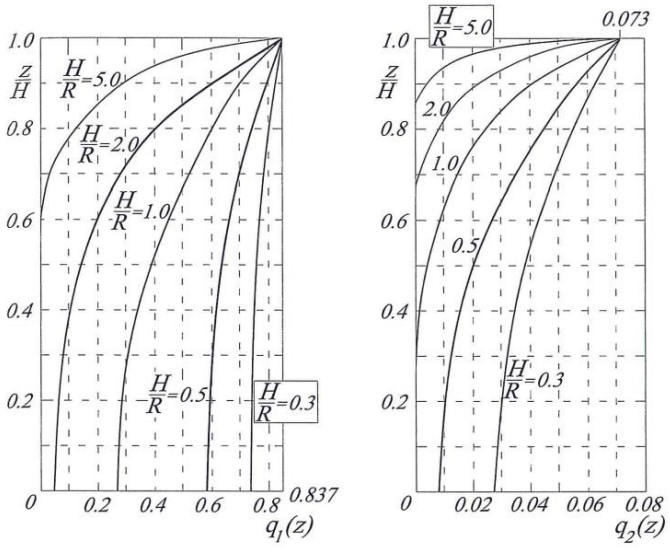

Figure 2-9. Trend of the convective pressure coefficient for the first convective mode (a) and the second one (b) [31]

Pressure resultants

In the NZSEE (Eqs. (C3.12), (C3.13) paragraph C3.3.1) the contribution of the first convective mode to the base shear Q_1 and to the base moment M_1 immediately above the tank bottom plate are:

$$Q_1 = S_e(T_1)m_1 \tag{2.42}$$

$$M_1 = Q_1 h_1 \tag{2.42b}$$

where:

T_1 is the natural period of the first sloshing motion (Eq. 2.14) ;

$S_e(T_1)$ is the elastic spectrum in terms of acceleration, obtained considering a damping ratio equal to 0.5% for water and other liquid (EC8-4 at paragraph 2.3.3.2 and NZSEE at paragraph 3.2) and 10% for granular material (EC8-4 at paragraph 2.3.3.2);

m_1 is obtained from Figure 2-8 (a) as a function of the total liquid mass m and the slenderness ratio;

h_1 is the equivalent height of the mass m_1 above the tank bottom, obtained from the graph in Figure 2-8 (b).

The base moment M_1' immediately below the tank bottom plate is the following:

$$M_1' = Q_1 h_1' \tag{2.43}$$

Vertical pressure

In the NZSEE, the contribution of the vertical seismic motion to the dynamic pressure on the shell is given by the expression (Eq. (C3.7) paragraph C3.3.1):

$$p_V(z) = \left(1 - \frac{z}{H}\right)\frac{S_{ve}(T_V)}{g}\gamma_w H \tag{2.44}$$

where γ_ω represents the specific weight of the liquid stored (kN/m^3), $S_{ve}(T_V)$ is the vertical component of the elastic spectrum corresponding to the vibration period T_V (Eq. (2.50)); the NZSEE at paragraph C2.8 suggests for the vertical component a damping ratio of 7.5% for a

soft soil, and 5% for a compact and rocky soil. Pressure linearly increases as the depth increases. According to the mechanical model depicted in Figure 2-10 maintaining the hypothesis of rigid tank, the total vertical seismic force is the following:

$$V = S_{ve}(T_V)m_V \tag{2.45}$$

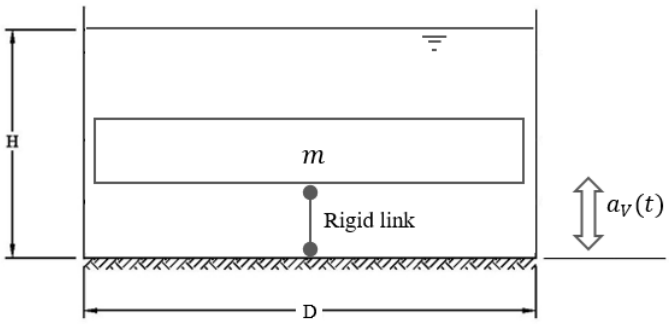

Figure 2-10. Mechanical model of rigid tank under vertical ground acceleration

where $m_V = m + m_b + m_p + m_r$, where m is the total liquid mass, m_b, m_p and m_r are respectively the mass of the foundation, vertical wall and roof. Generally, the effect of the vertical component V on the internal stress of the tank can be neglected.

Convective wave height and pressure on the roof

The maximum vertical displacement of the free surface with respect to the liquid level in absence of motion can be obtained from the expression provided by Veletsos in [23] (Eq. (C3.36) Paragraph C3.9 NZSEE):

$$d_{\max} = R\sqrt{\left(0.837\frac{S_e(T_1)}{g}\right)^2 + \left(0.073\frac{S_e(T_2)}{g}\right)^2 + \left(0.028\frac{S_e(T_3)}{g}\right)^2 + \ldots} \tag{2.46}$$

in which $S_e(T_1)$ is the elastic spectrum in acceleration obtained with a damping ratio of 0.5% for water and other liquids (EC8-4 paragraph 2.3.3.2; NZSEE paragraph 3.2; API 650 (2005) paragraph E.1; ASCE 7 Paragraph 15.7.2). T_1, T_2, T_3 are respectively the period of the first convective mode, the second, the third, obtained from Eq. (2.14). The most significant

Natural period of the tank-fluid system

As already shown in case of EC8-4 (see Eq.2.14 of this chapter), the natural period of the first convective motion of the fluid contained can be obtained from the same expression of ω_{cn}, given in Eq. 2.8 of the current work, for $n = 1$ (Eq. (C3.24) Paragraph C3.6 NZSEE and Eq. (A.9) Paragraph A.2.1.3 EC8-4):

The calculation on the impulsive period T_0 requires the soil-structure interaction to be taken into account. For a rigid tank set on a rigid soil, $T_0 = 0$ and then, $S_e(T_0) = Sa_g$, where S I related to the soil stratigraphy. Actually, the deformability of foundation and soil tends to elongate the impulsive period and then to increase the seismic response and damping. On the other hand, the influence of the soil-structure interaction on the sloshing frequencies is negligible. Therefore, the impulsive period T_0 is calculated through the expression proposed by Jennings and Bielak in [40,41] and simplified by Veletsos in [23] (Eq. (C3.30) Paragraph C3.6 NZSEE and Eq. (A.52) paragraph A.7.2.2 EC8-4):

$$T_0 = 2\pi\sqrt{\frac{m_0 + m_b}{K_x} + \frac{m_0 h_0^2}{K_\theta}} \tag{2.48}$$

where:

- m_0 and m_b are respectively the impulsive mass and the foundation mass, h_0 represents the centroid of the impulsive pressure; m_0 must include the mass of the wall m_p when the inertia effect is included.

- $K_x = \frac{8}{2-\nu_s} G_s R_b \alpha_x$ is the foundation stiffness (N/m) against the horizontal translation;

- $K_\vartheta = \frac{8}{3(2-\nu_s)} G_s R_b{}^3 \alpha_\vartheta$ is the foundation stiffness (N/m) against the rocking motion;

- ν_s is the Poisson ratio of soil;

- G_s is the tangential elastic modulus of soil;

- R_b is the foundation radius;

- α_x and α_ϑ convert the static values of the stiffness K_x and K_ϑ in dynamics values. These dimensionless coefficients are obtained from graphs in Figure 2-11 (a) and (b) as function of the frequency parameter α and for fixed values of the Poisson ratio of soil. The dimensionless parameter α is defined as:

$$\alpha = \frac{2\pi R_b}{T_0 v_s} \tag{2.49}$$

The coefficient α, used for the calculation of T_0, contains the unknown T_0, then the iterative procedure consists of fixing a trial value for α_x and α_ϑ, calculating K_x, K_ϑ and T_0 and verifying in Figure 2-11 (a) and (b) the values of α_x and α_ϑ previously defined.

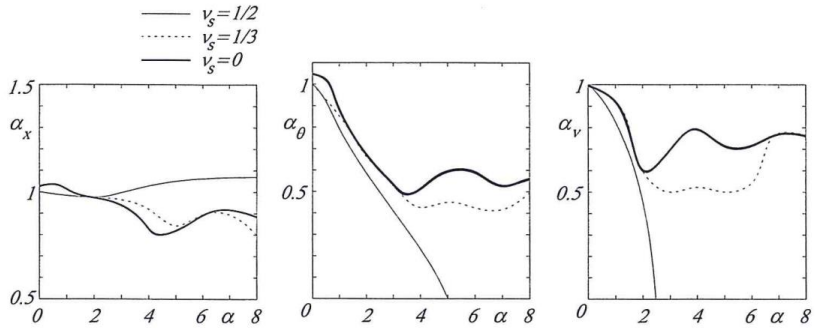

Figure 2-11. Coefficients α_x, α_θ, α_V, for the calculation of the vibration period considering the effects of soil-structure interaction [31]

Figure 2-11 (c) provides values for the coefficient α_V used in calculation of the tank vertical vibration period T_V, whose expression is provided in NZSEE (Eq. (C3.33) Paragraph C3.6) and in EC8-4 (Eq. (A.54) Paragraph A.7.2.2):

$$T_v = 2\pi\sqrt{\frac{m_V}{k_V}} \tag{2.50}$$

where:

$$K_V = \frac{4}{1-\nu_s} G_s R_b \alpha_v \tag{2.51}$$

in case in which the parameter α is involved in the calculation of the vertical vibration period, T_0 is replaced by T_V.

Combination of pressures, ductility and damping factor

The total pressure acting on the tank wall consists of three contributions (paragraph A.2.1.6 of EC8-4):

- the impulsive pressure p_i, governed by $a(t)$ (Eq. (2.35));
- the convective pressure p_{c1}, governed by $a_{c1}(t)$ (Eq. (2.40);
- the vertical pressure p_V, (Eq. (2.44)).

The NZSEE at the paragraph C4.2, the ACI 350.3-06 at the section 4, the API 650 (2005) at the paragraph E.6, the AWWA D110-04 and D115-06 at the paragraph 4.3.1 adopt the SRSS rule, since there is a low probability that maxima values of each contribute occur at the same time. Then, the hydrostatic pressure is added in order to determine the total hydrodynamic pressure acting on the tank wall:

$$p(z,\theta) = \sqrt{p_i^{\,2}(z,\theta) + p_{c1}^{\,2}(z,\theta) + p_v^{\,2}(z,\theta)} + p_h(z) \tag{2.52}$$

The NZSEE at paragraph 3.2 do not provide any dissipation to the convective and vertical modes of the fluid, then the ductility factor in terms of displacement is $\mu = 1$. At contrast, according to the tank typology, the code assume higher values for the impulsive component as described at the paragraph 2.2.1 of the current work [15].

The damping ratio ξ for convective modes is assumed 0.5. With regard to damping associated to the impulsive mode, the NZSEE refers to graphs in Figure 2-12 for horizontal modes and Figure 2-13 for vertical modes. The damping value is given as a function of the tank geometry, through the ratios H/R and t/R, and the foundation soil stiffness, through the shear waves velocity.

The NZSEE defines the seismic design action as:

$$S_d(T) = S_e(T) K_f(\mu, \xi) \tag{2.53}$$

where $S_e(t)$ is the elastic response spectrum and K_f is a factor given as function of ductility and damping factors (Table 2.6 adapted from Table 3.2 in NZSEE).

Table 2.6. Factor K_f as function of ductility factor μ and damping factor ξ

μ	ξ_h[%]	k_f							
		$\xi = 0.5\%$	$\xi = 1\%$	$\xi = 2\%$	$\xi = 5\%$	$\xi = 10\%$	$\xi = 15\%$	$\xi = 20\%$	$\xi = 30\%$
1.0	0.0	1.67	1.53	1.32	1.00	0.76	0.64	0.56	0.47
1.25	3.5	1.08	1.04	0.96	0.82	0.67	0.58	0.52	0.44
2.0	5.9	0.91	0.89	0.84	0.74	0.63	0.55	0.50	0.43

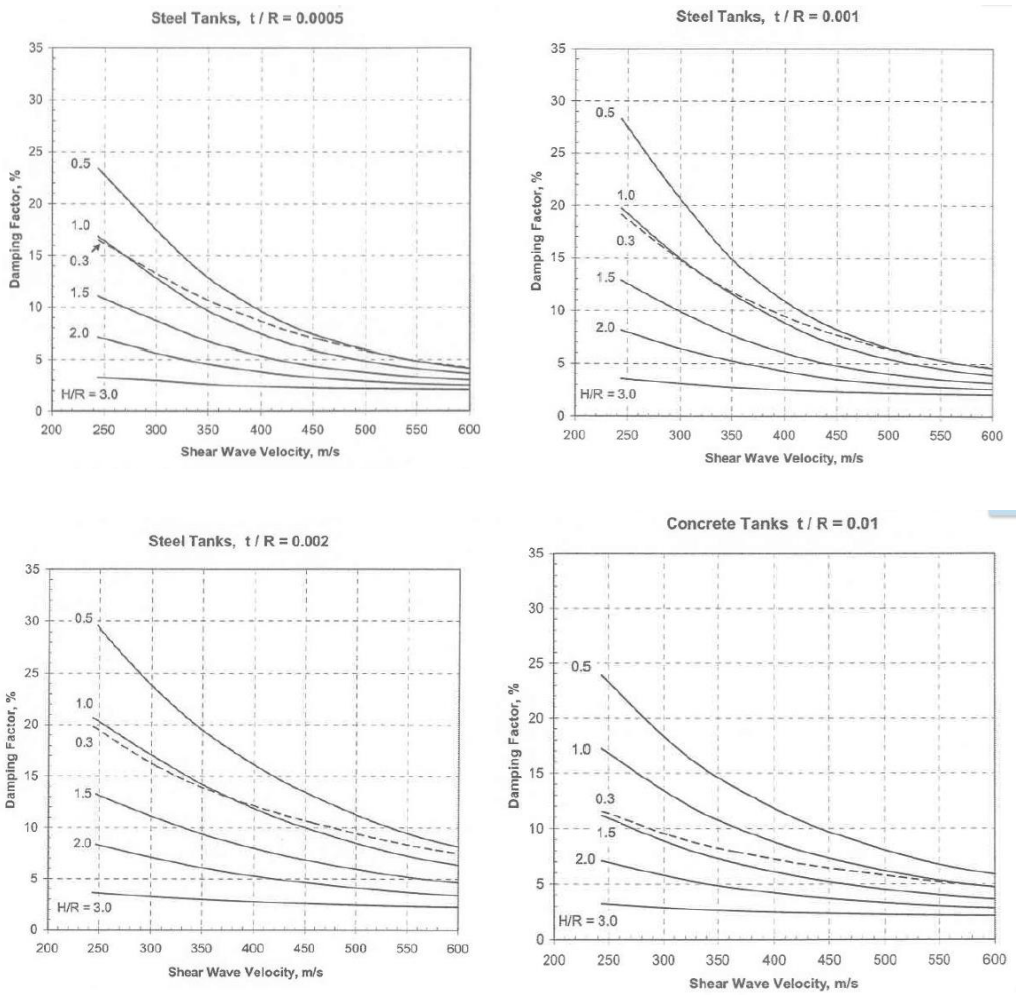

Figure 2-12. Damping factor ξ for horizontal impulsive modes

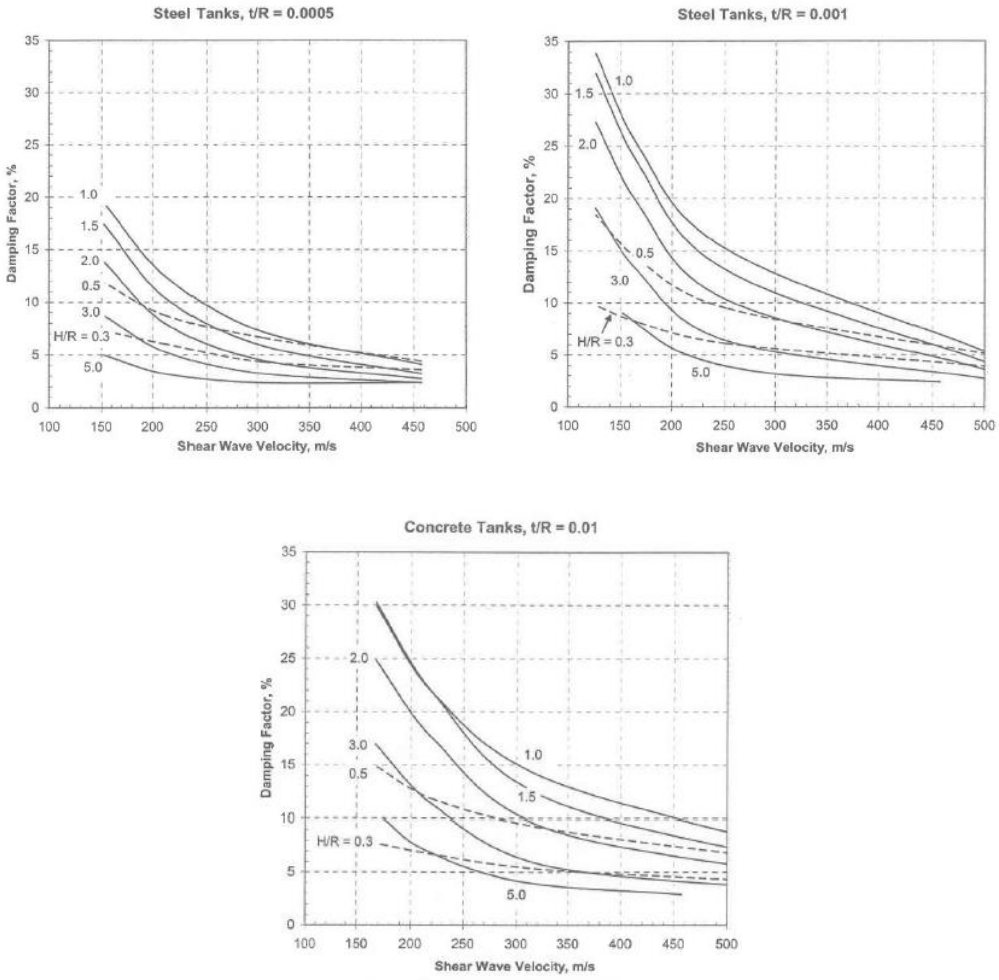

Figure 2-13. Damping factor ξ for vertical impulsive modes

Soil-structure interaction

Tanks set on deformable soils are subject to a more complex type of motion. The translational displacement is modified by a rocking component. As the soil flexibility increases, the period of the tank-fluid system elongates and the maximum force to which the structure is subjected decreases because of an increasing of the total damping. Therefore, for a certain soil flexibility, the elongation of the fundamental period is more pronounced for slender tanks than for squat tanks, since the rocking effects decrease as the tank aspect ratio decrease. However, in case of slender structures, the reduction of the maximum force is generally less significant since damping associated with rocking motion is smaller than damping associated with the horizontal translation.

A simple procedure is proposed by Veletsos in [42] and consists in an increase of the fundamental period and damping of the structure considered set on a rigid soil and subjected to the free field motion. Later, this method has been extended to the impulsive components (rigid and deformable) of the tank response [27,43,44]. The convective periods and pressures are assumed to be unmodified from soil-structure interaction. A reasonable approximation is obtained by using an equivalent single degree of freedom with parameters modified in order to correspond to the frequency and the peak response of the real system. The SDOF system properties are given by Veletsos and Tang in [27,43,44] and by Habenberger and Schwarz in [45].

A further simplified procedure is presented by Priestley et al. in the NZSEE and it consists in changing separately periods and damping of the rigid impulsive contribution. The expressions used for defining periods are given by the Eqs. (2.48) and (2.50) for rigid tanks and Eq. (2.63) for flexible tanks, whereas the damping estimation is obtained from researchers of Bielak and Veletsos [23,46] (Paragraph A.7.2.3 of the EC8-4; Eq. (C3.34) paragraph C3.7 of the NZSEE):

$$\xi_f = \xi_s + \frac{\xi_m}{\left(\frac{T_f^*}{T_f}\right)^3} \tag{2.54}$$

where ξ_s is the radiation damping in the soil and ξ_m is the material damping in the tank. Both these parameters depend on the specific vibration mode. In particular, ξ_s:

- for the horizontal impulsive "rigid tank" mode:

$$\xi_s = \frac{2\pi^2 m_i \alpha}{K_x T_0^2}\left(\frac{\beta_x}{\alpha_x} + \frac{K_x h_i^{'2}}{K_\theta}\frac{\beta_\theta}{\alpha_\theta}\right) \tag{2.55}$$

  where m_i is the impulsive mass, h_i is the height of the centroid of the impulsive pressure and α is dimensionless frequency parameter (Eq. (2.49)); α_x and α_ϑ are obtained from graphs in Figure 2-11 (a) and (b); β_x and β_ϑ convert the static values of damping associated with translation and rocking to dynamic values and are obtained from graphs in Figure 2-15 (a) and (b) as function of the frequency parameter α;

- for the horizontal impulsive "flexible tank" mode:

$$\xi_s = \frac{2\pi^2 m_f \alpha}{K_x T_f^{*2}}\left(\frac{\beta_x}{\alpha_x} + \frac{K_x h_f^{\ 2}}{K_\theta}\frac{\beta_\theta}{\alpha_\theta}\right) \tag{2.56}$$

where m_f is the impulsive horizontal mass in case of flexible tank and h_f is the height of the centroid of this mass; α is dimensionless frequency parameter in which T_0 is replaced by T_f^*, obtained from Eq. (2.64).

- for the vertical impulsive "rigid tank" mode:

$$\xi_s = \frac{2\pi^2 m_V \alpha}{K_V T_V^2} \frac{\beta_V}{\alpha_V} \tag{2.57}$$

where α is dimensionless frequency parameter (Eq. (2.49)) in which T_0 is replaced by T_V. The period T_V and the coefficient K_V are obtained from Eq. (2.50) and (2.51); α_V and β_V are given by Figure 2-11 (c) and Figure 2-15 (c).

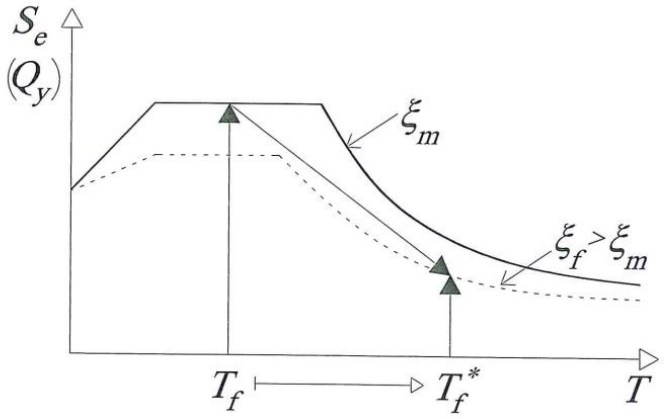

Figure 2-14. Reduction of the spectrum S_e (or reduction of the base shear) considering the soil-structure interaction [31]

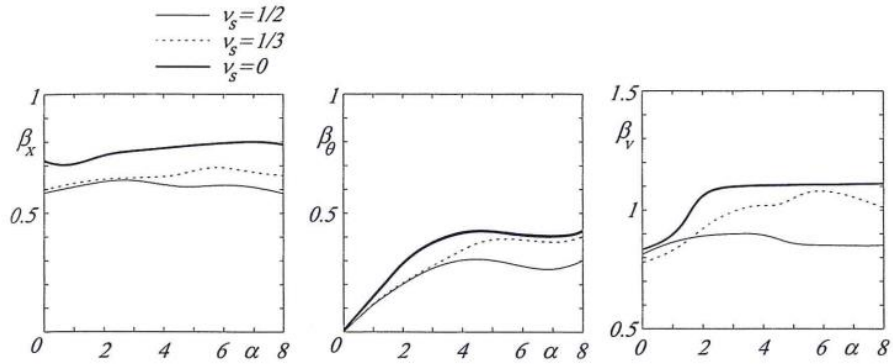

Figure 2-15. Coefficients β_x, β_θ, β_V, for the calculation of the damping ratio considering the effects of soil-structure interaction [31]

Unanchored tanks

Unanchored tanks can be subjected to uplift of the bottom plate when the overturning moment M_y induced by the earthquake overcomes the restoring moment M_R [47]. The tank bottom uplift can cause plastic deformation at the base plate and liquid leakage. Usually, the effects of uplift and rocking on the pressure distribution are neglected (Paragraph A.9.1, EC8-4). This approach is considered conservative since rocking motion adds flexibility to the tank-fluid system and then the natural period is shifted in a region of lower stress dynamic amplification [48]. The first simplified approach that considers the effects of the uplifting phenomenon for a rigid tank was proposed by Clough in [49]. This method was subsequently modified based on experimental data obtained by Clough and Niwa in [50], at the paragraph C4.4.2 of the NZSEE, in which an expression of the overturning moment M_R is proposed in Figure 2-16:

$$M_R = W_s(kR) + W_f(R - r) \tag{2.58}$$

where $W_s = W + W_p + W_r - W_f$ in which W is the total weight in (kN) of the liquid content, W_p and W_r are respectively the weight of wall and roof and W_f is the reaction exerted by the liquid acting on the portion of base plate of radius r directly in contact with the foundation. The compressive axial force $\bar{N}_y$ of the wall in vertical direction is determined by means an iterative procedure given at the paragraph C4.4.2 of the NZSEE, under the hypothesis that the reaction on the shell wall W_s is distributed among an arc of circle of angular extension $2\vartheta^*$, in contact with the foundation (Figure 2-16). ϑ^* is function of the dimensionless parameter $\mu = r/R$. The procedure starts by fixing a trial value of μ, and then a value of ϑ^*. The overturning moment is determined, in which k is a simple function on ϑ^*. These steps are repeated until $M_R = M_y$. When this condition is satisfied, one can calculate $\bar{N}_y$ and the membranal axial stress $\bar{\sigma}_y$.

In case of unanchored flexible tank, the elastic spectrum S_e, used in the calculation of the tank base shear and moment, is obtained by assuming a damping of (paragraph C2.8 NZSEE, Edition 1986):

- 15% on a soft soil and 10% on a compact and rocky soil, for horizontal motion;
- 7.5% on a soft soil and 5% on a compact and rocky soil, for vertical motion.

After Clough [49], a more sophisticated model was proposed by Wozniak and Mitchell in [51] and adopted in Appendix E of the API 650 (2005). The new model introduces a rigid-plastic behavior to take into account the bottom plate flexibility through the formation of plastic hinges.

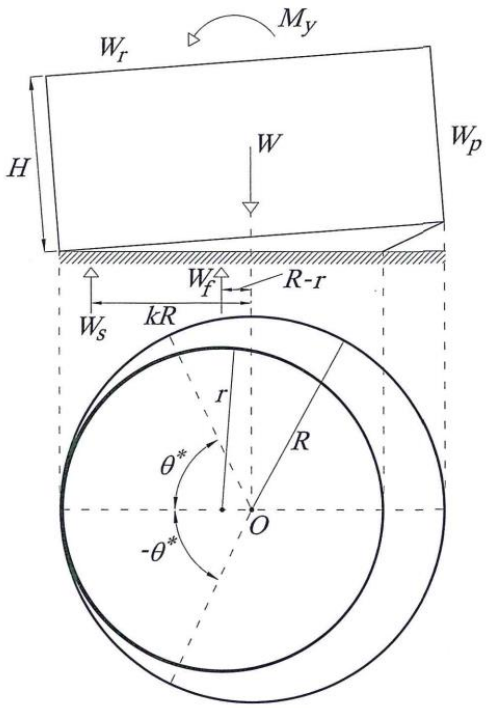

Figure 2-16. System of forces acting on a cylindrical tank in uplifting condition [31]

A further model of the bottom plate uplift for cylindrical tanks was studied by Fischer et al. in [33]. This study takes into account the dynamic nature of the phenomenon and the interaction with the roof. Authors provides design tables, as those in Figure 2-17 and Figure 2-18, for specific values of parameters as: the ratio between the wall thickness and the tank radius s/R, the slenderness ratio H/R and the type of foundation soil. The influence of the wall-roof connection described by Scharf in [52] has been confirmed by the experimental campaign conducted by Sakai et al. in [53]. Non-linear simplified method suitable for numerical implementations were proposed by Malhotra and Veletsos in [20,54,55] and by Peek and Jenning in [56,57]. More accurate non-linear models for flexible tank in uplift condition require finite elements simulations that include the structural properties of tank as well as properties of soil, foundation and soil-fluid-structure interaction [58,59].

Once the hydrodynamic pressure resulting from the tank uplifting are determined using one of the model described above, the next step is to calculate the tank stresses. The main effect of the bottom uplifting is to increase the compressive membrane force $\overline{N}_y$ in the tank wall, that represents a critical issue for collapse modes due to instability. Moreover, the flexural yielding in the bottom plate is allowed, then the radial membrane stress level in the plate must be checked.

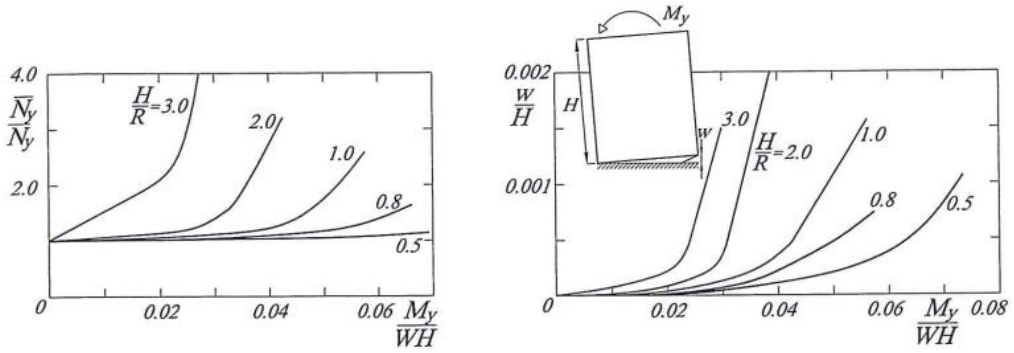

Figure 2-17. (a) Ratio of the compressive axial force in unanchored tanks to compressive axial force in tanks fixed to the base; (b) uplift displacement as function of the dimensionless overturning moment [31]

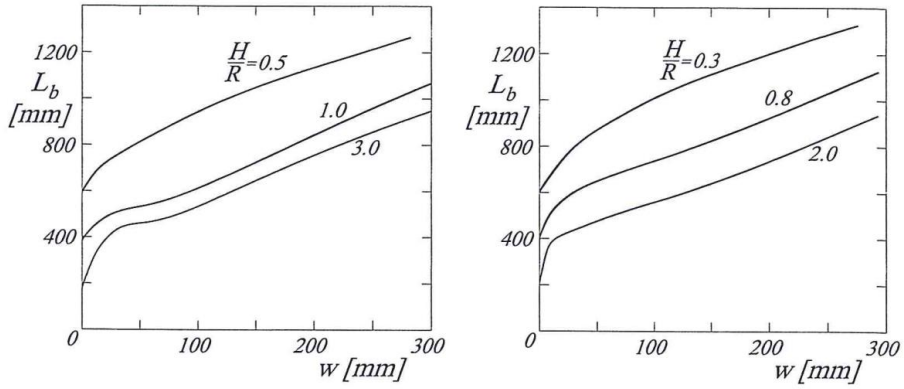

Figure 2-18. Uplift width of the tank bottom plate as a function of the uplift vertical displacement [31]

Compressive axial force in the tank wall

The ratio between the axial force $\overline{N}_y$ caused by the tank uplift and the compressive membrane force N_y in case of tank fixed at the base is shown in Figure 2-17 (a) as a function of slenderness $\gamma = H/R$ and dimensionless overturning moment M_y/WH where W is the total liquid weight (in kN). Figure 2-17 is referred to fixed roof tanks.

Bottom plate uplift

The uplift displacement value w as a function of the dimensionless ratio M_y/WH and of the aspect ratio H/R is given in Figure 2-17 (b) for fixed roof tank. The expression for w proposed by Cambra in [60] and properly modified in the NZSEE in order to take into account the base plate yielding (Eq. C4.25 Paragraph C4.4.2 NZSEE) is:

$$w = \frac{1}{A}\left[\frac{f_y s_b^2}{6N_x} + \frac{p_0 L_b}{N_x}\left(\frac{L_b}{2} - \sqrt{\frac{\bar{E}s_b^3}{12N_x}}\right)\right] \tag{2.59}$$

where $\bar{E} = E/(1-\nu^2)$, E and ν are the elastic modulus and the Poisson ratio of the material of which the base plate of thickness s_b is made; $p_0 = \gamma_\omega H$ is the hydrodynamic pressure at the tank base; $L_b = 2R(1-\mu)$ where $\mu = r/R$; the membrane resultant on the base plate is $N_x = \sigma_x s_b$, where σ_x is obtained from Eq. C4.24 Paragraph C4.4.2 of the NZSEE and Paragraph A.9.4 of the EC8-4; f_y is the steel yielding nominal value of the base plate (Tab. 3.1 at the point 3 of the UNI ENV 1993-1.1:2005); A is the foundation stiffness factor equal to 0.5 for flexible foundation and 1.0 for rigid foundation.

Flexible tanks

The evaluation of the tank stresses in the context of the seismic design can be un-conservative if shell wall is assumed to be rigid, especially in case of steel tanks. The fluid pressure in a flexible wall tank consists of four contributes:

- impulsive pressure for flexible tank $p_f(z,\vartheta)$ determined from Eq. (2.60);
- convective pressure $p_{c1}(z,\vartheta)$ determined for the first n sloshing modes from the expression (2.40);
- vertical pressure for flexible tank $p_{vf}(z)$ determined from Eq. (2.61).

Impulsive pressure

According to the NZSEE at Point C3.3.2, the maximum spatial-temporal value (ς,ϑ,t) of the impulsive component associated with the tank wall flexibility is obtained from Eq. (2.35) describing the rigid impulsive component:

$$p_f(z,\theta) = q_0(z)\frac{S_e(T_f)}{g}\gamma_w R\cos\theta \tag{2.60}$$

where T_f (Eqs. (2.61) and (2.63)) is the fundamental period of the first impulsive mode for flexible tank, neglecting the soil-structure interaction.

Vertical pressure

In the NZSEE, the contribution of the vertical seismic motion to the dynamic pressure on the shell associated to the wall flexibility is given by the expression (Eq. (C3.7) paragraph C3.3.2):

$$p_{Vf}(z) = \left(1 - \frac{z}{H}\right) \frac{S_{ve}(T'_{Vf})}{g} \gamma_w H \tag{2.61}$$

where T'_{Vf} is the fundamental period of the first impulsive mode associated to the flexible tank wall and neglecting the soil-structure interaction, given at paragraph C3.6 of NZSEE:

$$T'_{vf} = \frac{5.61\pi H}{K_v} \sqrt{\frac{\gamma_w}{Eg}} \tag{2.62}$$

Natural period of the tank-fluid system

As already presented in the paragraph "impulsive pressure", in case of flexible tanks, the natural period of the first horizontal impulsive mode neglecting the soil-structure interaction is described as follows:

- for cylindrical tank with H in meter (Eq. (c.3.26) paragraph C3.6 NZSEE):

$$T_f = \frac{5.61\pi H}{K_h} \sqrt{\frac{\gamma_w}{Eg}} \tag{2.63}$$

where K_h is function of the slenderness ratio H/R and ratio between thickness and radius, s/R. The Eq. (2.63) is determined by Haroun and Housner and it is valid in case of steel tanks with constant thickness and full of water; however, it may be extended also to other material and liquid contained in cases in which the shell mass is small compared with the mass of the stored material;

- for cylindrical and rectangular tank with height H (Eq. (C3.29) paragraph C3.6 of the NZSEE and paragraph A.7.2.2 of the EC8-4):

$$T_f^* = T_f \sqrt{1 + \frac{k_f}{k_x}\left[1 + \frac{k_x h_f^2}{k_\theta}\right]} \tag{2.64}$$

where $K_f = 4\pi^2 m_f / T_f^2$ in (N/m), K_x and K_ϑ are obtained from expression defined at the paragraph 2.3.1, considering that in the expression of α (Eq. (2.49)), the period T_0 is replaced by T_f^*; m_f is the horizontal impulsive mass in case of deformable tank, set at the height h_f measured from the tank base. The value of T_f is obtained from Eq. (2.63).

2.3.3. Seismic design of on-grade steel tanks according to AWWA D100-05

The standard AWWA D100-05 do not provide the evaluation of pressures distribution since the values of circumferential stresses are obtained from a direct formula (paragraph 12 of AWWA) that takes into account the three following contributes:

- impulsive contribute;
- convective contribute;
- vertical contribute.

For the sake of comparison with other codes (EC8-4 and NZSEE), this work obtains the pressure distribution associated to each stress component by dividing them by the tank radius. It should be noted that this relation is valid only under the hypothesis of membrane behavior of the shell wall, and far from the bonded edges and concentrated loads.

Impulsive pressure

As aforementioned, AWWA D100-05 do not provide the evaluation of the impulsive pressure distribution. However, it can be obtained from the ratio between the formulation of circumferential stress given in the codes and the tank ratio:

- If $D/H \geq 1.333$ (Eq. (13-43) Paragraph 13.5.4.2.3 AWWA D100-05):

$$p_i = \frac{8.480 \cdot A_i \cdot G_l \cdot D \cdot H \cdot \left[\frac{Y}{H} - 0.5 \cdot \left(\frac{Y}{H} \right)^2 \right] \cdot \tanh\left(0.866 \cdot \left(\frac{D}{H} \right) \right)}{R} \tag{2.65}$$

- If $D/H < 1.333$ and $Y/D < 0.75$ (Eq. (13-44) Paragraph 13.5.4.2.3 AWWA D100-05):

$$p_i = \frac{5.220 \cdot A_i \cdot G_l \cdot D^2 \cdot \left[\frac{Y}{0.75 \cdot D} - 0.5 \cdot \left(\frac{Y}{0.75 \cdot D} \right)^2 \right]}{R} \tag{2.66}$$

- If $D/H < 1.333$ and $Y/D \geq 0.75$ (Eq. (13-44) Paragraph 13.5.4.2.3 AWWA D100-05):

$$p_i = \frac{2.620 \cdot A_i \cdot G_l \cdot D^2}{R} \tag{2.67}$$

where Y is the distance (mm) measured from the free liquid surface, D and H are respectively the tank diameter and height (m), G_l is the ratio between the specific weight of the liquid contained and that of water, A_i is the design impulsive acceleration (g) defined as follow (Eq. (13-17) paragraph 13.2.9.2 AWWA D100-05):

$$A_i = \frac{S_{ei} \cdot I_E}{1.4 R_i} \geq \frac{0.36 S_{ei} \cdot I_E}{R_i} \tag{2.68}$$

where S_{ei} represents the elastic response spectrum corresponding to a time period $T = 0.2$ s and a damping ratio of 5%, whereas S_{e1} is the elastic response spectrum corresponding to $T = 0.1$s; I_E is the seismic importance factor, whose value is 1.5 for tank of strategic importance for the emergency management, and 1.25 for tanks of considerable importance and 1 for all other tanks (Paragraph 13.2.2 AWWA D100-05). R_i represents the seismic force reduction coefficient associated to the impulsive component and it is defined in a following paragraph of this chapter as a function of the tank typology.

Convective pressure

The convective pressure distribution for AWWA D100-05 can be evaluated with the same approach used for the impulsive component at the previous paragraph (Eq. (13-46) paragraph 13.5.4.2.3 AWWA D100-05):

$$p_i = \frac{1.850 \cdot A_c \cdot G_l \cdot D^2 \cdot \cosh\left[\frac{3.68 \cdot (H - Y)}{D} \right]}{R \cdot \cosh\left[\frac{3.68 \cdot H}{D} \right]} \tag{2.69}$$

where Y is the distance (mm) measured from the free liquid surface, D and H are respectively the tank diameter and height (m), G_l is the ratio between the specific weight of the liquid contained and that of water, A_i is the design impulsive acceleration (g) defined as follow (Eq. (13-18) paragraph 13.2.9.2 AWWA D100-05):

$$A_c = \frac{S_{ec} \cdot I_E}{1.4 R_c} \tag{2.70}$$

where S_{ec} represents the elastic response spectrum corresponding to a time period of the first convective mode T_c, defined as follows (Eq. (23-22) paragraph 13.5.1 AWWA D100-05):

$$T_c = 2\pi \sqrt{\frac{D}{3.68 g \cdot \tanh\left[\frac{3.68 \cdot H}{D}\right]}} \tag{2.71}$$

For a damping ratio of 0.5%. I_E is the seismic importance factor defined in the previous paragraph. R_i represents the seismic force reduction coefficient associated to the convective component and it is defined in a following paragraph of this chapter as a function of the tank typology.

Vertical pressure

The pressure distribution due to the vertical component of the ground motion for the standard AWWA D100-05 can be derived by using the procedure described for the impulsive and convective component:

$$p_v = \frac{N_h \cdot A_v}{R} \tag{2.72}$$

where A_V (g) is the vertical design acceleration, defined at paragraph 13.5.4.3 of AWWA D100-05 as follows:

$$A_v = 0.14 S_{ei} \tag{2.73}$$

where S_{ei} represents the elastic response spectrum corresponding to a time period $T = 0.2$ s and a damping ratio of 5%. N_h is the circumferential tensile internal force due to the hydrostatic pressure and defined as

$$N_h = g\,G\,D\,y \tag{2.74}$$

Reduction factor for the seismic force and damping factor

The AWWA standards employ different seismic force reduction factor for impulsive and convective modes to take into account the damping effect, the overstrength and the ductility of the system. Values adopted for the force reduction factor are defined at paragraph 13.2.6 of AWWA and reported herein in Table 2.7 as function of the tank typology and analyzed component.

Table 2.7. Reduction factor for seismic forces, R

Tipologia	$\mathbf{R_i}$	$\mathbf{R_c}$
Serbatoi ancorati meccanicamente	3.0	1.5
Serbatoi non ancorati	2.5	1.5

The AWWA standards, at paragraph 13.2.7.3.2 consider different damping factor for impulsive and convective modes: for the convective component of response, the seismic action is modified through a damping factor of 0.5%; for the impulsive mode, AWWA standards suggest a damping factor of 5%.

Combination of pressures

AWWA D100-05 at paragraph 13.5.4.2.3 provides a direct formula for the evaluation of the circumferential tensile stresses due to the hydrodynamic pressures generated by the seismic action (Eq. 13-42) paragraph 13.5.4.2.3 AWWA D100-05):

$$\sigma_s = \sqrt{\frac{N_i^{\,2} + N_c^{\,2} + (N_h A_v)^2}{1000\,t_s}} \tag{2.75}$$

where t_s (mm) is the wall thickness, N_i (N/mm) in the internal tensile force induced by the impulsive pressure, N_c (N/mm) in the internal tensile force induced by the convective pressure, N_h (N/mm) in the internal tensile force induced by the hydrostatic pressure.

In order to obtain the total pressure distribution, a formulation very similar to Eq. (2.75) has been used; in particular, the three contributes are combined according to the SRSS rules, then the contribution of hydrostatic pressure is added to the results:

$$p_{tot} = \sqrt{p_i^{\,2} + p_c^{\,2} + p_v^{\,2}} + p_h \tag{2.76}$$

Convective wave height

The evaluation of the maximum height of the convective wave is given in AWWA D100-05 at paragraph 13.5.4.4 (Eq. 13-52):

$$d_{\max} = 0.5 \cdot D \cdot A_f \tag{2.77}$$

where A_f (g) is the design convective acceleration employed for the evaluation of the sloshing effects, and it is defined as (Eq. 13-53 and Eq. 13-54, paragraph 13.5.4.4, AWWA):

- for $T_c \leq 4s$

$$A_f = \frac{S_{ec1} \cdot I_E}{T_c}$$

- for $T_c > 4s$

$$A_f = \frac{4S_{ec1} \cdot I_E}{T_c^{\,2}}$$

where S_{ec1} is the elastic response spectrum corresponding to $T = 1.0$ and a damping factor of 0.5%, I_E is the seismic importance factor defined in a previous paragraph, and T_c is the time period of the first convective mode evaluated in Eq. (2.71).

2.3.4. Comparison between design procedures in terms of pressures

In the current section, the distributions of hydrodynamic pressures proposed by the different codes (EC8-4, NZSEE and AWWA D100-05) are compared for the purpose of evaluating and quantifying the main differences among them. The proposed comparison focuses on the impulsive, convective and total pressures and on the different values of behavior factor used by the different codes. In order to solve complex functions (e.g. Bessel functions) and iterative

procedures, the comparison procedure has been carried out through the use of Matlab. Steel tanks analyzes have different aspect ratios. However, the radius R and the ratio t/R are constant. The tank wall is considered to be flexible. In the following, data of the tanks, seismic action and soil type involved in the analysis are summarized as follows:

- Tank radius: 5m;
- Wall thickness: 0.01 m;
- Density of the fluid content 1020 kg/m^3;
- Density of the tank shell material: 7950 kg/m^3;
- Young modulus of the tank shell material: 210000000 kN/m^2;
- Poisson modulus: 0.30;
- Shear modulus of the tank shell material: 81000000 kN/m^2;
- Peak ground horizontal acceleration a_g: 0.38g;
- Soil category according to EC8: A;

Impulsive pressures

In Figure 2-19 and Figure 2-20 is shown the behavior between the distribution of the impulsive component of the hydrodynamic pressures for the different codes considered (EC8-4, NZSEE and AWWA D100-05), evaluated in case of squat tank ($H/R = 0.4$) and slender tank ($H/R = 3.5$). In both cases the ratio between shell thickness and tank radius is $t/R = 0.002$ and $R = 5m$. The pressures normalized with respect to the quantity ($\rho_l \cdot R \cdot a_g \cdot g$) are plotted in Figure 2-19 and Figure 2-20.

For all the codes considered, in case of slender tank the impulsive pressure achieves higher values than those obtained in case of squat tanks. Indeed, as discussed in Chapter 1, the increasing of the slenderness ratio lead to an increment of the liquid percentage moving in unison with the tank wall. The NZSEE code provides a single formulation for slender and squat tanks. The only difference consists on the spectral acceleration associated to two different periods. Therefore, only the intensity of pressure changes among the two tank models. On the contrary, in EC8-4 and AWWA codes, in addition to an intensity variation between squat and slender tanks, it is possible to observe a different shape of the pressure distribution as well. Indeed, the impulsive pressure distribution slender tanks shows the peak value in the upper part of the wall. Then, in case of AWWA the peak value remains constant, while in case of EC8-4 it decreases near the base. This behavior is due to the flexible contribute to the impulsive pressure, that is not considered in the NZSEE. Figure 2-22 shows that the relevance of this contribute increases as the slenderness ratio increases, while in case of squat tanks (H/R=1), the

impulsive rigid contribute is dominant. For this reason, the impulsive pressure distributions according to EC8-4 and NZSEE for squat tanks are very similar (Figure 2-19 and Figure 2-20).

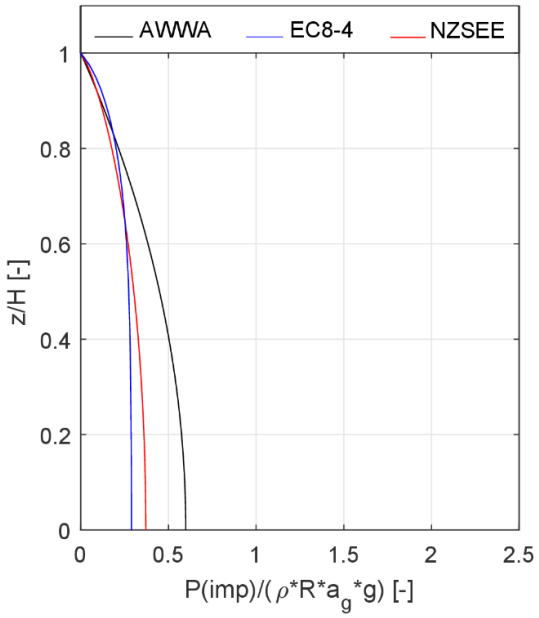

Figure 2-19. Normalized impulsive pressure in case of H/R=0.4

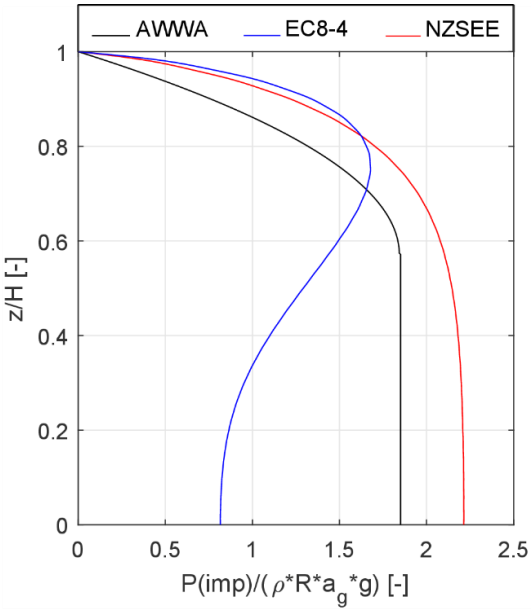

Figure 2-20. Normalized impulsive pressure in case of H/R=3.5

The maxima values of the normalized impulsive pressure for H/R=0.4 and H/R=3.5 are summarized in Table 2.8. Moreover, the percentage variation of maxima values obtained with AWWA and NZSEE are calculated with respect to the maxima values obtained for EC8-4.

Table 2.8. Maxima values of the normalized impulsive pressure and percentage variation with respect to EC8.

Maxima values of normalized impulsive pressure.	***EC8-4***	***NZSEE (%)***	***AWWA (%)***
H/R=0.4	0.30	0.37 (23%)	0.60 (100%)
H/R=3.5	1.69	2.21 (31%)	1.85 (9%)

Figure 2-21, 2-22, 2-23 represent the normalized distribution of the impulsive pressure as function of the slenderness ratio for the three codes examined and ratio t/R=0.002. The comparison confirms what discussed above: for the European standard, changes in slenderness ratio lead to substantial variation of intensity and shape of impulsive pressure; according to the

American code, for values of H/R higher than 1 (approximately 1.5), the value of pressure at the base remains constant, and it represents the maximum value. Moreover, for H/R higher than 1.5, this maximum value of pressure involves a bigger extent of the wall. In case of the NZSEE code, variation is observed only for the pressure intensity, not for the shape.

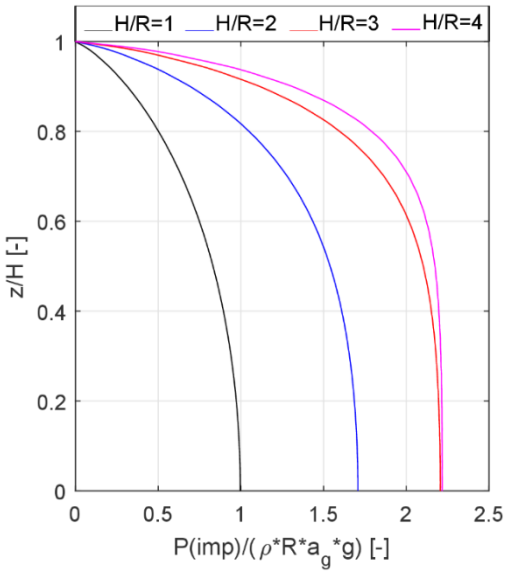

Figure 2-21. Normalized impulsive pressure for NZSEE as function of the slenderness ratio

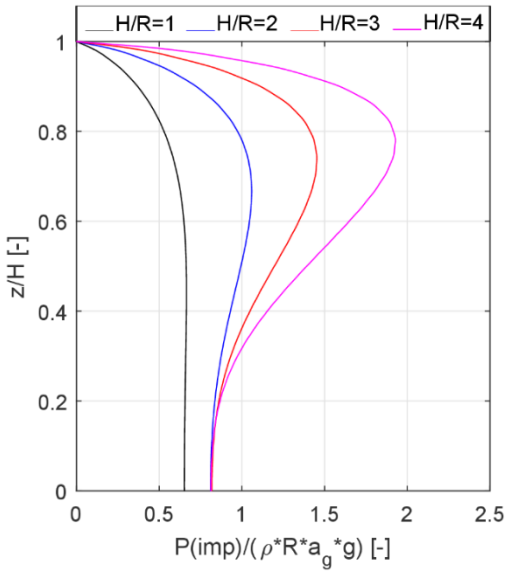

Figure 2-22. Normalized impulsive pressure for EC8-4 as function of the slenderness ratio

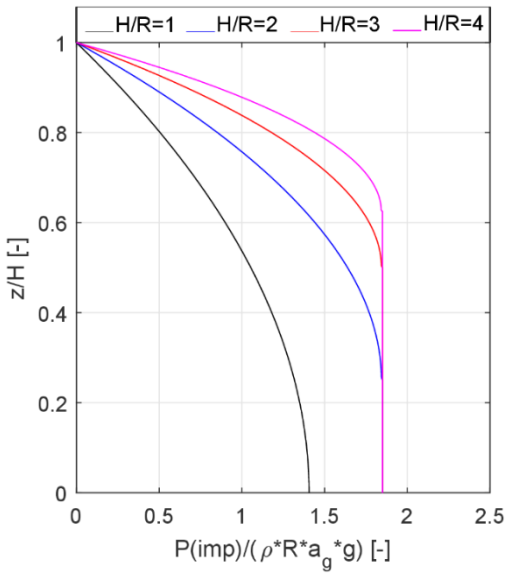

Figure 2-23. Normalized impulsive pressure for AWWA as function of the slenderness ratio

Convective pressures

Figure 2-24 and Figure 2-25 show the behavior between the distribution of the convective component of the hydrodynamic pressures for the different codes considered (EC8-4, NZSEE and AWWA D100-05), evaluated in case of squat tank ($H/R = 0.4$) and slender tank ($H/R = 3.5$). In both cases the ratio between shell thickness and tank radius is $t/R = 0.002$ and $R = 5m$. The pressures normalized with respect to the quantity ($\rho_l \cdot R \cdot a_g \cdot g$) are plotted in Figure 2-24 and Figure 2-25.

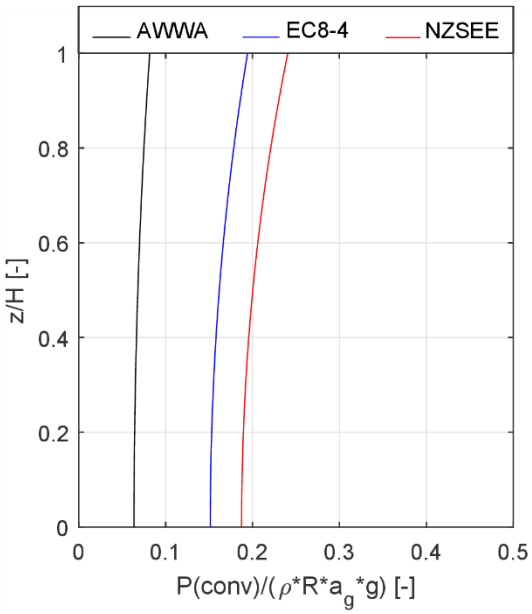

Figure 2-24. Normalized convective pressure in case of H/R=0.4

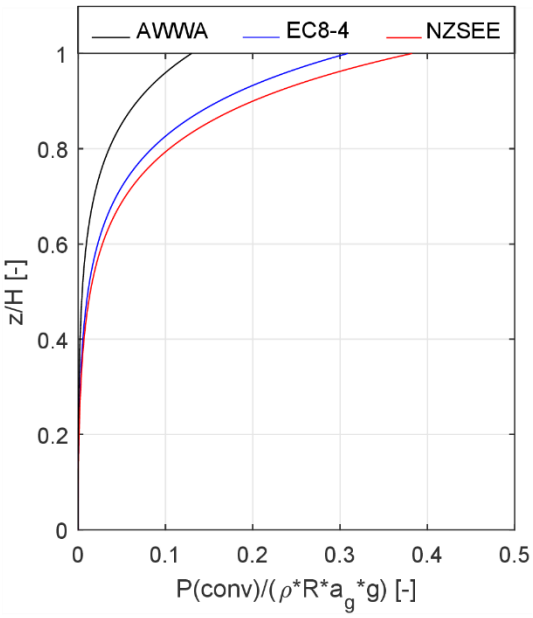

Figure 2-25. Normalized convective pressure in case of H/R=3.5

A first consideration should be made on the differences between pressures obtained in case of squat tank ($H/R = 0.4$) and pressure in case of slender tank ($H/R = 3.5$): as already explained in Chapter 1, the lower is aspect ratio H/R the bigger is the percentage of liquid mass involving in the convective motion. Then, in case of squat tanks, this generate high convective pressures on the tank wall, both at the top and at the base level. The maxima values of the normalized convective pressure for H/R=0.4 and H/R=3.5 are summarized in Table 2.9. Moreover, the percentage variation of maxima values obtained with AWWA and NZSEE are calculated with respect to the maxima values obtained for EC8-4.

Table 2.9. Maxima values of the normalized convective pressure and percentage variation with respect to EC8.

Maxima values of normalized convective pressure.	***EC8-4***	***NZSEE (%)***	***AWWA (%)***
H/R=0.4	0.19	0.24 (26%)	0.08 (-0.57%)
H/R=3.5	0.31	0.38 (23%)	0.13 (-58%)

In Figure 2-26, 2-27, 2-28 the distribution of the normalized convective pressures are plotted as function of the slenderness ratio for the three codes and t/R=0.002.

Figure 2-26, 2-27, 2-28 suggest some considerations: with respect to slender tanks, squat tanks are characterized by a bigger convective contribute to the hydrodynamic pressure. This is valid for all codes. Moreover, values of the convective pressures calculated according to the AWWA standard are lower than those obtained from the EC8-4 and NZSEE. This issue is probably due to the effect of the behavior factor. The next paragraph shows a comparison between total pressures calculated by including the behavior factor and total pressure calculated excluding it.

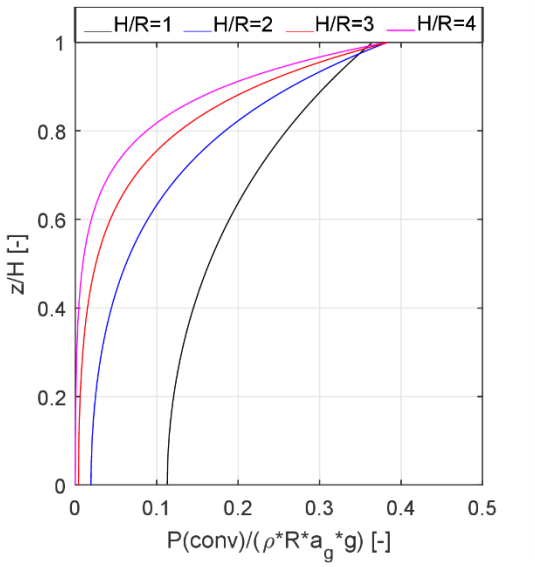

Figure 2-26. Normalized convective pressure for NZSEE as function of the slenderness ratio

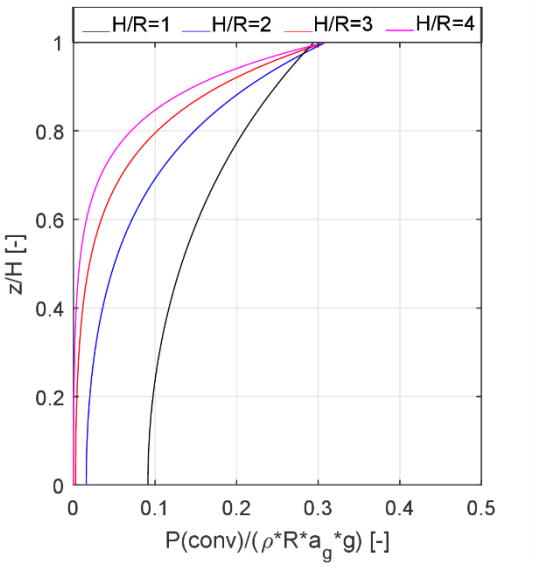

Figure 2-27. Normalized convective pressure for EC8-4 as function of the slenderness ratio

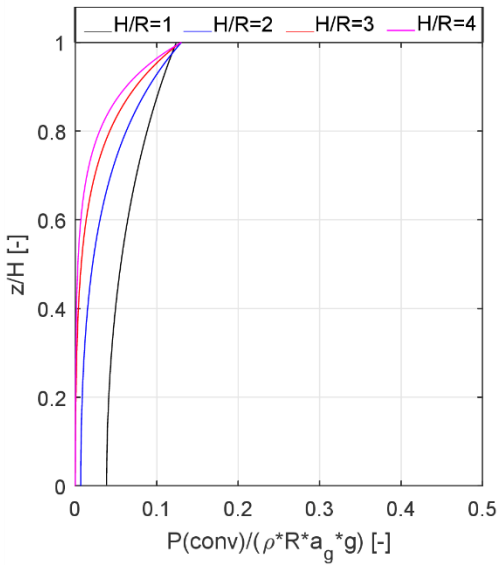

Figure 2-28. Normalized convective pressure for AWWA as function of the slenderness ratio

Total pressures

Figure 2-29, 2-30, 2-31, 2-32 shows the comparison between total pressures evaluated according to the combination rules provided in this Chapter for the different codes analyzed. Total pressures have been evaluated in case of squat tank ($H/R = 0.4$) and slender tank ($H/R = 3.5$). In both cases the ratio between shell thickness and tank radius is $t/R = 0.002$ and $R = 5m$. In figures, the total pressures are normalized with respect to the quantity ($\rho_l \cdot R \cdot a_g \cdot g$). In Figure 2-29 and Figure 2-31 pressures calculation includes the behavior factor, whereas in Figure 2-30 and Figure 2-32, pressures calculation excludes it. It should be noted as, in case of a squat tank (H/R=0.4), values of pressure calculated through AWWA standard are bigger compared to values of pressure obtained with the other codes if the behavior factor is not included in analyses. A comparison between Figure 2-29 and Figure 2-31 shows that pressures obtained from the American standard are lower because of the high values of the force reduction factor proposed by the code. In Figure 2-32 this behavior is not so evident since the tank shell height is bigger and the hydrostatic contribute tends to absorb the differences related to the other contributes. It should be noted that for a squat tank (H/R=0.4), NZSEE and EC8 curves are practically overlapped (Figure 2-32).

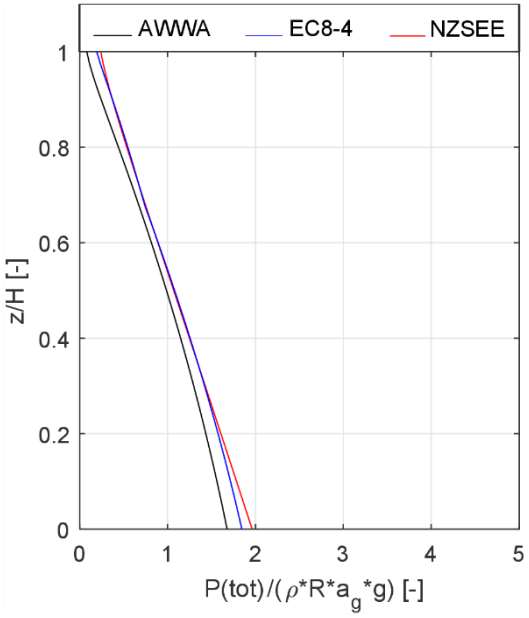

Figure 2-29. Normalized total pressure in case of H/R=0.4 and behavior factor

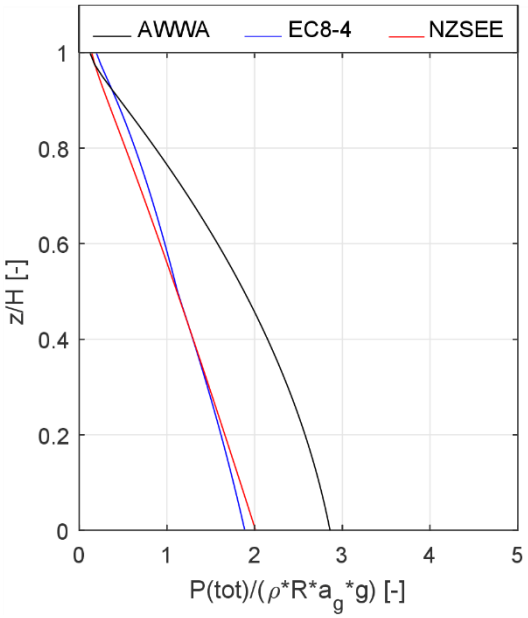

Figure 2-30. Normalized total pressure in case of H/R=0.4 and without behavior factor

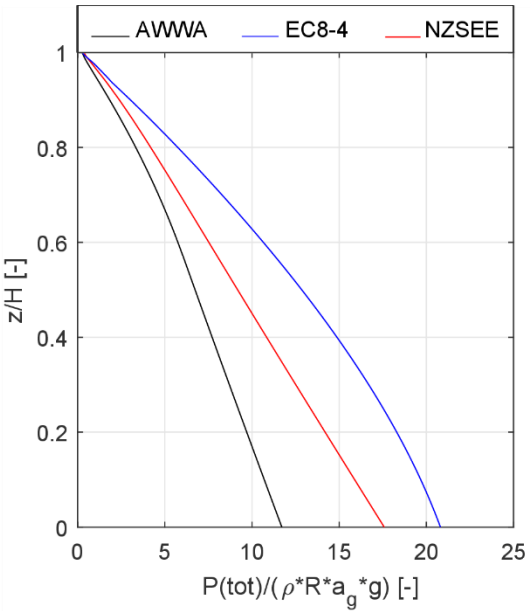

Figure 2-31. Normalized total pressure in case of H/R=3.5 and behavior factor

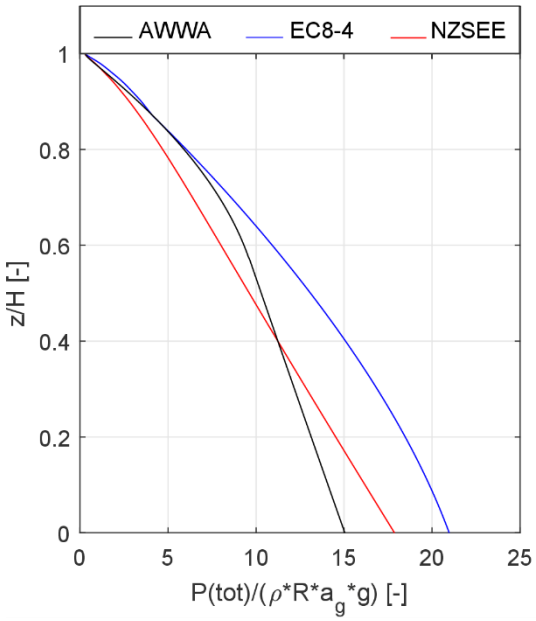

Figure 2-32. Normalized total pressure in case of H/R=3.5 and without behavior factor

The values of the normalized convective pressure at the base for H/R=0.4 and H/R=3.5 are summarized in Table 2.10 (considering behavior factor) and Table 2.11 (without considering behavior factor). Moreover, the percentage variation of maxima values obtained with AWWA and NZSEE are calculated with respect to the maxima values obtained for EC8-4.

Table 2.10. Values of the normalized total pressure at the tank base and percentage variation with respect to EC8 (considering behavior factor).

Values of normalized total pressure considering the behavior factor	***EC8-4***	***NZSEE (%)***	***AWWA (%)***
H/R=0.4	1.84	1.96 (6.5%)	1.68 (-8.7%)
H/R=3.5	20. 8	17.6 (-15%)	11.57 (-42%)

Table 2.11. Values of the normalized total pressure at the tank base and percentage variation with respect to EC8 (without considering behavior factor).

Values of normalized total pressure without considering the behavior factor	***EC8-4***	***NZSEE (%)***	***AWWA (%)***
H/R=0.4	1.88	2.01 (6.9%)	2.86 (52%)
H/R=3.5	20. 97	17.82 (-15%)	14.95 (-28%)

From the pressures values summarized in Table 2.10 and Table 2.11 the influence of the behavior factor and the differences among the codes can be examined. In particular, in case of squat tank (H/R=0.4), the behavior factor leads to a reduction of the total pressure of 41%. In NZSEE and EC8 this reduction effect is much smaller.

2.4. Conclusion

The current chapter is organized into three parts. The first section provides a list of the European and international codes and standards dealing with analysis, design and verification of storage tanks made of steel, pre-stressed or ordinary reinforced concrete located in areas of seismic activity. The second section deals with a critical comparison of the main design codes, focusing on provisions for the definition of reduction factor and damping factor, which represent two main topics in the framework of the lateral design seismic forces for liquid-containing tanks. Moreover, the section has the aim to compare the different approaches adopted by codes for modeling tank-fluid system and soil-structure interaction, combining impulsive and convective effects, evaluating hydrodynamic pressure on wall and base and sloshing wave height.

Some concluding remarks can be made on the critical comparison presented in the second section. Recognizing that liquid storage tanks possess low energy-dissipating capacity, all codes discussed specify lower values of the response modification factor compared to the conventional buildings. This lead to higher design seismic force for tanks. However, the manner and extent to which tank design seismic forces are increased in various codes might present several differences. There is a substantial variation in the values of the impulsive and convective base shear coefficients from American codes and standards, NZSEE and Eurocode 8. Indeed,

the formers (ACI 350.3, ACI 371, D-110, D-115, D-100, API 650) present a detailed classification of tanks and to each typology a different value of the response modification factor is assigned. On the contrary, NZSEE and Eurocode 8 do not provide such detailed classification of this factor based on the tank type. Among the differences in definition of design seismic force, it should be highlight that codes like ACI 350.3, D-110 and API 650 define the seismic design forces at the allowable stress design level, whereas ASCE 7 is at the strength design level. This is the reason for the bigger values of response modification factor in ACI 350.3, D-110 and API 650. Code D-100 as well defines design forces at the allowable stress design level. However, values of response modification factor are the same as those in ASCE 7, because a factor of 1.4 is used to convert design forces from strength design level to allowable stress design level. Differences among codes can be found in the context of the analysis of the tank-fluid system. NZSEE and EC8-4 adopts different mechanical models for tanks with rigid and flexible walls, whereas all other codes use the rigid tank model for all types of tanks. In particular EC8-4 introduces an impulsive component of pressure related to the wall flexibility; NZSEE uses a rigid tank model for reinforced concrete tanks and a flexible tank model for steel tanks. In these codes, the effects of the wall flexibility is taken into account by using a design acceleration corresponding to the impulsive mode natural period. For the purpose of combining impulsive and convective responses, Eurocode 8 uses the absolute summation rule, whereas ACI 350.3, D-110, D-115, D-100, API 650 and NZSEE adopt the SRSS rule. ASCE 7 claims that both rules may be employed for combination. NZSEE, Eurocode 8 and ACI 350.3 provide expressions for hydrodynamic pressure distribution on the tank wall. In contrast, expression for hydrodynamic pressure distribution on the tank bottom is given in NZSEE only. However, all the codes take into account the effect of hydrodynamic pressure on the bottom plate in the calculation of overturning moment. Provisions on the soil-structure interaction are given in NZSEE, ASCE 7 and Eurocode 8 only. These concluding remarks reveal the urgent need of a unified approach for the classification of tanks and the attribution of response modification factor to each tank typology, in order to overcome discrepancies presented in this chapter.

In the third section, a detailed analysis of the seismic design procedures of on-grade cylindrical steel storage tanks subjected to horizontal and vertical ground accelerations, according to the UNI EN 1998-4:2006, NZSEE and AWWA D100-05 is presented. Rigid and deformable tanks are considered in case of rigid or flexible foundation and in case of base perfectly or partially anchored to the foundation. Moreover, a comparison in terms of pressures distributions between the three codes examined is carried out as well. Analogies and differences between them are highlighted. For all the codes considered, in case of slender tank the impulsive pressure achieves higher values than those obtained in case of squat tanks.

Indeed, as discussed in Chapter 1, the increasing of the slenderness ratio lead to an increment of the liquid percentage moving in unison with the tank wall. The NZSEE code provides a

single formulation for slender and squat tanks. Therefore, only the pressure intensity change among the two tank models. On the contrary, in EC8-4 and AWWA codes, in addition to an intensity variation between squat and slender tanks, it is possible to observe a different shape of the pressure distribution as well. In case of impulsive pressure, both in squat and slender tanks the maxima values obtained with EC8-4 are smaller compared to those from NZSEE and AWWA. With regards to the convective component of pressure, the lower is aspect ratio H/R the bigger is the percentage of liquid mass involving in the convective motion. Then, in case of squat tanks, this generate high convective pressures on the tank wall, both at the top and at the base level. This is valid for all codes. Moreover, values of the convective pressures calculated according to the AWWA standard are lower than those obtained from the EC8-4 and NZSEE. This issue is probably due to the effect of the behavior factor. The influence of the behavior factor on the total pressures and the differences among the codes have been be examined. In particular, in case of squat tank, the behavior factor leads to a reduction of the total pressure of 41%. In NZSEE and EC8 this reduction effect is much smaller.

3. Definition of a new tank damage database

3.1. Introduction

One of the main purpose of the current study is to provide earthquake damage to ground motion relationships for on-grade steel storage tanks based on post-earthquake damage evaluation data. Also called empirical fragility curves, they are carried out from statistical procedures and describe the probability of experiencing or exceeding a particular level of damage as a function of ground-shaking intensity [61]. Past researchers developed fragility curves using relatively small collections of data. However, it is known that the number of samples affects the reliability of fragility estimation. In case of empirical data, this issue is much more emphasized because of measurement errors, indirect nature of observations and different uncertainties affecting information. In light of these considerations, one of the main step of the current work was defining a larger tank damage database. The current chapter provides all details on data source, seismic events considered, information collected, and criteria used for assigning to each database tank a reliable value of PGA. The tank damage database is attached to this work in Appendix A.

3.2. Effects of seismic loading on liquid storage tanks

In the following, a classification of the main failures of tank subjected to seismic event is presented (paragraph 3.2.1). Then, a synthetic description of the empirical performance of the tanks collected in database is provided for each earthquake involved, in order to highlight failure causes and consequences (paragraph 3.2.2). A more detailed description of damage is provided by the database in Appendix A.

3.2.1. Review of the main tank failures caused by earthquake

Reports on damages caused by past earthquakes reveals that liquid storage tanks show a complex dynamic behavior under seismic action. The occurrence of a certain failures rather than others depends on factors such as presence of anchors, slenderness ratio, roof type, fill rate, etc. The experience suggests that basing on the H/D ratio, the tank dynamic behavior can change completely. Usually, under seismic action slender tank behaves as a cantilever, with a concentration of high stresses near the base and a considerable value of the overturning

moment, due to the high position of the mass centroid. The most probable failures are uplifting and elephant foot buckling, rupture of the junction between the bottom and the base shell, buckling of the bottom shell, breakage of the inlet/outlet piping system, failure of anchors, shell buckling in the central part of the shell. Damage to the upper part and to the roof is not common for tall tanks. On the contrary, very squat tanks suffer mostly damages to the upper part because of the sloshing motion of the content inside, in particular buckling at the top of shell and at the roof, failure of the wall-roof shell connection, failure of rafters and columns sustaining the roof.

In the following, a technical description of the abovementioned seismic damages is provided.

- Shell buckling modes. The tank shell can be subjected to different kinds of instability: elastic and elastic-plastic. The first, usually involving the central part of the shell, is commonly known as "diamond buckling" due to the deformed configuration, and involves the elastic property of the shell material. It is caused by the excessive vertical compression meridional stress in combination with moderate hoop tensile stresses (this condition occurs in above the lower course of tank, where hydrodynamic pressure, which leads to an increase in the elastic buckling load, is small as compared to its magnitude at the tank base). On the contrary, elastic-plastic buckling, also known as "elephant foot buckling", extends around the tank circumference close to the lower course and it results from combined action of vertical compressive stresses exceeding the critical stress and hoop tension close to the yield limit. However, Rammestorfer et al. in [62] attributed the bulge formation to three components, the third is the local bending stresses due to the restraints at the tank base. Shell buckling modes can have different consequent scenarios such as failure of the weld between adjacent plates of the wall, failure at the bottom-wall connection (with or without leaking at junctions), deformation and rupture of the inlet/outlet piping system with probable loss of content, and in some cases total collapse of tank. Elastic buckling can also occur at the bottom plate, because of the presence of axial stresses in addition to the hydrostatic pressure, that pushes down the plate when it tends to uplift [63].

- Damage to the upper course and roof. Damage to the roof is usually caused by the sloshing motion of the convective mass, in the case in which the freeboard between the liquid surface and the roof is not sufficient. Often, the amplitude of the liquid waves can exceed several meters, as revealed by the presence of scratch marks in the upper course of the wall produced by the impact of floating roof [2]. In case of full or near full fixed roof tank, the sloshing motion results in increasing the pressure pushing onto the roof. Common codes and standards do not provide provisions for an adequate design of the roof under sloshing impact forces. Reports of past earthquakes revealed that, in the case of fixed roof, failure can occur at the joints between shell wall and roof, at the roof plate

in the form of buckling, in vents, in overflow piping and other appurtenances. Floating roof can be subjected to buckle of the deck plate, damage to the pontoon, roof drains, seals, antirotation devices, swing line and swing joints. Steel roof with curved knuckle joints appear to perform better [2], but supporting beams and columns can be damaged from sloshing impact forces. Extensive damage to roof and the upper part of the shell wall may lead liquid spillage. However, the loss of content related to this part of the tank structure is very small comparing with that caused by failures of the lower part.

- Anchorage failure. The anchorage system is widely used in case of slender tank, because of the high position of the center of liquid mass and then the need to counter the overturning moment. The most common anchorage system for steel tanks consists in hold-down bolts, straps or chairs. In case of strong earthquake, the anchorage system may be insufficient to withstand the seismic load and this usually results in anchor pull-out, stretching or failure. However, failure of anchors rarely leads to loss of tank contents.

- Foundation failure. The storage farms are often located in coastal areas, so this results in poor foundation soils and problem of liquefaction under seismic action. During the earthquake of Niigata in 1964, in Niigata Refinery Plant of Showa Oil Co. large crude oil tanks, built on not compacted ground, sustained settlements of several centimeters, base rotation and consequent troubles such as breakage of piping and leakages [64]. In similar situations, the loss of contents has caused a substantial reduction of the supporting materials under the tank base, and then an increase of the structural damages. During the Miyagi earthquake in 1978, the annular bottom plate of some tanks at the Tohoku Oil Sendai refinery, because of settlements, deformed so much that an acute angle was formed with the shell plate [65]. Field inspections detected other kinds of foundation failure as well, such as ring wall cracks and failure at the concrete pad. In case of tanks inadequately restrained against the uplift, vertical displacements cause additional tensile stresses in the base plate and in some cases the rupture of wall-bottom junction and of the base plate welds. In addition, sliding movements can damage tank and fittings, as the following paragraph will explain.

- Piping system failure. Piping failure can have several causes. Experience reveals that vertical and lateral tank movements result in breakage of valve, flanges and fittings, pipes disconnection and rupture. In particular, rigid piping is known to be highly prone to damages under seismic action. The presence of flexible loop in a pipe between the tank and the independent piping support should lead the complex to perform better. Damage to piping would entail repair costs of only 1% to 2% of the replacement value

of the tank, but would put the tank completely out of service immediately after the earthquake [66]. Indeed, depending on the extent of damage, the quantity of leakage can be different, as well as the consequent scenarios. Failure at piping can also occur in case of extensive buckling at the tank base, because of large shell deformations at the connection between the pipe and the tank. Buried pipes connected to the bottom plate broke in case of lateral movement and uplift, such as the case of the Loma Prieta earthquake in 1989 [2]. Obviously, damage to relief piping system is less severe in terms of loss of contents than damage to inlet/outlet piping.

3.2.2. Empirical performance of on-grade steel tanks under seismic action

A critical overview on the steel tanks dynamic performance observed during past earthquakes is one of the main tools for detecting critical issues and week points of this kind of structure. Following seismic events of significant intensity, damage information obtained from field inspections are collected in official post-earthquake reports and technical articles. Damage data collections are widely used especially for the evaluation of the empirical seismic fragility of tanks [8–10,67]. One of the bigger data collection available in current literature is NIST GCR 97-720, a technical report authored by Cooper [2], primarily concerned with the performance of petroleum storage tanks during major earthquakes ranging from the 1933 Long Beach earthquake through the 1995 Hyogoken-Nambu (Kobe) earthquake. Because of the similarity in construction of water tanks, their performance was included in the report. However, Cooper's collection is not the only data source on tank damages. A list of further reports and articles providing information on tanks damages caused by earthquakes have been provided as references of the current thesis. In this section, the empirical seismic performances of on-grade steel tanks are reported for 24 earthquakes occurred in the current century. A more detailed description of the tank damages is given in the database provided in Appendix A.

The 1933 Long Beach Earthquake

This moment magnitude 6.4 earthquake on March 10, 1933 originated offshore on the Newport-Inglewood fault [2]. Considering the concentration of oil production, storage, refining, and transport facilities in the affected area, actual failures were few. All tanks that failed, or sustained damage, were of riveted construction and located at a distance from the epicenter ranging from 3.5 to 45 Km. Damage to the roof seems to have its equivalent in later earthquakes damage to welded tanks. Sloshing in floating roof tanks also occurred in this earthquake, causing damage to the seals. The dearth of tank damage could be attributed to the relatively

small magnitude of the earthquake, “good” soil conditions at most tank locations, and most tanks not being full at the time of the earthquake. The destruction of the CLADWP Western Avenue riveted water tank (Figure 3-1) shows the possible effect of long period motion at a distance.

Figure 3-1. CLADWP Western Avenue riveted water tank, failure of the fourth shell course, Long Beach 1933

The 1952 Kern County Earthquake

The moment magnitude 7.3 earthquake occurred on July 21, 1952 was followed by a series of strong aftershock in a rather extended area in the northeast direction from the initial epicenter. The initial earthquake occurred in an area in close proximity to a number of tanks. Damage occurred to the General Petroleum tanks on their pipeline system from the San Joaquin Valley to the Los Angeles Basin. Virtually all the tanks observed in this area were riveted tanks with thick shells to allow for acceptable tensile stresses at the riveted splice between the shell plates. Considering the proximity of the facilities to the epicenter and the severity of the earthquake, one would expect more tank damage. Continental Station, located at 38 km from the epicenter, sustained no damage. Damage also occurred to tank floating roofs at the Pacific Gas and Electric Kern Power House, located at 42 km from the epicenter. The damage was principally to the floating roof seals accompanied by some sloshing and oil spillage. In most cases where damage to floating roof tanks occurred, there was also rotation of the roof and breakage of the roof anti-rotation guide and/or gage well. There were a number of smaller diameter bolted “production” tanks which either failed by elephant foot buckling, or in at least one case, the tank collapsed and fell over. The collapsed tank was nearly full. Most production tanks have heights and diameters that are approximately equal, and are of bolted shell construction [2,68].

The 1964 Alaska Earthquake

The Great Alaska moment magnitude 9.2 earthquake occurred on March 27, 1964. The epicenter of this earthquake was located in or near Prince William Sound. Damage to tanks and other structures in surrounding cities was extensive. This damage was caused not only by the strong shaking and ground failure, but also, for many sites, by the tsunami which followed the earthquake. In Anchorage, located 130 km from the epicenter, tanks were located in the dock area. Soils in the dock area consisted of silts and thick lens of "Bootlegger Clay". Damage to the larger tanks appeared to be minimal. Damage to smaller tanks appeared more frequently and more severely for those tanks situated closed to the water. Some tanks suffered elephant foot buckling as well as shell and roof damage (Figure 3-3) [2]. Reports on the earthquake noted that tanks less than half-full did not suffer damage. In Valdez, located 85 km from the epicenter, two tank farms were severely damaged by the earthquake and the resulting fire. The tank farms were built near the shoreline on poor soils [69]. The tanks appear to be not large (D/H from 1 to 2). Whittier was the closest community to the epicenter at 60 km. Tanks located near the shoreline suffered damage similar to those at Valdez[70] (Figure 3-2). The most tank in Nikiska, located at 210 km form the epicenter, suffered roof damage.

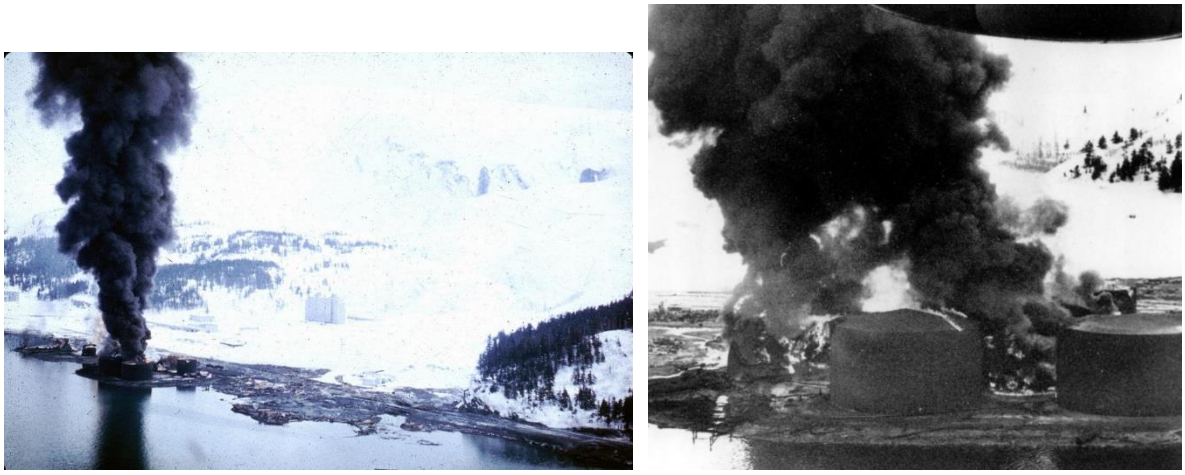

Figure 3-2. A tank farm in Whittier, Alaska was severely damaged by surge-waves developed by underwater landslides in Passage Canal, on March 27, 1964

Figure 3-3. Anchorage, Alaska, 1964. Vibration and ground fractures damaged some structures in the port area, including the fuel tank seen in the lower right

The 1964 Niigata Earthquake

The moment magnitude 7.6 earthquake occurred on June 16, 1964. It caused extensive damage in Niigata City, in Yamagata and Akita Prefectures. In Niigata City, two large oil refineries have been established, one belongs Showa Oil Co. and the other to Nippon Oil Co. These two plants were damaged severely by the Niigata earthquake, one of the large crude oil tanks in Showa Oil Co. began to burn immediately after the earthquake, and the damage was so severe that the most part of the plant were burned out completely. In Nippon Oil Co., there are several new oil tanks founded on improved ground by vibrofloatation, and they suffered almost no damage by the earthquake. However, so many tanks founded on natural ground suffered severe damage. Considerable unequal settlements were observed and the maximum settlement was about 50 cm [64,71,72].

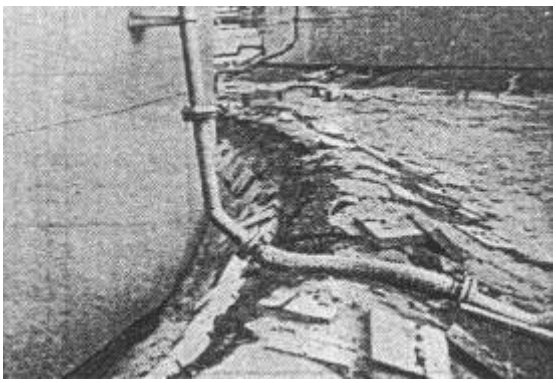

Figure 3-4. Settlement of tank on unimproved ground (Watanabe, 1966)

The 1971 San Francisco Earthquake

The moment magnitude 6.7 earthquake had its epicenter about 21 km north of the City on San Fernando. There was ground breakage or surface faulting south of the epicenter. Tank damage in this earthquake seems to have been confined to the general area north of where ground breakage occurred. A squat tank suffered roof and upper shell damage but not elephant foot buckling. It was one-half or two-third full at the time of earthquake. The tank had a knuckled roof/shell joint. Shell buckling damage was in the upper shell course but not in the knuckle joint [2]. Information for a lot of damaged tank was also available in technical reports. The main damages detected were floor plate ruptures, shell bucking, damage to roof seals in case of floating roof tanks, and damage to inlet/outlet fittings.

The 1972 Managua Earthquake

The moment magnitude 6.3 earthquake on December 23, 1972 occurred near Managua, the capital of Nicaragua. The epicenter was 28 kilometers northeast of the city center and a depth of about 10 kilometers. Few damage data are available for storage tanks. The grain storage tanks of the INCEI, showed uplifting of their anchor bolts to the south, and local buckling of the tanks to the north as well as near the top. Three tanks suffered elephant foot buckling, but they were left in service [66].

The 1978 Miyagi Earthquake

The moment magnitude 7.7 earthquake on June 23, 1978 damaged many buildings, structures and roads in Sendai city which is located about 100 km from the epicenter. At the Tohoku Oil Sendai Refinery, in the suburbs of Sendai city, three oil storage tanks were damaged severely, resulting in flow-out of the contents. Three tanks failed at the annular bottom plate along the inside fillet weld toe at the corner joint with the shell plate. Measurements made of the annular bottom plate thickness after the earthquake revealed that the bottom plate thickness in these tanks decreased by corrosion. Two tanks settled an average of about 10 to 14 cm along the perimeter. The anchor bolts of a water tank were uniformly pulled out about 15 cm. In many other tanks, the rolling ladder on the floating roof was buckled or deformed and oil flushed out on the floating roof [65,73]. Figure 3-5 shows one of the three failed storage tanks at Sendai Refinery, Tohoku Oil Company, Ltd. The damage illustrated is due to suction caused by rapid evacuation of the oil through the ruptured connection of the base and wall of the tank. The several tanks, of similar size, in the foreground are thought to be undamaged.

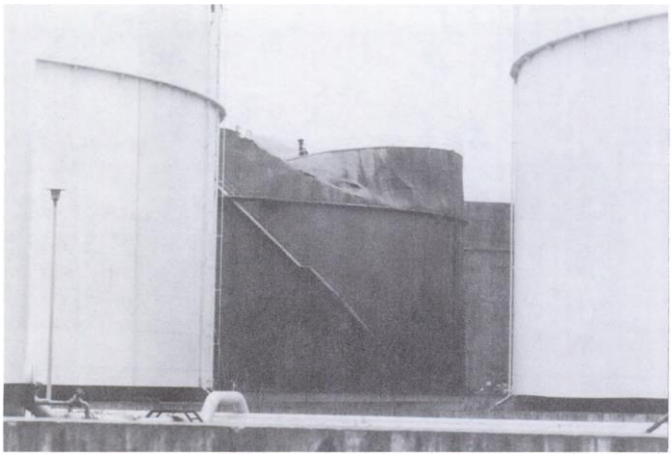

Figure 3-5. Miyagi 1978: failed storage tanks at Sendai Refinery, Tohoku Oil Company, Ltd.

The 1979 Imperial Valley Earthquake

The moment magnitude 6.4 earthquake provided the opportunity to evaluate the performance of tanks were near ground motions were recorded. Most of the information was obtained from EERI Reconnaissance Report [74] and the paper by Haroun [75]. The epicenter was located about 30 km from the site of the tanks. The tanks were located about 4-5 km west of the Imperial fault, where there was surface movement in the vicinity of the tanks. The full tanks at the Imperial Irrigation District (IID) power plant suffered roof damage which consisted of the roof separating from the shell at the roof/shell weld, allowing oil to spill. Sever damage at the Southern Pacific Pipe Lines (SPPL) terminal was to three tanks, consisted principally of elephant foot buckling. A number of eighteen tanks at this terminal sustained major damage. All tanks were built to API 650 in effect at the time of construction.

The 1980 Greenville Earthquake

The Greenville moment magnitude 5.8 earthquake on January 26, 1980, affected mostly wine tanks. A reconnaissance indicated that damage to the storage tanks at the Wente Bros. Winery near Livermore, California, was of engineering significance (Figure 3-6). A cursory study of the damage data indicates that the model of failure or the pattern of damage was a function of the following factors: 1) Fullness or emptiness of tanks: empty tanks suffered little or no damage; 2) Height-to-diameter ratio (H/D): the tanks with low value of H/D (H/D < 1.5) had predominantly large-amplitude “elephant foot” buckles all around (Figure 3-7 (a)). The tanks with intermediate values of H/D (1.5 <=H/D <=2.0) exhibited varying patterns and combinations of diamond-shaped buckles (Figure 3-7 (b)) and elephant foot buckles. Tanks

with high value of H/D (H/D > 2.0) suffered minor or no damage to the shell but had some failed anchorage welds or bolts; 3) Location of the cooling jackets: where this extra sheet of steel was close to the bottom of the tank, there was no damage to the shell. Where the jacket was located 3 or 4 feet above the base, the major buckling occurred between the cooling jacket and the base [76].

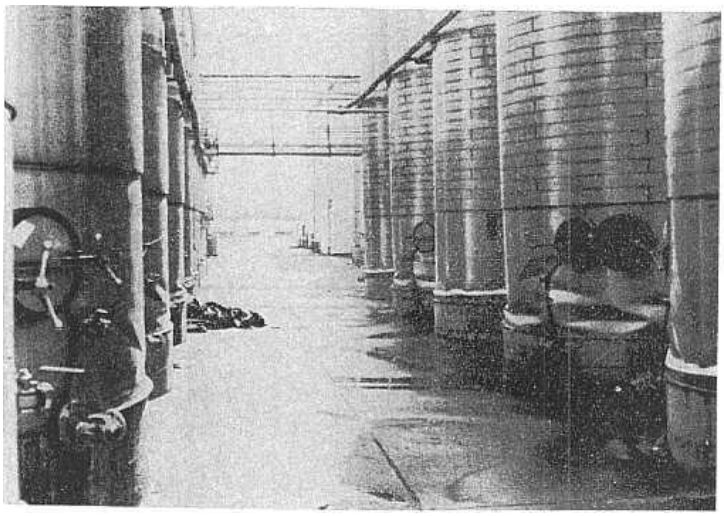

Figure 3-6. A general view of tank damage at Wente Bros. Winery, Greenville 1980

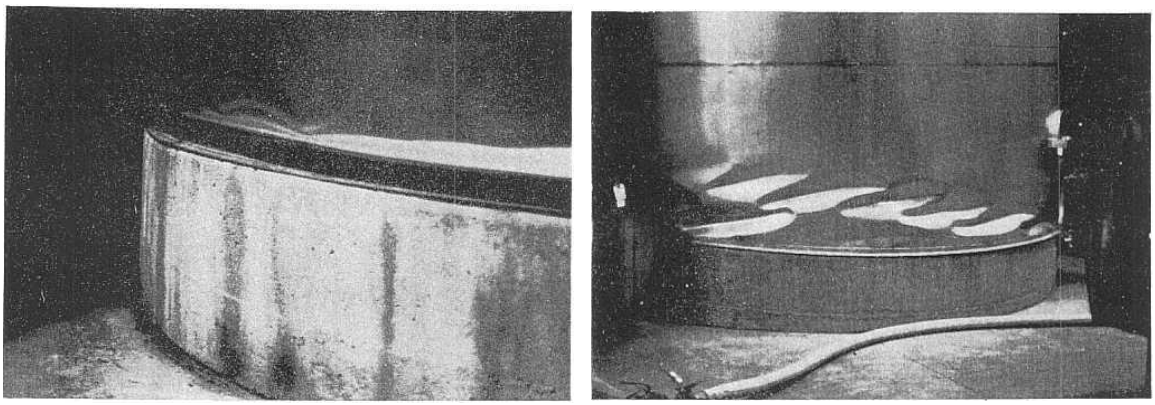

Figure 3-7. Typical elephant's foot buckling pattern (a); typical diamond-shaped buckling pattern (b)

The 1983 Coalinga Earthquake

The Coalinga moment magnitude 6.3 earthquake on May 2, 1983 presented the opportunity to observe performance of both large and medium sized tanks when subjected to strong ground motion at relatively short distance from the epicenter. The general terrain is rolling hills and

valleys, with primarily alluvial sols which are considered good foundation soils. This earthquake, which produced large accelerations, showed that large tanks do uplift, that sloshing in large floating roof tanks causes damage, that smaller bolted tanks with lower D/H ratios are vulnerable to damage and possible failure, and that large tanks are less vulnerable to elephant foot buckling than smaller tanks. Also evident from this earthquake is to not use bottom draw piping which is embedded in the earth below the tanks [2,77–79].

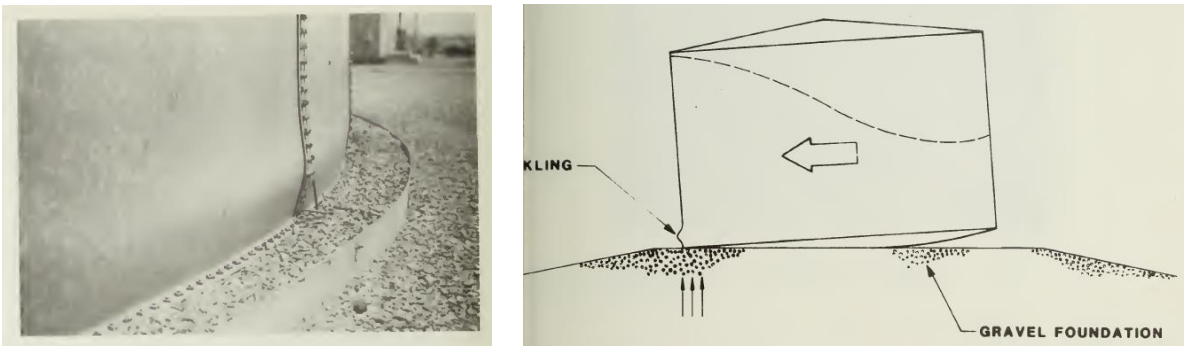

Figure 3-8. Elephant foot bulge at the base of a storage tank (a);diagram showing mechanism that causes elephant foot type damage to cylindrical storage tanks (b)

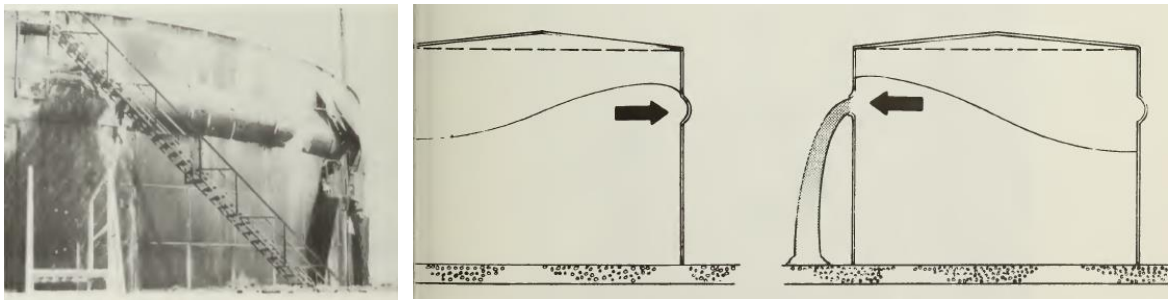

Figure 3-9. Bulge and rupture in one of Shell's storage tanks, probably caused by liquid slosh (a); Diagram of probable mechanism (liquid slosh) that caused damage sustained in the upper rings of cylindrical storage tanks (b)

The 1985 Chile Earthquake

On Sunday 3rd March 1985, at 19.47 local time, the central region of Chile was shaken by a major earthquake of moment magnitude 8.0 which caused heavy damage to a wide range of structures and left over 170 people dead and 1,000,000 people homeless. Many types of structures were damaged, ranging from adobe buildings to engineered bridges and harbor facilities. A large refinery at Concon, 30 km north east of Valparaiso, was damaged by the earthquake. One steel tank appeared to be leaning significantly and another could be seen to be buckled at the top, and to be stained by an oil spill. Although no information could be obtained

from the authorities, the refinery was apparently working normally, and no sign of serious fires or oil spills could be seen. Other damaged facilities were detected in Oxiquim chemical plant located at 50 km from the epicenter, Terquim Tank farm and Port of San Antonio at 55 km [80–83].

The 1986 Adak Earthquake

On May 7, 1986 a major earthquake of moment magnitude 8.0 occurred southeast of the Andreanof Island group in the Aleutian Islands chain. On the island of Adak there are diesel generator power plants, steam plants, electrical substations, and a large number of facilities. Storage tanks located in Fuel Pier Yard and Power Plant 3 and having aspect ratio H/D grater tank 1 suffered no damage.

The 1987 New Zealand earthquake

The 1987 New Zealand earthquake measured 6.5 on the moment magnitude scale and struck the Bay of Plenty region of New Zealand on 2 March. Industrial sites were badly affected. At Bay Milk Products in Edgecumbe, huge stainless-steel milk silos collapsed, spilling thousands of liters of milk. Two milk tankers were thrown on their sides. At the N.Z. Distillery Company, tanks of spirits collapsed, saturating the ground with vodka and gin. Although these damages, many storage tanks survived to the earthquake [66,84].

The 1991 Costa Rica earthquake

On April 22, 1991, the moment magnitude 7.7 Talamanca earthquake occurred with its epicenter located 39.5 km south of Limon, Costa Rica. The RECOPE oil refinery in Moin suffered severe damage to the plant facilities and to the oil storage tanks. The severe damage to different types of oil storage tanks together with the fact that many of these tanks had been filled on April 21, 1991, just one day before the earthquake, provide a rare opportunity to examine the different types of possible modes of failure. Tank no. 792, which was a temporary storage tank containing naphtha and diesel oil, exploded and landed about 50 m from its original location. Tanks 704,705, and 728 suffered severe damage to the roof and the tops of the walls due to sloshing of the contents, as shown in Figure 3-10. The forces due to hydrodynamic effects caused rupturing of the joint in the steel plates at the roof-wall junction (Figure 3-10 (b)). Five tanks containing gasoline had either total collapse or severe tilting of their floating roofs. Four

tanks experienced total loss of their contents due to the classical "elephant-foot" buckling of the vertical walls near the base, as shown in Figure 3-11 [85–87].

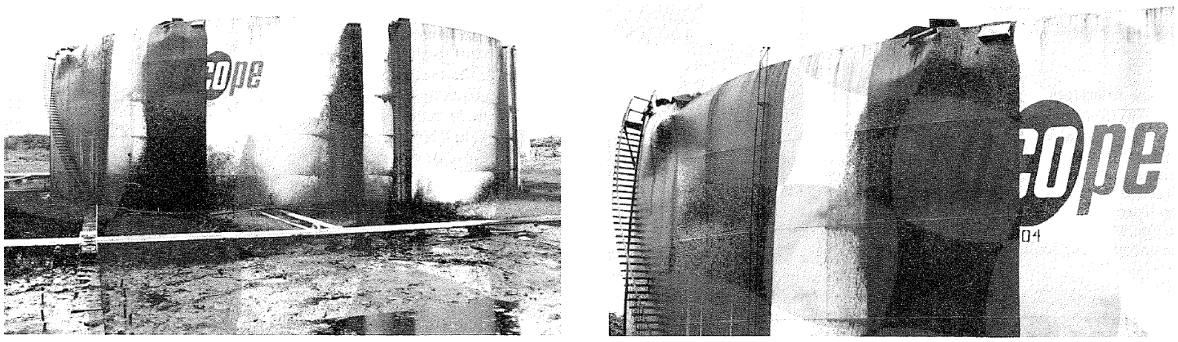

Figure 3-10. Overall view of the 12.19 m high by 44.2 m diameter oil storage tank showing oil spillage from top vents and from rupture of roof-wall junction (a); close-up of wall buckling and rupture of joint between steel plates at roof-wall junction (b)

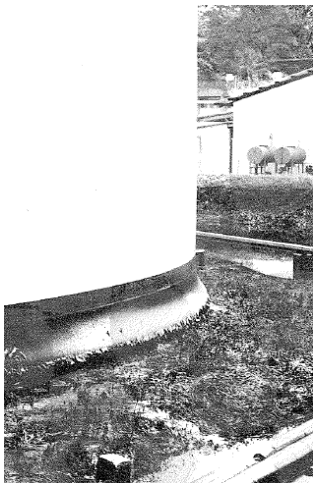

Figure 3-11. Close-up of elephant foot buckling at base of 9.75 m high by 21.14 m diameter tank

The 1989 Loma Prieta Earthquake

The Loma Prieta moment magnitude 6.9 earthquake of October 17, 1989 illustrated that tank damage can occur at considerable distance from the epicenter. Soil conditions obviously affect the performance of tanks, but different foundation design has led to different seismic performances of tanks located in the same area. Examination of the available information on water tanks near the area of strong shaking shows that the 100,000 gallons bolted tank which had elephant foot buckling probably had D/H on one or slightly greater. The remaining water

tanks were of a capacity that D/H would expected to be larger than two. No shell buckling was indicated in damage reports on these larger tanks [2,88–91].

The 1992 Landers Earthquake

The moment magnitude 7.3 Landers earthquake occurred on June 28, 1992. Though no petroleum storage tanks were damages in this earthquake, the large number of water tanks in the affected area and the small amount of damage, other than two total failures, make this a significant earthquake for tanks. Consideration for Landers include: most water tanks operate near full, hillside settings may provide “improved” foundation conditions. Most tanks in the Landers area were low, with heights less than 7.4 m. Sloshing and seal damage to large floating roof oil tanks occurred in the Los Angeles area, 180 km from Landers [2,92,93].

The 1994 Northridge Earthquake

The moment magnitude 6.7 earthquake occurred in January 17, 1994. It occurred on a blind thrust fault with the epicenter located in the San Francisco Valley near the community of Northridge. This earthquake significantly affected a number of tanks. Tanks located at north (20 km) and west (15 km) of the epicenter suffered damage. The Larwin tanks were totally destructed. From pictures of one of these tanks the shell appears to be raised from the floor in the manner that one would expect if floor/shell yielding at hinges were to take place (i.e., supporting the theory of the thicker annular ring). Also Newhall County Water District Tank 7 has a 12.7 mm bottom, and this tank did not have elephant foot buckling. Damage to smaller bolted tanks was again experienced in this earthquake. Roof damage to water tanks seemed to be a feature of this earthquake. The MWD Jensen Tank, which had upper shell damage and pulled anchor bolts in the 1971 San Francisco earthquake had its upper shell stiffened and the anchor bolts removed. This tank suffered no damage in this earthquake. The City of Simi had problems with buried and backfilled underdrains pulling out from the bottom of the tank (a similar problem occurred on a large oil tank at Coalinga and water tank at Loma Prieta) [94–96].

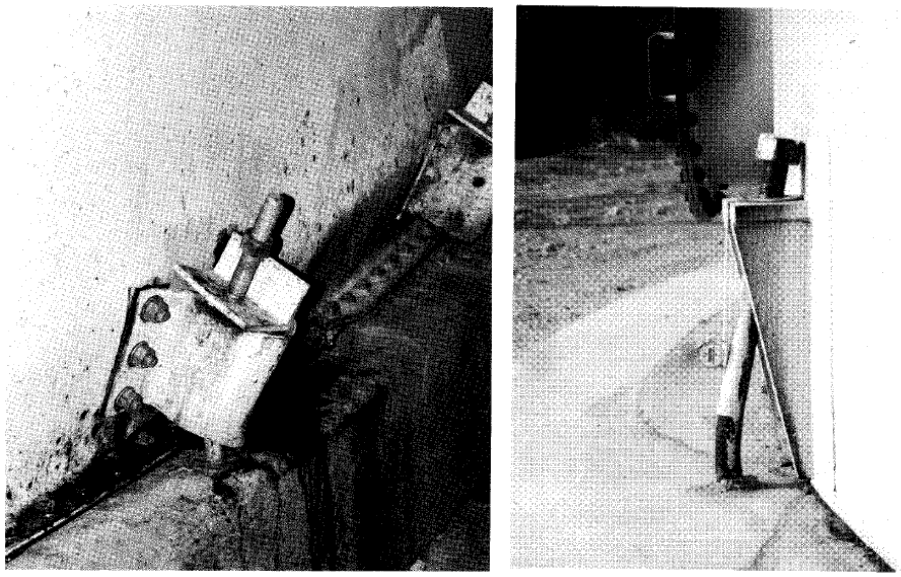

Figure 3-12. Stretched anchor bolts in two tanks affected by 1994 Northridge earthquake

The 1995 Kobe Earthquake

The moment magnitude 6.9 Kobe earthquake on 17 January 1995 fortunately did not provide the same tank problems resulted in prior Japanese earthquake (Tokyo 1923, Niigata 1964 and Miyagi-Ken-Oki (Sendai) 1978). The closest major refineries which had tanks at risk were located about 35 km from the epicenter at Osaka and Sakai. Acceleration at these three refineries is estimated to be 0.2g and apparently there was no major damage. A liquid storage tank terminal, about 10 km east of the epicenter and on the waterfront, was damaged from site liquefaction. There was no loss of product from damaged tanks. This terminal is built on reclaimed ground and probably experienced peak ground acceleration of 0.6-0.8 g. The terminal setting is 2-4 km from active faulting. The damage consisted principally of tank tilting, pipe support/piping loss of foundation support, and walkway-platform loss of support. Liquefaction was the principal cause of damage at this waterfront location [2,97–99].

Figure 3-13. Tanks in the port area. The ground shows signs of massive liquefaction and settlement. The tanks appear to be on pile-supported foundations

The 2003 Tokachi-oki Earthquake

The 2003 Tokachi-oki earthquake of moment magnitude 8.3 that occurred in the subduction zone southeast of Hokkaido, Japan, generated large-amplitude long-period ground motions with periods of several seconds to around 10 s in sedimentary basins in Hokkaido. These long period strong ground motions excited sloshing of liquid in large oil storage tanks, causing damage to many storage structures. The most severe damage occurred at a refinery in the city of Tomakomai, which lies in the Yufutsu sedimentary basin, southwestern Hokkaido. Seven oil storage tanks with floating roofs suffered fire damage and/or sinking of the roof. The liquid sloshing in those tanks that suffered severe damage had a fundamental-mode natural period of 5–12 s, comparable to the period of ground motions caused by the earthquake. The 2003 Tokachi-oki earthquake was the first M 8-class event to be recorded by the Japanese nationwide strong ground motion seismograph networks, K-NET and KiK-net. It was thus the first time that large-amplitude long-period ground motions, which are a characteristic of large earthquakes, were recorded at a high station density in Japan [100].

Figure 3-14 Tokachi-oki earthquake in 2003. From left to right: ring fire in a crude oil tank; open-top fire in a naphtha tank; sinking of floating roofs in two kerosene tanks

The 2003 Bam Earthquake

The 6.6 moment magnitude earthquake occurred on December 26, 2003 has the epicenter at 29.01 N - 58.26 E-SW of the city of Bam in southeastern Iran. Three out of six on-grade steel oil tanks at Roghan Jonub Company experienced leakage of liquid from roof-to-wall junctions because of sloshing during the quake. Other damage modes such as elephant foot buckling, rupture of rigid piping, and tank were not observed in these tanks. Figure (18) shows the leakage of oil from on-grade tanks [101–103].

Figure 3-15 Bam earthquake in 2003. Leakage of oil from tank due to sloshing

The 2007 Central Peru Earthquake

On August 15, 2007, an 8.0 moment magnitude earthquake occurred off the coast of Central Peru. Inspections were made of a number of industrial structures in the epicentral region, principally on the road between Pisco and the Port of San Martin. In general, both structural and non-structural damage was limited, despite these industrial sites being located close to Pisco in areas susceptible to ground subsidence. At the Port of San Martin, a water storage tank was located close to the access road near the port. The tank was anchored to a concrete base. There was no discernable damage or movement. At the Blue Pacific Oil, a large fish oil processing and storage facility on the coast. There are 10 large steel tanks about 12 m diameter and 10 m high, connected by pipework. They were built in 1967. Six of the tanks were reported to be on a 1.5 meter deep reinforced concrete raft. Three tanks classic elephant type buckling around a large extent of their perimeter. One tank showed buckling at the first strake level,1.5 m above ground (Figure 3-16). No product was lost due to pipe or tank failure, but some had sloshed out at the top through inspection holes. There was no sign of lateral movement or any restraints to prevent it, but there is a possibility that there was some settlement. At Epesca Peru, another fish oil plant next door to Austral with similar facilities, there was no damage. The Storage depot near Pisco takes oil and gas pipelines from offshore platforms and stores it. A water tank had buckled and split at the bottom, but this was a rusted skirt only and no product was lost. There were no signs of sideways movement. All other tanks were undamaged [104,105].

Figure 3-16 Central Peru earthquake in 2007.Blue Pacific oil facility view and tank damages

The 2010 Chile Earthquake

On February 27, 2010 a moment magnitude 8.8 earthquake struck the central part of Chile. During the 2010 Chilean earthquake there was no observed major fail in tanks, despite the high values recorded of vertical accelerations. One of the most important failure occurred in Santiago's airport. The airport had four fuel steel tanks and one for storing drink water, all of them were of welded steel. The tank containing water collapsed, while the four adjacent tanks of liquid fuels remained intact. The steel structure of Arturo Merino Benitez airport had major

nonstructural damages, which kept it out of service for a long time. The water tank was self-anchored and had a storage capacity of 1,300 m^3 which was full at the time of the earthquake. Tank collapse was likely due to repeated wall uplifts and subsequently shells plates buckling [80,106,107].

The 2011 Tohoku Earthquake

The 2011 off the Pacific coast of Tohoku Earthquake of moment magnitude 9.0 caused damage to oil storage tanks and other hazardous materials facilities. The damage of the oil storage tanks and hazmat facilities has a different aspect by area. The area for on-site survey is separated into three areas as 'the Pacific coast', 'the coast of the Japan Sea' and 'the Tokyo Bay'. Along the Pacific Coast: many tanks and pipelines floated and displaced by the buoyancy and the force of the tsunami; foundations of the tanks were swept away by the tsunami; no severe damage of the floating roofs by the liquid sloshing; few damage on storage tanks by the strong ground motions; liquefaction by the strong ground motions. Along the coast of the Japan Sea: sinking of the inner floating roof, fractures of the pontoons and oil spill onto the deck of the floating roofs due to the liquid sloshing and so on. Along the coast of the Tokyo Bay: sinking of the floating roof and other damage by the liquid sloshing [6,108,109].

Figure 3-17 Tohoku earthquake in 2011. Silos damaged by ground shaking at Sendai harbor (a), tank settled because of liquefaction around the foundation

The 2014 Napa Valley Earthquake

On August 24, 2014 a moment magnitude 6.0 earthquake occurred northwest of American Canyon, California. Of the 12 tanks in the City of Napa's water system, one (termed Montana "B") sustained significant damage (Figure 3-18). The tank is an unanchored 67' diameter, 37'

high circular welded steel tank with corrugated iron (CGI) roof supported by redwood beams on steel columns. The water sloshed with approximately 6' amplitude, damaging the roof. There was no buckling of the walls, but some rocking was evidenced by motion at the outtake slip joint. The tank drained immediately following the event due to a nearby pipe break. The Napa Valley has approximately 400 wine production facilities, about 300 of which have been built since 1966. An estimated 50 wineries sustained measurable damage to tanks, barrels and/or buildings. Stainless steel wine tanks used in the wine industry are generally not anchored or inadequately anchored. Damage limited to full tanks with limited base anchorage. The majority of tanks were empty in preparation for the harvest and crush in September [110,111].

Figure 3-18 Napa Valley in 2014. Roof damage in Montana B tank

3.3. Data sources and seismic events considered

The starting point for gathering the new collection of data presented in this work, as for previous works on tank fragilities [8–10], was the report authored by Cooper (NIST) [2]. However this data was here reviewed and expanded using other official post-earthquake reports and papers [112–119]. Information collected for each tank has the aim to present an adequate description of the overall conditions of the tank at the time of the earthquake occurrence. In particular:

- Information on the site in which tank is located, soil type, epicentral distance, Joyner-Boore distance [120], ground motion intensity parameters as horizontal and vertical peak ground accelerations and horizontal peak ground velocity;

- Information on tanks, i.e. dimensions, volume, foundation type, presence of anchorage, roof type, shell junction type and shell material, fluid level at the time of earthquake, date of construction and design code and finally damage suffered and extent of release.

The new database contains information on 5829 tanks, based on damage observed from earthquakes listed at the paragraph 3.2.2. However, not all tanks in database are taken into account for the fragility analysis presented in the current study, which is focused on atmospheric tanks used in chemical and process industries. For example, wine tanks (Greenville 1980 and Napa Valley 2014 [76,110]) have not been considered, since the material of which they are made and their geometry can lead to a different structural behavior with respect to that of oil tanks. Furthermore, in case of liquefaction of soil or ground failure beneath the tanks, a full understanding of the structural mechanism might be very complex and not always possible. For this reason, many tanks subjected to Niigata 1964, Kobe 1995 and Chile 1985 earthquakes were excluded from analyses. Similarly, since the cause of damage for tanks subjected to Tohoku 2011 earthquake is not so clear (many tanks were also affected by a severe tsunami occurred during the seismic event) they were not included in fragility analyses. This is also the case of a tank severely damaged and collapsed during the Northridge earthquake because of an adjacent tank. One of the 38 tanks experiencing the 1991 Costa Rica earthquake overturned and exploded. However, reports are not clear about the cause of this catastrophic failure, so it is not included in analyses. Then, the tanks involved in fragility formulations are 3026. Table 3.1, for each of the 24 events collected in database, shows the number of tanks in the database, the PGA range, the source from which PGA values were obtained and finally the source of the other earthquake data. The fourth column of this table specifies, for each earthquake, the number of tanks used in fragility analysis.

Table 3.1. Earthquake characteristics for tank database used in fragility analysis

Seismic Event	***Number of Tanks***	***PGA Range (g)***	***Number of Tanks Used in Analysis***	***Information Source***	***PGA Source***
Long Beach, 1933	52	0,358 – 0,448	52	[2,78]	This work
Kern County, 1952	64	0,113 – 0,351	64	[2,68]	This work
Alaska, 1964	40	0,20 – 0,384	40	[2,69,70,78]	This work
Niigata, 1964	189	0,16	-	[64,71,72]	[71,72]
San Fernando, 1971	35	0,12 – 0,86	35	[2,78,84,121]	This work, [66,84]
Managua, 1972	3	0,39	3	[78]	[78]
Miyagi, 1978	73	0,29	73	[65,122,123]	This work
Imperial Valley, 1979	29	0,378 – 0,467	29	[2,75,124]	This work
Greenville, 1980	177	0,167	1	[76]	This work
Coalinga, 1983	52	0,187 – 0,45	52	[2,77,78,84,125]	This work, [66,84]
Chile, 1985	168	0,23 – 0,28	163	[80–84]	This work, [66,83,84]
Adak, 1986	3	0,20	3	[84]	[66,84]
New Zealand, 1987	11	0,3 – 0,5	11	[84]	[66,84]
Loma Prieta, 1989	1824	0,065 – 0,55	1824	[2,88–91,126]	This work, [2,66]
Costa Rica, 1991	38	0,24	37	[85–87]	This work
Landers, 1992	33	0,19 – 0,553	33	[2,126]	This work, [2,66]
Northridge, 1994	105	0,23 – 0,90	104	[2,95,96,121,126,127]	This work, [2,66,95,126]
Kobe, 1995	426	0,36 – 0,74	-	[2,97]	This work, [2]
Tokachi-oki, 2003	177	0,10	177	[100]	This work
Bam, 2003	7	0,413 – 0,497	7	[101]	This work
Central Peru, 2007	104	0,34 – 0,427	104	[104,105]	This work, [104,105]
Chile, 2010	202	0,24 – 0,334	202	[80,106,107]	This work
Tohoku, 2011	1927	0,11 – 0,91	-	[6,108,128]	This work
Napa Valley, 2014	96	0,23 – 0,65	12	[110,111]	This work
Total	**5829**	**0,065 – 0,90**	**3026**		

3.4. Undamaged tanks

A crucial aspect of the creation of the present database is the introduction of a large population of undamaged tanks involved in past earthquakes and never included in previous fragility analyses. Information on these tanks, indeed, is not always clearly available in reports but in this work, it has been obtained by comparing data from different documents, analyzing the plant layouts from available pictures and comparing them with plant views provided by GIS archives. This has been the case of tanks subjected to earthquakes like Miyagi 1978, Northridge 1994, Kern County 1952, Tokachi-oki 2003, Coast of Central Peru 2007 and Chile 2010. These samples were not mentioned in Cooper's collection [2], that was the main source of all previous empirical fragility analysis on on-grade storage tanks. The absence of a large number of undamaged tanks might have led previous researches to overestimate tanks fragilities. In the following the undamaged tanks added for the aforementioned earthquakes are briefly presented.

Miyagi, 1978. A report authored by Kawano et al. [65] classifies tank damage occurred at the Tohoku Oil Sendai Refinery (100 km from the epicenter) in five basic categories: 1) failure of the annular bottom plate at bottom corner joint with oil spills; 2) settlement along the tank perimeter; 3) buckling of rolling ladder connected to floating roof; 4) pull-out of anchor bolts; 5) buckling of upper shell courses. Only six oil tanks, out of the total seventy-three, suffered substantial damage (i.e. categories 1 and 5), the remaining sixty-seven suffered only slight damage (i.e. categories 2,3 and 4). These kind of failures, in the aim of Damage States, are considered as DS1, i.e. no damage or slight damage, since they affect non-structural part of the tank.

Northridge, 1994. Damage data on ninety tanks were included in the data collection provided by ALA. In addition, the present work considers other fifteen tanks suffering only slight damage or no damage. Information on these tanks has been found in [126].

Kern County, 1952. Compared to the databases used in previous researches for developing fragility curves, the current work considers forty tanks additional tanks. They contained water, gasoline and oil and were located at a distance of 48-50 km from the epicenter. Most of them were undamaged. [68].

Tokachi-oki, 2003. This earthquake has never been included in previous fragility studies, as well as Coast of Central Peru 2007 and Chile 2010, discussed in this section. Information on damage of one hundred seventy-seven squat tanks, located at West Port of Tomakomai, has been extracted from [100] and GIS archives. Only seven tanks suffered sinking of the floating roof as a result of damage to the roof pontoons because of large amplitude sloshing. The remaining one hundred seventy tanks were undamaged.

Coast of Central Peru 2007. Information on one hundred-four oil and water storage tanks was obtained from [105], [104] and from GIS Archives. Tanks sites were the Port of San Martin, the Blue Pacific Oil plant and at other plants located on the coast near Pisco as Austral Fish Oil, Epesca Peru and Pluspetrol Peru (about 53-56 km from the epicenter). Only five tanks suffered damage: three fish oil tanks with fixed roof experienced elephant foot buckling around a large extent of their perimeter; another similar tank showed buckling at the first strake level, 1.5 m above ground (see Figure 3-16); a water tank had buckled and split at the bottom. All the remaining storage tanks did not suffer damage.

Chile 2010: damage data and information on tanks have been obtained from [80], [106],[107] and GIS archives. Most tanks had H/D ratio lower than 1, and only a tank out of two hundred-two collapsed. The others resulted undamaged.

3.5. Recent earthquakes

Previous database considered principally old seismic events. In particular, for his fragility curves, O'Rourke [8] used an inventory of nine seismic events occurred from 1933 to 1994; ALA 2001 [66] and Salzano [10] obtained fragility curves basing respectively on nineteen and about eleven seismic events occurred in the same period. The present database considers for the calculation of tank fragilities twenty-one earthquakes including five more recent events: 2003 Tokachi-oki earthquake ($M_w = 8.3$), 2003 Bam earthquake ($M_w = 6.6$), 2007 Central Peru earthquake ($M_w = 8$), 2010 Chile earthquake ($M_w = 8.8$), and 2014 Napa Valley earthquake ($M_w = 6$). It is expected and confirmed by damage data that recent seismic events have showed limited damage to tanks, since the most of them are new buildings and designed under recent seismic codes.

3.6. Information collected

Information on tanks and damage is extracted not only from previous databases. Indeed, many other reports and papers have been analyzed for obtaining additional data and confirming the reliability of past datasets. Information such as size and liquid stored is available for most of the tanks. For recent earthquakes (i.e. Tohoku, Napa Valley, etc.), for which reports provided limited data, information as the exact tank location in coordinates (often used for the evaluation of PGA value by ShakeMap), dimension and roof type is obtained by using GIS archives. This approach allowed to obtain data for a number of tanks much bigger than that involved in past

databases. Information about material is less frequently found in reports, but it can be deduced by the knowledge of the liquid contained. Indeed, for petroleum tanks, the material adopted is usually steel, instead for wine tanks aluminum and stainless steel are often used. Sometimes, source documents provide details about the plate thickness of bottom plate, shell courses and roof. The date of construction and/or the adopted design code are available for only 16% (477 out of the 3026 tanks) of the tank inventory used for fragility curves. Principal roof types are floating and fixed; for the latter typology, the most common shapes are dome, cone, flat and knuckle. However, cases of fixed roof with internal floating pan has been detected. Information on the foundation includes details on anchorage system and type of foundation structure. Tanks for which anchorage condition is known represent the 12% (375 out of 3026) of the tank inventory, and only 29% (109 out of 375) of them is anchored. Reports reveal that the most common foundation typologies used for atmospheric tanks are gravel or concrete pad, concrete ring, direct base on compacted soil or rock, pile foundation. The height of fluid at the time of earthquake is a crucial issue for the tank seismic response. Fill level in an oil tank can often be less than 50%, otherwise water system distribution tanks are kept at fill levels between 80% and 100% [9]. Percentage of filling is available for 14% of tanks in database (422 out of 3026). Information on structural damage and extent of release are deduced from reports for all tanks involved in the fragility analyses. It should be pointed out that reports do not provide the exact percentage of liquid losses and then, this information appears qualitative only. Further information on characterization of tank structural damage and amount of content released will be given later in a dedicated section. Table 3.2 provides a synthetic description of the physical characteristics of the database tanks. The number of tanks for which this information is available is also listed.

Table 3.2. Physical characteristics of database tanks

Parameter	Range	Average Value	Median Value	Number of Tanks
Size (H/D)	0.17 – 4.17	0.69	0.31	1336 (44%)
Percentage Full	0% - 100%	65%	75%	422 (14%)
Anchorage system	-	-	-	375 (12%)
Date of construction/Design code	-	-	-	477 (16%)
Roof type	-	-	-	505 (17%)
Foundation type	-	-	-	242 (8%)

3.7. Criteria used for defining PGA values

Different reports are often inconsistent on PGA. Discrepancies may result from several factors: i) the lack of ground motion recording stations close to the tanks, ii) the use of different

attenuation models for the PGA estimation, iii) the lack of information on soil properties, iv) the uncertainties on the location of tanks, v) the spatial variability of PGA.

In this work, in order to provide consistent values of PGA for each tank involved in fragility analysis, the following procedure was used:

- in case of a ground-motion recording station in the site of the plant, information from recorded data was used;
- in cases of tanks located far from recording stations, the PGA value was obtained from ShakeMap, a tool provided by the web site of "United States Geological Survey's (USGS) Earthquake Hazards Program"[129].
- Finally, in case of older earthquake, for which shake maps were not available, the attenuation model proposed by D. M. Boore et al. was used (provided by "Pacific Earthquake Engineering Research Centre" in *NGA-West2 Equations for Predicting Response Spectral Accelerations for Shallow Crustal Earthquakes* [120]).

Table 3.3 shows the PGA definition method used for each earthquake in database (only tanks involved in fragility analysis).

Table 3.3. Method of acquisition of PGA value for each seismic event involved in fragility analysis

Seismic event	***Method used for the PGA acquisition***
Long Beach, 1933	Attenuation model (PEER Center)
Kern County, 1952	Attenuation model (PEER Center) Recorded acceleration
Alaska, 1964	Recorded acceleration
San Fernando, 1971	ShakeMap USGS Recorded acceleration
Managua, 1972	Recorded acceleration
Miyagi, 1978	Recorded acceleration
Imperial Valley, 1979	ShakeMap USGS
Greenville, 1980	ShakeMap USGS
Coalinga, 1983	Attenuation model (PEER Center) Shake Map USGS Recorded acceleration
Chile, 1985	ShakeMap USGS Recorded acceleration
Adak, 1986	Recorded acceleration
New Zealand, 1987	Recorded acceleration
Loma Prieta, 1989	ShakeMap USGS Recorded acceleration
Costa Rica, 1991	ShakeMap USGS
Landers, 1992	ShakeMap USGS Recorded acceleration
Northridge, 1994	ShakeMap USGS Recorded acceleration
Tokachi-oki, 2003	ShakeMap USGS
Bam, 2003	ShakeMap USGS
Central Peru, 2007	ShakeMap USGS
Chile, 2010	ShakeMap USGS Recorded acceleration
Napa Valley, 2014	ShakeMap USGS

The diagram shown in Figure 1 synthetizes the procedure used for acquiring the PGA value for earthquake considered.

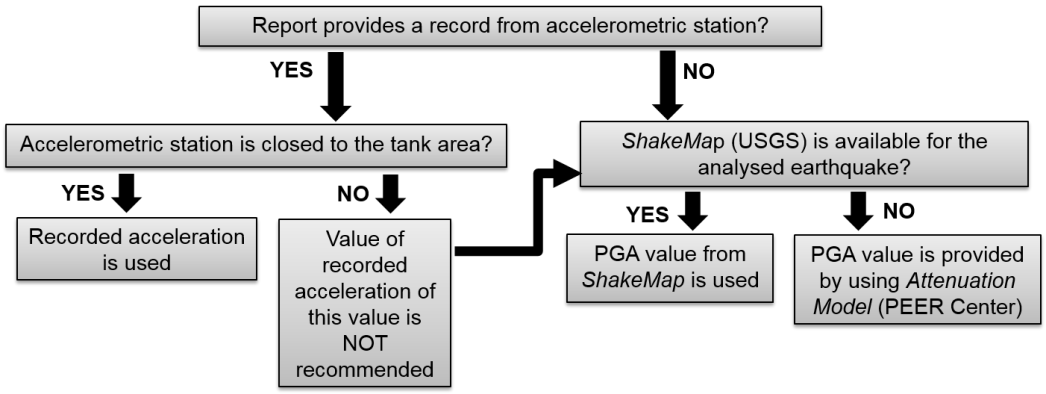

Figure 3-19. Procedure used for acquisition of PGA value

3.7.1. ShakeMap

ShakeMap is a tool used to portray the extent of potentially damaging shaking following an earthquake. It can be used for emergency response and loss estimation. ShakeMap was first developed for earthquakes in southern California as part of the TriNet Project, a joint effort by U.S. Geological Survey (USGS), California Institute of Technology (Caltech), and the California Geological Survey (CGS) [121]. Following the Northridge earthquake in 1994, older analog instruments were replaced with a state-of-the-art seismic network with digital communications in real time. Deployment was completed in 2002. Because the earthquake happens over a faults surface, not at a single point, the location of the earthquake (the epicenter) tells us only where the earthquake started, not necessarily where the shaking was the greatest. For a large earthquake, damage can sometimes occur hundreds of miles from the epicenter. Other factors, such as rupture direction and local geology, influence the amount of shaking in a particular area. It is the distribution of intensity (local severity of shaking), rather than the magnitude (the total energy released by earthquake), that provides useful information about areas prone to damage.

Philosophy of estimating and interpolating ground motions

The overall strategy for the deployment of stations relies on dense instrumentation concentrated in urban areas with high seismic hazards (USGS, 1999) and fewer stations in outlying areas [130]. Based on this philosophy, maps generated in these urban regions are expected to be most accurate where the population at risk is the greatest, and therefore, where emergency response and recovery efforts will likely be most urgent and complex. Even so, significant gaps in the observed shaking distribution will likely remain, especially in the transition from urban to more rural environments. Likewise, many critical facilities and lifelines are widely distributed, away from population centers and their dense seismic sensor networks. Thus, as a fundamental strategy for ShakeMap, USGS has developed algorithms to best describe the shaking in more remote areas by utilizing a variety of seismological tools.

If there were stations at each of the tens of thousands of map grid points needed to adequately portray shaking, then the creation of shaking maps would be relatively simple. Of course, stations are not available for the overwhelming majority of these grid points, and in many cases grid points may be tens of kilometers or more from the nearest reporting station. The overall mapping philosophy is then to combine information from individual stations, site amplification characteristics, and ground-motion prediction equations for the distance to the hypocenter (or to the causative fault) to create the best composite map. The procedure should produce

reasonable estimates at grid points located far from available data while preserving the detailed shaking information available for regions where there are stations nearby.

Recorded ground-motion parameters

ShakeMap requires estimates of magnitude, location, and (optionally) shaking IMs at seismic stations. As such, ShakeMap has been interfaced with several types of seismic processing systems. The ShakeMap system, however, is a stand-alone software package and itself contains no data acquisition component. It is assumed that station data delivered to ShakeMap are free-field sites that have been vetted by the contributing network. For global and historic earthquake ShakeMap generation, USGS has developed scripts to preprocess various forms of seismic waveform (as well as macroseismic) data which are openly available around the world.

Parametric data from stations serving ShakeMap should include peak ground acceleration (PGA), peak ground velocity (PGV), and peak response spectral acceleration amplitudes (at 0.3, 1.0, and 3.0 sec). For all maps and products, the motions depicted are peak values as observed; that is, the maximum value observed on the two horizontal components of motion.

Macroseismic intensity

Intensity data can fill important gaps where ground-motion recordings are not available, and often provide the only control in sparsely instrumented areas. This is particularly true for historic earthquakes, for which macroseismic data provide important constraints on shaking intensities. The ShakeMap Atlas (Allen et al., 2008, 2009a; Garcia et al., 2012a) is a collection of important historic earthquake shaking maps which are now widely used for scientific analyses and for loss model calibration (e.g., Wald et al., 2008; Jaiswal and Wald, 2010; Pomonis and So, 2011).

Macroseismic intensity data can also be an important constraint on peak ground motions, since ground motion amplitudes can be derived from intensity through the use of a suitable Ground-Motion/Intensity Conversion Equation (GMICE). Because a GMICE represents a statistical (probabilistic) relationship, the conversion to and from intensity has a higher uncertainty than direct ground-motion observation. ShakeMap accounts for this higher uncertainty by down-weighting converted observations in the interpolation process.

Ground motion and intensity predictions

In areas distant from the control of seismic instrumentation or reported intensity, ground motions must be estimated using the available earthquake source parameters and GMPEs or Intensity Prediction Equations (IPEs). GMPEs are available for a wide range of magnitudes, source mechanisms, and tectonic settings. IPEs are still comparatively uncommon.

3.7.2. Attenuation model

Attenuation model used in the current work for estimation of tank PGA has been provided by the *Pacific Earthquake Engineering Research (PEER) Center* in "NGA-West2 Equations for Predicting Response Spectral Accelerations for Shallow Crustal Earthquakes" [120]). This work proposed ground-motion prediction equations (GMPEs) for the computation of a median peak ground motions and response spectra for shallow crustal earthquakes in active tectonic regions. The equations were developed as a part of the NGA-West 2 project and are based on a composite data set [131] that includes global events from 1935 to 2011 spanning a wide magnitude range, plus a large number of small-to-moderate magnitude events from California principally from 1998 to 2011.

Ground-motion prediction equations (GMPEs) are used in seismic hazard applications to specify the expected levels of shaking as a function of predictor variables such as earthquake magnitude and distance. GMPEs for active crustal regions are typically developed from an empirical regression of observed amplitudes against an available set of predictor variables. Early GMPEs were very simple equations giving peak ground acceleration as a function of magnitude and epicentral distance (e.g., Douglas in [132]). Modern GMPEs express peak motions and response spectra as functions of moment magnitude, distance to the rupture surface, and site condition variables such as the time-weighted average shear-wave velocity over the upper 30 m of the profile (V_{S30}). The Prediction of horizontal-component peak ground acceleration (PGA), peak ground velocity (PGV) and response spectra (PSA, the 5% damped pseudo response spectral acceleration) is limited to the case of earthquakes of moment magnitude 3.0 to 8.5, at distances from 0 to 400 km, at sites having V_{S30} in the range from 150 m/sec to 1500 m/sec, for periods between 0.01 sec and 10 sec.

Form of the equation

The functional forms of the equation for predicting ground motions is:

$$\ln Y = F_E(M, mech) + F_{P,B}(R_{JB}, M) + F_{S,B}(V_{s30}, R_{JB}, M) + \varepsilon_n \sigma(M, R_{JB}, V_{S30}) \quad (3.1)$$

where lnY represents the natural logarithm of a ground-motion IM (PGA, PGV, or PSA); F_E , $F_{P,B}$, and $F_{S,B}$ represent the source-dependent function ("E" for "event"), path function ("P"), and site amplification function ("S"), respectively (subscript 'B' indicates base-case model; not used for event function since the same equations are used for the base-case and adjusted models). The predictor variables are M, *mech*, R_{JB} , and V_{S30} , which represent moment magnitude, fault type, Joyner-Boore distance (defined as the closest distance to the surface projection of the fault), and time-weighted average shear-wave velocity over the top 30 m of the site, respectively; ε_n is the fractional number of standard deviations of a single predicted value of lnY away from the mean value of lnY; σ is the total standard deviation of the model. The F_E , $F_{P,B}$, and $F_{S,B}$ and σ functions are period dependent.

Path and Source Functions

The base-case path-dependent function is given by:

$$F_{P,B}(R_{JB,}M) = [c_1 + c_2(M - M_{ref})]\ln(R / R_{ref}) + c_3(R - R_{ref}) \quad (3.2)$$

where

$$R = \sqrt{R_{JB}{}^2 + h^2} \quad (3.3)$$

and c_1, c_2, c_3, M_{ref}, R_{ref}, and h are the coefficients determined by regression.

The event-specific function is given by:

$$F_E(M, mech) =$$

$$e_0 U + e_1 SS + e_2 NS + e_3 RS + e_4(M - M_h) + e_5(M - M_h)^2 \qquad M \le M_h \quad (3.4)$$

$$e_0 U + e_1 SS + e_2 NS + e_3 RS + e_6(M - M_h) \qquad M \ge M_h \quad (3.5)$$

where $U, SS, NS,$ and RS are dummy variables (taking on value of 1 or 0, as indicated in Table 3.4) used to specify unspecified, strike-slip, normal-slip, and reverse slip fault types, respectively; M_h, the "hinge magnitude" for the shape of the magnitude scaling, is a coefficient to be set during the analysis. M_h is period-dependent; in the case of PGA prediction ($T = 0$), $M_h = 5.5$.

Table 3.4Values of dummy variables for different fault types [120]

Fault Type	U	SS	NS	RS
Unspecified	1	0	0	0
Strike-slip	0	1	0	0
Normal-slip	0	0	1	0
Reverse-slip	0	0	0	1

Site Term

The nonlinear site amplification component of the base-case GMPE (introduced in Eq. (3.1)) is comprised of two additive terms representing V_{S30}-scaling and nonlinearity as follows:

$$F_{S,B} = \ln(F_{lin}) + \ln(F_{nl}) \tag{3.6}$$

where $F_{S,B}$ represents site amplification in natural logarithmic units; F_{lin} represents the linear component of site amplification, which is dependent on V_{S30}; and F_{ln} represents the nonlinear component of site amplification, which depends on V_{S30} and the amplitude of shaking on reference rock (taken as $V_{S30} = 760$ m/sec).

The linear component of the model (F_{lin}) describes the scaling of ground motion with V_{S30} for linear soil response conditions (i.e., small strains) as follows:

$$\ln(F_{lin}) = \begin{cases} c \ln\left(\dfrac{V_{S30}}{V_{ref}}\right) & V_{S30} \le V_c \quad (3.7) \\ c \ln\left(\dfrac{V_c}{V_{ref}}\right) & V_{S30} > V_c \quad (3.8) \end{cases}$$

where c describes the V_{S30}-scaling in the model, V_c is the limiting velocity beyond which ground motions no longer scale with V_{S30}, and V_{ref} is the site condition for which the amplification is unity (taken as 760 m/sec). Parameters c and V_c are period-dependent and are determined by regression.

The nonlinear term in the site amplification model (F_{ln}) modifies the linear site amplification so as to decrease amplification for strong shaking levels. The F_{ln} term is constructed so as to produce no change relative to the linear term for low PGA_r levels. The functional form for the F_{ln} term is as follows:

$$\ln(F_{nl}) = f_1 + f_2 \ln\left(\frac{PGA_r + f_3}{f_3}\right) \quad (3.9)$$

where f_1, f_2 and f_3 are coefficients in the model and PGA_r is the median peak horizontal acceleration for reference rock (taken as 760 m/sec). The coefficient f_1 is taken equal to zero to force $\ln(F_{ln})$ to zero for $PGA_r \ll f_3$, whereas the coefficient f_3 is taken equal to 0.1g. Finally f_2 is a function of period and V_{S30} as follows:

$$f_2 = f_4[\exp\{f_5(\min(V_{s30}, 760) - 360)\} - \exp\{f_5(760 - 360)\}] \quad (3.10)$$

In order to apply the site amplification function, one must first evaluate PGA_r for applicable magnitude and distance using Eq. (3.1) for rock site conditions.

4. Seismic fragility formulations

4.1. Introduction

This section provides a technical description of the seismic fragility analysis carried out for on-grade steel storage tanks. The development of fragility formulation has been widely used by many researchers in the past as a means to investigate the seismic behavior of liquid storage tanks. This approach has the advantage to directly provide an estimate of damage and loss of content, parameters required for risk assessment. O'Rourke and So [8] characterized the seismic behavior of cylindrical on-grade steel storage tanks developing fragility curves using a logistic regression analysis of the performances of 397 tanks in nine earthquake events. The damage states adopted to characterize damage were consistent with the damage state description in the HAZUS methodology. Fragility relations were obtained as a function of the aspect ratio and filling percentage. Comparison with HAZUS fragilities and other seismic performance relations contained in literature, as *ATC 13* (1985) [133] and *ATC 25* (1991) [134], was also provided. American Lifeline Alliance (hereafter ALA, [135]) obtained tank fragilities using a bigger collection of data including 532 tanks exposed to 21 earthquakes and a slightly different definition of damage states, based on tank functionality. Least square regression was used for estimation of the median acceleration to reach a particular damage state and the associated lognormal dispersion parameter. The influence of filling level and anchorage was also investigated. Berahman [67] analyzed steel storage tanks with fill level higher than 50% from ALA's database and calculated seismic fragility of unanchored tanks adopting a Bayesian approach. The author adopted ALA's damage states. The comparison with tank fragilities available in literature suggested that the actual tank performance was better than that proposed in ALA and O'Rourke. Salzano et al. [10] proposed empirical fragilities in terms of content release intensity, adopting probit analysis. The tank database used was almost the same of previous studies, but in this case authors divided tanks into release states, depending on the loss of content caused by damage. Seismic tank performance and release entity were analyzed and discussed in the framework of Quantitative Risk Analysis.

Although a consistent number of researches have been conducted on this issue, past databases counted a relatively small number of samples. Moreover, in most cases, development of fragility curves was based on the usage of damage matrixes, in which tanks were divided into PGA bins, and the value of dispersion parameter was bounded a priori [8–10]. In light of that, the objective of the study reported herein is to evaluate the seismic fragility of atmospheric on-grade steel tanks using a bigger collection of damage information (presented and discussed Chapter 3) and trying to overcome the limits of previous works.

The current section presents first a critical overview of data collection and fragility relations available in current literature, pointing out the main problems related to the management of damage information from visual inspections, choice of criteria for classifying damage into ranges, relation between reparability and functionality after damage occurrence, choice of appropriate method for fitting empirical function and interpretation of results. The present work establishes two sets of Damage States. The first set characterizes failures in terms of tank structural performance, the second in terms of loss of content. A Bayesian approach has been used to fit fragility curves. Generalized linear model with probit and logit functions have been employed in order to derive seismic fragilities as function of tank aspect ratio, filling level of the liquid content and presence of base anchorage system. One of these models has been formulated in order to take into account simultaneously the effects on fragility of these crucial aspects. A critical comparison with previous works in terms of damage states, analysis method adopted and results obtained is also presented.

4.2. Statistical procedures for developing seismic fragility curves

Earthquake damage to ground motion relationships is a key component for earthquake loss estimation and the performance-based analysis of the risk of structures [61]. These relationships, also known as fragility curves, describe the probability of experiencing or exceeding a certain damage level as a function of ground-shaking intensity.

It is possible to distinguish three general classes of fragility functions basing on the method used to create them [136]:

1. *Empirical fragility curves* are based on post-earthquake damage evaluation data. They are obtained by fitting a function to approximate observational data from the laboratory or the real world. The observational data can be: (1) ordered pairs of environmental excitation and a binary indicator of failure (i.e., reaching or exceeding the specified limit state), for each of a set of individual assets; or (2) ordered sets of environmental excitations, number of assets exposed to that level of excitation, and the number of those that failed when subjected to the environmental excitation [8–10,67,137,138].

2. *Analytical fragility curves* based on structural modeling and response simulations. The performance of the structure is a function of some vector of "basic" variables. These variables determine both the capacity of a structure to withstand a load and the demand placed on the structure. Once the limit function, or limit state, is defined the probability of exceedance the limit states is calculated [139–141].

3. *Expert opinion or judgment-based fragility curves* are created by polling one or more people who have experience with the asset class in question, where the experts guess or judge failure probability as a function of environmental excitation. ATC- 13 (Applied Technology Council 1985) compiles a large number of judgment-based fragility functions for California buildings [142,143].

Fragility functions can also be obtained by a combination of these methods. For example, many of the fragility curves in HAZUS-MH's earthquake module are created by such a hybrid approach. As before mentioned, in this work the empirical method has been used to develop seismic fragility curves of tanks. Information about damage is provided by the database assembled for purpose of analysis (described in Chapter 3 and given in Appendix A).

4.3. Critical analysis of fragility models available in literature

In the context of fragility curves based on post-earthquake damage data, one of the most significant researches proposed in literature is the statistical study on on-grade steel tanks provided by O'Rourke and So in 1999 [8]. The authors developed fragility curves by building a database on the seismic performance of 423 tanks damaged by nine earthquakes (379 out of the total number were involved in analysis). PGA values ranged from 0.10 to 1.20g. Based upon the physical description of each tank seismic performance, derived from the database source documents, O'Rourke and So assigned to each tank one of the five HAZUS damage states, formulated in terms of functionality, as described below in Table 4.1

Table 4.1. O'Rourke damage state definition and distribution within database (adapted from [8])

Damage State	***Description***	***Number of Tanks***
DS1	No damage to tank or I/O pipes	257
DS2	Damage to roof, minor loss of content, minor shell damage, minor piping damage, no elephant foot buckling	102
DS3	Elephant foot buckling with no leak or minor loss of contents	33
DS4	Elephant foot buckling with major loss of contents, severe damage	15
DS5	Total failure, tank collapse	16

Table 4.2. HAZUS damage states used for building-type structures

HAZUS Damage State	***Description***
DS1	No damage
DS2	Slight damage
DS3	Moderate damage
DS4	Extensive damage
DS5	Complete (collapse) damage

A possible issue related to these Damage States is that they do not distinguish the severity of failure at the piping system and treat in the same manner damage to inlet/outlet pipes, pressure relief line, overflow pipe and other pipe appurtenances. In fact, all piping failures were associated uniquely to Damage State 2. In terms of functionality, this choice may result inappropriate since the entity of content loss is completely different according to the location of piping-shell coupling. A further issue is that the HAZUS Damage States, described in Table 4.2 and developed for use with building-type structures, were adopted. For buildings it is reasonable to assume that increasing damage states also relate to increasing severity of failure and decreasing functionality. Contrarily, in case of tanks, this criterion is not always reliable. Failure to piping, categorized as DS2, can lead to a complete loss of content and put tank out of service, even if repair costs could be inexpensive. On the other hand, repair cost of the shell in case of occurrence of elephant foot buckling without loss of content, regarded as DS3, could be much more expensive, yet the tank might not lose any functionality immediately after the earthquake. Table 4.3, defined by combining the damage states used by O'Rourke and information on repair costs and loss functionality reported by ALA 2001, confirms that in case of storage tanks, there is not a direct correlation between repair costs and functionality, as assumed for common buildings.

Table 4.3. Repair costs and impact on functionality related to DSs obtained by following HAZUS criteria

Damage State (O'Rourke and So)	***Failure Mode***	***Repair Costs as a Percentage of Replacement Cost***		***Impact on Functionality as a Percentage of Contents Lost Immediately After the Earthquake***	
		For Each Failure Mode	***For Damage State***	***For Each Failure Mode***	***For Damage State***
DS1	No damage to tank or I/O pipes	0%	0%	0%	0%
DS2	Rupture of overflow pipe	1% - 2%	1% - 30%	0% - 2%	0%-100%
	Rupture of drain pipe	1% - 2%		50%-100%	
	Rupture of Inlet/Outlet Pipe	1% - 5%		100%	
	Roof system partial damage	2% - 20%		0%-10%	
	Roof system collapse	5% - 30%		0%-20%	
DS3	Elephant foot buckling with no leak	30% - 80%	30% - 80%	0%	0%
DS4	Elephant foot buckling with leak	40% - 100%	40% - 100%	100%	100%
DS5	Total failure, tank collapse	100%	100%	100%	100%

O'Rourke binned tanks into 8 PGA intervals and calculated the logit function for each PGA range and Damage State. Linear regression was then used to define fragility as a function of PGA. However, a regression in which data is binned based on the value of the covariate (in this case IM) is highly sensitive to the binning scheme. The authors calculated tank fragilities for their full database, for tanks with aspect ratio $H/D \geq 0.7$ and $H/D < 0.7$, and for tanks with filling level $FL \geq 50\%$ and $FL < 50\%$. In order to allow comparisons with the HAZUS model, lognormal fragility functions were deducted from logistic regression curves. Median value of the lognormal distribution m_j and standard deviation σ_j of $ln(PGA)$ for each Damage States are summarized in Table 4. In order to allow a direct comparison with results obtained in this work, the median value μ_j of the associated normal distribution of $ln(PGA)$ has been reported in table as well. By examining results, authors concluded that squat tanks behave better than slender tanks and filling level contributes to worsen tank seismic performance.

Table 4.4. O'Rourke empirical parameters for fragility curves (adapted from [15]*)*

	Damage States			
Fragility parameters	$\boldsymbol{DS \geq 2}$	$\boldsymbol{DS \geq 3}$	$\boldsymbol{DS \geq 4}$	$\boldsymbol{DS = 5}$
All tanks (N=397)				
$\boldsymbol{m[g]}$	0.70	1.10	1.29	1.35
$\boldsymbol{\mu[ln(g)]}$	-0.36	0.10	0.25	0.30
$\boldsymbol{\sigma[ln(g)]}$	0.48	0.35	0.28	0.22
Tanks with H/D < 0.70				
$\boldsymbol{m[g]}$	0.67	1.18	1.56	1.79
$\boldsymbol{\mu[ln(g)]}$	-0.40	0.17	0.44	0.58
$\boldsymbol{\sigma[ln(g)]}$	0.50	0.34	0.35	0.29
Tanks with H/D ≥ 0.70				
$\boldsymbol{m[g]}$	0.45	0.69	0.89	1.07
$\boldsymbol{\mu[ln(g)]}$	-0.80	-0.37	-0.12	0.07
$\boldsymbol{\sigma[ln(g)]}$	0.47	0.32	0.21	0.15
Tanks with FL < 50%				
$\boldsymbol{m[g]}$	0.64	-	-	-
$\boldsymbol{\mu[ln(g)]}$	-0.45	-	-	-
$\boldsymbol{\sigma[ln(g)]}$	0.41	-	-	-
Tanks with FL ≥ 50%				
$\boldsymbol{m[g]}$	0.49	0.86	0.99	1.17
$\boldsymbol{\mu[ln(g)]}$	-0.71	-0.15	-0.01	0.16
$\boldsymbol{\sigma[ln(g)]}$	0.55	0.39	0.27	0.21

Another significant contribution was provided by ALA 2001 [9]. The authors reviewed and amplified the inventory developed by Cooper [2]. The new database contained 532 tanks in a PGA range from 0.10-1.20g with an average value of 0.32 g. Moreover, ALA modified the definition of Damage States, in particular for the case of piping damage: slight damage to pipe causing only minor leaks (such as damage to overflow or relief pipe) was treated as DS=2, while broken inlet/outlet pipe allowing a consistent loss of content was assigned to DS=4. This way of classifying damage is more consistent with functionality than with repair costs. Substantial buckling to the upper courses is defined as DS=3, contrarily to O'Rourke's work, in which it was classified as DS=2. In order to fit fragility models, authors divided tanks into 9 PGA ranges. For each range the PGA was defined as the average of the PGA values of each tank in that range and the percentage of tanks reaching or exceeding a Damage State was calculated. A least square regression analysis was performed to fit lognormal fragility curves. The dispersion parameter σ was bounded in the interval 0.01 to 0.80. Fragility parameters m, μ and σ are shown in Table 4.5 and Table 4.6 as a function of the effect of filling level and presence of anchorage.

From a critical analysis of their results the authors deducted that an increasing filling level leads to a decrement of the median acceleration levels to reach a certain damage states. Furthermore, they concluded that tanks with filling levels below 50% do not experience elephant foot buckling with leakage or collapse. Moreover, anchored tanks perform better than unanchored tanks. It should be noted, however, that database counted only 46 anchored tanks against the 251 unanchored, and tanks with unknown anchorage condition were assumed to be unanchored.

Table 4.5. ALA empirical parameters for fragility curves as a function of fill level (adapted from [9])

	Damage States			
Fragility parameters	$DS \geq 2$	$DS \geq 3$	$DS \geq 4$	$DS = 5$
All tanks (N=531)				
$m[g]$	0.38	0.86	1.18	1.16
$\mu[ln(g)]$	-0.97	-0.15	0.17	0.15
$\sigma[ln(g)]$	0.80	0.80	0.61	0.07
Tanks with FL < 50% (N=95)				
$m[g]$	0.56	>2.00	-	-
$\mu[ln(g)]$	-0.58	-	-	-
$\sigma[ln(g)]$	0.80	0.40	-	-
Tanks with FL ≥ 50% (N=251)				
$m[g]$	0.18	0.73	1.14	1.16
$\mu[ln(g)]$	-1.71	-0.31	0.13	0.15
$\sigma[ln(g)]$	0.80	0.80	0.80	0.40
Tanks with FL ≥60% (N=209)				
$m[g]$	0.22	0.70	1.09	1.16
$\mu[ln(g)]$	-1.51	-0.36	0.09	0.15
$\sigma[ln(g)]$	0.80	0.80	0.80	0.41
Tanks with FL ≥ 90% (N=120)				
$m[g]$	0.13	0.67	1.01	1.15
$\mu[ln(g)]$	-2.04	-0.40	0.01	0.14
$\sigma[ln(g)]$	0.07	0.80	0.80	0.10

Table 4.6. ALA empirical parameters for fragility curves as a function of filling level and anchorage (adapted from [9])

	Damage States			
Fragility parameters	$DS \geq 2$	$DS \geq 3$	$DS \geq 4$	$DS = 5$
Tanks with FL ≥ 50% (N=251)				
$m[g]$	0.18	0.73	1.14	1.16
$\mu[ln(g)]$	-1.71	-0.31	0.13	0.15
$\sigma[ln(g)]$	0.80	0.80	0.80	0.80
Tanks with FL ≥ 50%, Anchored, (N=46)				
$m[g]$	0.71	2.36	3.72	4.26
$\mu[ln(g)]$	-0.34	0.86	1.31	1.45
$\sigma[ln(g)]$	0.80	0.80	0.80	0.80
Tanks with FL ≥ 50%, Unanchored, (N=205)				
$m[g]$	0.15	0.62	1.06	1.13
$\mu[ln(g)]$	-1.90	-0.48	0.06	0.12
$\sigma[ln(g)]$	0.12	0.80	0.80	0.10

Some critical remarks should be made on the regression procedure adopted by ALA (2001). As already mentioned, a least square regression analysis was performed to fit lognormal fragility curves, and the dispersion parameter σ was bounded in the interval 0.01 to 0.80. It should be noticed that in many cases (see Table 4.5 and Table 4.6) the estimated value for σ corresponds to the upper bound assumed by the authors. In these cases, $\sigma = 0.80$ is not the true dispersion of the data used, since it was bounded a priori in the regression procedure, which might be questionable because it forces the shape of fragility curve. Indeed, if no bounds were applied to the dispersion parameter, results from the same statistical procedure would be different. In order to demonstrate that, the ALA method (i.e. regression procedure and tank database) has been used in this work for deriving fragility curves without bounding the dispersion parameter, hereafter "unforced procedure". On the contrary, the procedure adopted by ALA (2001) in [9,66] and whose results are shown in Table 4.5 and Table 4.6, hereafter is called "forced procedure" since it bounds the dispersion parameter and forces the shape of fragility curves. In particular, the analyses on all tanks of the ALA database has been compared in this section. Table 4.7 shows results in terms of fragility parameters m, μ and σ from the "unforced procedure" above explained. These values must be compared with results from the "forced procedure" for all tanks in Table 4.5.

Figures 4.1 - 4.4 compare for each damage states, the fragility curve obtained from the forced procedure (red) and that from the unforced one (black). Comparison between results shows that, when in the regression procedure the dispersion parameter is bounded (Table 4.5, all tanks, $DS \geq 2$ and $DS \geq 3$), its value can be far from the "true" value obtained from the not bounded analysis (Table 4.7, all tanks, $DS \geq 2$ and $DS \geq 3$) . Median values has been found to change as well. It should be noted that no differences between the two calculations are obtained for $DS \geq 4$ and $DS = 5$, since in these cases the true dispersion parameter σ was already under the limit 0.80.

Table 4.7. "Unforced procedure":Empirical parameter for fragility curves obtained in this work by adopting the ALA method (procedures and tank database) without bounding the dispersion parameter

	Damage States			
Fragility parameters	$\boldsymbol{DS \geq 2}$	$\boldsymbol{DS \geq 3}$	$\boldsymbol{DS \geq 4}$	$\boldsymbol{DS = 5}$
All tanks (N=531)				
$\boldsymbol{m[g]}$	0.52	1.17	1.18	1.16
$\boldsymbol{\mu[ln(g)]}$	-0.65	0.16	0.17	0.15
$\boldsymbol{\sigma[ln(g)]}$	1.65	1.28	0.61	0.07

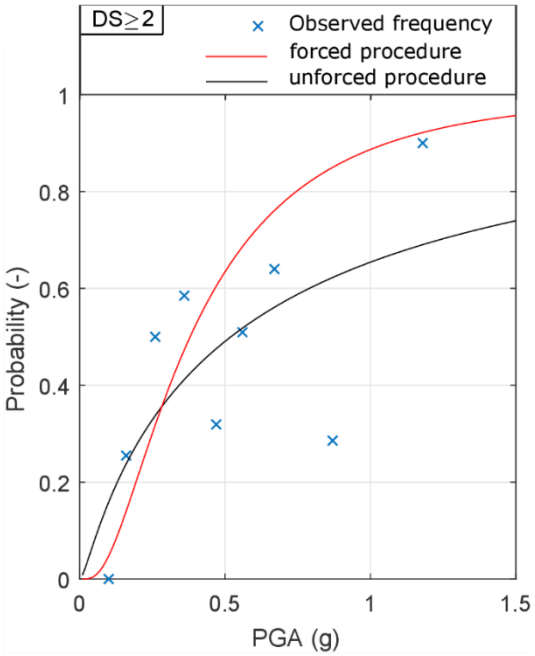

Figure 4-1. Comparison between forced (Table 4.5,4.6) and unforced procedure (Table 4.7) on ALA database for DS≥2 (all tanks N=531)

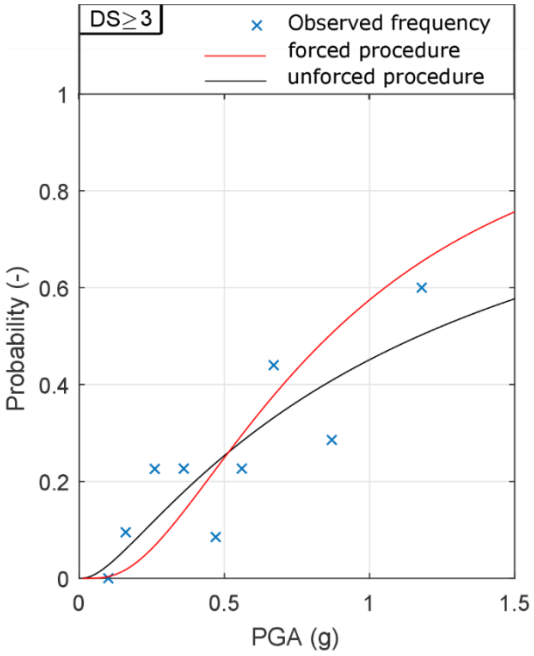

Figure 4-2. Comparison between forced (Table 4.5,4.6) and unforced procedure (Table 4.7) on ALA database for DS≥3 (all tanks N=531)

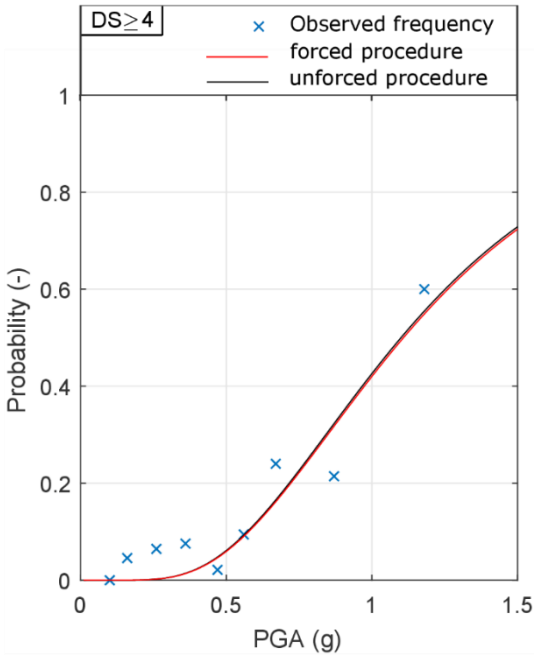

Figure 4-3. Comparison between forced (Table 4.5,4.6) and unforced procedure (Table 4.7) on ALA database for DS≥4 (all tanks N=531)

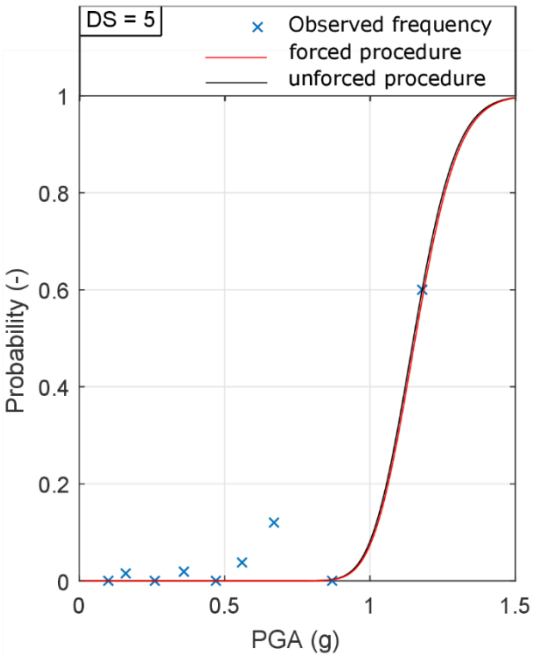

Figure 4-4. Comparison between forced (Table 4.5,4.6) and unforced procedure (Table 4.7) on ALA database for DS=5 (all tanks N=531)

The third significant contribution to the technical literature was provided by Salzano et al. [10]. Authors obtained fragility curves based on damage states in terms of content release by analyzing the collection of data provided by ALA (2001). The dataset was reorganized in term of Risk States (RS) with reference to the loss of content, as shown in Table 4.8.

Table 4.8. Salzano et al. damage state definition and distribution within database (adapted from [10])

Risk State	***Description***	***Number of Tanks***
RS1	Negligible loss of content	332
RS2	Structural damage of shell or auxiliary equipment allowing slight loss of content	159
RS3	Extended or catastrophic damage resulting in total loss of content	41

In case of RS2, it was assumed that safety procedures and technical staff are able to avoid or mitigate the risk of major accident and to restore plant functions in ten minutes at least. On the contrary, RS3 represented catastrophic failure of tank or piping system, causing huge quantity of released content, so it is not possible to mitigate subsequent accidents like pool fire, flash fire, vapor cloud explosion and toxic dispersion. Also in this case, tanks in database were divided into PGA bins and probit regression was adopted to obtain the probability of damage in terms of loss of content with respect to PGA. Also in this case, the authors set the highest value of the dispersion parameter σ to be equal to 0.80. As above demonstrated in case of ALA fragility curves, this regression procedure might be questionable because it forces the shape of fragility curve and values of μ and σ can be far from the "true" ones obtained from the not bounded analysis. Fragility parameters m, μ and σ are given in Table 4.9. As obtained from previous works analyzed, results showed that full tanks are more fragile than either empty or half-filled tanks. Base anchors increase the median acceleration to reach RS2 and RS3 for any filling level.

Table 4.9. Salzano et al. empirical parameters for fragility curves as a function of filling level and anchorage (adapted from [10])

	Risk States	
Fragility parameters	$\boldsymbol{RS \geq 2}$	$\boldsymbol{RS = 3}$
All tanks		
$\boldsymbol{m[g]}$	0.38	1.18
$\boldsymbol{\mu[ln(g)]}$	-0.97	0.17
$\boldsymbol{\sigma[ln(g)]}$	0.80	0.61
Tanks with FL < 50%, All anchorage conditions		
$\boldsymbol{m[g]}$	0.18	1.14
$\boldsymbol{\mu[ln(g)]}$	-1.71	0.13
$\boldsymbol{\sigma[ln(g)]}$	0.80	0.80
Near full tanks, Anchored		
$\boldsymbol{m[g]}$	0.30	1.25
$\boldsymbol{\mu[ln(g)]}$	-1.20	0.22
$\boldsymbol{\sigma[ln(g)]}$	0.60	0.65
Tanks with FL ≥50%, Anchored		
$\boldsymbol{m[g]}$	1.71	3.72
$\boldsymbol{\mu[ln(g)]}$	0.54	1.31
$\boldsymbol{\sigma[ln(g)]}$	0.80	0.80
Near full tanks, Unanchored		
$\boldsymbol{m[g]}$	0.15	1.06
$\boldsymbol{\mu[ln(g)]}$	-1.90	0.06
$\boldsymbol{\sigma[ln(g)]}$	0.70	0.80
Tanks with FL ≥50%, Unanchored		
$\boldsymbol{m[g]}$	0.15	1.06
$\boldsymbol{\mu[ln(g)]}$	-1.90	0.06
$\boldsymbol{\sigma[ln(g)]}$	0.12	0.80

4.4. Characterization of tank damage

The present work establishes two sets of Damage States, the first based on structural damage and the second base on loss of content severity.

4.4.1. Definition of damage states

The first set of damage states characterizes failures in terms of tank structural performance and it consists of five Damage States. Table 4.10 provides a description of each damage state and the number of tanks classified accordingly.

Table 4.10. Damage State definition used in the present work

Damage State	***Description***	***Number of Tanks***
DS1	No damage or slight damage to tank wall, bottom plate, minor damage to piping system	2786
DS2	Damage to roof and upper part of shell due to sloshing	72
DS3	Damage to piping system	59
DS4	Slight elephant foot buckling, damage to the shell-bottom plate junction	59
DS5	Extensive elephant foot buckling, damage to the shell-bottom plate junction, severe damage to the shell or bottom plate, total failure, tank collapse, overturning.	50

Damage states proposed herein introduce some differences compared to those originally established by HAZUS methodology for building-type structure, and later adopted for tanks by O'Rourke and ALA [8,9]. In fact, normally the severity of failure increases as the damage state increases. Whereas, following the definition of DSs adopted in this work, the severity of failure increases from DS1 to DS5 except for DS2, the damage state related to failure at roof and upper shell courses. This consideration has been suggested by a critical analysis of the relation between the intensity measure adopted, i.e. the peak ground acceleration, and tank damage. Contrary to the other failures, damage to the upper part of tank is strictly related to the sloshing motion of the liquid contained. In case of squat tanks, convective hydrodynamic pressure becomes very high compared to the corresponding component in slender tanks and the strong impact of liquid waves can easily cause damage to the upper part of the wall, to roof and to roof-wall junction, allowing liquid spillage [2]. On the other hand, failures included in Damage States from DS3 to DS5, (failure at piping system, lower part of shell, bottom-shell junction, EFB etc.), are related to the tank bulging motion, i.e. the motion of liquid moving in unison with shell wall, and also to the tank rocking motion, for unanchored tanks. The natural period of sloshing system is known to be far from that of bulging [144]. The bulging motion is excited mainly by short period accelerations, while sloshing motion by longer period accelerations. In addition, PGA is not strongly correlated to the spectral acceleration for long periods, so it might not be a very effective intensity measure for damage states associated with tank sloshing. This is also demonstrated by analyzing distribution of damage versus PGA, for tanks with filling level greater or equal to 50%, as shown in Figure 4-5. In particular, this figure shows the ratio between the number of damaged tanks and the total number in different PGA intervals. Damage modes related to rocking and bulging motions clearly show an increasing trend, contrarily, damage modes related to sloshing are more uniformly distributed among the PGA axis. The boundary values of each PGA range in Figure 4-5 are set in order to divide tanks into groups of approximately the same number. In conclusion, it is reasonable to assume that DS2 depends on mechanical phenomena not significantly related to Damage States from 3 to 5. Thus, a tank supposed to be in DS5, for example, might not necessarily feature damage related to DS2.

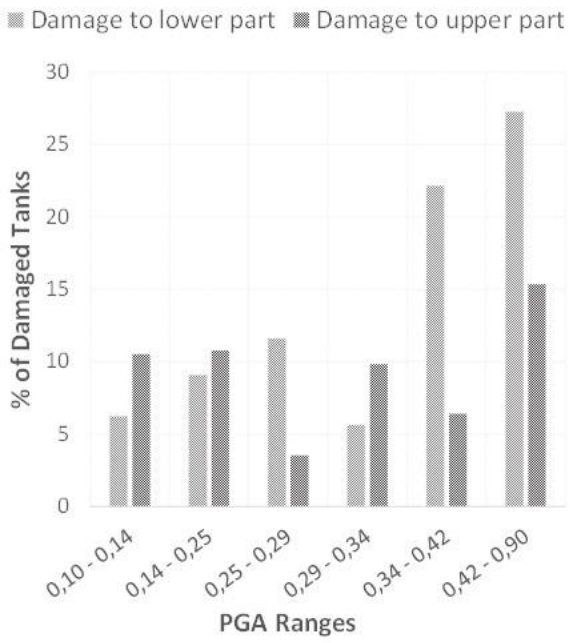

Figure 4-5. Percentage of damaged tanks for each PGA range

Development of fragility curves will take into account this issue, as discussed later. Compared to the damage classification used in past researches [8,9], the one propose herein distinguishes piping system damage into DS1 and DS3, depending on the entity of failure and its location, as well as the pipe type involved. For example, damage to an overflow pipe creates only slight leaks, while damage to either inlet/outlet or drain piping can have much more relevant consequences. Finally, when elephant foot buckling is associated to rips at the shell-bottom junction, a huge quantity of fluid can flow-out, because of location of failure. This is why, if occurring together with other crises, it is regarded as DS5.

4.4.2. Definition of risk levels

The second set of damage states classifies damage data in terms of loss of content and it consists of three Risk Levels. In the framework of seismic risk assessment of plants, the quantitative evaluation of release of dangerous substances is a fundamental topic [145]. Indeed, depending on the amount of content lost and on toxicity, flammability and reactivity of stored substances, liquid leakages can trigger hazardous chains of events whose consequences affect not only the

plant but also the surrounding environment. Quantitative Risk Analysis uses information on releases in order to estimate the likelihood and consequences of hazardous events, and expresses quantitatively results in terms of risk to people and environment. Based on the amount of release caused by failure at the shell or at the piping system, each database tank has been associated to a Risk Level, following the criteria given in Table 4.11. It should to be noted that spillage from the top of the shell is not considered as release, in order to be consistent with considerations on sloshing made before.

Table 4.11. Risk Level definition used in the present work

Risk Level	***Description***	***Number of Tanks***
RL1	No release, spillages from roof	2893
RL2	Minor leaks from shell tearing or damaged piping	41
RL3	Major leaks from shell rupture or broken pipe, inlet/outlet pipe or outflow pipe disconnected from tank. Leaks from tearing in correspondence of bottom-shell junction	92

4.5. Parametric fragility curves

4.5.1. General approach

Fragility curves were fitted using the two set of damage states described at paragraph 4.4 (DSs and RLs). Lallemant et al. [61] discussed the most commonly used methods for fitting fragility curves from observational data. In this work Bayesian approach is used to estimate parameters of seismic fragility relation for on-grade storage tanks [146].

In the Bayesian approach adopted a general parametric fragility model is defined as a function of ground-motion intensity IM (i.e. PGA) and of a set of unknown regression parameters $\boldsymbol{\Theta}$:

$$P_f(IM) = f(IM; \boldsymbol{\Theta}) \tag{4.1}$$

The current knowledge of parameters $\boldsymbol{\Theta}$, in Bayesian statistics is described by a joint density function $f(\boldsymbol{\Theta})$ referred to as *priori* distribution. If $\boldsymbol{y}$ is defined as the vector of observed data, the Bayes theorem is applied to update the knowledge of the regression parameters and then obtain a *posterior* distribution:

$$f(\boldsymbol{\Theta}|\,\boldsymbol{y}) = \frac{P(\boldsymbol{y}\,|\boldsymbol{\Theta})f(\boldsymbol{\Theta})}{P(\boldsymbol{y})} = \frac{P(\boldsymbol{y}\,|\boldsymbol{\Theta})f(\boldsymbol{\Theta})}{\int P(\boldsymbol{y}\,|\boldsymbol{\Theta})\,f(\boldsymbol{\Theta})d\boldsymbol{\Theta}} \tag{4.2}$$

where $P(\boldsymbol{y}\,|\boldsymbol{\Theta})$ is named likelihood function L. The integrals at denominator can be solved using computational algorithms based on Markov Chain Monte Carlo methods (MCMC) and Gibbs sampling [147].

Generally, the minimum dimension of a database to select in order to construct a fragility function depend on the level of uncertainty the study can accept. Simple rules for establishing the minimum number of samples necessary to predict the observed behavior in case of linear models are available in literature [148–154]. Guidelines for Empirical Vulnerability Assessment (Rossetto et al. in [155] suggests a database size of minimum 100 observations and a at least 30 of them should have reached or exceed a given damage state [156], with the data point located among a wide range of IM values.

4.5.2. Fragility curves based on individual damage states

This paragraph provides a description of the procedure used to fit parametric fragility curves basing on the general damage exceedance condition $D \geq D_j$. For this purpose, for each damage state D_j, the observed damage data is converted into a binary variable y_{ij} which is equal to 1 if damage the i-th tanks is greater or equal to D_j and 0 otherwise. Assuming the binary variables y_{ij} independent and identically distributed, the likelihood function L_j for the damage state D_j is defined as [61,157,158]:

$$L_j = P\left(\boldsymbol{y_j}\,|\boldsymbol{\Theta_j}\right) = \prod_{i=1}^{N}\left(1 - p_{i,j}(IM_i;\boldsymbol{\Theta_j})\right)^{(1-y_{i,j})} p_{i,j}(IM_i;\boldsymbol{\Theta_j})^{y_{i,j}} \tag{4.3}$$

where N is the total number of tanks observed, $p_{i,j}$ indicates the failure probability related to the damage state D_j for the ground motion intensity IM_i, $\boldsymbol{\Theta_j}$ represents the vector of unknown regression parameters and $\boldsymbol{y_j}$ is a vector containing observed damage data for the damage state D_j, i.e. $\boldsymbol{y_j} = \left|y_{i,j}, \ldots, y_{N,j}\right|$. Equation (4.3) corresponds to assuming that y_{ij} follows a Bernoulli distribution B, with probability $p_{i,j}$:

$$y_{i,j} \sim B\left(1, p_{i,j}\left(IM, \boldsymbol{\Theta_j}\right)\right) \tag{4.4}$$

In the present work, two generalized linear models (hereafter GLM) have been used: the first GLM employs a probit link function, whereas the second GLM uses a logit link function. For each GLM, five different expressions are used for defining the probability of failure as a function of ground-motion intensity.

In particular, for both the GLMs:

- the first expression is used to investigate tank fragility by considering all tanks in database;
- the second expression is used to investigate the effect of the aspect ratio H/D on tank fragility;
- the third expression is used to investigate the effect of the filling level;
- the fourth expression is used to investigate the presence of base anchorage system;
- the fifth expression is used to take into account simultaneously the effects of the tank aspect ratio and presence of base anchorage system on tank fragility.

GLM with probit link function

As aforementioned, at first, the fragility for all tanks in database is determined. It should be noted that a GLM using a probit function can be rewritten in terms of lognormal model. The probability of failure $p_{i,j}$ is defined as by

$$p_{i,j} = \Phi\left(\frac{\ln(IM_i) - \mu_j}{\sigma_j}\right) = \Phi\left(\alpha_{0,j} + \beta_{0,j}\ln(IM_i)\right) \quad (4.5)$$

where $\Phi(.)$ represents the standard normal cumulative distribution function and $\alpha_{0,j}$ and $\beta_{0,j}$, are unknown regression parameters fitted from the GLM described as follows:

$$\Phi^{-1}(p_{i,j}) = \alpha_{0,j} + \beta_{0,j}\ln(IM_i) \quad (4.5b)$$

The regression parameters $\alpha_{0,j}$ and $\beta_{0,j}$ are clearly related to the median value μ_j of $\ln(IM_i)$ and the dispersion parameter σ_j by the expressions:

$$\mu_j = -\alpha_{0,j} \cdot {\beta_{0,j}}^{-1} \quad (4.6)$$

$$\sigma_j = 1/\beta_{0,j} \quad (4.7)$$

In order to avoid zero damage probability for $IM = 0$, the logarithm of the ground motion intensity has been considered as covariate.

For the purpose of investigating the influence of aspect ratio, the filling level and the presence of anchorage system on the tank fragilities, further expressions are adopted for defining the probability of failure as a function of IM. In case in which the fragility analysis involves the effects of aspect ratio H/D, the probability of failure $p_{i,j}$ has the following structure:

$$p_{i,j} = \Phi\left(\alpha_{0,j} + \alpha_{HD,j} \cdot \left(\frac{H}{D}\right)_i + \beta_{0,j} \cdot \ln(IM_i)\right) \tag{4.8}$$

where $(H/D)_i$ is the value of the aspect ratio relative to the i-th observation; $\alpha_{HD,j}$ is a regression coefficient relative to the j-th Damage State, expressing the influence of the aspect ratio on the tank fragility. In order to provide a correspondence with the first model given in Eqs. (4.5) - (4.7), the median value μ_j of the associated normal distribution and the dispersion parameter σ_j are derived for the lognormal function in Eq. (4.8):

$$\mu_j = -\left(\alpha_{0,j} + \alpha_{HD,j} \cdot \left(\frac{H}{D}\right)_i\right) \cdot {\beta_{0,j}}^{-1} \tag{4.9}$$

$$\sigma_j = 1/\beta_{0,j} \tag{4.10}$$

The effect of filling level FL on the tank seismic performance has been studied by employing an expression analogous to that given in Eq. (4.8) used to investigate effects of aspect ratio. In particular, the probability of failure $p_{i,j}$ has the form:

$$p_{i,j} = \Phi\left(\alpha_{0,j} + \alpha_{FL,j} \cdot (FL)_i + \beta_{0,j} \cdot \ln(IM_i)\right) \tag{4.11}$$

where $(FL)_i$ is the value of the filling level corresponding to the i-th observation, and $\alpha_{FL,j}$ is a regression coefficient expressing the influence of FL on the tank fragility. As before, a correspondence in terms of parameters μ_j and σ_j between the model in Eq. (4.11) and that presented by Eqs. (4.5) - (4.7) is provided by Eqs. (4.9) and (4.10) in which, in the expression of μ_j, the term $\alpha_{HD,j} \cdot (H/D)_i$ is substituted by $\alpha_{FL,j} \cdot (FL)_i$.

In case in which tank fragility analysis involves effects of anchorage system, the probability of failure $p_{i,j}$ is described as

$$p_{i,j} = \Phi\left(\alpha_{0,j} + \alpha_{A,j} \cdot (A)_i + \alpha_{NA,j} \cdot (NA)_i + \beta_{0,j} \cdot \ln(IM_i)\right) \tag{4.12}$$

where $(A)_i$ is equal to 1 for anchored tanks and 0 otherwise, and $(NA)_i$ is inversely defined; $\alpha_{A,j}$ and $\alpha_{NA,j}$ represent respectively the effects of the presence and absence of anchorage system on the seismic tank fragility. The parameters μ_j and σ_j can be described by Eqs. (4.9), (4.10) in which, in the expression of μ_j, the term $\alpha_{HD,j} \cdot (H/D)_i$ is substituted by $\alpha_{0,j} + \alpha_{A,j} \cdot (A)_i + \alpha_{NA,j} \cdot (NA)_i$.

The approach described by Eqs. (4.8) - (4.12) consists of three different fragility functions that consider separately the effects on tank fragility of the three aspects investigated (aspect ratio,

filling level and presence of anchorage). Other researches have proposed different fragility models depending on H/D, filling level and anchorage, even though they fitted these models independently using different subsets of their database [8–10]. Taking into account the effects of the aforementioned parameters through specific regression coefficients, as proposed here, allows to perform significance tests on these latter, and therefore evaluate which parameters are statistically more relevant for the definition of fragility. However, this criterion does not consider the combined effect of these parameters. Therefore, an overall fragility function taking into account simultaneously the effects of the tank aspect ratio and anchorage system is provided. In this last case, the probability of failure $p_{i,j}$ is described as follows:

$$p_{i,j,tot} = \Phi\left(\alpha_{0,j} + \alpha_{HD,j} \cdot \left(\frac{H}{D}\right)_i + \alpha_{A,j} \cdot (A)_i + \alpha_{NA,j} \cdot (NA)_i + \beta_{0j} \cdot \ln(IM_i)\right) \tag{4.13}$$

For this last expression, the parameters μ_j and σ_j can be obtained from Eqs. (4.9), (4.10) in which the expression of μ_j is adjusted by replacing the term $\alpha_{HD,j} \cdot (H/D)_i$ with $\alpha_{0,j} + \alpha_{HD,j} \cdot \left(\frac{H}{D}\right)_i + \alpha_{A,j} \cdot (A)_i + \alpha_{NA,j} \cdot (NA)_i$.

GLM with logit link function

Also in this case, at first, all tanks in database are used to evaluate tank fragility. The probability of failure $p_{i,j}$ is defined as by

$$p_{i,j} = \frac{e^{(\gamma_{0,j} + \eta_{0,j} \ln(IM_i))}}{1 + e^{(\gamma_{0,j} + \eta_{0,j} \ln(IM_i))}} \tag{4.14}$$

where $\gamma_{0,j}$ and $\eta_{0,j}$, are unknown regression parameters fitted from the GLM described as follows:

$$\ln\left(\frac{p_{i,j}}{1 - p_{i,j}}\right) = \gamma_{0,j} + \eta_{0,j} \ln(IM_i) \tag{4.14b}$$

In case in which the fragility analysis involves the effects of aspect ratio H/D, the probability of failure $p_{i,j}$ has the following structure:

$$p_{i,j} = \frac{e^{(\gamma_{0,j} + \gamma_{\mathrm{HD},j} \cdot \left(\frac{H}{D}\right)_i + \eta_{0,j} \ln(IM_i))}}{1 + e^{(\gamma_{0,j} + \gamma_{\mathrm{HD},j} \cdot \left(\frac{H}{D}\right)_i + \eta_{0,j} \ln(IM_i))}} \tag{4.15}$$

where $(H/D)_i$ is the value of the aspect ratio relative to the i-th observation and $\gamma_{\mathrm{HD},j}$ is a regression coefficient relative to the j-th Damage State, expressing the influence of the aspect ratio on the tank fragility.

The effect of filling level FL on the tank seismic performance has been studied by employing the expression:

$$p_{i,j} = \frac{e^{(\gamma_{0,j}+\gamma_{\mathrm{FL},j}\cdot(FL)_i+\eta_{0,j}\ln(IM_i))}}{1+e^{(\gamma_{0,j}+\gamma_{\mathrm{FL},j}\cdot(FL)_i+\eta_{0,j}\ln(IM_i))}} \tag{4.16}$$

where $\gamma_{\mathrm{FL},j}$ is a regression coefficient expressing the influence of FL on the tank fragility.

In case in which tank fragility analysis involves effects of anchorage system, the probability of failure $p_{i,j}$ is described as

$$p_{i,j} = \frac{e^{(\gamma_{0,j}+\gamma_{\mathrm{A},j}\cdot(A)_i+\gamma_{\mathrm{NA},j}\cdot(NA)_i+\eta_{0,j}\ln(IM_i))}}{1+e^{(\gamma_{0,j}+\gamma_{\mathrm{A},j}\cdot(A)_i+\gamma_{\mathrm{NA},j}\cdot(NA)_i+\eta_{0,j}\ln(IM_i))}} \tag{4.17}$$

where $\gamma_{\mathrm{A},j}$ and $\gamma_{\mathrm{NA},j}$ represent respectively the effects of the presence and absence of anchorage system on the seismic tank fragility.

The fragility formulation that takes into account simultaneously the effects of the tank aspect ratio and anchorage system is described as follows:

$$p_{i,j,tot} = \frac{e^{\left(\gamma_{0,j}+\gamma_{\mathrm{HD},j}\cdot\left(\frac{H}{D}\right)_i+\gamma_{\mathrm{A},j}\cdot(A)_i+\gamma_{\mathrm{NA},j}\cdot(NA)_i+\eta_{0,j}\ln(IM_i)\right)}}{1+e^{\left(\gamma_{0,j}+\gamma_{\mathrm{HD},j}\cdot\left(\frac{H}{D}\right)_i+\gamma_{\mathrm{A},j}\cdot(A)_i+\gamma_{\mathrm{NA},j}\cdot(NA)_i+\eta_{0,j}\ln(IM_i)\right)}} \tag{4.18}$$

For GLMs with probit and logit link functions, Bayesian regression has been performed using the software R and JAGS [159,160] and the model parameters $\boldsymbol{\theta_j} = [\alpha_{r,j}, \beta_j]$ and $\boldsymbol{\theta_j} = [\gamma_{r,j}, \eta_j]$ have been estimated for each damage state D_j, for the all formulations presented. Three MCMC chains are used and their convergence is checked by computing the potential scale reduction factor [147]. Uninformative distributions are adopted as *priori* distributions of the model parameters.

Compared to the previous works [8–10], data are not divided into PGA bins whose boundaries could significantly affect results, and therefore regression is calculated directly from the entire dataset. Following this approach, fragility relations are not influenced or forced by the choice of range bounds. Moreover, the value of dispersion parameter is not subjected to any boundary. The ground motion IM used for defining tank fragilities is the Peak Ground Acceleration, since it is the most widely available parameter from reports. However, this might not be the most

efficient IM for all types of tank damage, as discussed when DSs have been defined, at paragraph 4.4.

4.6. Results

4.6.1. Fragility curves for damage states

Fragility curves in terms of Damage States are derived for all database tanks by employing the generalized linear models presented in Eqs. (4.5) - (4.7) for probit link function, and in Eq. (4.14) for logit link function. Their plot for damage states from 2 to 5 and the respective observed frequencies are shown in Figure 4-6 (in case of GLM with probit link function) and Figure 4-15 (in case of GLM with logit link function). Table 4.12 shows estimates of the model parameters $\alpha_{0,j}$ and $\beta_{0,j}$. For the ease of comparison with other works in literature, in Table 4.12 the median value μ_j and the standard deviation σ_j of the normal distribution associated to $ln(PGA)$ are also reported for each damage state j. However, this has been done only for the GLM with probit link function, since as shown in Eq. (4.5), it corresponds to a lognormal model. Table 4.17 depicts estimates of the model parameters $\gamma_{0,j}$ and $\eta_{0,j}$, as well as the median value μ_j of $ln(PGA)$. Note that for Damage State 2 as well as Damage State 5, fragility models were defined considering the probability of achieving those DS rather than their exceedance probability. The reason of this choice has been clarified in the paragraph dealing with Damage States description (paragraph 4.4). It should be noted that fragility curve for $DS = 2$ has been shown in figure only for fragility involving all database tanks (Eqs. (4.5) - (4.7) and Eq. (4.14)). Figures associated with the further models proposed in this work show fragility curves for $DS \geq 3$, $DS \geq 4$ and $DS = 5$, since PGA might not be an effective intensity measure for $DS = 2$.

As already mentioned, the influence of the H/D ratio, filling level and anchorage system on tank seismic performance is also investigated. The median value of H/D in present tank database is 0.31. In particular, out of 3026 tanks, 662 tanks have H/D ratio greater or equal to 0.31, 674 tanks have H/D ratio less than 0.31, while for 1690 tanks this information is not available. The median value of filling level in tank database is 0.75 and most tanks are unanchored (266 out of 375 tanks for which information on anchorage system is available).

The effects of tank aspect ratio H/D on seismic fragility has been analyzed by adopting the GLM with probit link function described by Eqs. (4.8) - (4.10) and the GLM with logit function described by Eq. (4.15). Results in terms of fragility parameters $\alpha_{0,j}$, $\alpha_{HD,j}$ and β_{0j} are presented in Table 4.13. By substituting values obtained for $\alpha_{0,j}$, $\alpha_{HD,j}$ and β_{0j} into Eqs. (4.9),

(4.10), median value μ_j and dispersion σ_j of the associated normal distribution are obtained for $H/D = 0.2$ and 0.6 and presented in Table 4.13; the corresponding fragility curves are plotted in Figure 4-8. Similarly, results in terms of fragility parameters $\gamma_{0,j}$, $\gamma_{HD,j}$, η_{0j}, and median value μ_j of $ln(PGA)$ are presented in Table 4.18, whereas the corresponding fragility curves are plotted in Figure 4-17. For the sake of comparison, Figure 4-8 and Figure 4-17. show fragility curves for all tanks as well (in red line).

Tank fragility as a function on the filling level was studied by using the GLM with probit link function described in Eq. (4.11), and the GLM with logit function described by Eq. (4.16). Table 4.14 contains value of model parameters $\alpha_{0,j}$, $\alpha_{FL,j}$ and β_{0j}, as well as the median value μ_j and the standard deviation σ_j of $ln(PGA)$ calculated for $FL = 0.2, 0.5$ and 0.9 . Corresponding fragility curves are represented in Figure 4-10. Likewise, Table 4.19 provides fragility parameters $\gamma_{0,j}$, $\gamma_{FL,j}$, η_{0j}, and the median value μ_j of $ln(PGA)$, and Figure 4-19 plots the corresponding fragility curves.

The influence of the anchorage system on the tank dynamic performances was investigated by employing the GLM with probit link function in Eq. (4.12) and the GLM with logit link function in Eq. (4.17). Since from a first analysis the parameter α_{jA} has been found not to be significant, a further analysis has been conducted without considering anchored tanks (in Eqs. (4.12) and (4.17) the term $\alpha_{jA} \cdot (A)_i$ has been omitted). Indeed, it should be noted that information on the presence of base anchorage is available for only 109 and its irregular distribution among PGA does not allow to carry out a consistent statistical analysis. Therefore, Table 4.15 summarizes value of $\alpha_{0,j}$, $\alpha_{NA,j}$ and β_{0j} obtained from analysis as well as value of μ_j and σ_j for unanchored tanks. Fragility curves for unanchored tanks are plotted in Figure 4-12. On the other hand, Table 4.20 shows fragility parameters $\gamma_{0,j}$, $\gamma_{NA,j}$,η_{0j} and the median value μ_j of $ln(PGA)$; in Figure 4-21 the corresponding fragility curves are plotted.

Finally, fragility parameters obtained for the last overall GLM in case of probit link function, described by Eq. (4.13), are provided in Table 4.16. Values for μ_j and σ_j assuming $H/D = 0.5,\ 1$ and 2 and absence of anchorage system ($NA = 1$) are shown as well. The corresponding fragility curves are shown in Figure 4-14. Table 4.21 shows fragility parameters for the GLM with logit function described by Eq. (4.18) and in Figure 4-23 the corresponding fragility curves are depicted. Also for these two overall GLMs, the parameter α_{jA} has been found to be not significant, then a further analysis has been conducted without considering anchored tanks, (the corresponding term $\alpha_{jA} \cdot (A)_i$ in Eq. (4.13) and (4.18) is omitted). Note that all tables show the significance $p - values$ corresponding to the significance tests carried out in the parameters

$\alpha_{HD,j}$, $\alpha_{FL,j}$ $\alpha_{NA,j}$ $\gamma_{HD,j}$, $\gamma_{FL,j}$ $\gamma_{NA,j}$ [147]. All the regression parameters included in the models appear to be statistically significant.

The Akaike information criterion (AIC) has been used in order to estimate the relative quality of the two statistical models used (probit and logit models) for the given set of data. The GLM with probit link function has been found to represent in a more reliable way the observed data.

Results from fragility analyses overall confirms some general trends from other researchers [8,9] in terms of influence on the tank performances of filling level, presence of base anchorage system and tank aspect ratio: squat tanks show better seismic performances than slender tanks, since median PGA to reach or exceed a certain damage state decreases as the aspect ratio increases (see Table 4.13, Table 4.16, Figure 4-8 and Figure 4-14). Moreover, Salzano et al. [10] remark that for low values of the aspect ratio, tanks only suffer damage to roof. Filling level affects the tank seismic performance reducing the PGA level relative to each damage state (see Table 4.14 and Figure 4-10), as found in [8,10,67]. Finally, the presence of anchorage system improves the seismic performance level of tank (see Table 4.15, Table 4.16, Figure 4-12 and Figure 4-14), as claimed by Salzano and ALA in [10,135].

Table 4.22 and Figure 4-24 allow a quick comparison between fragility curves obtained in the current work and those available in literature in terms of Damage States. It should be noted that, with regard to the current work, comparison involves the fragility obtained by using the probit model, since it has been found to represent the observed data in a more reliable way, as aforementioned. Moreover, the tank fragility obtained in case of "all tanks" has been analyzed. The comparison excludes $DS2$ for the reasons discussed in this chapter at paragraph 4.4.

Fragility curves obtained in the present work, are characterized by higher PGA median values than those provided in literature by O'Rourke and So (2000) and ALA (2001) [8–10]. It is an expected result since database used in the present work represents a bigger collection of data, including larger number of seismic events and tanks. For more recent events, moreover, it is supposed that tanks involved would perform better than older riveted tanks. On the other hand, the older databases used by previous researchers included almost exclusively damaged tanks; a great number of undamaged tanks, considered in the present database, were omitted in the previous ones. These aspects have certainly led to overestimate tank fragilities in the past.

Moreover, in ALA (2001) the fragility curves were fitted by performing a regression (least square regression) using a bounded range of possible σ values ($\sigma = 0.01$ to $\sigma = 0.80$). However, if no bounds were applied to the dispersion parameter, results from the same statistical procedure would be different (this statement has been demonstrated at paragraph 4.3). Therefore, the parameter $\sigma = 0.80$ obtained for $DS \geq 2$ and $DS \geq 3$ was not the true

dispersion of the data used, because it was bounded a priori in the regression procedure, and this forced the results. In contrast, in the current work, the value of dispersion parameter is not subjected to any boundary. This aspect has led to reduce the dispersion parameter of ALA fragility curves for $DS \geq 2$ and $DS \geq 3$, and also to obtain smaller median values μ of $ln(IM_i)$.

4.6.2. Fragility curves for risk levels

The same approach has been used for deriving fragility curves in term of risk levels (or release states). It is noted from literature that very squat tanks are not vulnerable to elephant foot buckling while they are easily subjected to cracks in fixed roof connection or damage to the upper part of wall by floating panel [10,126]. However, as explained above, damage and spillage caused by sloshing in this work are considered as not damage. Consequently, these fragilities are relative to losses from damage to the lower part of shell (releases from elephant foot buckling, bottom-shell junction, piping-shell coupling, etc.). Moreover, it should be pointed out that spillage from the roof is usually of secondary importance with respect to releases from the bottom, since in the latter case, location of failure and weight of the liquid column above can induce the complete escape of content.

Fragility curves in terms of Risk Levels are derived for all database tanks by employing the GLMs presented in Eqs. (4.5) - (4.7) and Eq. (4.14). Their plot for risk levels 2 and 3 and the respective observed frequencies are shown in Figure 4-7 in case of probit function, and in Figure 4-16 in case of logit function. The GLM parameters for probit function, i.e. the coefficients $\alpha_{0,j}$ and $\beta_{0,j}$, the median value μ_j and the standard deviation σ_j of $ln(PGA)$ for the j-th Risk Level are provided in Table 4.12, whereas the GLM parameters for logit function are shown in Table 4.17. As for damage states, also in case of risk levels fragility curves are derived as function of aspect ratio, filling level and anchorage system. Fragility parameters relative to probit function are shown in Tables 4.11 - 4.15, while those associated with logit function are summarized in Tables 4.16 - 4.20. Fragility curves are depicted in Figures 4.3, 4.5, 4.7, 4.9 (probit function) and Figures 4.12, 4.14, 4.16, 4.18 (logit function).

Results from analysis in terms of risk levels confirms what obtained in case of damage states with regard to the tank performances and to the effects of aspect ratio, filling level and anchorage system on tank seismic fragility.

Table 4.23 and Figure 4-25 allow a quick comparison between fragility curves obtained in the current work and those available in literature in terms of Risk Levels [10]. In particular, the tank fragility obtained in case of “all tanks” has been analyzed. Moreover, with regard to the

current work, comparison involves the results from the probit model, since it has been found to represent the observed data in a more reliable way, as aforementioned.

As found for damage states, the current study has obtained lower fragilities also in terms of risk levels with respect to what found in literature [10]. The same considerations made at paragraph 4.6.1 are valid in this case of risk levels as well.

Moreover, Salzano et al. (2003), as ALA (2001) in case of damage states (see paragraph 4.6.1), fitted fragility curves in a bounded range of possible σ values ($\sigma = 0.01$ to $\sigma = 0.80$). Therefore, the parameter $\sigma = 0.80$ obtained for $RL \geq 2$ was not the true dispersion of the data used. In contrast, the current work has not bounded the value of dispersion parameter.

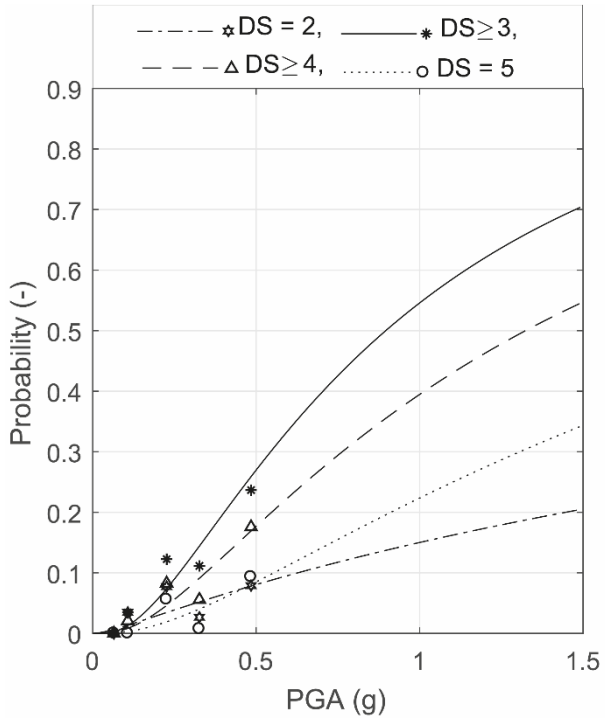

Figure 4-6. Fragility curves for all tanks in database in terms of Damage States (Eqs. (4.5)-(4.7))

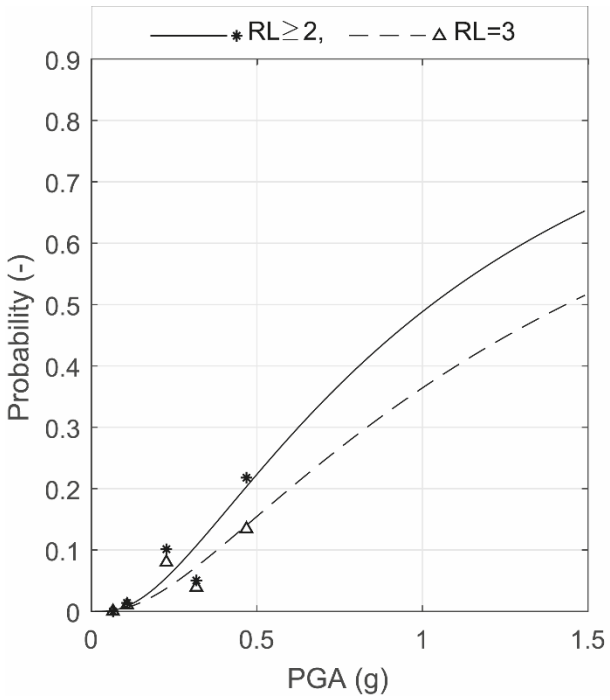

Figure 4-7. Fragility curves for all tanks in database in terms of Risk Levels (Eqs. (4.5)-(4.7))

Table 4.12. Fragility parameters obtained adopting the model presented in Eqs. (4.5)-(4.7) for Damage States and Risk Levels.

	Damage States				***Risk Levels***	
Fragility parameters	$\boldsymbol{DS = 2}$	$\boldsymbol{DS \geq 3}$	$\boldsymbol{DS \geq 4}$	$\boldsymbol{DS = 5}$	$\boldsymbol{RL \geq 2}$	$\boldsymbol{RL = 3}$
$\boldsymbol{\alpha_{0,j}[-]}$	-1.036	0.115	-0.267	-0.762	-0.029	-0.347
$\boldsymbol{\beta_{0j}[ln(g)^{-1}]}$	0.527	1.051	0.952	0.884	1.056	0.965
Associated normal distribution of $\boldsymbol{ln(PGA)}$						
$\boldsymbol{\mu_j\ [ln(g)]}$	1.967	-0.109	0.281	0.862	0.028	0.360
$\boldsymbol{\sigma_j[ln(g)]}$	1.899	0.951	1.050	1.130	0.947	1.037

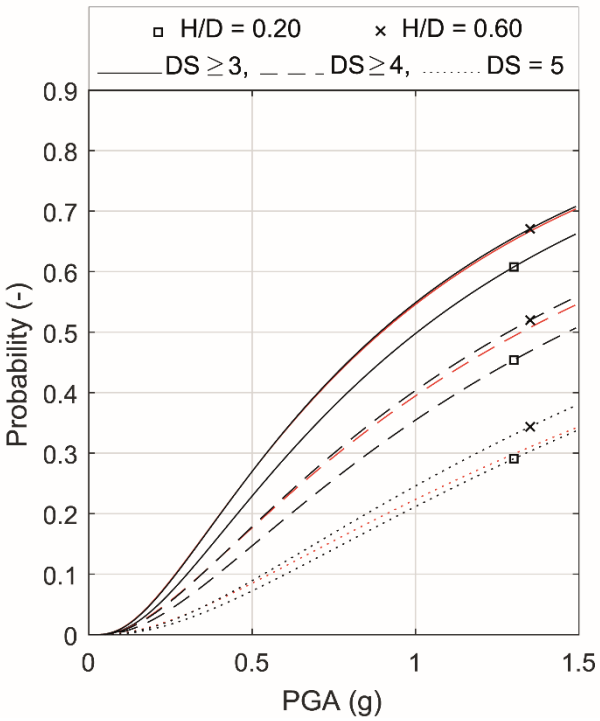

Figure 4-8. Fragility curves for H/D=0.2 and 0.6 in terms of Damage States (Eqs. (4.8)-(4.10)). Red lines correspond to all tanks (see Fig. 4-6)

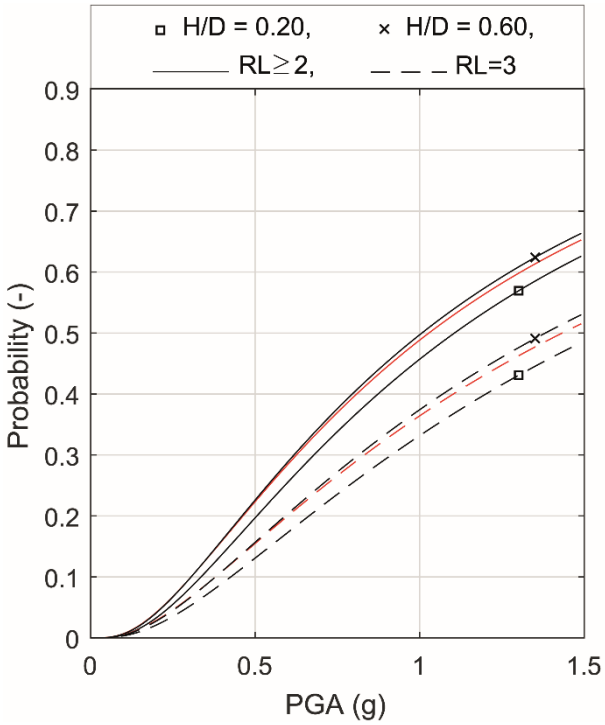

Figure 4-9. Fragility curves for H/D=0.2 and 0.6 in terms of Risk Levels (Eqs. (4.8)-(4.10)). Red lines correspond to all tanks (see Fig. 4-7)

Table 4.13. Fragility parameters obtained adopting the model presented in Eqs. (4.8)-(4.10) for Damage States and Risk Levels.

	Damage States				***Risk Levels***	
Fragility parameters	$\boldsymbol{DS = 2}$	$\boldsymbol{DS \geq 3}$	$\boldsymbol{DS \geq 4}$	$\boldsymbol{DS = 5}$	$\boldsymbol{RL \geq 2}$	$\boldsymbol{RL = 3}$
$\boldsymbol{\alpha_{0,j}[-]}$	-0.967	-0.070	-0.437	-0.857	-0.158	-0.492
$\boldsymbol{\alpha_{HD,j}[-]}$	-0.021	0.321	0.322	0.282	0.252	0.286
$\boldsymbol{p - value}$	0.837	$4.9 \cdot 10^{-6}$	$3.2 \cdot 10^{-5}$	$5.6 \cdot 10^{-3}$	$1.5 \cdot 10^{-3}$	$6.8 \cdot 10^{-4}$
$\boldsymbol{\beta_{0j}[ln(g)^{-1}]}$	0.532	1.062	0.977	0.949	1.074	0.991
Associated normal distribution of $\boldsymbol{ln(PGA)}$ for $\boldsymbol{H/D = 0.2}$						
$\boldsymbol{\mu_j[ln(g)]}$	1.827	0.005	0.382	0.844	0.100	0.439
$\boldsymbol{\sigma_j[ln(g)]}$	1.880	0.942	1.024	1.054	0.931	1.009
Associated normal distribution of $\boldsymbol{ln(PGA)}$ for $\boldsymbol{H/D = 0.6}$						
$\boldsymbol{\mu_j[ln(g)]}$	1.843	-0.115	0.250	0.725	0.007	0.323
$\boldsymbol{\sigma_j[ln(g)]}$	1.880	0.942	1.024	1.054	0.931	1.009

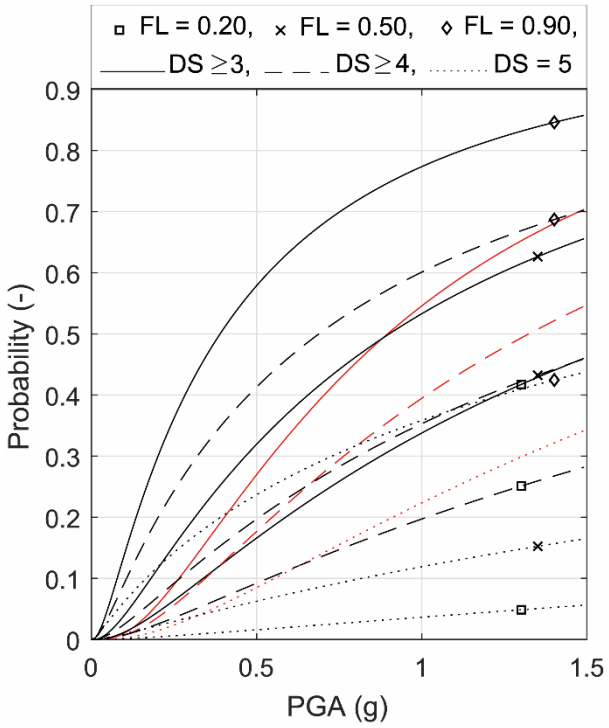

Figure 4-10. Fragility curves for FL=0.2, 0.5 and 0.9 in terms of Damage State (Eq. (4.11)). Red lines correspond to all tanks (see Fig. 4-6)

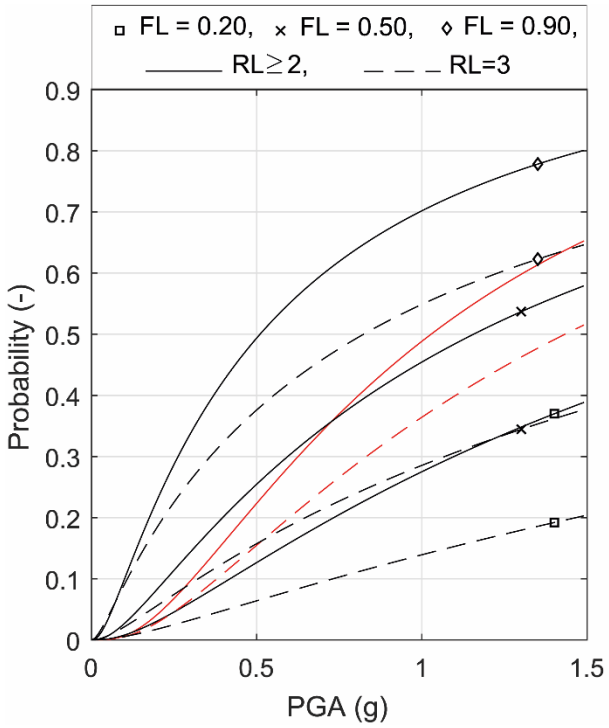

Figure 4-11 Fragility curves for FL=0.2, 0.5 and 0.9 in terms of Risk Levels (Eq. (4.11)). Red lines correspond to all tanks (see Fig. 4-7)

Table 4.14. Fragility parameters obtained adopting the model presented in Eq. (4.11) for Damage States and Risk Levels.

	Damage States				***Risk Levels***	
Fragility parameters	$\boldsymbol{DS = 2}$	$\boldsymbol{DS \geq 3}$	$\boldsymbol{DS \geq 4}$	$\boldsymbol{DS = 5}$	$\boldsymbol{RL \geq 2}$	$\boldsymbol{RL = 3}$
$\boldsymbol{\alpha_{0,j}[-]}$	-2.184	-0.752	-1.168	-2.200	-0.920	-1.428
$\boldsymbol{\alpha_{FL,j}[-]}$	1.737	1.670	1.582	2.042	1.610	1.723
$\boldsymbol{p - value}$	$< 2 \cdot 10^{-16}$	$< 2 \cdot 10^{-16}$	$< 2 \cdot 10^{-16}$	$< 2 \cdot 10^{-16}$	$< 2 \cdot 10^{-16}$	$< 2 \cdot 10^{-16}$
$\boldsymbol{\beta_{0j}[ln(g)^{-1}]}$	0.12829	0.79609	0.68623	0.5103	0.787	0.632
Associated normal distribution of $\boldsymbol{ln(PGA)}$ for $\boldsymbol{FL = 0.2}$						
$\boldsymbol{\mu_j[ln(g)]}$	14.317	0.526	1.241	3.512	0.759	1.714
$\boldsymbol{\sigma_j[ln(g)]}$	7.795	1.256	1.457	1.960	1.271	1.581
Associated normal distribution of $\boldsymbol{ln(PGA)}$ for $\boldsymbol{FL = 0.5}$						
$\boldsymbol{\mu_j[ln(g)]}$	10.256	-0.104	0.549	2.311	0.145	0.896
$\boldsymbol{\sigma_j[ln(g)]}$	7.795	1.256	1.457	1.960	1.271	1.581
Associated normal distribution of $\boldsymbol{ln(PGA)}$ for $\boldsymbol{FL = 0.9}$						
$\boldsymbol{\mu_j[ln(g)]}$	4.840	-0.943	-0.373	0.710	-0.673	-0.194
$\boldsymbol{\sigma_j[ln(g)]}$	7.795	1.256	1.457	1.960	1.271	1.581

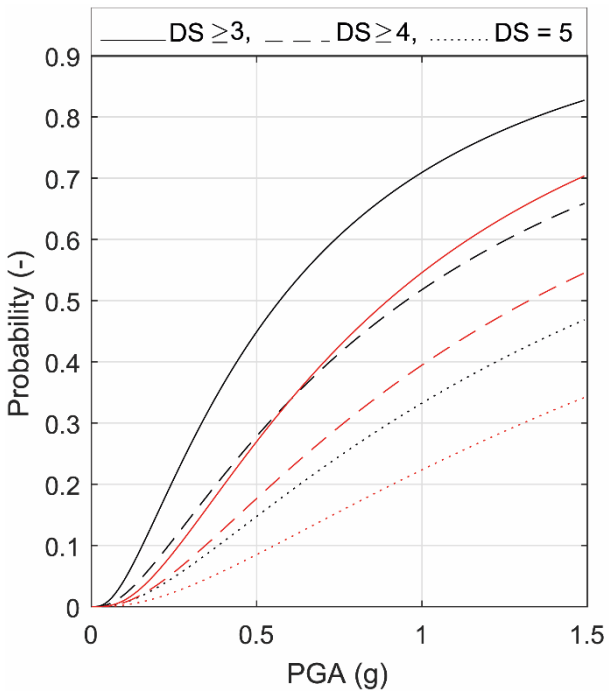

Figure 4-12. Fragility curves for unanchored tanks in terms of Damage States (Eq. (4.12)). Red lines correspond to all tanks (see Fig. 4-6)

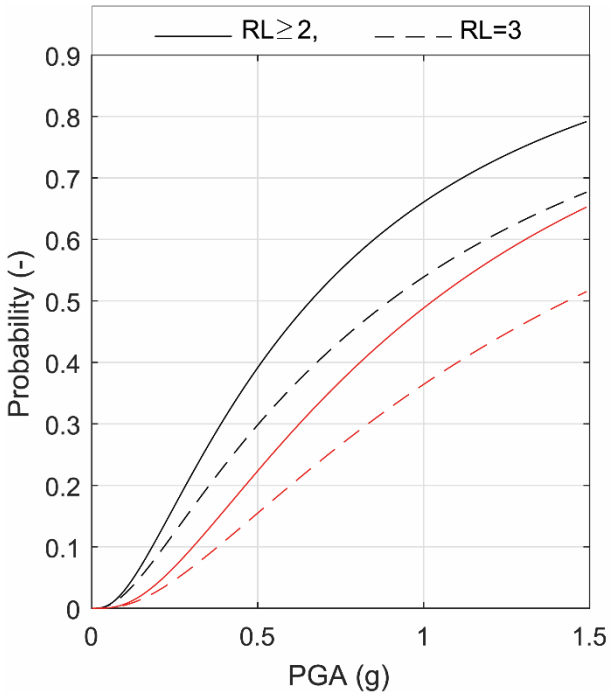

Figure 4-13. Fragility curves for unanchored tanks in terms of Risk Levels (Eq. (4.12)). Red lines correspond to all tanks (see Fig. 4-7)

Table 4.15. Fragility parameters obtained adopting the model presented in Eq. (4.12) for Damage States and Risk Levels.

	Damage States				***Risk Levels***	
Fragility parameters	$\boldsymbol{DS = 2}$	$\boldsymbol{DS \geq 3}$	$\boldsymbol{DS \geq 4}$	$\boldsymbol{DS = 5}$	$\boldsymbol{RL \geq 2}$	$\boldsymbol{RL = 3}$
$\boldsymbol{\alpha_{0,j}}[-]$	-1.208	-0.160	-0.438	-0.872	-0.300	-0.638
$\boldsymbol{\alpha_{A,j}}[-]$	-	-	-	-	-	-
$\boldsymbol{p-value}$	-	-	-	-	-	-
$\boldsymbol{\alpha_{NA,j}}[-]$	0.455	0.712	0.482	0.439	0.714	0.736
$\boldsymbol{p-value}$	$4.0 \cdot 10^{-4}$	$5.6 \cdot 10^{-12}$	$3.2 \cdot 10^{-5}$	$2.6 \cdot 10^{-3}$	$5.9 \cdot 10^{-11}$	$6.2 \cdot 10^{-10}$
$\boldsymbol{\beta_{0j}}[\boldsymbol{ln(g)^{-1}}]$	0.446	0.981	0.912	0.887	0.996	0.905
Associated normal distribution of $\boldsymbol{ln(PGA)}$ for unanchored tanks						
$\boldsymbol{\mu_j}[\boldsymbol{ln(g)}]$	1.690	-0.563	-0.049	0.488	-0.41616	-0.10779
$\boldsymbol{\sigma_j}[\boldsymbol{ln(g)}]$	2.243	1.020	1.096	1.128	1.004	1.105

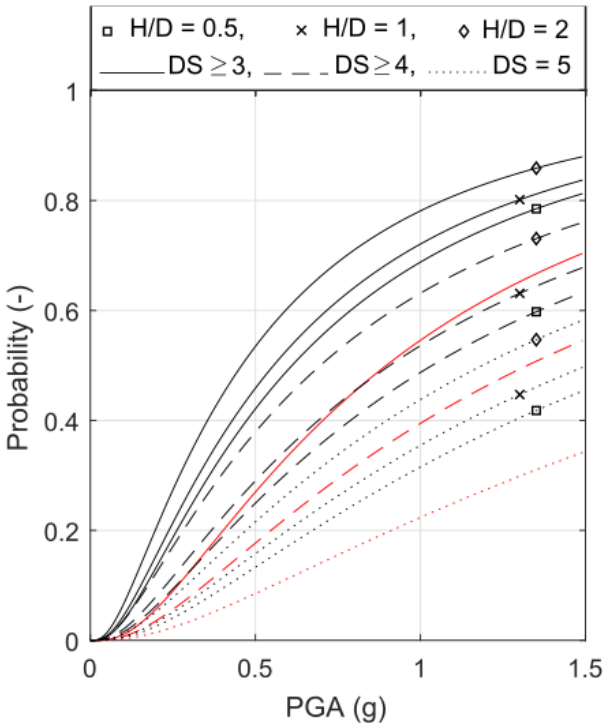

Figure 4-14. Fragility curves for unanchored tanks as function of H/D, in terms of Damage States (Eq. (4.13)). Red lines correspond to all tanks (see Fig. 4-6)

Table 4.16. Fragility parameters obtained adopting the model presented in Eq. (4.13) for Damage States

	Damage States			
Fragility parameters	$\boldsymbol{DS = 2}$	$\boldsymbol{DS \geq 3}$	$\boldsymbol{DS \geq 4}$	$\boldsymbol{DS = 5}$
$\boldsymbol{\alpha_{0,j}[-]}$	-1.138	-0.246	-0.553	-0.969
$\boldsymbol{\alpha_{HD,j}[-]}$	-0.111	0.191	0.245	0.216
$\boldsymbol{p - value}$	0.292	$1.0 \cdot 10^{-2}$	$2.5 \cdot 10^{-3}$	0.04
$\boldsymbol{\alpha_{A,j}[-]}$	-	-	-	-
$\boldsymbol{p - value}$	-	-	-	-
$\boldsymbol{\alpha_{NA,j}[-]}$	0.494	0.640	0.398	0.380
$\boldsymbol{p - value}$	$2.8 \cdot 10^{-4}$	$3.2 \cdot 10^{-9}$	$5.3 \cdot 10^{-4}$	0.012
$\boldsymbol{\beta_{0j}[ln(g)^{-1}]}$	0.463	0.994	0.929	0.911
Associated normal distribution of $\boldsymbol{ln(PGA)}$ for unanchored tanks with and $\boldsymbol{H/D = 0.5}$				
$\boldsymbol{\mu_j[ln(g)]}$	1.511	-0.493	0.035	0.528
$\boldsymbol{\sigma_j[ln(g)]}$	2.162	1.005	1.077	1.098
Associated normal distribution of $\boldsymbol{ln(PGA)}$ for unanchored tanks with and $\boldsymbol{H/D = 1}$				
$\boldsymbol{\mu_j[ln(g)]}$	1.631	-0.588	-0.097	0.409
$\boldsymbol{\sigma_j[ln(g)]}$	2.162	1.005	1.077	1.098
Associated normal distribution of $\boldsymbol{ln(PGA)}$ for unanchored tanks with and $\boldsymbol{H/D = 2}$				
$\boldsymbol{\mu_j[ln(g)]}$	1.871	-0.780	-0.361	0.172
$\boldsymbol{\sigma_j[ln(g)]}$	2.162	1.005	1.077	1.098

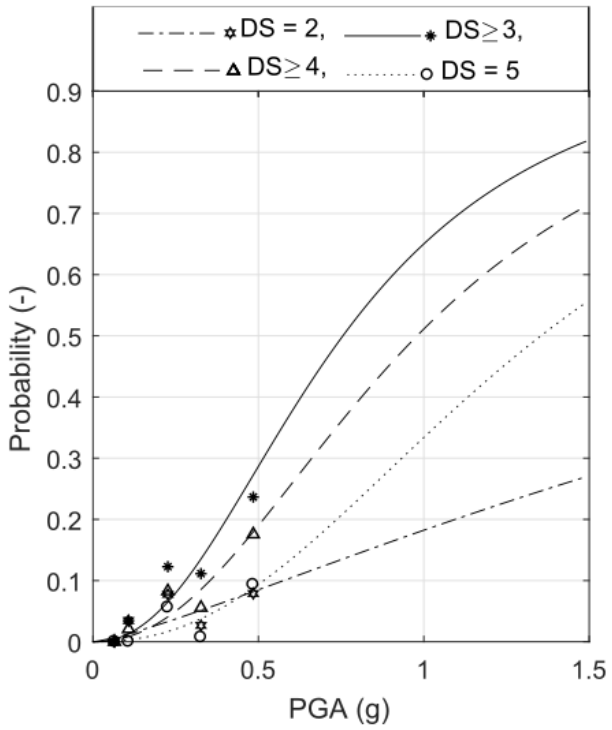

Figure 4-15. Fragility curves for all tanks in database in terms of Damage States (Eq. (4.14))

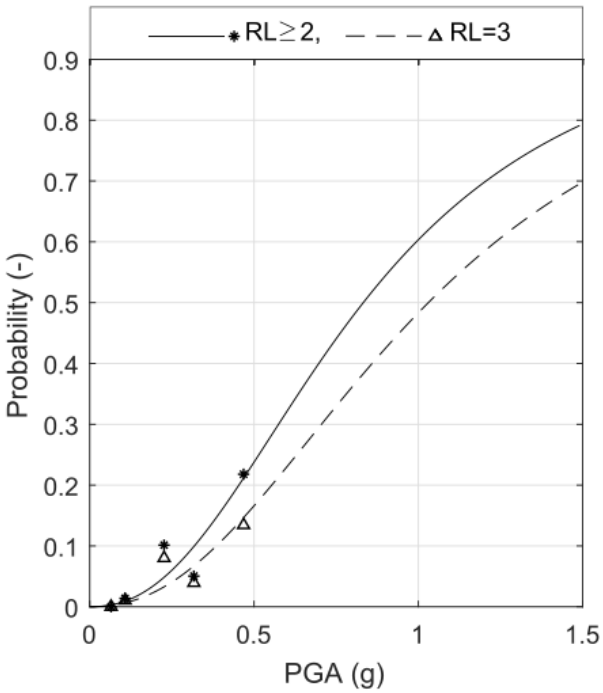

Figure 4-16. Fragility curves for all tanks in database in terms of Risk Levels (Eq. (4.14))

Table 4.17. Fragility parameters obtained adopting the model presented in Eqs. (4.14) for Damage States and Risk Levels.

	Damage States				***Risk Levels***	
Fragility parameters	$\boldsymbol{DS = 2}$	$\boldsymbol{DS \geq 3}$	$\boldsymbol{DS \geq 4}$	$\boldsymbol{DS = 5}$	$\boldsymbol{RL \geq 2}$	$\boldsymbol{RL = 3}$
$\boldsymbol{\gamma_{0,j}[-]}$	-1.501	0.620	0.044	-0.691	0.419	-0.067
$\boldsymbol{\eta_{0,j}[ln(g)^{-1}]}$	1.264	2.211	2.157	2.279	2.286	2.232
Median value of ln(PGA)						
$\boldsymbol{\mu_j[ln(g)]}$	0.500	-0.273	-0.019	0.316	-0.185	0.031

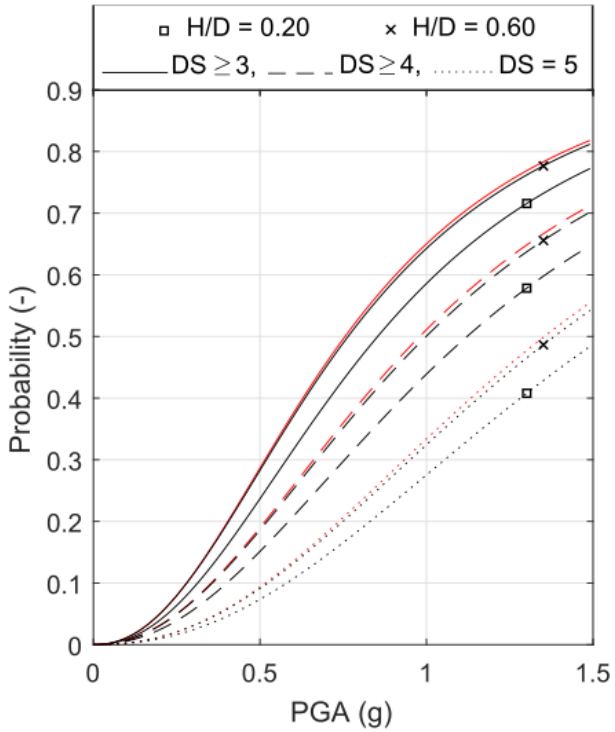

Figure 4-17. Fragility curves for H/D=0.2 and 0.6 in terms of Damage States (Eqs. (4.15)). Red lines correspond to all tanks (see Fig. 4-15)

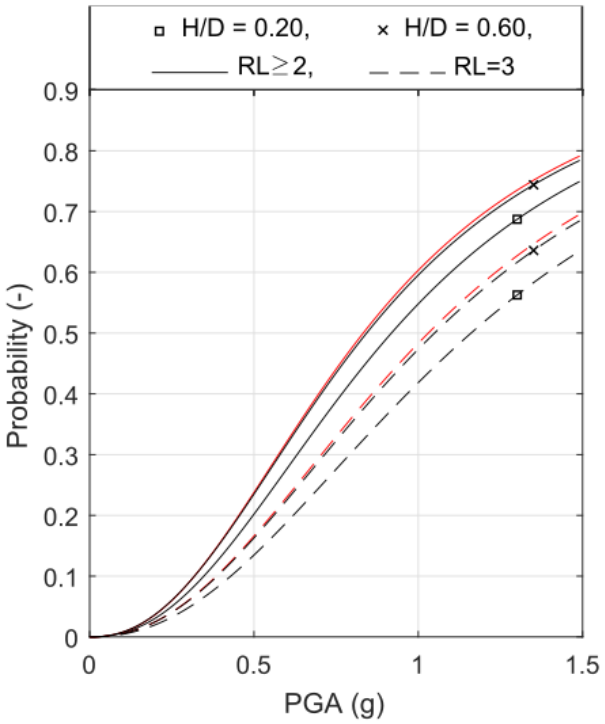

Figure 4-18. Fragility curves for H/D=0.2 and 0.6 in terms of Risk Levels (Eqs. (4.15)). Red lines correspond to all tanks (see Fig. 4-16)

Table 4.18. Fragility parameters obtained adopting the model presented in Eqs. (4.15) for Damage States and Risk Levels.

			Damage States			***Risk Levels***
Fragility parameters	$\boldsymbol{DS = 2}$	$\boldsymbol{DS \geq 3}$	$\boldsymbol{DS \geq 4}$	$\boldsymbol{DS = 5}$	$\boldsymbol{RL \geq 2}$	$\boldsymbol{RL = 3}$
$\boldsymbol{\gamma_{0,j}[-]}$	-1.501	0.227	-0.369	-1.084	0.096	-0.440
$\boldsymbol{\gamma_{HD,j}[-]}$	-0.059	0.601	0.620	0.584	0.485	0.556
$\boldsymbol{p - value}$	0.407	$2.1 \cdot 10^{-6}$	$1.1 \cdot 10^{-5}$	$5.7 \cdot 10^{-3}$	$3.3 \cdot 10^{-5}$	$6.4 \cdot 10^{-3}$
$\boldsymbol{\eta_{0,j}[ln(g)^{-1}]}$	1.171	2.189	2.134	2.259	2.259	2.208
Median value of ln(PGA) for $\boldsymbol{H/D = 0.2}$						
$\boldsymbol{\mu_j[ln(g)]}$	1.542	-0.163	0.114	0.406	-0.094	0.148
Median value of ln(PGA) for $\boldsymbol{H/D = 0.6}$						
$\boldsymbol{\mu_j[ln(g)]}$	1.584	-0.274	0.001	0.322	-0.174	0.488

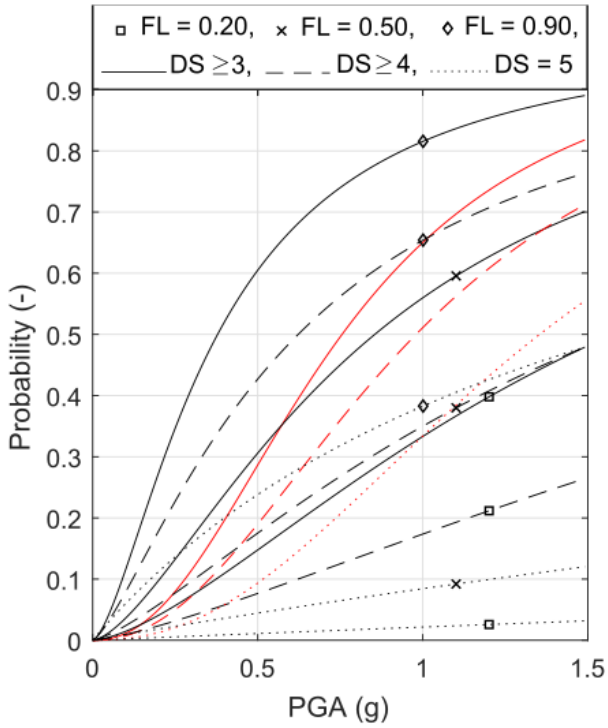

Figure 4-19. Fragility curves for FL=0.2, 0.5 and 0.9 in terms of Damage State (Eq. (4.16)). Red lines correspond to all tanks (see Fig. 4-15)

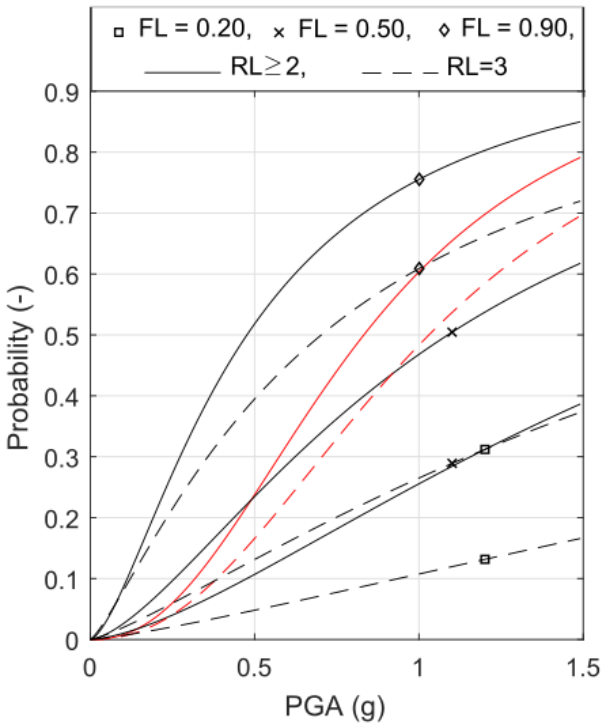

Figure 4-20 Fragility curves for FL=0.2, 0.5 and 0.9 in terms of Risk Levels (Eq. (4.16)). Red lines correspond to all tanks (see Fig. 4-16)

Table 4.19. Fragility parameters obtained adopting the model presented in Eqs. (4.16) for Damage States and Risk Levels.

		Damage States			***Risk Levels***	
Fragility parameters	$\boldsymbol{DS = 2}$	$\boldsymbol{DS \geq 3}$	$\boldsymbol{DS \geq 4}$	$\boldsymbol{DS = 5}$	$\boldsymbol{RL \geq 2}$	$\boldsymbol{RL = 3}$
$\boldsymbol{\gamma_{0,j}}[-]$	-4.785	-1.316	-2.188	-4.768	-1.696	-2.848
$\boldsymbol{\gamma_{FL,j}}[-]$	3.969	3.113	3.137	4.767	3.136	3.655
$\boldsymbol{p - value}$	$< 2 \cdot 10^{-16}$	$< 2 \cdot 10^{-16}$	$< 2 \cdot 10^{-16}$	$< 2 \cdot 10^{-16}$	$< 2 \cdot 10^{-16}$	$< 2 \cdot 10^{-16}$
$\boldsymbol{\eta_{0,j}[ln(g)^{-1}]}$	0.045	1.528	1.342	0.987	1.520	1.254
Median value of ln(PGA) for $\boldsymbol{FL = 0.2}$						
$\boldsymbol{\mu_j[ln(g)]}$	13.478	0.451	1.157	3.850	0.704	1.684
Median value of ln(PGA) for $\boldsymbol{FL = 0.5}$						
$\boldsymbol{\mu_j[ln(g)]}$	10.150	-0.151	0.445	2.398	0.077	0.820
Median value of ln(PGA) for $\boldsymbol{FL = 0.9}$						
$\boldsymbol{\mu_j[ln(g)]}$	4.567	-0.968	-0.460	0.476	-0.734	-0.357

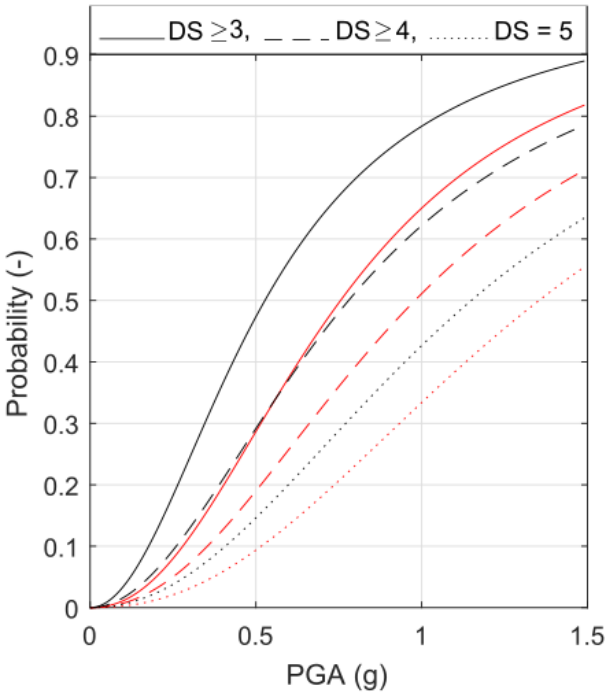

Figure 4-21. Fragility curves for unanchored tanks in terms of Damage States (Eq. (4.17)). Red lines correspond to all tanks (see Fig. 4-15)

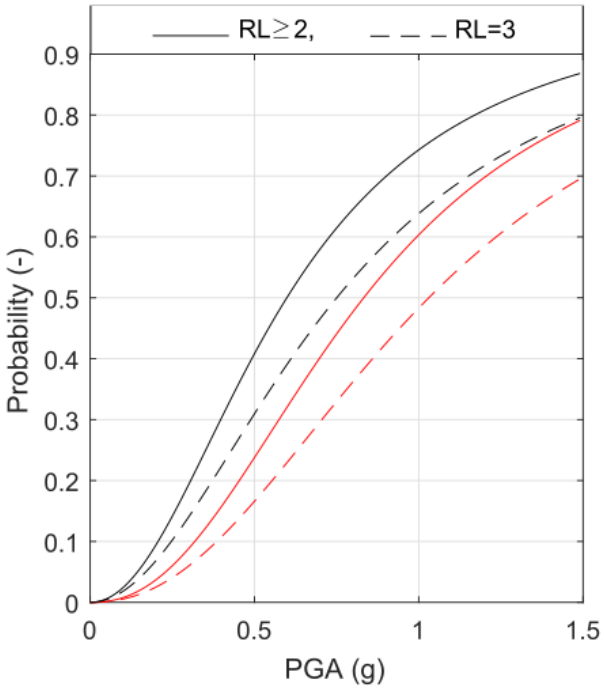

Figure 4-22. Fragility curves for unanchored tanks in terms of Risk Levels (Eq. (4.17)). Red lines correspond to all tanks (see Fig. 4-16)

Table 4.20. Fragility parameters obtained adopting the model presented in Eqs. (4.17) for Damage States and Risk Levels.

			Damage States		***Risk Levels***	
Fragility parameters	$\boldsymbol{DS = 2}$	$\boldsymbol{DS \geq 3}$	$\boldsymbol{DS \geq 4}$	$\boldsymbol{DS = 5}$	$\boldsymbol{RL \geq 2}$	$\boldsymbol{RL = 3}$
$\boldsymbol{\gamma_{0,j}[-]}$	-2.061	0.0365	-0.379	-1.103	-0.206	-0.791
$\boldsymbol{\gamma_{A,j}[-]}$	-	-	-	-	-	-
$\boldsymbol{p - value}$	-	-	-	-	-	-
$\boldsymbol{\gamma_{NA,j}[-]}$	1.007	1.249	0.877	0.807	1.266	1.359
$\boldsymbol{p - value}$	$4.3 \cdot 10^{-4}$	$3.3 \cdot 10^{-12}$	$2.8 \cdot 10^{-5}$	$6.7 \cdot 10^{-3}$	$6.6 \cdot 10^{-11}$	$1.2 \cdot 10^{-10}$
$\boldsymbol{\eta_{0,j}[ln(g)^{-1}]}$	0.978	2.009	1.999	2.120	2.066	1.977
Median value of ln(PGA) for unanchored tanks						
$\boldsymbol{\mu_j[ln(g)]}$	1.430	-0.654	-0.248	0.131	-0.511	-0.288

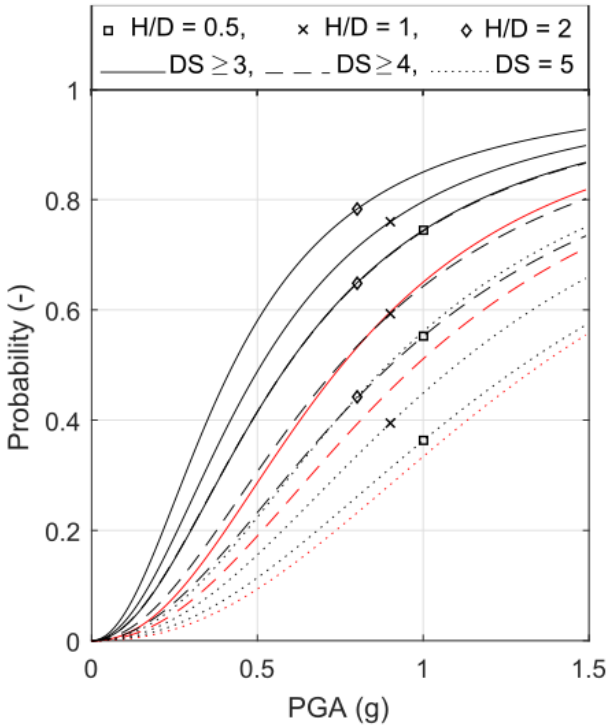

Figure 4-23. Fragility curves for unanchored tanks in terms of Damage States (Eq. (4.18)). Red lines correspond to all tanks (see Fig. 4-15)

Table 4.21. Fragility parameters obtained adopting the model presented in Eq. (4.13) for Damage States

	Damage States			
Fragility parameters	$\boldsymbol{DS = 2}$	$\boldsymbol{DS \geq 3}$	$\boldsymbol{DS \geq 4}$	$\boldsymbol{DS = 5}$
$\boldsymbol{\gamma_{0,j}[-]}$	-1.897	-0.126	-0.603	-1.320
$\boldsymbol{\gamma_{HD,j}[-]}$	-0.278	0.371	0.473	0.448
$\boldsymbol{p - value}$	0.292	$1.0 \cdot 10^{-2}$	$2.5 \cdot 10^{-3}$	0.040
$\boldsymbol{\gamma_{A,j}[-]}$	-	-	-	-
$\boldsymbol{p - value}$	-	-	-	-
$\boldsymbol{\gamma_{NA,j}[-]}$	1.103	1.119	0.717	0.667
$\boldsymbol{p - value}$	$2.8 \cdot 10^{-4}$	$3.2 \cdot 10^{-9}$	$5.3 \cdot 10^{-4}$	0.012
$\boldsymbol{\eta_{0j}[ln(g)^{-1}]}$	1.014	2.035	2.024	2.144
Median value of ln(PGA) for $H/D = 0.5$, unanchored				
$\boldsymbol{\mu_j[ln(g)]}$	1.401	-0.528	-0.105	0.262
Median value of ln(PGA) for $H/D = 1$, unanchored				
$\boldsymbol{\mu_j[ln(g)]}$	1.598	-0.673	-0.301	0.095
Median value of ln(PGA) for $H/D = 2$, unanchored				
$\boldsymbol{\mu_j[ln(g)]}$	1.765	-0.868	-0.528	-0.128

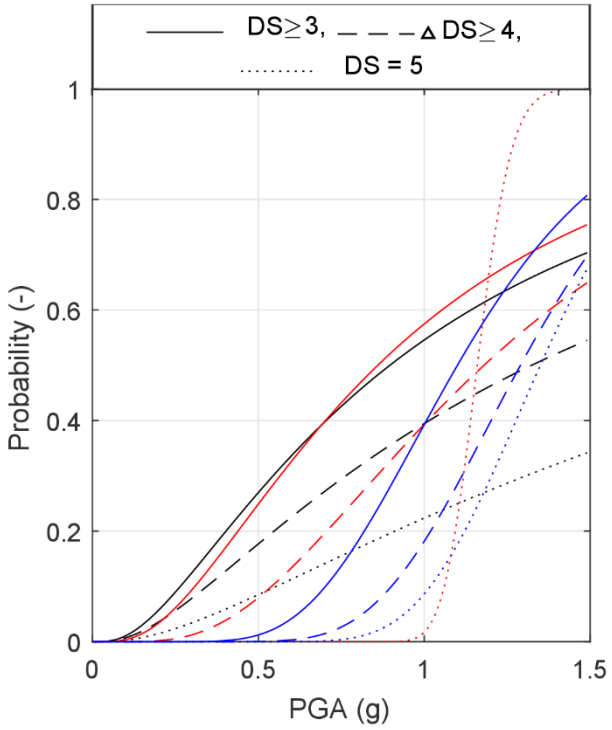

Figure 4-24. Fragility curves for all tanks in database in terms of Damage States: probit model of the current work (Eqs. (4.5)-(4.7)), black lines; ALA (2001), red lines; O'Rourke and So (2000), blue lines.

Table 4.22. Comparison in terms of fragility parameters obtained for Damage States and all database tanks in :i) the current work by using probit model presented in Eqs. (4.5)-(4.7), ii) O'Rourke and So (2000), iii) AlA (2001).

	Fragility parameters					
	Current study		***O'Rourke and So (2000)***[8]		***ALA (2001)***[9]	
Damage States	$\mu_j\,[ln(g)]$	$\sigma_j[ln(g)]$	$\mu_j\,[ln(g)]$	$\sigma_j[ln(g)]$	$\mu_j\,[ln(g)]$	$\sigma_j[ln(g)]$
$DS \geq 3$	-0.11	0.95	0.10	0.35	-0.15	0.80
$DS \geq 4$	0.28	1.05	0.25	0.28	0.17	0.61
$DS = 5$	0.86	1.13	0.30	0.22	0.15	0.07

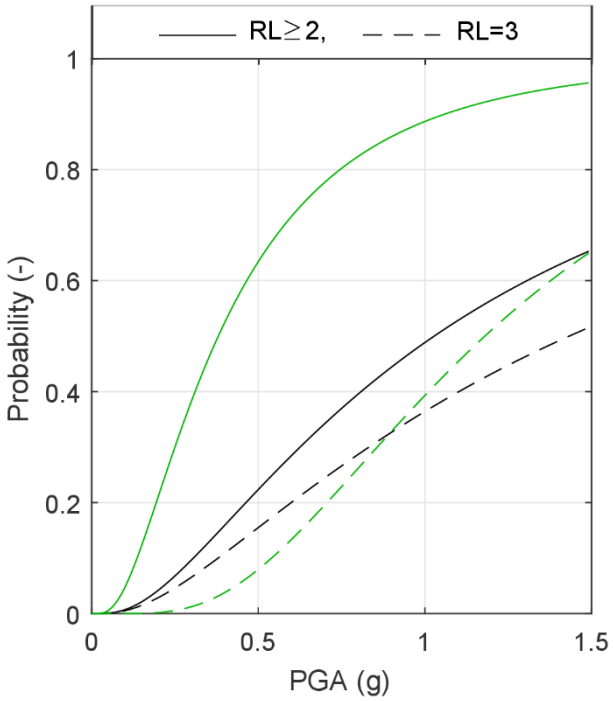

Figure 4-25. Fragility curves for all tanks in database in terms of Risk Levels: probit model of the current work (Eqs. (4.5)-(4.7)), black lines; Salzano et. al (2003), green lines;

Table 4.23. Comparison in terms of fragility parameters obtained for Risk Levels and all database tanks in :i) the current work by using probit model presented in Eqs. (4.5)-(4.7), ii) Salzano et al. (2003).

	Fragility parameters			
	Current study		***Salzano et al. (2003) [10]***	
Damage States	$\mu_j\,[ln(g)]$	$\sigma_j[ln(g)]$	$\mu_j\,[ln(g)]$	$\sigma_j[ln(g)]$
$\boldsymbol{RL \geq 2}$	0.03	0.95	-0.97	0.80
$\boldsymbol{RL = 3}$	0.36	1.04	0.17	0.61

4.7. Conclusion

The evaluation of seismic fragility of on-grade steel storage tanks based on empirical damage data constitutes the first main step carried out in the context of this PhD research. At the date, the bigger collection of damage data available in literature was provided by Cooper in [2]. His technical report collects data on about 500 tanks in 10 earthquakes ranging from 1933 through 1995. All previous statistical studies based on tank empirical damage data [8–10,67] were performed by using this dataset. The current study provides to the technical state of art a bigger tank damage data collection of 5829 on-grade steel storage tanks involved in 24 seismic events from 1933 through 2014. Database includes tanks of different size, fabrication type, date of construction, code adopted, liquid stored, roof and foundation type. For recent earthquakes, tank average dimension and location have been obtained from GIS archives. Reliable PGA values for tanks in absence of ground-motion recording have been obtained by using the program ShakeMap or attenuation models. Of this initial collection, 3026 tanks have been selected for the purpose of analysis, while the others have been excluded because of different construction material and geometry, and damage related to soil liquefaction.

A further novel introduced by the current study has been the new definition of Damage States, basing on a critical analysis of the different mechanisms involved in the tank seismic performance. Tank damages have been classified into 5 damage states and 3 risk levels. In particular, compared to previous researches, this work analyzes in different way damage to the lower shell courses and damage to the upper part of tank, since the dynamic mechanisms involved (i.e. bulging and sloshing) are excited by different frequencies.

Bayesian regression was used to calculate tank fragility curves. Different generalized linear models with probit and logit link functions have been employed for expressing the probability related to the damage state under investigation as a function of ground-motion intensity. The effects on the tank seismic performance of the aspect ratio H/D, filling level of the liquid stored at the time of the earthquake occurrence, and presence of anchorage system have been investigated. One of this model provides the advantage to take into account simultaneously the effects on fragility of these crucial aspects. Results demonstrate that past studies tend to overestimate the seismic fragility of tanks, since with respect to the present work, (1) smaller data collections were used, (2) a significant number of undamaged tanks, considered herein, were omitted and (3) newer seismic event were not taken into account. However, the current results overall confirms some general trends from other researchers in terms of influence on the tank performances of filling level, presence of base anchorage system and tank aspect ratio. In particular, slender tanks are more vulnerable than comparatively squat tanks, as well as anchored tanks performed better than comparatively unanchored tanks. Finally, tank seismic performance decreases as the filling level increases.

5. Simplified analysis of the tank rocking motion

5.1. Introduction

The main purpose of this chapter is to provide a simplified analysis of the rocking motion of cylindrical tanks focusing on the role of dynamic forces involved in rocking-bulging interaction.

As well known, the dynamic response of unanchored cylindrical tanks to the horizontal ground acceleration is governed by the interaction between bulging and rocking motions [161]. Despite many researches have been conducted on this topic, their contribution to an effective treatment was limited to numerical simulations and experimental tests. Even in the framework of seismic design code, the rocking motion is determined using a diagram carried out by a study performed with finite element analyses on sample tanks (see Chapter 1). In particular, uplift of the tank bottom plate is given as a function of the overturning moment for different values of the aspect ratio of the tank [162]. Therefore, in order to provide an effective tool for the evaluation of the main tank response, this work presents an analytical treatment of the tank bulging motion that takes into account the effect of rocking. Indeed, during the seismic event, the tank bulging motion is affected by the rotational inertia forces associated with the bottom plate uplift, then, considering the bulging and rocking motions separately can lead in error. In particular, the analyses carried out will demonstrate that rocking motion causes a reduction of the bulging response.

After a critical analysis of the current literature, the first section of this chapter provides an overview of the main steps of Taniguchi's research carried out in the framework of the tank rocking-bulging motion, in order to describe the technical background on which the current study is founded.

A next section provides a detailed description of the analytical model developed by Taniguchi in [163], the so-called two degree of freedom system (2DOF) that constitutes the starting point of the current study. The aim of the 2DOF system is to simulate the dynamic behavior of tanks taking into account both rotational motion and horizontal translational motion. It should be mentioned that no plasticity of the model is considered; moreover, the sliding motion is not taken into account.

In order to validate the accuracy of the 2DOF system in describing the effects of rotational-translational interaction on the main response, the second order system of differential equations is solved using a numerical software (MATLAB). Results obtained in terms of time history of

relative displacement and rotation are compared with those of the experimental test carried out by recording, through a high-speed camera, the motion of a physical model whose features are calibrated in order to properly represent the dynamic behavior of the 2DOF model. Once validated through the comparison, the 2DOF system provides the tank model equations by replacing the physical quantities of the 2DOF model with those of a sample tank. The equations of motion for the tank model are simplified in order to easily obtain the two main quantities that describe the tank rocking-bulging motion: the maximum angular acceleration $\ddot{\vartheta}_{max}$ and the absolute maximum response acceleration $(\ddot{x}_1 + \ddot{z}_H)_{max}$ that takes into account the reduction of bulging motion due to the occurrence of rocking.

Despite a previous study conducted by Taniguchi [163] provides a simplified analysis obtained from the same differential equations of the tank model, the author does not keep in simplified equations the terms related to the rocking-bulging interaction. However, as the comparison between analytical and experimental results obtained in the present work corroborates, the rocking-bulging interaction is governed by rotational inertia, centrifugal and Coriolis forces that play a leading role in the dynamic response of the tank. Therefore, the behavior of a tank experiencing rocking-bulging motion is far from that of a tank experiencing exclusively bulging or rocking motions, because different forces are involved in each of these cases. In light of this, the present work proposes a new treatment of the second order differential system, that unlike the previous study, maintains terms related to rotational inertia, centrifugal and Coriolis forces also in the simplified analysis. By following this procedure, reasonable values both for angular acceleration and horizontal absolute response acceleration are obtained.

The last section of this work proposes the seismic analysis of an unanchored steel storage tank carried out in LS-DYNA software. Value of the response obtained from numerical analysis is compared with that provided by the analytical one, in order to validate the accuracy of the latter.

It should be noted that the proposed procedure does not take into account the effect of sloshing motion. Actually, as confirmed by a previous study [161], the natural period of the sloshing system is far from that of the bulging one. Moreover, the main shock, principally consisting of short period ground accelerations exciting the bulging system, appears during the first instants of a recorded accelerogram. At these moments, shake table tests show that only small waves occur on the fluid surface at the two opposite ends of the tank diameter parallel to the seismic action. This little splashing is attributed to the rocking-bulging motion of the liquid. Sloshing motion occurs later, excited by the long period accelerations. For this reason, it is reasonable to neglect the sloshing system in the proposed analysis.

5.2. Rocking-bulging motion in literature

Bulging motion represents the motion of the liquid inside the tank undergoing the translational inertia force. It is also known as impulsive motion (see Chapter 1 for details). In the context of clamped tanks, the mechanical investigation on the tank-fluid system subjected to horizontal acceleration was first begun by Housner [18]. Housner considered the tank to be infinitely rigid so that the motion of the tank shell and roof together with a portion of the liquid content moving in unison with the shell, coincides with ground motion. This theory has been widely recognized and used in American and European seismic design codes. Actually, tanks are not rigid and typically have a natural period in horizontal vibration that affects the tank response. Veletsos in [22] concluded that the impulsive force can be reasonable estimated from the solutions derived for a rigid tank except that the maximum ground acceleration is replaced by the spectral value of the pseudo-acceleration corresponding to the fundamental natural frequency of the tank-fluid system. Sakai and Ogawa [164] solved the shell-liquid couple vibration problems (so called "bulging problem") through a variational approach and presented the calculation of the natural periods of tanks. Simplified mechanical models proposed in literature [16–20] employed spring-mass models to take into account the effect of the impulsive mass for rigid (spring constant $k \to \infty$) and flexible wall. That is reasonable since the tank-fluid system is regarded as a continuous system. It should be noted that, in case of fixed tanks, the sum of bulging and sloshing mass provides the total liquid mass.

In case of unanchored tanks, the dynamic behavior of the tank-fluid system becomes more complex, due to the discontinuous nature of the rocking phenomenon, and to the strongly nonlinear fluid-shell-soil interaction problem. The rocking motion of the unanchored tank has been the subject of both experimental and analytical study. Clough [49] investigated the uplift displacement of the tank bottom plate and hypothetically identified the crescent like uplift region of bottom plate. Clough and Niwa [50] experimentally the stress distribution around the junction between shell wall and bottom plate through static tilt tests. Isoe [165] and Peek [57,166] provided the analytical procedure to obtain the stress distribution of the same problem. Assuming the development of two elastic hinges in the bottom plate, the calculation of its deflection was presented by Wozniak and Mitchell in 1978 [51]. Veletsos and Tang [167], in analyzing the rocking motion of unanchored tanks described the tank-fluid system through a mechanical model similar to that used for investigating the transient response of laterally excited fixed tanks. Their mechanical model consisting of impulsive and convective spring-mass systems was excited through an angular base motion about a horizontal axis at the center of the tank base. This is a first simplification of the formulation, since actually tank rotation occurs alternately about the right and the left tank bottom edges. Several components of the response for the rocking tank were evaluated from existing data related to the tank response in

case of lateral excitation. However, as demonstrated by later studies, in case of base uplift occurrence, the total liquid mass does not count only impulsive and convective components. Veletsos and Malhotra [168,169] studied the uplifted resistance of the tank bottom plate and presented a reasonable and efficient analysis method for the asymmetrically uplifted plates. The same authors in [55] thoroughly investigated the effects of the bottom plate uplifting on the tank liquid system. However, their works did not take into account the mechanical role of the liquid content responding to the tank rocking motion. Although the behavior of partially uplifting plate was largely investigated, the effects of uplifting on the response of the tank-liquid system has not been not fully understood. Moreover, a mechanical model which considers all physical quantities involved in the tank rocking response and relationships among them was not not provided. Then, in order to fully understand the problem of tank rocking, it was necessary to investigate the problem from a kinematic point of view. Under this consideration, the first simpler model analyzed was a rigid body. Housner in [170] analyzed the rocking response of a free-standing rigid body subjected to the ground motion. Spanos [171], Anooshehpoor [172] and Shenton [173] found the minimum overturning ground motion acceleration. Pompei [174] and Zhang [175] pointed out the importance of rotational inertia forces in analyzing the kinematics of the rocking motion of a body. Using the variational approach, Taniguchi [176–178] investigated the rocking motion of bodies including the effects of rotational inertia forces. Later, in Ref. [48,179,180] the author employed the mechanical analogy between the rocking motion of the rigid body and that of the tank. In his studied he considered the rocking-bulging interaction motion. In Ref. [161] Taniguchi provided a first method for the evaluation of the dynamical quantities involved in rocking motion, i.e. the effective mass of liquid for rocking motion and that for rocking-bulging interaction, and discussed about the fundamental role of the rotational inertia forces. Later, in [162], the author proposed a more accurate procedure consisting in adopting the so-called “slice model” for evaluating the masses of fluid contributing to the rocking motion of cylindrical tanks. Details on this work are given in the next paragraph.

5.3. Technical background on tank rocking-bulging motion

In the framework of this PhD thesis, one of the main topics analyzed has been the dynamic behavior of the tank-fluid system, with particular regard to the tank rocking-bulging interaction motion. This study has been developed during a research period at the Tottori University, under the supervision of Prof. Tomoyo Taniguchi. The present section aims to provide an overview of the main steps of Taniguchi’s research in order to underline the key concepts and main achievements constituting the background on which the current study is founded.

As already mentioned, Taniguchi understood the importance of analyzing the rocking motion of unanchored tanks starting from the kinematic study of a rectangular rigid body subjected to horizontal and vertical acceleration [178]. By deriving equations of motion, commencement and termination conditions, and reaction forces of the rigid body modes, he analytically described the lift-off motion, slip motion and lift-off-slip interaction. Figure 5-1 depicts the two possible motions of the rigid block starting from the rest position (i.e. lift-off motion and slip motion) and the four subsequent responses, accordingly to the equations of motion governing the rigid body modes and boundary conditions corresponding to the commencement and termination of the motions.

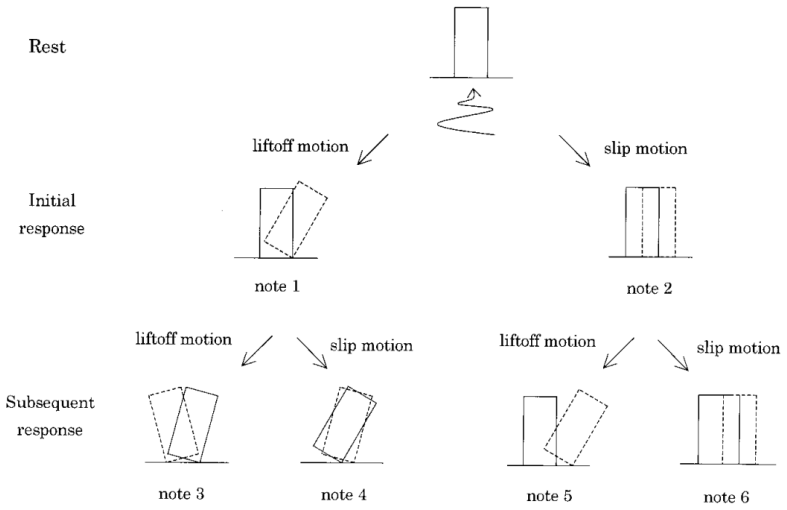

note 1 : equations of liftoff motion[*1]
liftoff commencement conditions
note 2 : equations of slip motion[*2]
slip commencement conditions
note 3 : equations of liftoff motion[*1]
liftoff termination conditions[*5]
overturning conditions[*6]
note 4 : equations of liftoff-slip interaction motion[*3]
slip commencement conditions including liftoff motion effects
termination conditions[*4]
liftoff termination conditions[*5]
overturning conditions[*6]
note 5 : equations of liftoff-slip interaction motion[*3]
liftoff commencement conditions including slip motion effects
slip termination conditions[*4]
liftoff termination conditions[*5]
overturning conditions[*6]
note 6 : equations of slip motion[*2]
slip termination conditions[*4]

Figure 5-1. Classification of the response of a rigid body subjected to horizontal and vertical ground acceleration [178]

From observation of the lift-off motion he categorized the lift-off as a not vibrant phenomenon but a bouncing phenomenon. Indeed it has no natural frequency and there is no conservative force which is proportional to the lift-off angle. Employing the mechanical analogy between the lift-off motion of the rigid bodies and the tanks, Taniguchi investigated the dynamical system of the tank rocking motion.

As already mentioned, the effective mass of liquid for bulging motion represents the portion of the liquid mass undergoing the horizontal inertia forces. A fundamental step in Taniguchi's research consisted in founding that the rocking motion of a body is governed by the effects of rotational inertia forced on the non-inertial coordinate system, i.e. the centrifugal, inertia, and Coriolis forces. This consideration led the author to observe that as for the bulging motion, it is possible to derive the analytical formulation for the effective mass of liquid for rocking motion. The distribution of this mass was supposed to be linear among the entire height of the tank wall. Figure 5-2 shows a simple sketch of the liquid masses distribution along the tank wall (bulging and rocking masses).

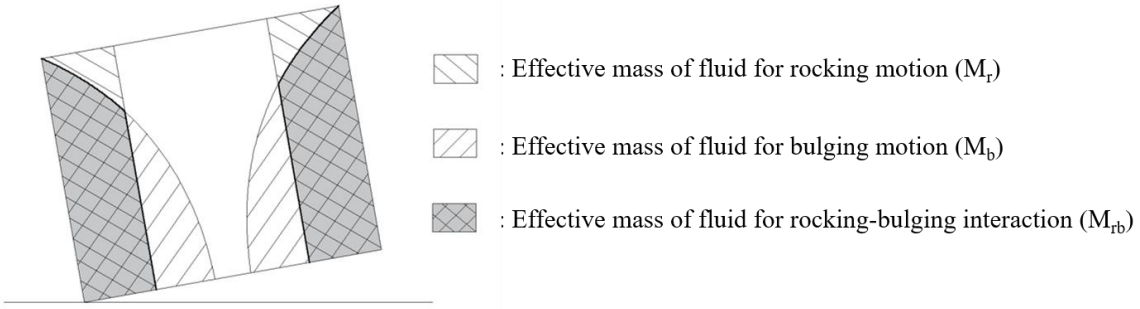

Figure 5-2. Liquid masses distribution among the tank wall

However, the effective mass for rocking motion was not the only subject of investigation. From Figure 5-2 it should be noted that the distribution of the effective mass of fluid for bulging motion and that for rocking motion partially overlap. A part of the effective mass of fluid for tank bulging motion may be also under the influence of the rotational inertia forces. Under this consideration, Taniguchi introduced a third effective mass, i.e. the effective mass of fluid for rocking-bulging interaction motion. As many results by past investigators show, the uplift region of the tank bottom plate is partial. It may yield the hypothesis that the influences of rotational inertia forces exerted by the tank rocking motion on the bulging system are limited to a part of the effective mass of liquid for bulging motion which overlaps with the distribution of the effective mass of liquid for rocking motion.

The effects of rotational inertia forces as well as the effective mass for rocking and rocking-bulging interaction were employed in Ref. [161], in which the author defined an analytical procedure for the analysis of the dynamics of rocking tanks that computes the effective masses involved in the tank rocking motion. A spring-mass-rigid-body combined system has been adopted to describe the mechanism of the tank rocking motion. In addition, the contribution of the rotational inertia forces involved in the tank rocking motion to the bulging response was thoroughly examined. Figure 5-4 shows the analized tank model in rotated position. The height of the liquid content is h, the tank radius R. Rotation can occur alternately about the left and the right bottom edges (O and O'). The model has a rigid-doughnut-shaped bottom plate and stiffen-less membrane in its central part. The effective mass for bulging motion, M_I, which is the same as the effective mass of liquid for impulsive motion, is attached to the tank wall by horizontal sping, whose stifness is calibrated in order to meet the natural frequency of the first bulging mode of the tank. Curves for determining mass M_I and its height from the base h_I can be found in [181]. This research considers the effective liquid mass for rocking motion distributed along the filling height of content and from the inner surface of the tank wall up to the edge of the rigid doughnut-shaped bottom ring (see Figure 5-3 and Figure 5-4).

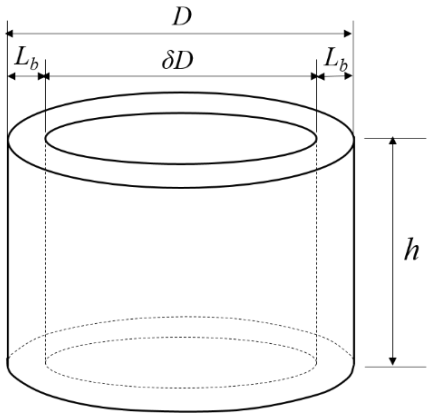

Figure 5-3. Idealized form of the effective mass for rocking [161]

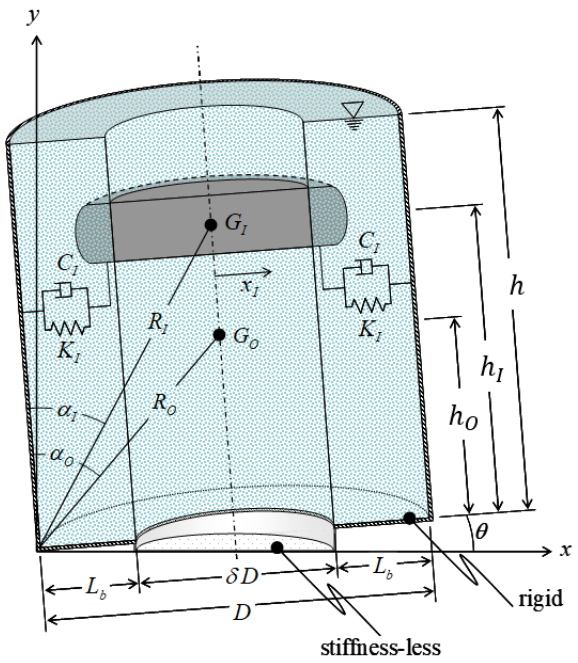

Figure 5-4. Spring-mass-rigid-body combined system in rotated position [161]

The appearance of the effective mass of liquid for rocking motion can be regarded as the hollow cylinder in Figure 5-3 or Figure 5-4. Its wall thickness is the same as the width of the rigid-doughnut-shaped bottom plate, L_b. From the geometry shown in Figure 5-3, the effective mass of liquid for rocking motion and the moment of inertia of this mass has been calculated. Their expressions are the following:

$$\delta = 1 - 2L_b / D \tag{5.1}$$

$$M_E = (1-\delta^2)M_0 \tag{5.2}$$

$$I_E = \frac{M_0 h^2}{48}\left\{3\gamma^2(\delta^2+5)(1-\delta^2)+16(1-\delta^2)\right\} \tag{5.3}$$

where M_0 is the total mass of the liquid content and $\gamma = D/h$ is the tank aspect ratio.

The effective mass of liquid for rocking-bulging interaction has been calculated based on the Housner's theory. Housner [18] determined the effective mass of liquid for impulsive motion in accordance with fluid pressure as if the mass were moving with the tank. From the same analogy, the lateral pressure exerted by the fluid above the uplift region of the bottom plate (i.e. by the hollow cylinder content) is given as if an equivalent mass M_{rb} were moving with

impulsive motion of the tank. This part is also moving with the rocking motion of the tank and consequently subjected to the rotational inertia force. The ratio of the effective mass for rocking-bulging motion to the effective mass bor bulging motion is obtained as:

$$\frac{M_{rb}}{M_l} = 1 - \frac{\sinh\left(\sqrt{3}\dfrac{R - L_b}{h}\right)}{\sinh\left(\sqrt{3}\dfrac{R}{h}\right)} \quad \left(\frac{h}{R} \le 1.5\right) \tag{5.4}$$

$$\frac{M_{rb}}{M_l} = \frac{\dfrac{R}{h}\left[1.06 - 0.745\sinh\left\{1.15\left(1 - \dfrac{L_b}{R}\right)\right\}\right] + \dfrac{L_b}{h}\left(2 - \dfrac{L_b}{R}\right)\left(\dfrac{h}{R} - 1.5\right)}{1 - 0.436\dfrac{R}{h}} \quad \left(\frac{h}{R} > 1.5\right) \tag{5.5}$$

Figure 5-5 presents values of this ratio for various h/R.

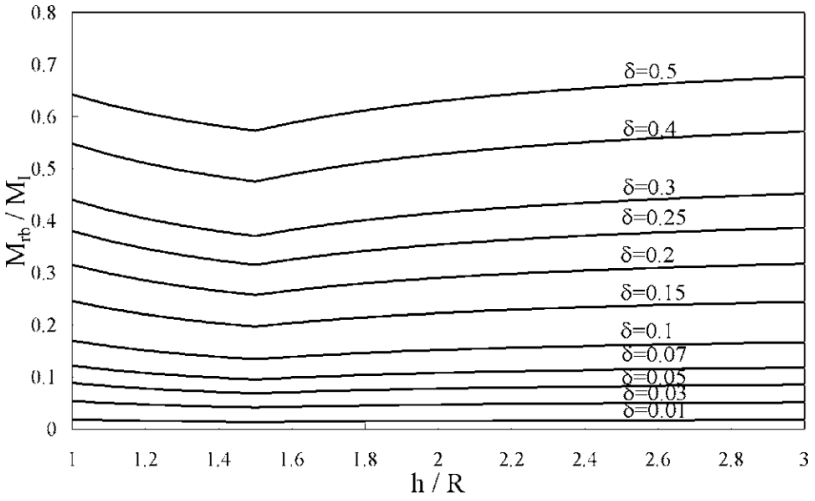

Figure 5-5. Ratio of effective mass of liquid for rocking-bulging interaction motions to that for impulsive mass [161]

Through this study, Taniguchi demonstrated that the effective mass of fluid for rocking motion and that for rocking-bulging interaction can reach significant values with respect to the impulsive mass, and then, they play a significant role in the framework of tank rocking motion. Under this consideration, other investigations were carried out by the author with the purpose to rigorously quantify them. A simplification employed in the spring-mass-rigid-body combined system was the rigid-doughnut-shaped bottom plate. Generally, the tanks have a flexible bottom plate, then rotation ϑ involves only a crescent-like uplifted part that appears eccentrically on the periphery of the tank bottom plate. In Ref. [162], Taniguchi focused on this issue by considering the effects of the deformed tank bottom plate on the fluid pressure. Then,

he proposed an analytical procedure for evaluation of the effective mass of fluid for rocking motion and that for rocking-bulging interaction of cylindrical tanks having the crescent-like uplift part in the bottom plate. The cylindrical tank was studied through the so-called slice model. Figure 5-6 shows a tank with undeformable shell wall. It rotates around the Y-axis with the angular velocity $\dot{\vartheta}_0(t)$ pivoting at its left bottom edge, at the origin O of the global Cartesian coordinates $X-Y-Z$, and its bottom plate has a crescent-like uplifted part as a consequence. The value of $2\delta l$ gives the width of the uplifted part of the tank bottom plate, while $l-\delta l$ gives the diameter of the circular unuplifted part of the tank bottom plate.

A thin rectangular tank, i.e. the slice model, is set inside the cylindrical tank at a distance a from the X-axis and perpendicular to the Y-axis. The element coordinates $x-z$ of the slice model has the origin at O' and is parallel to the $X-Z$ plane of the global coordinates. Figure 5-7 and Figure 5-9 show a plane view of the tank bottom plate where the hatched part represents the crescent-like uplifted part of the tank bottom plate. The bottom part of the slice model is shown as a segment $O'-N$.

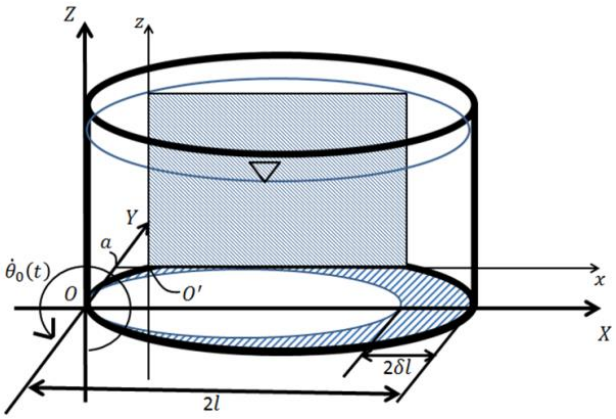

Figure 5-6. Cylindrical tank and slice model [162]

The boundary conditions applied to the slice model change in accordace with the location of the slice model in the cylindrical tank model. If the slide model is located between $Y=0$ and $Y=\pm l-\delta l$, i.e. if the slice model contains an unuplifted part on its bottom, then the boundary condition for the bottom part are shown in Figure 5-8. In contrast, if the slice model is located between $Y=\pm l-\delta l$ and $Y=\pm l$, i.e. if the bottom of the slice model consists of only uplifted part of the tank bottom plate, the boundary condition are depicted in Figure 5-10. It should be noted that the bottom plate of the cylindrical tank is assumed to uplift rectilinearly.

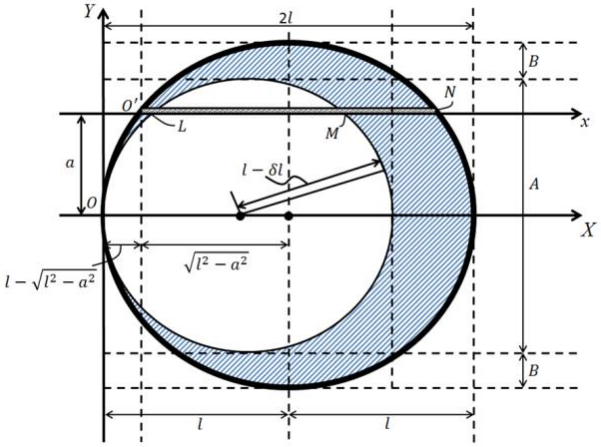

Figure 5-7. Slice model which has unuplifted bottom part [162]

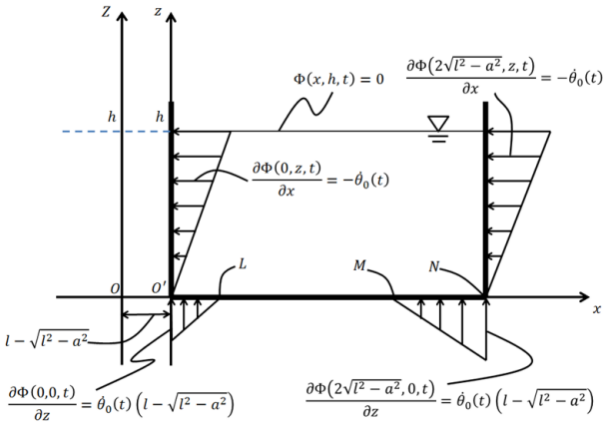

Figure 5-8. Boundary conditions for the slice model which has unuplifted bottom part [162]

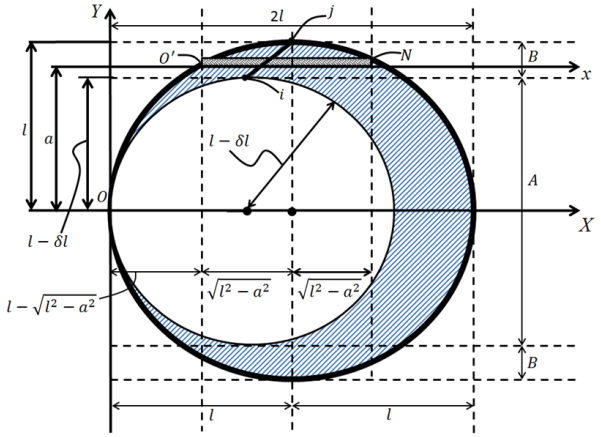

Figure 5-9. Slice model whose all bottom part uplifts [162]

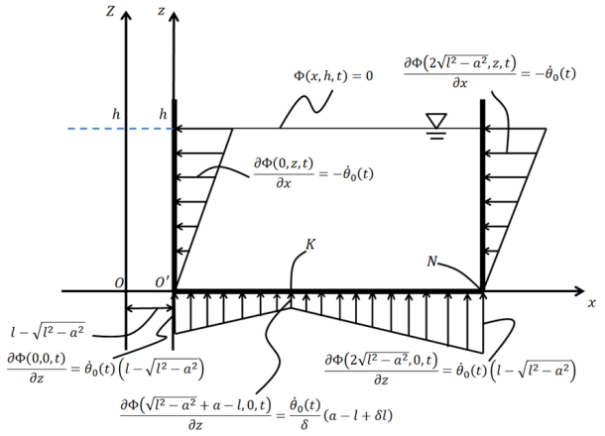

Figure 5-10. Boundary conditions for the slice model whose all bottom part uplift [162]

The solution of the Laplace equation in Cartesian coordinate that satisfies all boundary conditions is obtained by applying the Fouriet transformation. Fouriet inverse transformation is then applied to it and finds a solution of the velocity potential function of the slice model. Its derivative with respect to time gives the fluid pressure at an arbitrary point inside the slide model of interest.

Effective mass of fluid for rocking motion of cylindrical tanks

Once the fluid pressure has been obtained, the pressure gradient of fluid in a given direction gives the effective density of fluid moving in unison with the tank in the given direction at an arbitrary point inside the tank. Therefore, from the equilibrium of forces acting on a small volume in the rotational direction (Figure 5-11), the effective density of fluid for rocking motion at an arbitrary point inside the slice model is given as a function of the pressure gradient in the rotational direction:

$$\rho_{eff}(r,\theta) = -\frac{1}{r^2\ddot{\theta}_0(t)} \cdot \frac{\partial P(r,\theta,t)}{\partial \theta} \tag{5.6}$$

Employing the expression for $P(r,\theta,t)$ obtained as described before and coordinate transformation, Eq. (5.6) becomes:

$$\rho_{eff}(x,z) = \ f_A(x,z)\rho \ \text{ or } \ f_B(x,z)\rho \tag{5.7}$$

where $f_A(x,z)$ and $f_B(x,z)$ are the ratios of the effective density of fluid for rocking motion to the original density of fluid at an arbitrary point. In particular, $f_A(x,z)$ is that for the slice model located between $Y = 0$ and $Y = \pm l - \delta l$ (see Figure 5-7), while $f_B(x,z)$ is that for the slice model located between $Y = \pm l - \delta l$ and $Y = \pm l$ (see Figure 5-9). Expression for $f_A(x,z)$ and $f_B(x,z)$ are given in Ref. [162]. The effective mass of fluid for rocking motion of the cylindrical tank M_r is given by summing up the mass of all small volumes inside all slice models:

$$M_r = f_r M_{Total} \tag{5.8}$$

$$f_r = \frac{1}{l^2 h\pi}\left[\int_0^h \int_0^{2\sqrt{l^2-a^2}} \int_{-(l-\delta l)}^{l-\delta l} f_A \, dadxdz \ + 2\int_0^h \int_0^{2\sqrt{l^2-a^2}} \int_{l-\delta l}^{l} f_B \, dadxdz\right] \tag{5.9}$$

where f_r is the ratio of the effective mass of fluid for rocking motion of cylindrical tank M_r to the total mass of the fluid M_{Total}.

Table 5.1 shows values of the ratio of the effective mass of fluid for rocking motion to the total mass of fluid fulfilled in the tank for different values of the tank aspect ratio $h/2l$. Employing values of δ from 1% to 10% (according to Ref. [5], the value of δ is up to 6% to 7% for broad tanks), the effective mass of fluid for rocking motion is computed. The value of f_r increases as the tank becomes tall, and as the uplift part extends (se graph in Figure 5-12). In slender tanks, since it is about a half of the total mass of fluid fulfilled in the tank, ignoring its effects in analyzing the tank rock motion may yield erroneous results.

Following a similar procedure, the effective moment of inertia of fluid for rocking motion, as well as the horizontal and vertical distance between the pivot O and the centroid of effective mass of fluid for rocking motion, $d_{r,x}$ and $d_{r,z}$ have been calculated and tabulated (respectively Table 5.2, Table 5.3, Table 5.4) for the tank commonly used geometry as a function of the tank aspect ratio $h/2l$ for different values of δ.

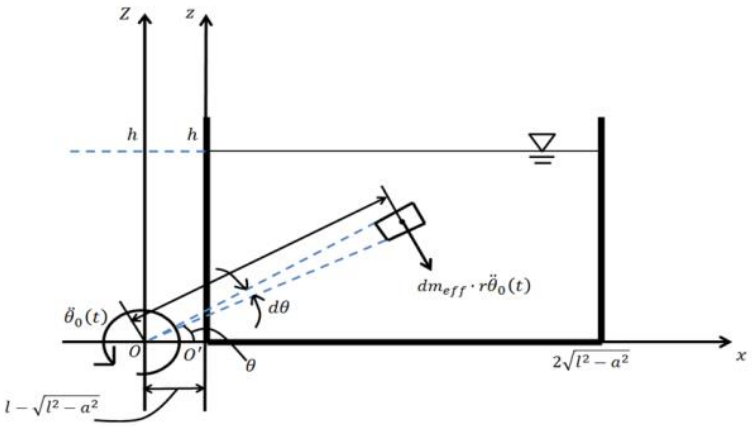

Figure 5-11. Equilibrium of forces acting on a small volume in the slice model in rocking motion [162]

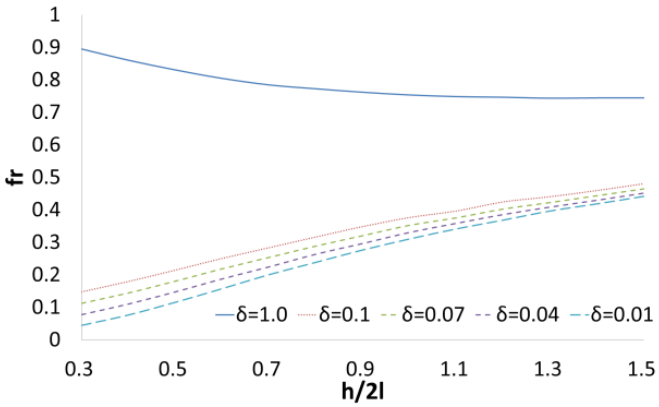

Figure 5-12. Effective mass of fluid for rocking motion [162]

Table 5.1 Values of the ratio of the effective mass of fluid for rocking motion to the total mass of fluid fulfilled in the tank

	h/2l												
	0.3	0.4	0.5	0.6	0.7	0.8	0.9	1.0	1.1	1.2	1.3	1.4	1.5
δ =1.0	0.895	0.861	0.831	0.805	0.785	0.773	0.762	0.754	0.749	0.747	0.744	0.745	0.745
δ =0.1	0.148	0.180	0.215	0.251	0.284	0.317	0.349	0.377	0.397	0.425	0.441	0.460	0.481
δ =0.09	0.136	0.168	0.203	0.239	0.276	0.308	0.338	0.369	0.390	0.415	0.438	0.458	0.472
δ =0.08	0.124	0.157	0.192	0.229	0.264	0.300	0.330	0.361	0.383	0.409	0.429	0.450	0.467
δ =0.07	0.113	0.145	0.181	0.219	0.254	0.289	0.321	0.353	0.376	0.403	0.423	0.444	0.465
δ =0.06	0.101	0.134	0.170	0.208	0.244	0.280	0.313	0.345	0.369	0.397	0.418	0.440	0.458
δ =0.05	0.089	0.122	0.159	0.197	0.235	0.272	0.305	0.338	0.363	0.391	0.415	0.435	0.456
δ =0.04	0.078	0.111	0.148	0.188	0.225	0.264	0.297	0.331	0.359	0.386	0.409	0.430	0.452
δ =0.03	0.066	0.099	0.137	0.177	0.216	0.254	0.289	0.324	0.353	0.379	0.404	0.427	0.448
δ =0.02	0.055	0.088	0.126	0.166	0.207	0.246	0.282	0.317	0.347	0.373	0.399	0.423	0.444
δ =0.01	0.045	0.077	0.116	0.158	0.201	0.239	0.277	0.311	0.342	0.369	0.397	0.419	0.442

Table 5.2 Values of the ratio of horizontal distance between the centroid of M_r and O to the diameter of tank

	h/2l												
	0.3	0.4	0.5	0.6	0.7	0.8	0.9	1	1.1	1.2	1.3	1.4	1.5
δ =1.0	0.5164	0.5159	0.5141	0.5116	0.5087	0.5056	0.5026	0.4998	0.4973	0.4950	0.4931	0.4915	0.4902
δ =0.1	0.6162	0.5543	0.5086	0.4774	0.4566	0.4434	0.4356	0.4313	0.4289	0.4291	0.4293	0.4310	0.4331
δ =0.09	0.6151	0.5508	0.5041	0.4726	0.4525	0.4394	0.4318	0.4283	0.4263	0.4264	0.4278	0.4296	0.4310
δ =0.08	0.6131	0.5463	0.4989	0.4676	0.4475	0.4356	0.4283	0.4254	0.4236	0.4242	0.4253	0.4273	0.4293
δ =0.07	0.6103	0.5412	0.4930	0.4621	0.4420	0.4309	0.4246	0.4222	0.4213	0.4219	0.4233	0.4255	0.4283
δ =0.06	0.6072	0.5348	0.4862	0.4558	0.4368	0.4264	0.4209	0.4191	0.4183	0.4195	0.4212	0.4238	0.4263
δ =0.05	0.6023	0.5271	0.4783	0.4485	0.4309	0.4216	0.4170	0.4159	0.4156	0.4172	0.4198	0.4220	0.4250
δ =0.04	0.5952	0.5174	0.4692	0.4408	0.4246	0.4171	0.4131	0.4128	0.4134	0.4155	0.4178	0.4204	0.4234
δ =0.03	0.5856	0.5054	0.4584	0.4320	0.4183	0.4119	0.4094	0.4097	0.4108	0.4129	0.4159	0.4190	0.4220
δ =0.02	0.5700	0.4898	0.4459	0.4233	0.4122	0.4073	0.4058	0.4068	0.4083	0.4109	0.4140	0.4175	0.4207
δ =0.01	0.5456	0.4696	0.4325	0.4146	0.4062	0.4029	0.4027	0.4040	0.4064	0.4093	0.4128	0.4161	0.4198

Table 5.3 Values of the ratio of vertical distance between the centroid of M_r and O to the depth of fluid

	h/2l												
	0.3	0.4	0.5	0.6	0.7	0.8	0.9	1	1.1	1.2	1.3	1.4	1.5
δ =1.0	0.4733	0.4630	0.4520	0.4454	0.4408	0.4377	0.4360	0.4354	0.4359	0.4366	0.4378	0.4396	0.4411
δ =0.1	0.4947	0.4921	0.4873	0.4860	0.4857	0.4860	0.4869	0.4892	0.4910	0.4933	0.4958	0.4978	0.5006
δ =0.09	0.4965	0.4940	0.4895	0.4886	0.4882	0.4884	0.4900	0.4915	0.4935	0.4956	0.4982	0.5000	0.5035
δ =0.08	0.4986	0.4962	0.4921	0.4914	0.4911	0.4915	0.4928	0.4943	0.4962	0.4983	0.5006	0.5025	0.5059
δ =0.07	0.5011	0.4991	0.4949	0.4943	0.4941	0.4946	0.4954	0.4969	0.4988	0.5010	0.5033	0.5051	0.5083
δ =0.06	0.5046	0.5022	0.4980	0.4976	0.4976	0.4978	0.4985	0.4996	0.5015	0.5037	0.5058	0.5087	0.5111
δ =0.05	0.5090	0.5059	0.5020	0.5014	0.5010	0.5011	0.5015	0.5025	0.5044	0.5066	0.5081	0.5107	0.5122
δ =0.04	0.5144	0.5103	0.5062	0.5053	0.5049	0.5043	0.5045	0.5056	0.5067	0.5085	0.5105	0.5131	0.5146
δ =0.03	0.5220	0.5161	0.5110	0.5096	0.5081	0.5079	0.5076	0.5084	0.5097	0.5109	0.5132	0.5155	0.5170
δ =0.02	0.5322	0.5231	0.5164	0.5136	0.5120	0.5108	0.5106	0.5111	0.5124	0.5138	0.5159	0.5179	0.5195
δ =0.01	0.5448	0.5308	0.5214	0.5177	0.5151	0.5136	0.5134	0.5137	0.5146	0.5158	0.5179	0.5193	0.5215

Table 5.4 Values of the ratio of the effective moment inertia of fluid for rocking motion to the moment inertia of total mass

	h/2l												
	0.3	0.4	0.5	0.6	0.7	0.8	0.9	1	1.1	1.2	1.3	1.4	1.5
δ =1.0	0.5833	0.6252	0.6549	0.6685	0.6853	0.7029	0.7235	0.7474	0.7760	0.8056	0.8376	0.8728	0.9079
δ =0.1	0.1208	0.1363	0.1577	0.1859	0.2206	0.2625	0.3112	0.3652	0.4180	0.4800	0.5364	0.5969	0.6651
δ =0.09	0.1111	0.1266	0.1481	0.1762	0.2126	0.2542	0.3030	0.3581	0.4123	0.4717	0.5362	0.5974	0.6569
δ =0.08	0.1014	0.1171	0.1382	0.1672	0.2032	0.2475	0.2959	0.3516	0.4031	0.4674	0.5284	0.5893	0.6545
δ =0.07	0.0915	0.1070	0.1290	0.1584	0.1943	0.2386	0.2883	0.3448	0.4015	0.4624	0.5248	0.5865	0.6563
δ =0.06	0.0817	0.0971	0.1193	0.1489	0.1860	0.2309	0.2814	0.3383	0.3951	0.4577	0.5195	0.5864	0.6498
δ =0.05	0.0718	0.0873	0.1098	0.1398	0.1776	0.2233	0.2724	0.3323	0.3903	0.4536	0.5190	0.5824	0.6485
δ =0.04	0.0618	0.0777	0.1003	0.1310	0.1692	0.2166	0.2656	0.3265	0.3865	0.4505	0.5145	0.5792	0.6471
δ =0.03	0.0502	0.0677	0.0908	0.1219	0.1613	0.2086	0.2614	0.3206	0.3820	0.4439	0.5117	0.5792	0.6414
δ =0.02	0.0419	0.0578	0.0816	0.1137	0.1543	0.2017	0.2555	0.3151	0.3768	0.4405	0.5087	0.5772	0.6437
δ =0.01	0.0323	0.0485	0.0729	0.1061	0.1473	0.1956	0.2505	0.3096	0.3734	0.4375	0.5072	0.5717	0.6445

Effective mass of fluid for bulging motion of cylindrical tanks

In order to investigate the effective mass of fluid for bulging motion, a slice model set a distance a from the X-axis and perpendicular to the Y-axis has been analyzed (Figure 5-6). The Laplace equation is solved specifying boundary conditions shown in Figure 5-13.

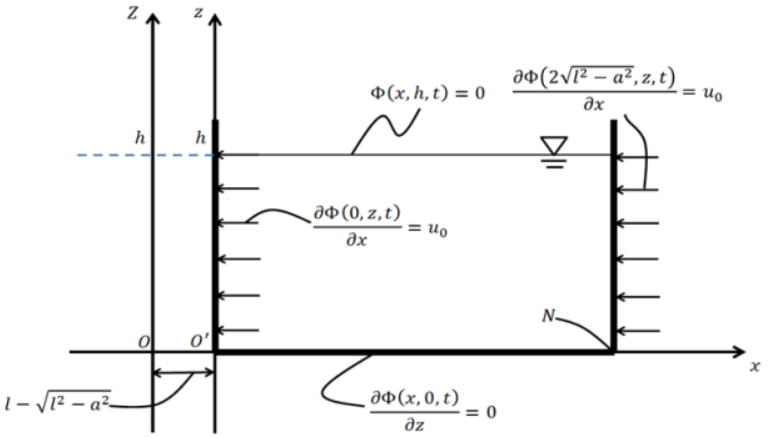

Figure 5-13. Boundary conditions of slice model for specifying the tank bulging motion [162]

The velocity potential has been calculated and its derivative with respect to time gives the fluid pressure at an arbitrary point inside the slice model of interest. The pressure gradient of fluid in the horizontal direction gives the effective density of fluid for bulging motion (see Figure 5-14)

$$\rho_{eff} = -\frac{1}{\ddot{u}_0}\frac{\partial P(x,z,t)}{\partial x} \tag{5.10}$$

Employing the expression of the fluid pressure, the effective density of fluid for bulging motion of the slice model is given as:

$$\rho_{eff}(x,z) = f_{b1}(x,z)\rho \tag{5.11}$$

where $f_{b1}(x,z)$ is the ratio of the effective density of fluid for bulging motion to the original density of fluid in the tank. Expression for $f_{b1}(x,z)$ is given in Ref. [162]. The effective mass of fluid for bulging motion of the cylindrical tank M_b is given by summing up the mass of all small volumes inside all slice models:

$$M_b = f_b M_{Total} \tag{5.12}$$

$$f_b = \frac{1}{l^2 h\pi}\left[\int_0^h \int_0^{2\sqrt{l^2-a^2}} \int_{-l}^{l} f_{b1}(x,z)\,da\,dx\,dz\right] \tag{5.13}$$

where f_b is the ration of the effective mass of fluid for bulging motion M_b and the total liquid mass M_{Total}. Values of f_b have been found to be in good agreement with those in literature [182]. Figure 5-15 shows this comparison as a function of the tank aspect ratio.

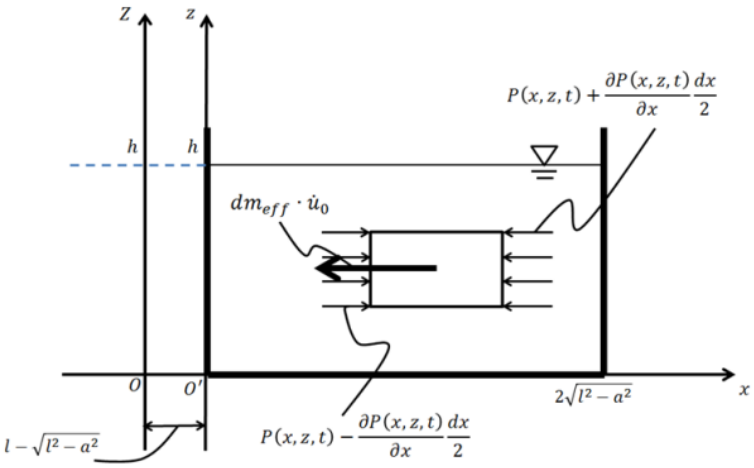

Figure 5-14. Equilibrium of forces acting on a small volume in the slice model in bulging motion [162]

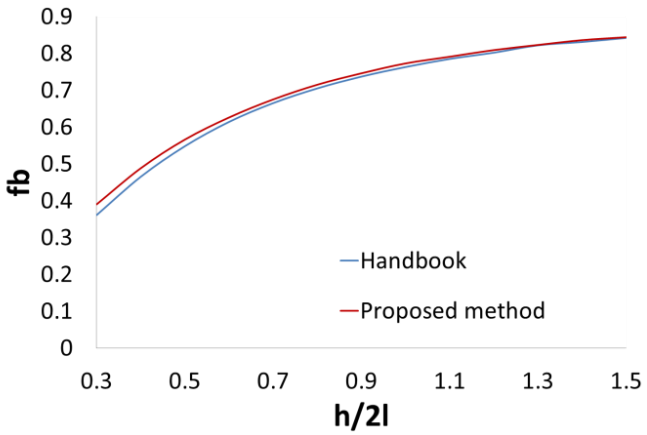

Figure 5-15. Effective mass of fluid for bulging motion [162]

Effective mass of fluid for rocking-bulging interation

Finally, the effective density of fluid for rocking-bulging interaction was given as the quotient of the product between the effective density of fluid for rocking motion and that for bulging motion divided by the original density of the fluid content. Summing up the effective mass of all small volumes inside all slice models, the effective mass of fluid for rocking-bulging interaction of the cylindrical tank was defined as

$$M_{rb} = f_{rb} M_{Total} \tag{5.14}$$

$$f_{rb} = \frac{1}{l^2 h\pi}\left[\int_0^h \int_0^{2\sqrt{l^2-a^2}} \int_{-(l-\delta l)}^{l-\delta l} f_A f_{b1} dadxdz + 2\int_0^h \int_0^{2\sqrt{l^2-a^2}} \int_{l-\delta l}^{l} f_B f_{b1} dadxdz\right] \tag{5.15}$$

where f_{rb} is the ratio of the effective mass of fluid for rocking -bulging interaction M_{rb} and the total fluid mass M_{Total}. Values of f_{rb} were calculated and given in Table 5.5 and Figure 5-16 as a function of the aspect ratio for different value of δ. The value of f_{rb} increases as the tank becomes tall, and as the uplift part extends (see graph in Figure 5-16). In slender tanks, it is about a third of total mass of fluid fulfilled in the tank, then ignoring effects of rocking-bulging interaction in analyzing the tank rock motion may yield erroneous results.

Table 5.5 Values of ratio of effective mass of fluid for rocking-bulging interaction to the total mass of fluid fulfilled in the tank

			h/2l										
	0.3	0.4	0.5	0.6	0.7	0.8	0.9	1	1.1	1.2	1.3	1.4	1.5
δ =1.0	0.3575	0.4351	0.4929	0.5346	0.5648	0.5879	0.6048	0.6185	0.6290	0.6394	0.6468	0.6558	0.6630
δ =0.1	0.0757	0.1041	0.1408	0.1749	0.2079	0.2418	0.2750	0.3048	0.3282	0.3564	0.3756	0.3972	0.4199
δ =0.09	0.0695	0.0978	0.1333	0.1662	0.2016	0.2342	0.2660	0.2978	0.3218	0.3486	0.3735	0.3967	0.4113
δ =0.08	0.0639	0.0924	0.1259	0.1586	0.1925	0.2284	0.2587	0.2912	0.3155	0.3425	0.3649	0.3881	0.4068
δ =0.07	0.0590	0.0845	0.1183	0.1519	0.1849	0.2192	0.2516	0.2843	0.3097	0.3367	0.3596	0.3834	0.4059
δ =0.06	0.0526	0.0780	0.1107	0.1432	0.1771	0.2120	0.2447	0.2775	0.3033	0.3310	0.3542	0.3783	0.3979
δ =0.05	0.0466	0.0715	0.1032	0.1353	0.1696	0.2048	0.2377	0.2710	0.2972	0.3257	0.3522	0.3738	0.3970
δ =0.04	0.0413	0.0655	0.0957	0.1286	0.1619	0.1988	0.2311	0.2646	0.2940	0.3222	0.3468	0.3695	0.3938
δ =0.03	0.0348	0.0577	0.0882	0.1203	0.1549	0.1906	0.2248	0.2589	0.2883	0.3151	0.3422	0.3672	0.3895
δ =0.02	0.0281	0.0502	0.0809	0.1139	0.1489	0.1844	0.2189	0.2533	0.2828	0.3103	0.3380	0.3633	0.3857
δ =0.01	0.0235	0.0448	0.0742	0.1074	0.1429	0.1786	0.2140	0.2477	0.2789	0.3071	0.3348	0.3587	0.3829

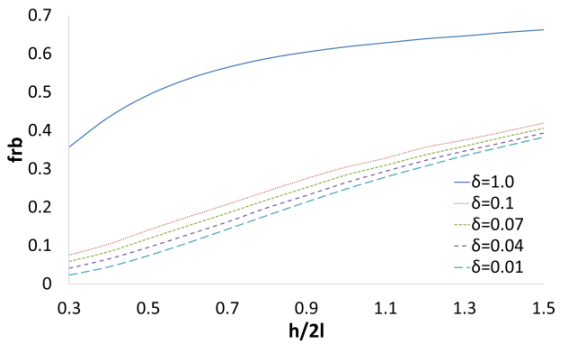

Figure 5-16. Effective mass of fluid for rocking-bulging interaction [162]

5.4. The two degrees of freedom model

Nomenclature

A list of the variables involved in the 2DOF model and tank model analyzed in the following is provided herein.

k : Spring constant

m_1 : Mass of the Spring-Mass System (SMS)

m_2 : Mass attached to the base of the SMS

I_1 : Moment of inertia of m_1 at the gravity center

I_2 : Moment of inertia of m_2 at the gravity center

R_1 : Length between origin *O* and gravity center of m_1

R_2 : Length between origin *O* and gravity center of m_2

G_1 : Center of mass m_1

G_2 : Center of mass m_2

x_1 : Displacement of m_1

$\ddot{z}_H$: Horizontal ground acceleration

α_1 : Angle between vertical line y and R_1

α_2 : Angle between vertical line y and R_2

θ : Rotation angle of 2DOF model

5.4.1. Geometry, masses and degrees of freedom

The starting point of the study on tank rocking motion carried out in the framework of this PhD thesis is represented by the 2DOF system provided by Taniguchi et al. [163,183]. It consists of two masses connected by an elastic spring, whose constant value is k; the entire 2DOF model (m_1 and m_2) can rotate pivoting at the left and at the right bottom edges (see Figure 5-17). The

variable ϑ describes this motion. According to the pivot, in the first case, the positive rotation is anti-clockwise, in the second case, clockwise. Rotation angle ϑ is measured on the global coordinates (X, Y), set in the first case at the left bottom edge of the 2DOF model, in the second case at the right one. The upper mass m_1 can vibrate around the rest position, according to the stiffness of the spring. Its displacement x_1 is measured on the inclined element coordinates (x, y), a local reference system that follows the rotation of the 2DOF model. The position of the reference systems is clarified in the following Figure 5-17

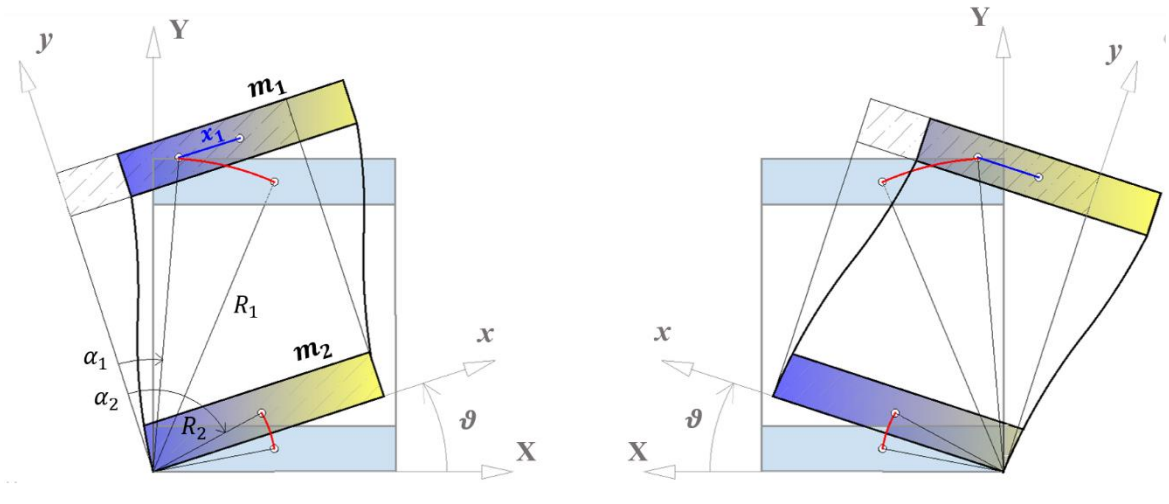

Figure 5-17.The 2DOF model in rotated and displaced position [163,183]

The system composed by the upper mass m_1 and the spring hereafter is called Spring-Mass (SM) system. The SM system starts to vibrate when the 2DOF model is subjected to the ground acceleration, while the entire 2DOF model begins to rotate from the horizontal position when the Overturning Moment (OM), mainly induced by the motion of the SM system, overcomes the Restoring Moment (RM), related to the weight of the entire 2DOF model.

The mechanical model proposed in this section can properly describe the coexistence of rotational and translational motions in a tank subjected to the ground shaking. Indeed, the mass of the liquid content displacing in unison with the shell is simulated by the vibrant mass m_1. The mass m_2 includes all the other masses of the tank system that only contribute to the rocking motion.

5.4.2. Derivation of equation of motion for the 2DOF model

The system of equations for the 2DOF model has been derived through the variational approach and it consists of two simultaneous second order equations in the variables ϑ and x_1. As well known, Lagrange's equations for a system subjected to conservative and not conservative forces have the following form:

$$\frac{d}{dt}\left(\frac{\partial L}{\partial \dot{q}_i}\right) - \frac{\partial L}{\partial q_i} = Q_i \tag{5.16}$$

where:

q_i are the independent generalized coordinates, in this case the two degrees of freedom of the system, θ and x_1;

$\dot{q}_i$ are the generalized velocity $\dot{\vartheta}$ and $\dot{x}_1$;

$L = T - V$ is the Lagrangian of the system and it is given;

T is the total kinetic energy;

V is the total potential energy;

Q_i are the generalized forces.

Then, the Lagrange's Equations for the 2DOF system are

$$\frac{d}{dt}\left(\frac{\partial L}{\partial \dot{x}_1}\right) - \frac{\partial L}{\partial x_1} = Q_{x_1} \tag{5.17}$$

$$\frac{d}{dt}\left(\frac{\partial L}{\partial \dot{\vartheta}}\right) - \frac{\partial L}{\partial \vartheta} = Q_{\vartheta} \tag{5.18}$$

In order to derive the Lagrangian function, kinetic and potential energy have been derived.

The kinetic energy of the 2DOF model consists of two contributes:

- Kinetic energy of the mass m_1

$$T_1 = \frac{1}{2}\left[\left(I_1 + m_1 {R_1}^2\right) + m_1\left({\dot{x}_1}^2 + {x_1}^2\dot{\vartheta}^2 - 2R_1\dot{x}_1\dot{\vartheta}cos\alpha_1 + 2R_1x_1\dot{\vartheta}^2 sin\alpha_1\right)\right] \tag{5.19}$$

- Kinetic energy of the mass m_2:

$$T_2 = \frac{1}{2}\left[\left(I_2 + m_2 {R_2}^2\right)\right] \tag{5.20}$$

Then, the total kinetic energy has the following form

$$T = T_1 + T_2 = \frac{1}{2}\left[\left(I_1 + m_1{R_1}^2\right) + \left(I_2 + m_2{R_2}^2\right) + m_1\left({\dot{x}_1}^2 + {x_1}^2\dot{\vartheta}^2 - 2R_1\dot{x}_1\dot{\vartheta}cos\alpha_1 + 2R_1x_1\dot{\vartheta}^2sin\alpha_1\right)\right] \tag{5.21}$$

The potential energy of the 2DOF model consists of three contributes:

- Potential energy of the mass m_1

$$V_1 = m_1g[R_1cos(\alpha_1 - \vartheta) + x_1sin\vartheta - R_1cos\alpha_1] \tag{5.22}$$

- Potential energy of the mass m_2

$$V_2 = m_2g[R_2cos(\alpha_2 - \vartheta) - R_2cos\alpha_2] \tag{5.23}$$

- Potential energy of the elastic spring

$$V_{spring} = \frac{1}{2}k{x_1}^2 \tag{5.24}$$

Then, the total potential energy has the following form

$$V = V_1 + V_2 + V_{spring} = = m_1g[R_1cos(\alpha_1 - \vartheta) + x_1sin\vartheta - R_1cos\alpha_1] + m_2g[R_2cos(\alpha_2 - \vartheta) - R_2cos\alpha_2] + \frac{1}{2}k{x_1}^2 \tag{5.25}$$

The expression of the generalized forces of the 2DOF model are derived from that of the work done by the external forces. The work of external forces on mass m_1 is

$$W_1 = -m_1\ddot{z}_H(R_1sin(\alpha_1 - \vartheta) + x_1cos\vartheta - R_1sin\alpha_1) \tag{5.26}$$

whereas for mass m_2

$$W_2 = -m_2\ddot{z}_H(R_2sin(\alpha_2 - \vartheta) - R_2sin\alpha_2) \tag{5.27}$$

The total virtual work for the 2DOF model is

$$\delta W = \delta W_1 + \delta W_2 = \delta x_1[-m_1\ddot{z}_Hcos\vartheta] + \delta\vartheta\left[m_1\ddot{z}_H(R_1cos(\alpha_1 - \vartheta) + x_1sin\vartheta) + m_2\ddot{z}_H\left(R_1cos(\alpha_1 - \vartheta)\right)\right] \tag{5.28}$$

Then, the generalized forces

- for the independent generalized coordinate x_1 is

$$Q_{x_1} = -m_1 \ddot{z}_H cos\vartheta \tag{5.29}$$

- for the independent generalized coordinate ϑ is

$$Q_{\vartheta} = m_1 \ddot{z}_H (R_1 cos(\alpha_1 - \vartheta) + x_1 sin\vartheta) + m_2 \ddot{z}_H \big(R_1 cos(\alpha_1 - \vartheta)\big) \tag{5.30}$$

Once all quantities have been obtained, the first Lagrange's equation provides the equation of translational motion of the vibrant mass of the 2DOF model:

$$\begin{aligned} & m_1 \ddot{x}_1 - \lambda m_1 R_1 \ddot{\theta} \cos\alpha_1 + \lambda m_1 g \sin\theta - m_1 \left(x_1 + \lambda R_1 \sin\alpha_1\right) \dot{\theta}^2 \\ & \quad + k x_1 + m_1 \ddot{z}_H \cos\theta = 0 \end{aligned} \tag{5.31}$$

It should be noted that, in Eq. (5.31), the damping effects of the SM system response are taken into account in the inertia force of the tank bulging system by introducing the spectral response acceleration in the framework of simplified analysis.

Similarly, the second Lagrange's equation provides the equation for the rocking motion of the 2DOF model:

$$\begin{aligned} & \left\{ m_1 \left(x_1^2 + 2\lambda x_1 R_1 \sin\alpha_1 + R_1^2\right) + I_1 + I_2 + m_2 R_2^2 \right\} \ddot{\theta} - \lambda m_1 \ddot{x}_1 R_1 \cos\alpha_1 \\ & \quad + 2 m_1 \dot{x}_1 \dot{\theta} \left(x_1 + \lambda R_1 \sin\alpha_1\right) + m_1 g \left\{ R_1 \sin\left(\alpha_1 - \theta\right) + \lambda x_1 \cos\theta \right\} \\ & \quad\quad + m_2 g R_2 \sin\left(\alpha_2 - \theta\right) \\ & \quad\quad\quad - \left[m_1 \left\{ \lambda R_1 \cos\left(\alpha_1 - \theta\right) + x_1 \sin\theta \right\} + \lambda m_2 R_2 \cos\left(\alpha_2 - \theta\right) \right] \ddot{z}_H = 0 \end{aligned} \tag{5.32}$$

It should be noted that, in the case in which the equations of motion are derived for the opposite rotational direction (the pivot is the right bottom edge), the overall structure of the differential equations does not change, but some terms appear with opposite sign. Therefore, by introducing the index λ, which specifies the rotational direction, the equations have been unified.

The SM system starts to vibrate from the rest position when the 2DOF model is subjected to the ground acceleration (see Figure 5-18).

The condition to initiate the rocking motion of the 2DOF model is that the overturning moment, due to the horizontal acceleration, overcomes the restoring moment, related to the weight force (see Figure 5-19).

$$RM<OM \tag{5.33}$$

$$RM = (m_1 R_1 \sin\alpha_1 + m_2 R_2 \sin\alpha_2) g$$

$$OM = m_1 R_1 \cos\alpha_1 \left(\ddot{x}_1 + \ddot{z}_H\right) + m_2 R_2 \cos\alpha_2 \ddot{z}_H$$

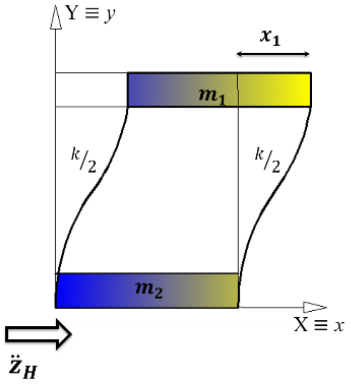

Figure 5-18. 2DOF model in displaced position [163,183]

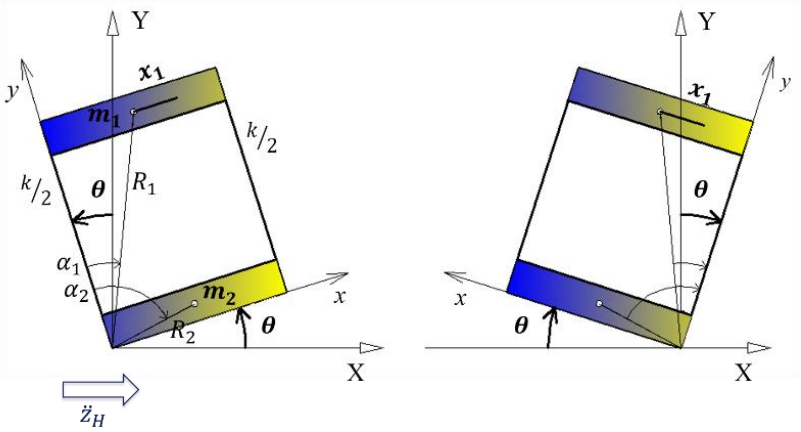

Figure 5-19. 2DOF model in rotated position pivoting respectively at the left and at the right bottom edges position [163,183]

From the equilibrium among translational and rotational forces on the inclined element coordinates, the reaction forces R_x and R_y, i.e. the forces to support rotation of the 2DOF model pivoting at the left bottom edge of the lower mass. Expression of these forces in the inclined system is the following:

$$R_x = F_{Ix} + F_{ext,x} \tag{5.34}$$

$$R_y = F_{Iy} + F_{ext,y} \tag{5.35}$$

where

F_{Ix} and F_{Iy} are respectively the x and y-component of the inertia force

$F_{est,x}$ and $F_{est,y}$ are respectively the x and y-component of the external forces, i.e. the force due to the horizontal ground-acceleration and the weight force.

Once obtained in the local inclined system, these forces have been projected on the global system as follows

$$R_X = R_x cos\vartheta - R_y sin\vartheta \tag{5.34}$$

$$R_Y = R_x sin\vartheta + R_y cos\vartheta \tag{5.35}$$

Then, the vertical and horizontal components of the reactions have been found:

$$\begin{aligned} R_X = {} & (m_1 + m_2)\ddot{z}_H - m_1 R_1 \ddot{\vartheta} cos(\alpha_1 - \vartheta) - m_1 R_1 \dot{\vartheta}^2 sin(\alpha_1 - \vartheta) \\ & + m_1 \ddot{x}_1 cos\vartheta - 2m_1 \dot{x}_1 \dot{\vartheta} sin\vartheta - m_1 x_1 \ddot{\vartheta} sin\vartheta - m_1 x_1 \dot{\vartheta}^2 cos\vartheta \\ & - m_2 R_2 \ddot{\vartheta} cos(\alpha_2 - \vartheta) - m_2 R_2 \dot{\vartheta}^2 sin(\alpha_2 - \vartheta) \end{aligned} \tag{5.36}$$

$$\begin{aligned} R_Y = {} & (m_1 + m_2)g + m_1 R_1 \ddot{\vartheta} sin(\alpha_1 - \vartheta) - m_1 R_1 \dot{\vartheta}^2 cos(\alpha_1 - \vartheta) + m_1 \ddot{x}_1 sin\vartheta \\ & + 2m_1 \dot{x}_1 \dot{\vartheta} cos\vartheta + m_1 x_1 \ddot{\vartheta} cos\vartheta - m_1 x_1 \dot{\vartheta}^2 sin\vartheta \\ & + m_2 R_2 \ddot{\vartheta} sin(\alpha_2 - \vartheta) - m_2 R_2 \dot{\vartheta}^2 cos(\alpha_2 - \vartheta) \end{aligned} \tag{5.37}$$

These represent respectively the base shear and the vertical reaction at the pivoting left bottom edge of the model.

The transition from the lift-off around an edge to the lift-off around the other one in accompanied by an impact. The associated loss of energy is taken into account by reducing the angular velocity of the system after the impact. In particular, it can be expressed as follow:

$$\dot{\theta}\left(t^+\right) = e\dot{\theta}\left(t^-\right) \qquad 0 \le e \le 1 \tag{5.38}$$

where e is the restitution coefficient; t^+ is the time just after the impact; t^- is the time just before the impact. Changes in angular velocity are assumed to occur instantaneously.

5.5. Experimental test

In order to validate the accuracy of the 2DOF system equations and their adequacy in simulating the complex motion of a body that translates and rotates simultaneously, both experimental test and analytical simulation have been conducted. This section provides a detailed description of the experimental test carried out and a presentation of results obtained.

The experimental test consists on recording the free fall and free rocking of a steel model through a high-speed camera, with the aim to obtain the displacement of a particular point of the model and the rotation of the entire body.

5.5.1. Steel model

The sample investigated consists in a 2-story model composed of two rigid masses connected by two flexible columns (see Figure 5-20).

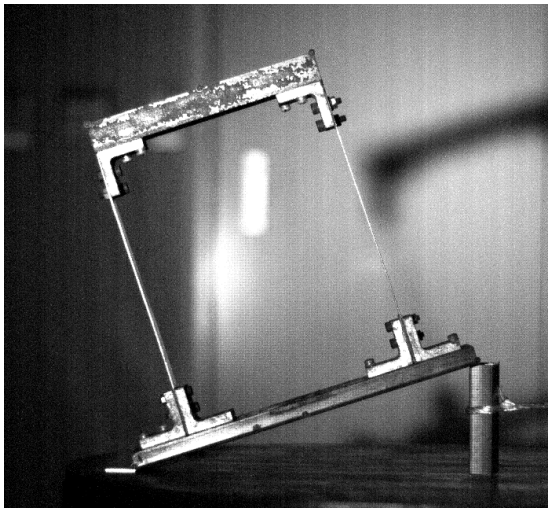

Figure 5-20. Steel model used in free fall experimental test [183]

The construction materials are steel for masses and junctions, aluminum for columns. The upper mass m_1 is $3.33\,kg$, the lower mass m_2 is $2.34\,kg$ (these values include mass of steel junctions). The distance R_1 between the pivot of rotation and the gravity center of m_1 is $299mm$, while for the lower mass R_2 is $101mm$.

The angles between the axis y and respectively R_1 and R_2 are 0.341 and $1.446\,rad$. The natural frequency of the vibrant mass m_1 is $3.9\,Hz$. The sample model is set on a steel rigid plane. In order to avoid sliding motion, not considered in the analytical model, the two contact surfaces have been coated with sandpaper. The restitution coefficient is assumed to be 0.85. Figure 5-21 provides some details on the model size and clarifies the mass position with respect to the rotation pivot (quotes in figure are given in mm).

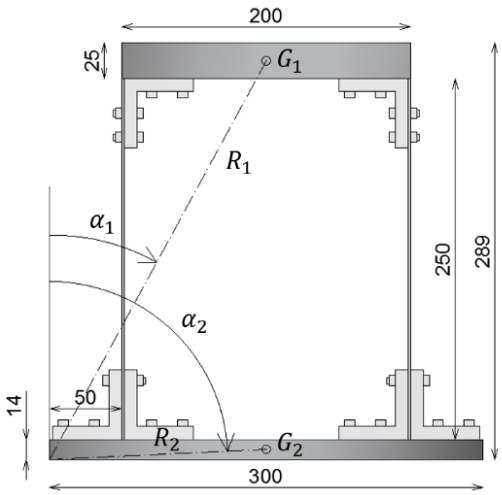

Figure 5-21. Geometry of the sample model used in experimental test [183]

The analogy between the steel sample and the mechanical model in terms of degrees of freedom, masses involved, global and rotating reference systems is clarified in Figure 5-22.

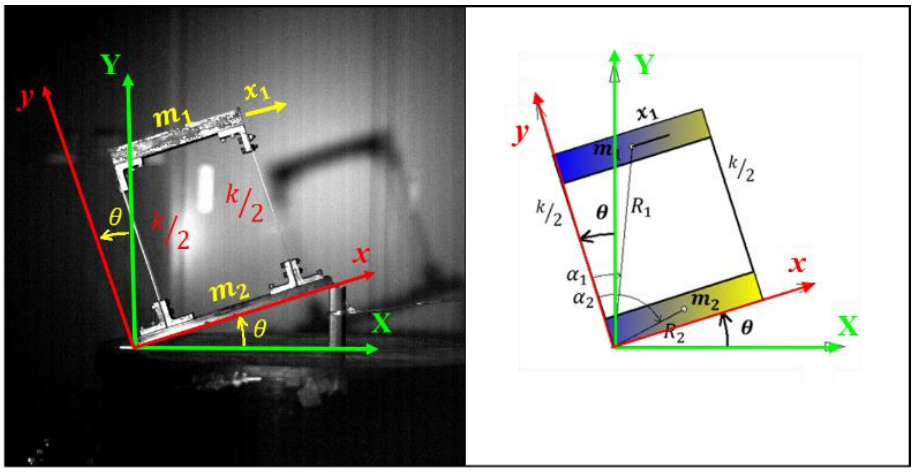

Figure 5-22. Analogies between the 2-story steel model and the 2DOF system [183]

5.5.2. Test instrumentation and set-up

The motion is acquired in high-speed photography whose time interval is 1/3000 second. The experimental test is recorded by controlling the high speed camera functions through Photron Fastcam. The Photron FASTCAM Viewer is an application software program that makes possible to control high-speed cameras from the PC, including operations such as camera setup, framing and downloading. Once the motion has been recorded, the responses of interest are measured with an image processor, i.e. Deep Motion. Instrumentation used in laboratory and the overall output of the experimental test are shown in Figure 5-23.

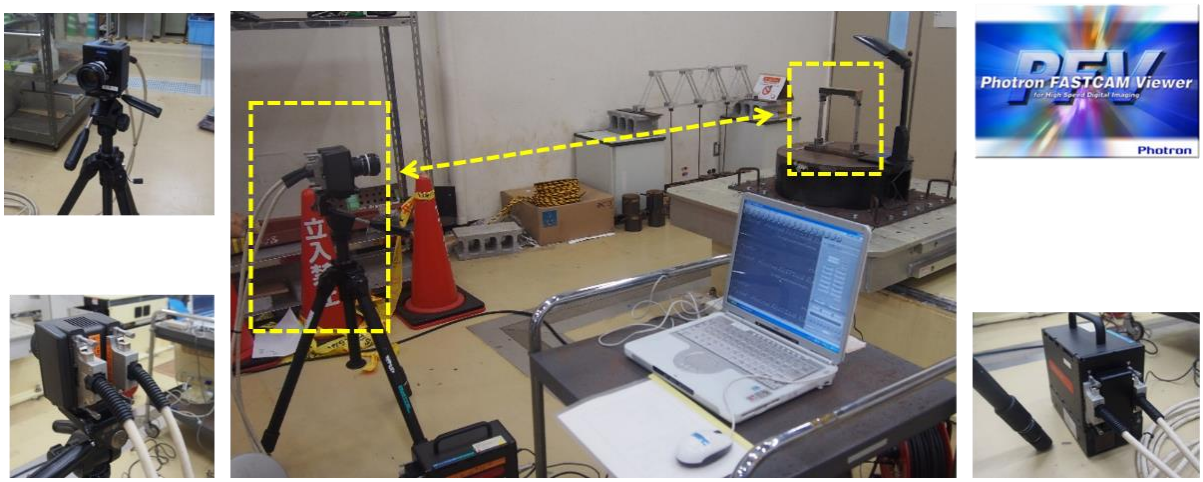

Figure 5-23. Instrumentation used for the experimental test [183]

It should be noted that there is a certain distance between the camera and the sample. It has been calibrated so that the camera lens can properly catch the points of control and follow them during the motion. Moreover, for this purpose an appropriate lightening has been adopted. In order to prevent getting distorted images during the motion recording, the sample model is kept parallel to the camera lens.

The points of control of the sample model, i.e. the points of which high speed camera records the position in time, consist in white points surrounded by black circle. They are made of paper and attached to the upper and lower masses of the steel model. The reference point R consists in a point of control fixed to the base where the steel model is set. Location of points of control is clarified in Figure 5-24.

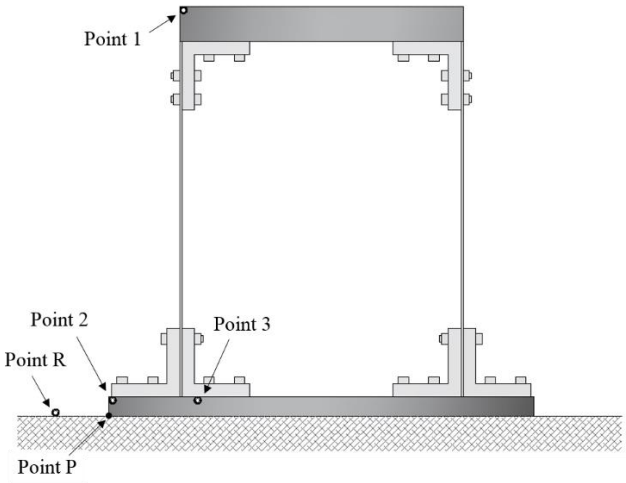

Figure 5-24. Location of the points of control in the model [183]

The free fault test begins from an inclined initial position. In details, an initial uplift angle about the left bottom edge $\vartheta_0 = 0.125$ rad is enforced to the model; consequently, a displacement of the upper mass $x_{1,0} = 2.035$ mm occurs due to the inclined component of the weight force (in Figure 5-25, the red line parallel to the upper mass). From this initial configuration, depicted in Figure 5-25, the free fall test is performed.

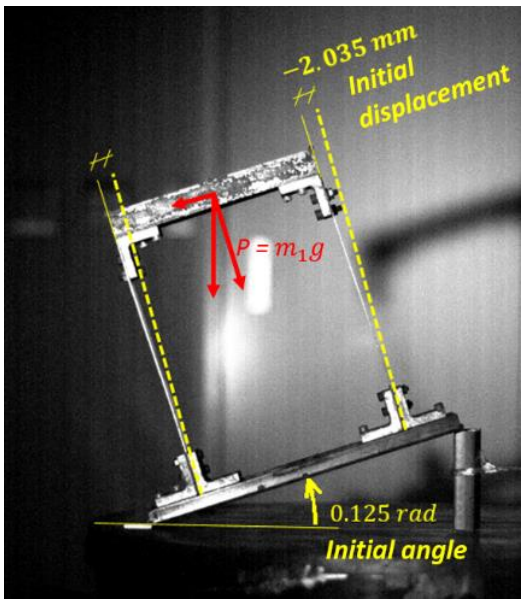

Figure 5-25. Initial conditions of the free fall test in terms of initial rotation angle and initial displacement [183]

5.5.3. Coordinates reference systems

Before to explain the procedure for obtaining the response of interest, i.e. relative displacement x_1 of the vibrating upper mass and rotation $\vartheta(t)$ of the entire model around the pivot P, some considerations should be made on the three coordinates systems used. The first coordinates system to be introduced is that used by Deep Motion to refer the time history of the points of control; it is centered in the reference point R as already explained; axes are called (X', Y') and are depicted in blue in Figure 5-26. The second coordinate system considered (X, Y), depicted in green in Figure 5-26, is parallel to the previous one and it is centered on the rotation pivot P. The third coordinates system (x, y), depicted in red in Figure 5-26, is centered on the rotation pivot P and follows the rotation of the model. Note that in Figure 5-26, the model has been rigidly rotated: that configuration should not be confused with the initial condition of the experimental test, depicted in Figure 5-25 and consisting of initial rotation and displacement.

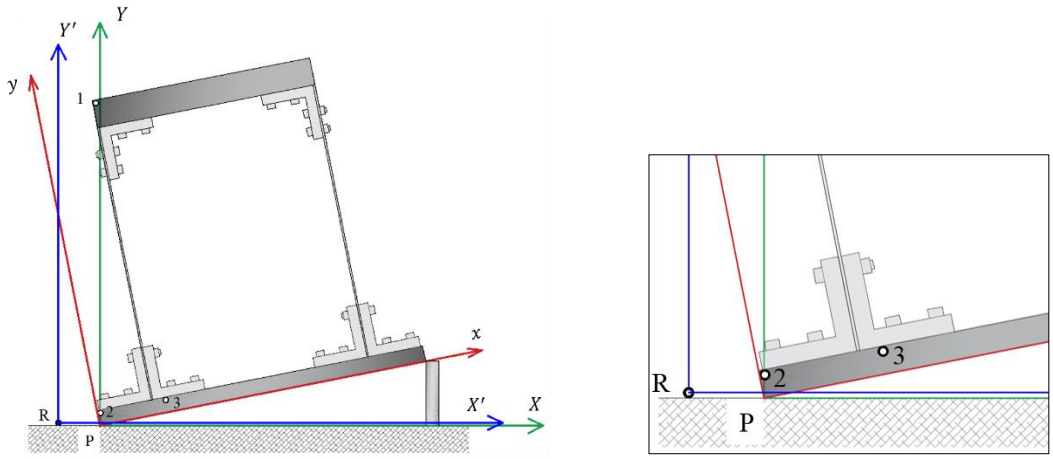

Figure 5-26. Coordinates reference systems [183]

5.5.4. Outputs and analysis of results

Once the motion has been recorded, the image processor Deep Motion is used to measure the time history of the absolute displacement of points 2 ($X_2'(t)$, $Y_2'(t)$), and 3 ($X_3'(t)$, $Y_3'(t)$), located at the lower mass and 1 ($X_1'(t)$, $Y_1'(t)$), located at the upper mass, with respect to the reference system (X', Y') centered at point R.

However, as deducted by the comparison between the 2DOF model and the 2-story steel model explained in Figure 5-22, the degrees of freedom of this latter are

- rotation ϑ of the entire body about the pivot located alternatively at the left and at the right bottom edge;

- relative displacement x_1 of the vibrating upper steel mass with respect to a rotating reference system centered at the bottom edge of the lower mass (x, y).

In order to obtain time history of rotation $\vartheta(t)$, the displacements of points 2 and 3 referred to the system (X', Y') are employed into the equation

$$\vartheta(t) = \frac{[Y_3'(t) - Y_2'(t)]}{[X_3'(t) - X_2'(t)]} \tag{5.39}$$

The time history of the relative displacement $(x_1(t), y_1(t))$ is calculated as the composition between the displacement $(X_1'(t), Y_1'(t))$ obtained by Deep Motion and referred to the system (X', Y') and the displacement of point 1, $(X_{1r}'(t), Y_{1r}'(t))$, due to the rigid rotation of the model around the pivot and measure on the same reference system. Since displacement $(X_{1r}'(t), Y_{1r}'(t))$ is read on the reference system with center in R that does not coincide with the center of rotation P (see Figure 5-26), it is described by the expressions:

$$\begin{aligned} X_{1r}'(t) &= X_{1r}(t) + d_{X(P,R)} = d_{Y(1,P)}\, sin\vartheta(t) + d_{X(1,P)}\, cos\vartheta(t) + d_{X(P,R)} \\ Y_{1r}'(t) &= Y_{1r}(t) - d_{Y(P,R)} = d_{Y(1,P)}\, cos\vartheta(t) - d_{X(1,P)}\, sin\vartheta(t) - d_{Y(P,R)} \end{aligned} \tag{5.40}$$

where X_{1r} and Y_{1r} are the coordinates of the displacement of point 1 due to the rigid rotation of the model around the pivot and measure on the reference system center in the pivot P; $d_{X(1,P)}$ and $d_{Y(1,P)}$ are the components of the distance between point 1 and the rotation pivot P, whereas $d_{X(P,R)}$ and $d_{Y(P,R)}$ are components of the distance between the pivot P and the reference point R.

Finally, the relative displacement $(x_1(t), y_1(t))$ has the following expression:

$$\begin{aligned} x_1(t) &= X_1'(t) + X_{1r}'(t) \\ y_1(t) &= Y_1'(t) - Y_{1r}'(t) \end{aligned} \tag{5.41}$$

Values of distances employed in Eqs. (5.40) summarized in Table 5.6 and depicted in Figure 5-27.

Table 5.6 Distance between points P and 1, and between R and P

$\boldsymbol{d_{X(1,P)}}$	52.73 mm
$\boldsymbol{d_{Y(1,P)}}$	286.34 mm
$\boldsymbol{d_{X(P,R)}}$	37.5 mm
$\boldsymbol{d_{Y(P,R)}}$	2.72 mm

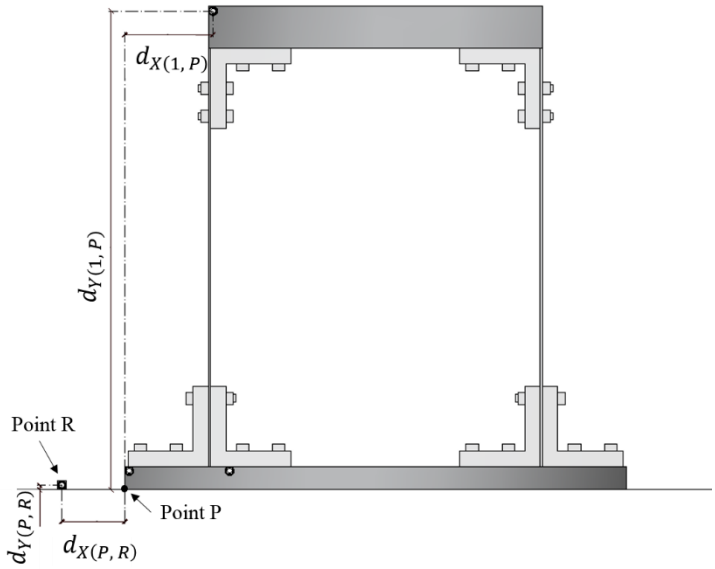

Figure 5-27. Distance between points P and 1, and between R and P, employed in Eqs. (5.40) [183]

Figure 5-28 shows a sequence of pictures depicting the main phases of the free fault test. Pictures 1 and 2 represent respectively the initial position of the sample model and the first instants of its rotation about the pivot P. During these phases, the relative position of the upper mass is displaced at left respect to the lower one. Picture 3 captures the instant in which the model touches the ground. In this configuration the relative displacement x_1 of the upper mass, and consequently the elastic force, is almost zero, since the columns are in rest position. After the impact, for a time span of $0.05\ s$, the upper mass continues to move to the right, while the rotation of the entire model is zero. When the upper mass reaches the maximum displacement (picture 4), the model starts to rotate around the pivot on the right bottom edge and the relative displacement of columns decreases and becomes zero in correspondence of the maximum rotation (picture 5). After this point the experimental response is no longer analyzed because of noise problem inducted by impact.

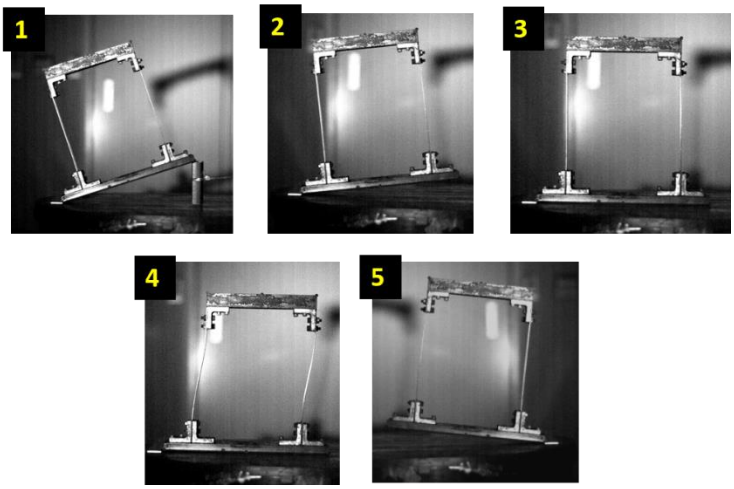

Figure 5-28. Main phases of the free fault-free rocking test [183]

5.6. Numerical simulation

On the other hand, the simultaneous equations of motion of the 2DOF model provided at paragraph 5.4.2 are solved by using the numerical software MATLAB. The unknown of the differential system are six: angular acceleration $\ddot{\vartheta}$, angular velocity $\dot{\vartheta}$, rotation angle ϑ, relative acceleration $\ddot{x}_1$, relative velocity $\dot{x}_1$ and relative displacement x_1. The initial condition employed for solving the system of differential equations are the same of the experimental test (Figure 5-25):

$$\vartheta_0 = 0.125$$

$$\dot{\vartheta}_0 = 0$$

$$x_{1,0} = -2.035\ mm \tag{5.42}$$

$$\dot{x}_{1,0} = 0\ mm/s^2$$

In MATLAB, the system of simultaneous differential equations is solved by using the ODE (Ordinary Differential Equation) solver. This function integrates the differential system from t_0 to t_f, respectively initial and final time instants, with the given initial conditions. The numerical model simulates the loose of energy associated with the impact by setting new initial conditions for the differential equations when the model touches the ground ($\vartheta_0 = 0$). In particular, values of rotation ϑ_i, relative displacement $x_{1,i}$ and relative velocity $\dot{x}_{1,i}$ at the time

step i, are set equal to those at the previous time step, $i-1$, whereas the angular velocity $\dot{\vartheta}_i$ is set as the product between its value at the previous time step (with opposite sign) and the restitution coefficient (see also Eq. (5.38) at paragraph 5.4.2):

$$\begin{aligned} \vartheta_i &= \vartheta_{i-1} \\ \dot{\vartheta}_i &= -\dot{\vartheta}_{i-1} \cdot e \\ x_{1,i} &= x_{1,i-1} \\ \dot{x}_{1,0} &= \dot{x}_{1\,,i-1} \end{aligned} \tag{5.43}$$

The numerical solution obtained from MATLAB is the time history of ϑ, $\dot{\vartheta}$, x_1 and $\dot{x}_1$.

5.7. Comparison between experimental and numerical results

Summarily, numerical results in terms of time history of x_1 and ϑ consists in the exact solution of the simultaneous equations of motion of the 2DOF system presented in section 5.4.2; on the other hand, experimental test provides time history of x_1 and ϑ for a 2-story steel model designed and realized with the aim to physically reproduce the behavior of the 2DOF system. A critical comparison between results from the two analyses is conducted in this section in order to confirm the reliability of the 2DOF system in describing the combined translational-rotational motion.

Figure 5-29 shows the time history of the rotation angle θ obtained both from experimental test (gray line) and analytical resolution (black line). Figure 5-30 provides the same comparison in terms of time history of relative displacement x_1.

As figures show, the analytical response is well simulated by the experimental test. In the case of rotation angle θ, the two curves match well in terms of maxima values and bouncing timing. In both cases, the first part of the θ curve is not parabolic as is obtained by Taniguchi from numerical and experimental analyses carried out on a similar model with rigid columns [184]. In particular, the current θ curve shows a small deflection when the relative displacement x_1 reaches the maximum value (between 0.05 and $0.1\ s$). This reduction observed in rotation with the respect to the case of rigid columns is obviously due to the effect of translational motion on the overall response.

At the time $0.135\ s$, the model touches the ground. It is worth to clarify the trend of the two curves after this first impact. As confirmed by the experimental test, once touched the ground, the steel model rests in horizontal position for a time span of about $0.05\ s$ (pictures 3 and 4 in Figure 5-28), during which the upper mass continues to displace but rotation of the entire model is zero. This behavior can be justified by analyzing the instantaneous value of forces acting on the model and the equilibrium between overturning and restoring moments. When the model touches the ground ($\vartheta = 0$) the upper mass is approximately in the rest position (spring force is close to zero). Overturning moment, that in case of absence of ground acceleration counts only the term linked to the inertia force of the mass m_1 ($OM = m_1 \ddot{x}_1 R_1 cos\alpha_1$), does not allow the initiation of rocking motion about the right bottom edge immediately after the impact. It is worth to point out that the behavior of the same model with rigid columns has been proved to be different [184]: in that case, the duration of rest in rotation is comparable to that of the impact, i.e. close to zero. Time history of rotation in experimental and analytical cases confirms the role of the equilibrium of moments described above (see Figure 5-29).

In the framework of the experimental test, after the first impact curve shows a flat trend accompanied by some irregularity due to the impact noise; on the other hand, analytical model simulates it in a more ideal but still reasonable way. Noise problem obviously does not appear and immediately after the impact, the model starts to uplift pivoting at the right bottom edge. However, for about the same time span measured in the experimental test, although the lower mass m_2 tries to keep rotating, rotation cannot grow up and reach the maximum value, so it depresses until the mass m_1 gets the maximum relative displacement x_1 and consequently the maximum value of the overturning moment, at the time 0.2 s. After this point, the rotation angle increases again until the displacement x_1 reaches the maximum absolute value in the other direction.

Both the analytical responses θ and x_1, after the first impact, are shifted in time respect to the experimental ones. This happens because the analytical model keeps following the ideal behavior, whereas in the real model, when impact occurs, the flexible columns receive a shock and consequently start to vibrate with a different frequency; this leads them to stop working for few instants and to lose the ideal behavior.

Overall, comparison between experimental and analytical results confirms the accuracy of the analytical model in simulating the simultaneous rotational-translational motion, especially before the first impact on the ground when problem related to noise is not yet occurred.

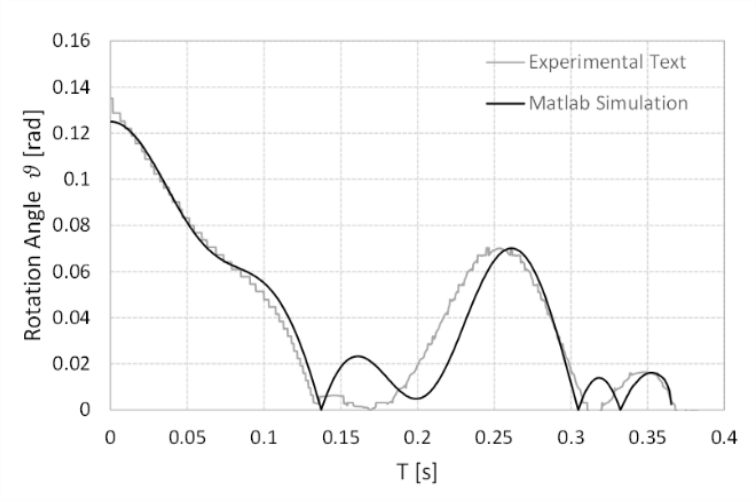

Figure 5-29. Comparison between analytical and experimental results in terms of rotation angle [183]

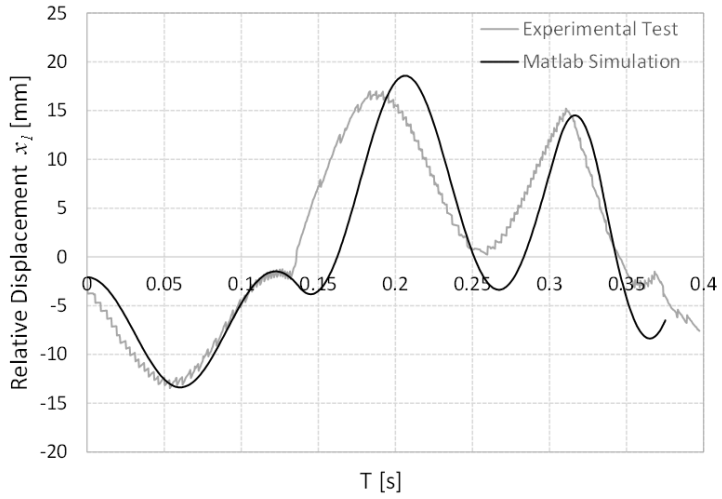

Figure 5-30. Comparison between analytical and experimental results in terms of relative displacement [183]

5.8. The tank model

Nomenclature

D : Diameter of the cylindrical tank

H_{rf} : Height of the gravity center of m_{rf}

H_{rb} : Height of the gravity center of m_{rb}

H_{sh} : Height of the gravity center of m_{sh}

I_{bpUL}: Moment of inertia of m_{bpUL} at the gravity center

I_{bpNUL}: Moment of inertia of m_{bpNUL} at the gravity center

I_{rf} : Moment of inertia of m_{rf} at the gravity center

I_{sh} : Moment of inertia of m_{sh} at the gravity center

I_r : Moment of inertia of m_r at the gravity center

m_b : Effective mass of fluid for bulging motion

m_{rb}: Effective mass of fluid for rocking-bulging interaction

m_{bp}: Mass of tank bottom plate

m_{bpUL}: Mass of tank bottom plate that uplifts

m_{bpNUL}: Mass of tank bottom plate that does not uplift

m_l : Mass of liquid contained in the tank

m_r : Effective mass of fluid for rocking motion

m_{rf}: Mass of tank roof

m_{sh}: Mass of tank shell

G_b : Center of effective mass of fluid for bulging motion

G_{rb} : Center of effective mass of fluid for rocking-bulging interaction

G_r : Center of effective mass of fluid for rocking motion

G_{rf} : Center of mass of the roof

G_{sh} : Center of mass of the shell wall

R_b : Length between origin *O* and gravity center of m_b

R_{bpUL}: Length between origin *O* and gravity center of m_{bpUL}

R_{bpNUL}: Length between origin *O* and gravity center of m_{bpNUL}

R_{rb} : Length between origin *O* and gravity center of m_{rb}

R_{rf} : Length between origin *O* and gravity center of m_{rf}

R_{sh} : Length between origin *O* and gravity center of m_{sh}

R_r : Length between origin *O* and gravity center of m_r

$S_{AH}^{ratio}(T_b, h_b)$: A ratio of response acceleration to the ground acceleration

T_b : Natural period of the tank bulging motion

$(\ddot{z}_H)_{max}$: Maximum horizontal ground acceleration

α_b : Angle between vertical line y and R_b

α_{rb} : Angle between vertical line y and R_{rb}

α_{bpUL}: Angle between vertical line y and R_{bpUL}

α_{bpNUL}: Angle between vertical line y and R_{bpNUL}

α_{rf} : Angle between vertical line y and R_{rf}

α_{sh} : Angle between vertical line y and R_{rf}

α_r : Angle between vertical line y and R_r

5.9. Equation of motion for the tank model

Once the 2DOF system has been proved to be a reliable tool for describing the combined translational-rotational motion, its equations of motion can be employed to provide an easy tool for calculation of the main response of tank undergoing rocking-bulging motion. Before to explain the simplified procedure proposed in this work, it is worth to show and discuss the complete differential equations of motion of the tank model derived from the equations of motion of the 2DOF model [163]. In particular, the equations for the tank rock motion have been obtained by substituting the physical quantities of the 2DOF with the corresponding dynamic properties of the tank in rock. The analogy between the two models is formulated by considering the following remarks. As shown in a Taniguchi's paper [162] (discussed at paragraph 5.3) the liquid masses involved in the rocking-bulging motion of a cylindrical tank are essentially: effective mass of fluid for bulging motion m_b, effective mass of fluid for rocking motion m_r and effective mass of fluid for rocking-bulging interaction m_{rb}. Values of m_r and m_{rb} are provided by tables as functions of the aspect of the tank and the ratio of the uplift width of the tank bottom plate to the diameter, while value of m_b is a function of the aspect of the tank only. The slice model [162] presented at paragraph 5.3 has been employed for calculation of these masses.

Since m_1 of the 2DOF model is a mass that translates and rotates simultaneously, it can simulate bulging motion, rocking motion, and combined bulging-rocking motion. In particular

- In Eq. (5.31), m_1 is replaced by
    - m_b in terms related to bulging forces;
    - m_{rb} in terms related to the horizontal component of forces depending on angular velocity or acceleration.
- In Eq. (5.32), it is replaced by
    - m_b in the terms related to the horizontal acceleration;
    - m_r in terms related to the rotational acceleration (in this case, m_2 is included as well);
    - m_{rb} in terms related both to rotational and to translational variables.

On the other hand, m_2 of the 2DOF model is a mass that only rotates, then in the analogy with the tank model it can represent the mass of shell, roof and bottom plate. Following the same

criterion used for replacing masses, all the other quantities involved in the equations of the 2DOF model, i.e. α_1, α_2, R_1, R_2, I_1, I_2, are replaced with the corresponding ones in the tank model.

Value of the spring constant *k* is adjusted to match the natural period of the tank bulging motion. In the formulation of the tank model, uplifted and un-uplifted parts of the bottom plate are distinguished. Moreover, Figure 5-31 shows the analytical model of the tank rocking-bulging motion. The equation for the tank bulging motion is rewritten as:

$$\begin{aligned} & m_b\ddot{x}_1 - \lambda m_{rb} R_{rb}\ddot{\theta}\cos\alpha_{rb} + \lambda m_b g\sin\theta \\ & \quad - m_{rb}\left(x_1 + \lambda R_{rb}\sin\alpha_{rb}\right)\dot{\theta}^2 + kx_1 + m_b\ddot{z}_H\cos\theta = 0 \end{aligned} \tag{5.44}$$

Similarly, the equation for the tank rocking motion becomes:

$$\begin{aligned} & \left\{m_{rb}(x_1^2 + 2\lambda x_1 R_{rb}\sin\alpha_{rb}) + \left(I_{rf} + I_{sh} + I_{bpUL} + I_r\right)\right. \\ & \left. + \left(m_{rf}R_{rf}^2 + m_{sh}R_{sh}^2 + m_{bpUL}R_{bpUL}^2 + m_r R_r^2\right)\right\}\ddot{\theta} \\ & -\lambda m_b\ddot{x}_1 R_b\cos\alpha_b + 2m_{rb}\dot{x}_1\dot{\theta}\left(x_1 + \lambda R_{rb}\sin\alpha_{rb}\right) \\ & + \left\{m_{rf}R_{rf}\sin\left(\alpha_{rf} - \theta\right) + m_{sh}R_{sh}\sin\left(\alpha_{sh} - \theta\right)\right. \\ & \left. + m_{bpUL}R_{bpUL}\sin\left(\alpha_{bpUL} - \theta\right) + m_r R_r\sin\left(\alpha_r - \theta\right)\right\} g \\ & -\left[m_b\left\{\lambda R_b\cos\left(\alpha_b - \theta\right) + x_1\sin\theta\right\}\right]\ddot{z}_H \\ & -\lambda\left\{m_{rf}R_{rf}\cos\left(\alpha_{rf} - \theta\right) + m_{sh}R_{sh}\cos\left(\alpha_{sh} - \theta\right)\right. \\ & \left. + m_{bpUL}R_{bpUL}\cos\left(\alpha_{bpUL} - \theta\right)\right\}\ddot{z}_H = 0 \end{aligned} \tag{5.45}$$

It should be noted that, in the rocking motion equation, there is not an equivalent term for $m_1 g x_1 cos\theta$ because the liquid mass working in vertical direction cannot give its contribution to the rotational motion, as in the case of solid materials like steel.

This study ignores response of shell and roof and assumes that the tank bottom plate is on the ground before the tank starts to rock. Therefore, a condition to initiate the tank rock motion is given as (Figure 5-32):

$$\begin{aligned} & RM < OM \\ & RM = (m_{rf} + m_{sh})Dg/2 \\ & OM = m_b H_b\left(\ddot{x}_1 + \ddot{z}_H\right) + (m_{rf}H_{rf} + m_{sh}H_{sh})\ddot{z}_H \end{aligned} \tag{5.46}$$

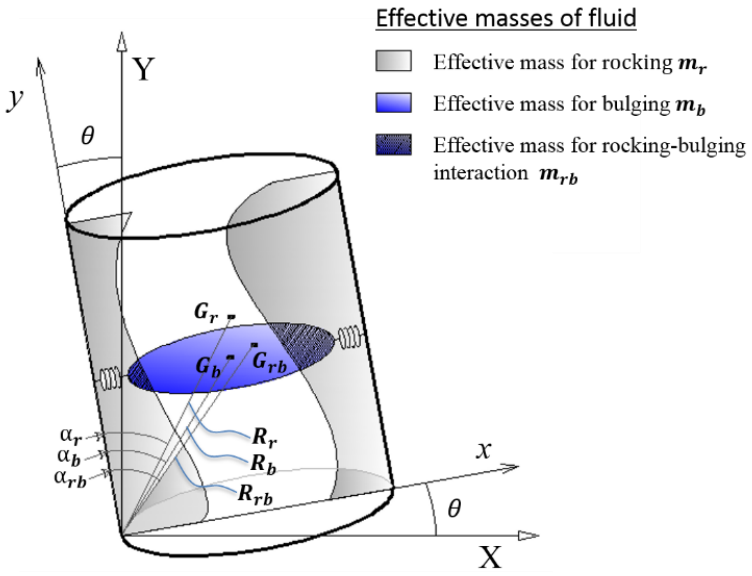

Figure 5-31. Analytical model of tank rocking-bulging motion [163,183]

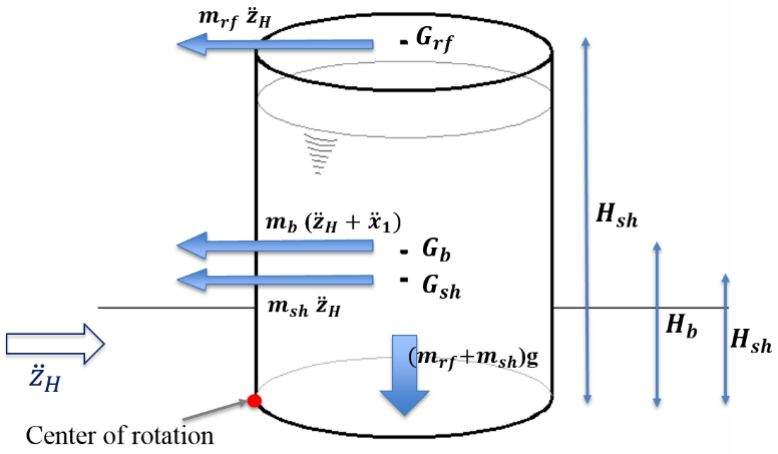

Figure 5-32. Forces at the initiation of the tank rocking motion [163,183]

Following the same criteria used for deriving Eqs. (5.44) and (5.45), the base shear R_X and R_Y

$$
\begin{aligned}
R_X = {} & (m_b + m_{rf} + m_{sh} + m_{bpUL} + m_{bpNUL})\ddot{z}_H \\
& - m_{rb}R_{rb}\dot{\vartheta}^2 sin(\alpha_{rb} - \vartheta) - m_{rb}R_{rb}\ddot{\vartheta}cos(\alpha_{rb} - \vartheta) \\
& + m_b\ddot{x}_1 cos\vartheta - m_{rb}(2\dot{x}_1\dot{\vartheta}sin\vartheta + x_1\ddot{\vartheta}sin\vartheta + x_1\dot{\vartheta}^2 cos\vartheta) \\
& - \left(m_{rf}R_{rf}cos\alpha_{rf} + m_{sh}R_{sh}cos\alpha_{sh}\right. \\
& \left. + m_{bpUPL}R_{bpUPL}cos\alpha_{bpUPL} + m_rR_rcos\alpha_r\right) \\
& \cdot \left[\ddot{\vartheta}cos\vartheta - \dot{\vartheta}^2 sin\vartheta\right] \\
& - \left(m_{rf}R_{rf}sin\alpha_{rf} + m_{sh}R_{sh}sin\alpha_{sh}\right. \\
& \left. + m_{bpUPL}R_{bpUPL}sin\alpha_{bpUPL} + m_rR_rsin\alpha_r\right) \\
& \cdot \left[\ddot{\vartheta}sin\vartheta + \dot{\vartheta}^2 cos\vartheta\right]
\end{aligned}
\tag{5.47}
$$

$$
\begin{aligned}
R_Y = {} & (m_l + m_{rf} + m_{sh} + m_{bpUL} + m_{bpNUL})g + m_{rb}R_{rb}\ddot{\vartheta}sin(\alpha_{rb} - \vartheta) \\
& - m_{rb}R_{rb}\dot{\vartheta}^2 cos(\alpha_{rb} - \vartheta) + m_b\ddot{x}_1 sin\vartheta \\
& + m_{rb}\left(2\dot{x}_1\dot{\vartheta}cos\vartheta + x_1\ddot{\vartheta}cos\vartheta - x_1\dot{\vartheta}^2 sin\vartheta\right) \\
& + \left(m_{rf}R_{rf}sin\alpha_{rf} + m_{sh}R_{sh}sin\alpha_{sh}\right. \\
& \left. + m_{bpUPL}R_{bpUPL}sin\alpha_{bpUPL} + m_rR_rsin\alpha_r\right) \\
& \cdot \left[\ddot{\vartheta}cos\vartheta - \dot{\vartheta}^2 sin\vartheta\right] \\
& - \left(m_{rf}R_{rf}cos\alpha_{rf} + m_{sh}R_{sh}cos\alpha_{sh}\right. \\
& \left. + m_{bpUPL}R_{bpUPL}cos\alpha_{bpUPL} + m_rR_rcos\alpha_r\right) \\
& \cdot \left[\ddot{\vartheta}sin\vartheta + \dot{\vartheta}^2 cos\vartheta\right]
\end{aligned}
\tag{5.48}
$$

The mass m_l in the expression of R_Y is added to maintain the total weight of fluid.

5.10. Simplified analysis of the tank model

The equations of motion shown in the previous section for tank in rock represent a second order differential system in six unknown. The computational effort associated with its resolution can be high and not convenient for design purpose. In light of that, a previous companion study [163] provided a simplified tool starting from the differential equations, but moving from tank model to simplified system it neglected all terms describing the interaction between rocking and bulging motions. However, as shown in previous sections (paragraph 5.7), rotational inertia forces affect the bulging motion, as well as translational inertia forces affect the rocking one. Under this consideration, a new approach that takes into account the rocking-bulging interaction has been derived in this section in order to fully exploit the reliability of an analytical model validated by experimental tests.

The unknown variables in the system of two second order equations are: angular acceleration $\ddot{\theta}$, angular velocity $\dot{\theta}$, rotation angle θ, relative acceleration $\ddot{x}_1$, relative velocity $\dot{x}_1$ and relative displacement x_1.

Both the differential equations of motion for tank (Eqs. (5.44), (5.45)) contain terms related to the bulging-rocking interaction. In the case of Eq. (5.44), the term

$$-m_{rb}x_1\dot{\theta}^2 \tag{5.49}$$

represents the centrifugal force component linked to the displacement x_1; its direction is the same of the displacement. In Eq. (5.45), terms related to the rocking-bulging interaction are

$$m_{rb}({x_1}^2 + 2\lambda x_1 R_{rb} sin\alpha_{rb})\ddot{\theta} \tag{5.50}$$

that is the moment of the rotational inertia force and

$$2m_{rb}(x_1 + \lambda R_{rb} sin\alpha_{rb})\dot{x_1}\dot{\theta} \tag{5.51}$$

representing the moment of the Coriolis force.

It should be noted that all these terms are related to m_{rb}. The present work, in order to take into account rocking-bulging interaction, keeps these actions also in the framework of the simplified analysis. Figure 5-33 clarifies the position of the application point and the direction of these forces and the arm in case of moments. Note that, for simplicity of representation, they are depicted in the 2DOF system.

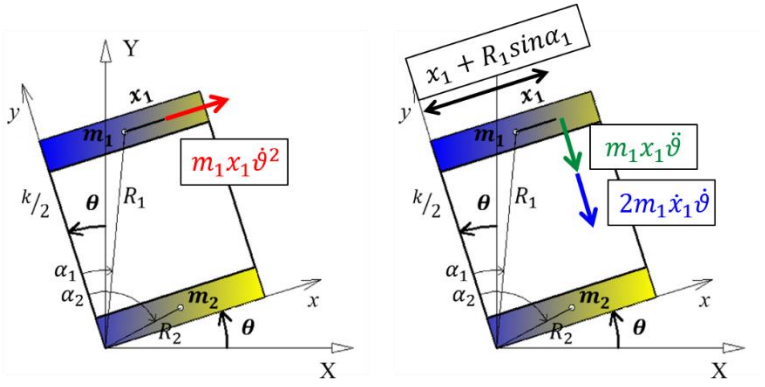

Figure 5-33. Forces and moments related to the rocking-bulging interaction [183]

According to Ref.[49], the uplift width of the tank bottom plate usually is up to 6-7% of the diameter of the tank. Therefore, the rotation angle of tank θ is very small and values of

trigonometric functions are regarded as $\sin\theta \cong 0$ and $\cos\theta \cong 1$. Moreover, contributions of inertia and weight forces arising from the uplifted part of the tank bottom plate are neglected.

With the aim to provide the maxima responses of tank bulging and rocking motions, the absolute acceleration of the tank bulging system $(\ddot{x}_1 + \ddot{z}_H)$ is replaced by the response acceleration spectrum, which is given as the product of the maximum ground acceleration $(\ddot{z}_H)_{max}$ by the value of a ratio of the maximum response acceleration to the maximum ground acceleration, $S_{AH}^{ratio}(T_b, h_b)$, which is function of the natural period of the tank bulging motion T_b and of its damping ratio h_b:

$$\left(\ddot{x}_1 + \ddot{z}_H\right)_{\max} = S_{AH}^{ratio}\left(T_b, h_b\right)\left(\ddot{z}_H\right)_{\max} \tag{5.52}$$

The relative displacement and the relative velocity are also replaced by the spectral values:

$$\left(x_1\right)_{\max} = \frac{S_{AH}^{ratio}\left(T_b, h_b\right)\left(\ddot{z}_H\right)_{\max}}{\omega_b^2} \tag{5.53}$$

$$\left(\dot{x}_1\right)_{\max} = \frac{S_{AH}^{ratio}\left(T_b, h_b\right)\left(\ddot{z}_H\right)_{\max}}{\omega_b} \tag{5.54}$$

Through these substitutions, damping effects are naturally included in the analysis. It should be pointed out that the maxima effects of tank rocking and bulging motions are assumed to be simultaneous. In addition, the proposed analysis assumes that the tank bulging motion reaches its maximum value specified by Eq. (5.52) even in presence of rocking motion.

After the introduction of the response spectra and the simplifications due to the small values of rotation, the tank model is described by a system of two simultaneous equations in the two variables $\ddot{\theta}$ and $\dot{\theta}$. In particular, Eq. (5.44) becomes:

$$\begin{aligned} & m_b S_{AH}^{ratio}\left(T_b, h_b\right)\left(\ddot{z}_H\right)_{\max} - m_{rb} H_{rb}\ddot{\theta} \\ & - m_{rb}\left(\left(S_{AH}^{ratio}\left(T_b, h_b\right)\left(\ddot{z}_H\right)_{\max} / \omega_b^2\right) + R_{rb}\sin\alpha_{rb}\right)\dot{\theta}^2 + \\ & + k\, S_{AH}^{ratio}\left(T_b, h_b\right)\left(\ddot{z}_H\right)_{\max} / \omega_b^2 = 0 \end{aligned} \tag{5.55}$$

while Eq. (5.45) becomes:

$$
\begin{aligned}
&\left\{ m_{rb}\left(S_{AH}^{ratio}\left(T_b, h_b \right)\left(\ddot{z}_H \right)_{\max} / \omega_b^2 \right)^2 + \right. \\
&+2\, m_{rb}\left(S_{AH}^{ratio}\left(T_b, h_b \right)\left(\ddot{z}_H \right)_{\max} / \omega_b^2 \right) D/2 + \\
&+\left(I_{rf} + I_{sh} + I_r \right) + \\
&\left. +\left(m_{rf} R_{rf}^2 + m_{sh} R_{sh}^2 + m_r R_r^2 \right) \right\} \ddot{\theta} + \\
&-m_b S_{AH}^{ratio}\left(T_b, h_b \right)\left(\ddot{z}_H \right)_{\max} H_b + \\
&+2 m_{rb} \dot{\theta}\left(S_{AH}^{ratio}\left(T_b, h_b \right)\left(\ddot{z}_H \right)_{\max} / \omega_b \right)\left[\left(S_{AH}^{ratio}\left(T_b, h_b \right)\left(\ddot{z}_H \right)_{\max} / \omega_b^2 \right) + D/2 \right] + \\
&+\left\{ m_{rf} + m_{sh} + m_r \right\} Dg/2 - \left\{ m_{rf} H_{rf} + m_{sh} H_{sh} \right\} \ddot{z}_H = 0
\end{aligned}
\tag{5.56}
$$

where the following substitutions are made:

$$
\begin{aligned}
&H_b = R_b \cos \alpha_b \\
&H_r = R_r \cos \alpha_r \\
&H_{rf} = R_{rf} \cos \alpha_{rf} \\
&H_{sh} = R_{sh} \cos \alpha_{sh}
\end{aligned}
\tag{5.57}
$$

Moreover, in order to simplify the notation

$$
\begin{aligned}
&R_r \sin \alpha_r \cong D/2 \\
&R_{rb} \sin \alpha_{rb} \cong D/2
\end{aligned}
\tag{5.58}
$$

are assumed. It should be noted that, in the simplified analysis, the index of rotational direction λ is not considered, since the aim of the analysis is not to investigate time history of the response but only its maximum value.

The expression of $\ddot{\theta}$ is derived from Eq. (5.56):

$$
\begin{aligned}
&\ddot{\theta} = \left\{ m_{rb}\left[S_d{}^2 + DS_d \right] + \left(I_{rf} + I_{sh} + I_r \right) + \left(m_{rf} R_{rf}^2 + m_{sh} R_{sh}^2 + m_r R_r^2 \right) \right\}^{-1} \cdot \\
&\cdot \left[m_b H_b S_a - 2 m_{rb} S_v \left(S_d + D/2 \right) \dot{\theta} - \left(m_{rf} + m_{sh} + m_r \right) gD/2 + \right. \\
&\left. +\left(m_{rf} H_{rf} + m_{sh} H_{sh} \right)\left(\ddot{z}_H \right)_{\max} \right]
\end{aligned}
\tag{5.59}
$$

Introducing Eq. (5.59) in Eq. (5.55), the following quadratic equation in $\dot{\theta}$ is provided:

$$
\begin{aligned}
&m_{rb}\left[S_d+\frac{D}{2}\right]\dot{\theta}^2-2{m_{rb}}^2H_{rb}S_v\left[S_d+\frac{D}{2}\right]\cdot\left\{m_{rb}\left[{S_d}^2+DS_d\right]+\right.\\
&\left.\left(I_{rf}+I_{sh}+I_r\right)+\left(m_{rf}R_{rf}^2+m_{sh}R_{sh}^2+m_rR_r^2\right)\right\}^{-1}\dot{\theta}+\\
&+m_{rb}H_{rb}\left\{m_{rb}\left[{S_d}^2+DS_d\right]+\left(I_{rf}+I_{sh}+I_r\right)+\left(m_{rf}R_{rf}^2+m_{sh}R_{sh}^2+m_rR_r^2\right)\right\}^{-1}\\
&\cdot\left[m_bH_bS_a-\left(m_{rf}+m_{sh}+m_r\right)gD/2+\left(m_{rf}H_{rf}+m_{sh}H_{sh}\right)\left(\ddot{z}_H\right)_{\max}\right]\\
&-\left\{m_bS_a+kS_d\right\}=0
\end{aligned}
\tag{5.60}
$$

in which, in order to simplify the notation, the expression of the spectral values are given by

$$
\begin{aligned}
S_a&=S_{AH}^{ratio}(T_b,h_b)(\ddot{z}_H)_{max},\\
S_v&=S_{AH}^{ratio}(T_b,h_b)(\ddot{z}_H)_{max}/\omega\\
S_d&=S_{AH}^{ratio}(T_b,h_b)(\ddot{z}_H)_{max}/\omega^2.
\end{aligned}
\tag{5.61}
$$

The spring constant of the tank bulging system is

$$
k=4\pi^2m_b/T_b^2 \tag{5.62}
$$

Solutions of the quadratic equation are given as:

$$
\dot{\theta}=\frac{\left(-b\pm\sqrt{b^2-4ac}\right)}{2a} \tag{5.63}
$$

where:

$$
a=m_{rb}\left[S_d+\frac{D}{2}\right]\dot{\theta}^2
$$

$$
\begin{aligned}
b=&-2{m_{rb}}^2H_{rb}S_v\left[S_d+\frac{D}{2}\right]\cdot\\
&\left\{m_{rb}\left[{S_d}^2+DS_d\right]+\left(I_{rf}+I_{sh}+I_r\right)+\left(m_{rf}R_{rf}^2+m_{sh}R_{sh}^2+m_rR_r^2\right)\right\}^{-1}\dot{\theta}
\end{aligned}
\tag{5.64}
$$

$$
\begin{aligned}
c=&m_{rb}H_{rb}\left\{m_{rb}\left[{S_d}^2+DS_d\right]+\left(I_{rf}+I_{sh}+I_r\right)+\left(m_{rf}R_{rf}^2+m_{sh}R_{sh}^2+m_rR_r^2\right)\right\}^{-1}\cdot\\
&\cdot\left[m_bH_bS_a-\left(m_{rf}+m_{sh}+m_r\right)gD/2+\left(m_{rf}H_{rf}+m_{sh}H_{sh}\right)\left(\ddot{z}_H\right)_{\max}\right]\\
&-\left\{m_bS_a+kS_d\right\}
\end{aligned}
$$

Only one of the two solutions of Eq. (5.63) is picked up, i.e. the value of $\dot{\theta}$ that maximizes $\ddot{\theta}$, since the aim of the analysis is to obtain the maximum value of the response in terms of rotational acceleration $\ddot{\theta}$.

Once angular velocity and angular acceleration of rocking motion are known, the second important task of this section is to provide a measure of the effects of rocking motion on the bulging response. For this purpose, Eq. (5.55) is compared with the bulging motion equation, Eq. (5.44), evaluated in absence of uplift, given as follows:

$$m_b\left(\ddot{x}_1+\ddot{z}_H\right)+kx_1=0 \tag{5.65}$$

Therefore, substitution of Eq. (5.65) into Eq. (5.55) provides the absolute response acceleration of the tank bulging motion that takes into account the rocking-bulging interaction effects:

$$\begin{aligned}\left(\ddot{x}_1+\ddot{z}_h\right)=&\left\{S_{AH}^{ratio}\left(T_b,h_b\right)\left(\ddot{z}_H\right)_{\max}\right\}-\frac{m_{rb}}{m_b}H_{rb}\ddot{\theta}\\&-\frac{m_{rb}}{m_b}\left\{\frac{S_{AH}^{ratio}\left(T_b,h_b\right)\left(\ddot{z}_H\right)_{\max}}{\omega_b}+\frac{D}{2}\right\}\dot{\theta}^2\end{aligned} \tag{5.66}$$

This expression shows as the appearance of rocking motion during the seismic event leads to a reduction of the absolute response acceleration of the tank bulging motion and then a decreasing of all response quantities involved such as bulging displacement and base shear.

The overturning moment is given in terms of the response acceleration spectrum by introducing Eq. (5.52) in Eq. (5.46c):

$$OM=m_bH_bS_{AH}^{ratio}\left(T_b,h_b\right)\left(\ddot{z}_H\right)_{\max}+\left(m_{rf}H_{rf}+m_{sh}H_{sh}\right)\left(\ddot{z}_H\right)_{\max} \tag{5.67}$$

Substituting Eq. (5.67) into Eq. (5.46a), the value of the ground acceleration demand for the appearance of the rocking motion is given by:

$$\left(\ddot{z}_H\right)_{\max}>\frac{\left(m_{rf}+m_{sh}\right)Dg}{2\left\{m_bH_bS_{AH}^{ratio}\left(T_b,h_b\right)+\left(m_{rf}H_{rf}+m_{sh}H_{sh}\right)\right\}} \tag{5.68}$$

5.11. Numerical analysis on a sample tank

For the purpose of validating the accuracy of the proposed procedure, this section provides a comparison between the tank response for rocking motion calculated by the simplified analysis and that computed by the Explicit Finite Element Analysis (EFEA) for a sample tank in LS-DYNA software. This study considers an unanchored flat bottom tank, set on an almost rigid foundation, without roof. Shell height and diameter are respectively $30.0\ m$ and $51.5\ m$. The construction material for cylindrical and bottom plates is an aluminium alloy. Thickness value varies in height from $54.5\ mm$ to $16.0\ mm$ for cylindrical shell, while for bottom plate it is $6.0\ mm$. The annular plate, whose width is $4.0\ m$, has $32.7\ mm$ in thickness. The tank stores liquefied natural gas (LNG) whose density is $0.47\ t/m^3$ and depth is $28.8\ m$. Since the proposed analysis does not take into account the out-of-round deformation of the shell, rigid stiffeners modelled by rigid elements are attached to the cylindrical shell with an interval of $0.6\ m$. Moreover, the relative displacement between the bottom plate and the foundation is constrained in order to prevent sliding. Cylindrical shell and bottom plate are modelled by shell elements consisting of 21,639 nodes and 21,640 elements (see Figure 5-34). The Arbitrary Lagrangian Eulerian (ALE) approach is employed in order to model fluid-structure interaction. The fluid content is modelled by eulerian elements consisting of 301,168 nodes and 301,400 elements. The tank is supported by a concrete foundation whose diameter and thickness are respectively $71.5\ m$ and $10\ m$. Foundation is modelled by solid elements consisting of 15,651 nodes and 10,640 elements. It should be pointed out that the FE modelling of the foundation does not take into account the soil-structure interaction and the dispersion of waves in soil. However, this choice is reasonable since it leads to a safe side evaluation of the tank model response. Dynamic excitation used in the seismic analysis is a recorded accelerogram of Kobe earthquake of 1995, shown in Figure 5-35.

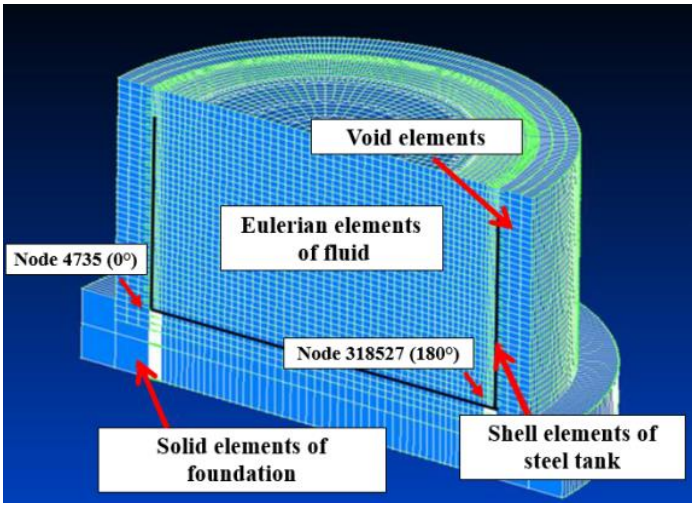

Figure 5-34. Numerical model of a sample tank [183]

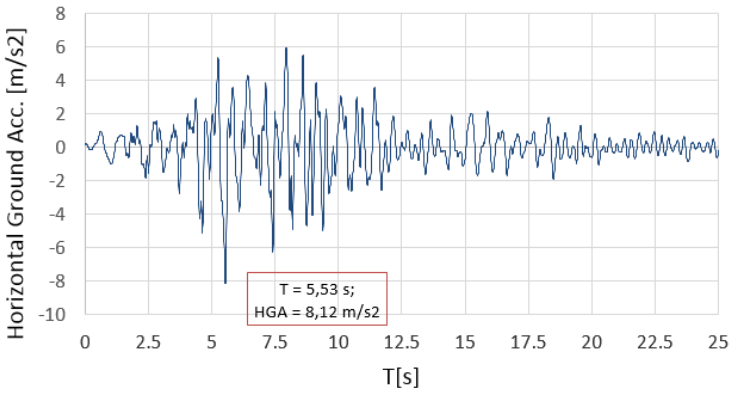

Figure 5-35. Recorded accelerogram (Kobe earthquake '95) [183]

In this case, time history analysis uses the first seconds to increase gravitational acceleration gradually in order to take into account the dead weight of the tank. For this reason, the response does not begin from $t = 0$.

Figure 5-36 shows time history of the vertical displacement of the two edge nodes of the bottom plate located along the diameter parallel to the ground acceleration. Figure 5-34 clarifies the location of the nodes analyzed for the uplift evaluation. As the alternate location of the peaks in vertical displacement demonstrates (Figure 5-36), the left and the right bottom edges reciprocally uplift because of the appearance of rocking motion. The maximum value of uplift displacement is $d_{z,max} = 0.704$ m.

Figure 5-37 provides the distribution of the uplift displacement of the tank bottom plate along the diameter parallel to the ground acceleration at the time $t = 10.3\ s$ (time in which the maximum value of the uplift displacement $d_{z,max}$ occurs). The corresponding uplift width of the tank bottom plate is $w_{z,max} = 3{,}98$ m (ratio of the uplift width to tank diameter is $\delta = 0.077$).

The effective mass for bulging motion and the position of its gravity center for the sample tank are obtained from literature [182]. Employing the uplift ratio reached from the numerical analysis, the effective masses for tank rocking motion and for tank rocking-bulging interaction, the position of their gravity centers and their moments of inertia are estimated from tables presented in [162].

Table 5.7 summaries values of these properties and all other data required to carry out the simplified analysis. The ratio of the maximum response acceleration to the maximum ground acceleration $S_{AH}^{ratio}(T_b, h_b)$ is 2.48. The maximum ground acceleration $(\ddot{z}_H)_{max}$ is 8.12 m/s^2.

From Eqs. (5.59), (5.63) and (5.64a, b, c), values of angular acceleration $\ddot{\theta}$ and angular velocity $\dot{\theta}$ are calculated. Moreover, employing these values into Eq. (5.66), the absolute maximum response acceleration $(\ddot{x}_1 + \ddot{z}_H)_{max}$ of the tank bulging motion that includes the rocking motion effects is derived.

In Table 5.8 results from simplified analysis are provided. For comparison purposes, the table presents also the value of the absolute maximum response acceleration calculated without considering rocking effects. It should be noted that the bulging absolute acceleration when the rocking motion occurs is about 16.5% of the bulging absolute acceleration in absence of rocking.

The tank response computed by EFEA in terms of angular and horizontal acceleration is affected by noise, caused by the impact of the tank on the foundation during the rocking motion. For this reason, a filter has been used in order to reduce this effect, paying attention not to modify the phase and the amplitude of the response.

Figure 5-38 shows the time history for angular acceleration $\ddot{\theta}$ and rotation angle θ. As expected, the two curves have different values of amplitude but the same phase, while their shapes are opposite respect to the time axis. This is evidence that the filter does not affect the period of the acceleration.

As mentioned before, the maximum uplift displacement of the tank bottom plate is reached at $t = 10.3\ s$; at the same time, also rotation angle is maximum, and angular acceleration value is around $0.24\ rad/s^2$.

Figure 5-39 shows the time history of the angular velocity computed by numerical analysis. When the maximum uplift displacement occurs, angular velocity is around $0.06\,rad/s$. Finally, in order to compare analytical and numerical results in terms of absolute bulging motion acceleration, some considerations should be made. The height of the gravity center of the effective mass for bulging motion of the sample tank is $H_b = 10.809\,m$. Therefore, in the numerical model, the absolute acceleration of the two shell nodes placed along the diameter parallel to the ground motion at the height H_b is analyzed. Since the motion of the LS-DYNA tank model is referred to an external global system, the absolute response acceleration of all nodes includes the contribution due to the displacement of the shell induced by the rotational motion, when the tank rocks. On the other hand, in the absolute response acceleration for bulging motion ($\ddot{x}_1 + \ddot{z}_H$) carried out by the simplified analysis, the term $\ddot{x}_1$ represents the relative bulging acceleration, i.e. the acceleration referred to a system of axis rotating in unison with the tank rocking motion. Therefore, in order to provide a consistent comparison between numerical and analytical results, the contribution of the rotation is removed from the absolute response acceleration obtained by the numerical analysis.

Figure 5-40 shows the time history of the absolute response acceleration and highlights the value of the response when the maximum uplift displacement of the bottom plate occurs. It should be noted that the response acceleration trend does not match that of a single degree of freedom system, given by a sinusoidal function antisymmetric respect to the horizontal axis. This is a reasonable result since the bulging acceleration and the other bulging responses are affected by the bulging-rocking interaction, as clarified in a previous section. In order to demonstrate the reliability of the absolute response acceleration trend for bulging motion provided by EFEA, Figure 5-41 shows the time history of the translational acceleration derived by numerical analysis in MATLAB for the 2-story steel model. It should be noted that it does not include the ground acceleration since the simple free fall of the model from an initial inclined position has been analyzed. However, the overall trend of the responses depicted in Figure 5-40 and Figure 5-41 shows a good match. The value of the EFEA absolute response acceleration ($\cong 16.5\,m/s^2$) corresponding to the maximum uplift displacement is given as the amplitude of the wave, that in this particular case does not coincide with the distance of the peak from the horizontal axis (see Figure 5-40). Moreover, since the angular acceleration graph is not smooth because of noise, it is recommended to pick up the medium value of the trend near the peak of the response.

Comparison between numerical and analytical results is provided in Table 5.8. It is evident that simplified analysis carries out very reasonable values of angular acceleration for rocking motion and absolute response acceleration for bulging motion. Moreover, results provided by EFEA in terms of bulging absolute acceleration, confirm that bulging response is reduced by the effect of the rocking-bulging interaction and simplified analysis can correctly estimate this reduction.

Otherwise, simplified analysis cannot provide reasonable evaluation of the angular velocity. This is an expected result, since a simplified procedure neglecting the contribution of the angular velocity has been employed for the calculation of the effective masses involved in the rocking-bulging motion. However, this is a reasonable simplification, since values of angular velocity are very small if compared to those of angular acceleration, so that the latter represents the main actor of the rocking-bulging interaction.

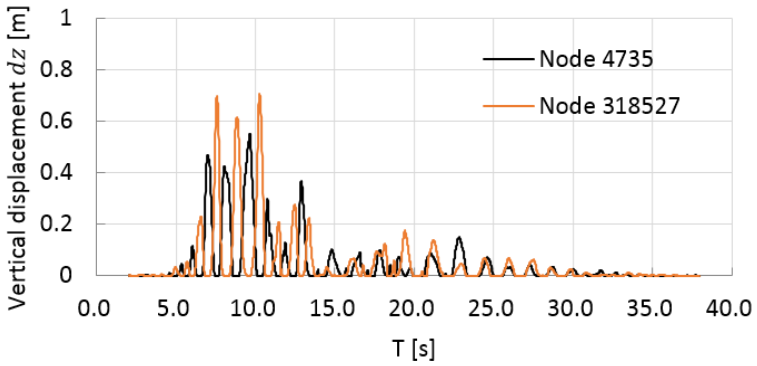

Figure 5-36. Time history of the vertical displacement of two edge nodes of the bottom plate [183]

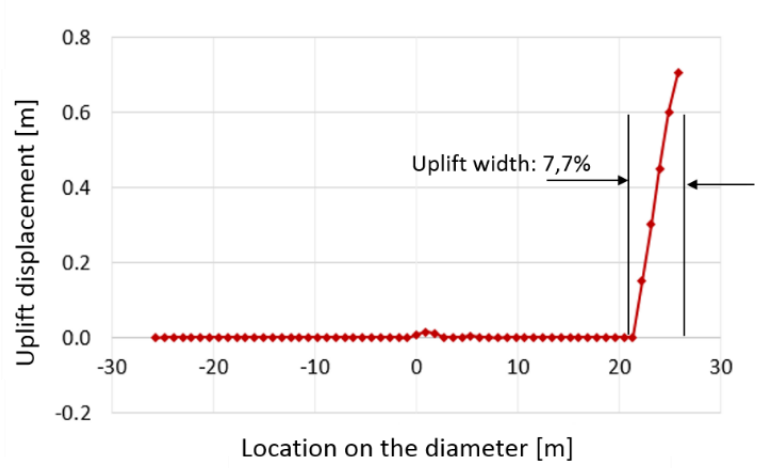

Figure 5-37. Distribution of the uplift displacement of the tank bottom plate at the time t = 10.3 s [183]

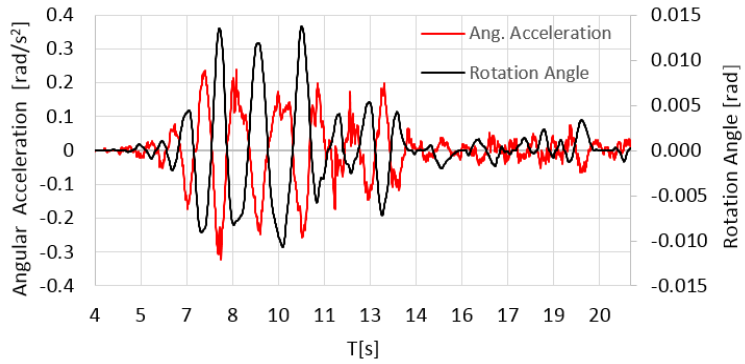

Figure 5-38. Time history of angular acceleration and rotation angle [183]

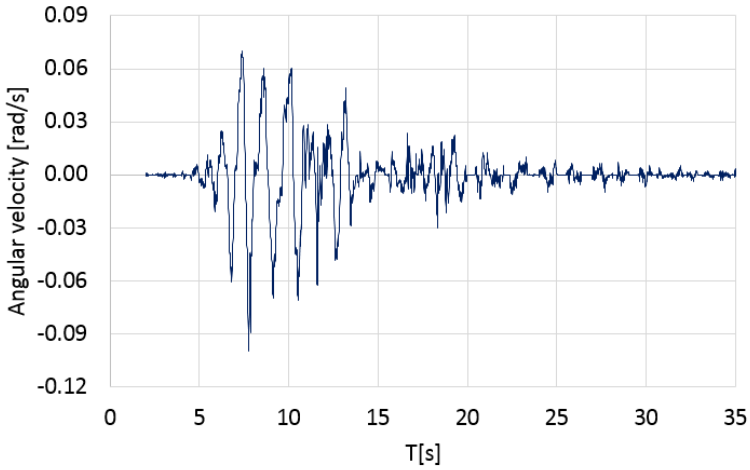

Figure 5-39. Time history of angular velocity [183]

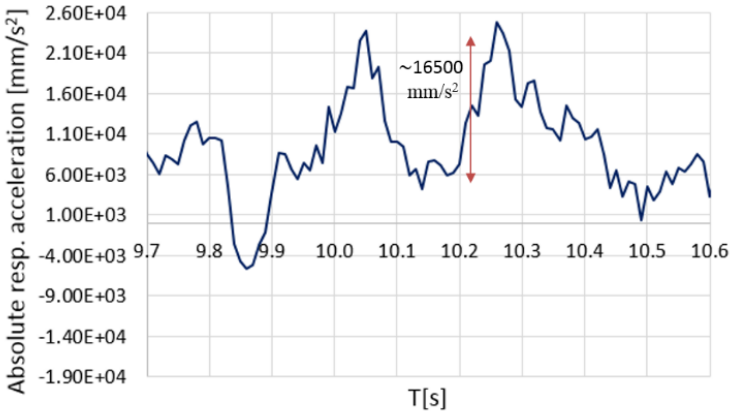

Figure 5-40. Time history of bulging absolute response acceleration [183]

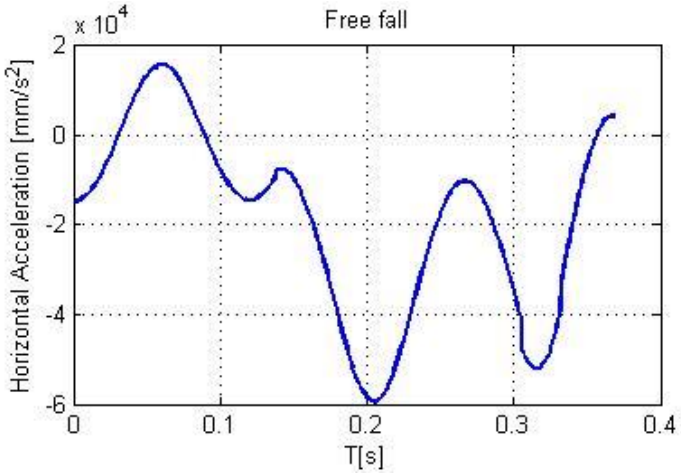

Figure 5-41. Time history of bulging response acceleration carried out by MATLAB in the case of steel model free fall [183]

Table 5.7 Dynamic properties of the sample tank model involved in simplified analysis [183]

Bottom plate uplift		***Heights of the gravity centers***	
Max uplift displ. $d_{z,max}$	0.704 m	H_{sh}	11.094 m
		H_r	25.307 m
Max uplift width $w_{x,max}$	3,98 m	H_b	10.809 m
		H_{rb}	22.274 m
Effective Masses		***Angles between vertical line y and R***	
m_b	17.488×10^6 kg	α_b	67.23 rad
m_r	6.459×10^6 kg	α_r	43.58 rad
m_{rb}	4.306×10^6 kg	α_{rb}	45.97 rad
m_{sh}	3.866×10^5 kg	***Moments of inertia of the masses***	
m_{bp}	7.588×10^4 kg		
m_{rf}	0.0 kg	I_{sh}	4.56×10^8 kg.m^2
Lengths between origin and gravity centers		I_r	5.215×10^9 kg.m^2
		Dynamic bulging properties	
R_{sh}	28.039 m		
R_r	34.933 m	T_b	0.4 s
R_b	27.926 m	k_b	4.310×10^9 kg/s^2
R_{rb}	32.051 m	h_b	0.05

Table 5.8 Tank responses calculated respectively by simplified and numerical analyses

Responses of interest	***Symplified Analisys***	***Numerical Analysis***
Angular acc. $\ddot{\theta}$ [rad/s^2]	0.202	0.240
Angular vel. $\dot{\theta}$[rad/s]	-2.570	0.06
Abs. response acc. for bulging motion $(\ddot{x}_1 + \ddot{z_H})_{max}$ [m/s^2] (including rocking effects)	16.82	16.5
Abs. response acc. for bulging motion $(\ddot{x}_1 + \ddot{z_H})_{max}$ [m/s^2] (not including rocking effects)	20.14	/

5.12. Conclusions

In order to investigate the dynamic response of unanchored tanks during seismic events, this study first analyses the mechanical analogy between the rocking-bulging motion of a tank and that of a 2DOF model, consisting of a spring-mass system and a lower mass attached to its base. For the 2DOF model, the equations of motion are derived. The system of second order differential equations is solved by using a numerical software. On the other hand, an experimental test is conducted by recording, through a high-speed camera, the motion of a physical model whose features are calibrated in order to properly represent the dynamic behavior of the 2DOF model analytically described. Then, the 2DOF model is validated by comparing the response in terms of displacement and rotation from numerical analysis with that from the experimental one. The equations for the tank rocking-bulging motion are derived from those of the 2DOF model by introducing the dynamic properties of a sample tank. Then, equations of motion for tank model are simplified in order to provide an easier tool whose the primary purpose is the evaluation of the two main quantities involved in the tank rocking-bulging response: the maximum angular acceleration $\ddot{\theta}_{max}$ and the absolute maximum response acceleration $(\ddot{x}_1 + \ddot{z}_H)_{max}$ including the reduction of the bulging motion due to the occurrence of rocking. In this framework, the fundamental role of rotational inertia and centrifugal forces governing the rocking-bulging interaction is investigated. Therefore, unlike a previous work [163], all terms of the 2DOF model equations related to these forces are kept in the simplified analysis. Finally, results of the seismic analysis conducted on a storage tank with LS-DYNA software are compared with those provided by the simplified method in order to validate the accuracy of the latters. The comparison reveals that the simplified analysis represents a reliable and accurate method for the evaluation of the tank rocking-bulging motion. Indeed, it can provide a good estimation for maximum angular acceleration and absolute maximum response acceleration. Less accuracy is detected in the evaluation of the angular velocity. This is attributed to a simplification in the method employed for the calculation of the effective masses involved in the tank rocking-bulging motion, which consists in procedure that

neglects the contribution of the angular velocity. However, this is a reasonable simplification, since values of angular velocity are very small compared to those of angular acceleration.

6. Concluding remarks

The main purpose of the research carried out in the aim of this PhD dissertation is the analysis of the dynamic behavior of on-grade cylindrical steel storage tanks. This has been done through two main research fields: the evaluation of tank seismic fragility and the analytical modeling of the dynamic of tank-fluid system subjected to the ground acceleration.

As well known, the seismic fragilities of storage tanks play a fundamental role in the context of the earthquake vulnerability assessment of industrial plants. The first part of the PhD study has tried to provide a contribution to that topic. New fragility models have been proposed with the aim to overcome limits and week points of past researches summarized in the following.

A first critical issue was the dimension of dataset: at the date, empirical fragility analyses in literature were carried out basing on small collection of data. Therefore, the first step of the present work has consisted in collecting a larger database on tank failure during past earthquakes. The present dataset contains a great number of undamaged tanks omitted in previous collections.

A further crucial point consists in the definition of damage states. Often in literature, classification of damage was based on HAZUS criteria, suitable for building-type structure but inadequate for cylindrical steel tanks. The present work classifies tank damages by using a set of damage states basing on tank-fluid system structural performances and a set of risk levels related to intensity of liquid releases.

Moreover, in most cases, development of fragility curves was based on the usage of damage matrixes, in which tanks were divided into PGA bins, and the value of dispersion parameter was bounded a priori. This regression procedure might be questionable because it forces the shape of fragility curve. The present work proposes fragility curves fitted by using the Bayesian approach. The advantage introduced by approach is that it is well suited to treat direct and indirect information obtained from field observations and to incorporate subjective engineering judgement. Data have been not divided into PGA bins and therefore regression is calculated directly from the entire dataset. Following this approach, fragility relations are not influenced or forced by the choice of range bounds. Moreover, the value of dispersion parameter is not subjected to any boundary.

Results from fragility analyses overall confirms some general trends from other researchers in terms of influence on the tank performances of crucial aspects as filling level, presence of base anchorage system and tank aspect ratio. Other researches have proposed different fragility

models depending on filling level, anchorage and H/D, even though they fitted these models independently using different subsets of their database. Taking into account the effects of the aforementioned parameters through specific regression coefficients, as proposed here, allows to perform significance tests on these latter, and therefore evaluate which parameters are statistically more relevant for the definition of fragility. In addition, an overall fragility function taking into account simultaneously the effects of these parameters is provided.

With respect to what found in literature, the current study has obtained lower tank fragilities. It is an expected results, since previous researches considered mostly damaged tanks, while a great number of undamaged tanks were omitted.

The second section of the present PhD study has focused on the mechanical modeling of unanchored tanks dynamics. These structures are known to show a complex behavior under seismic action, since their response involves the combination of vibrating and bouncing phenomena. Past researches provided simple tools for the seismic analysis of the tank-fluid system but they neglected the effects of the tank rocking-bulging motion interaction. However, as the comparison between analytical and experimental results corroborates in the present work, the rocking-bulging interaction is governed by rotational inertia, centrifugal and Coriolis forces that play a leading role in the dynamic response of the tank.

Then, the current study proposes an investigation on the role of inertial and centrifugal forces in the context of the interaction between rocking and translational motions. The simultaneous dynamic equations of a 2DOF model have been solved through a numerical software and results have been compared with those of experimental tests. Moreover, employing the dynamic properties governing the tank rocking-bulging motion into the simultaneous equations, a simplified method to determine the tank bulging response and the measure in which it is reduced by the rocking appearance is provided. Validation of the proposed analysis is conducted comparing its results with those computed through an Explicit Finite Element Analysis on a sample tank.

A future development of this work could deal with the derivation of analytical fragility curves based on structural modeling and response simulations. For this purpose, a proper numerical model simulating the seismic response of the tank-fluid system in case of unanchored tank will be employed. Indeed, one of the problems related with empirical fragility curves is that damage data corresponding to high PGA values are limited, therefore, in this case curves have to be extrapolated. By using analytical fragility, this issue can be overcome.

7. References

[1] ASCE, The Effects of Earthquakes on Power and Industrial Facilities and Implications for Nuclear Power Plant Design, (1987).

[2] T.W. Cooper, A Study of the Performance of Petroleum Storage Tanks during Earthquakes, 1933-1995 NIST GCR 97-720, 1997.

[3] C.F. Braun and Co, Western Gulf Oil Co., Paloma, Earthquake and Fire Damage Report on Inspection and Reconstruction, (n.d.).

[4] G.P.C.-E. Department, Report on Effects to General Petroleum Interests of the Tehachapi - Arvin Earthquake, Dep. Gen. Pet. Corp. - Eng. (n.d.).

[5] S. Girgin, The natech events during the 17 August 1999 Kocaeli earthquake: Aftermath and lessons learned, Nat. Hazards Earth Syst. Sci. 11 (2011) 1129–1140. doi:10.5194/nhess-11-1129-2011.

[6] S. Zama, H. Nishi, K. Hatayama, M. Yamada, H. Yoshihara, On Damage of Oil Storage Tanks due to the 2011 off the Pacific Coast of Tohoku Earthquake (Mw 9.0), Japan, in: 15 WCEE, Lisboa, 2012.

[7] HAZUS, Earthquake Loss Estimation Methodology, Natl. Inst. Build. Sci. Prep. by Risk Manag. Solut. (1997).

[8] M.J. O'Rourke, P. So, Seismic fragility curves for on-grade steel tanks, Earthq. Spectra. 16 (2000) 801–815. doi:10.1193/1.1586140.

[9] American Lifelines Alliance, Seismic Fragility Formulation For Water Systems, Part 1 - Guideline, (2001).

[10] E. Salzano, I. Iervolino, G. Fabbrocino, Seismic risk of atmospheric storage tanks in the framework of quantitative risk analysis, J. Loss Prev. 16 (2003) 403–409. doi:10.1016/S0950-4230(03)00052-4.

[11] P.K. Malhotra, Sloshing Loads in Liquid-Storage Tanks with Insufficient Freeboard, Earthq. Spectra. 21 (2005) 1185–1192.

[12] R.A. Ibrahim, Liquid sloshing dynamics. Theory and applications, Cambridge University Press, 2005.

[13] J.Y. Yang, Dynamic Behaviour of Fluid-Tank Systems, Ph.D. Thesis, Rice University, Houston, (1976).

[14] B. Hunt, M.N.J. Priestley, Seismic water waves in a storage tank, Bull. Seismol. Soc. Am. 68 (1978) 487–499.

[15] O.R. Jaiswal, D.C. Rai, S.K. Jain, Review of Seismic Codes on Liquid-Containing Tanks, Earthq. Spectra. 23 (2007) 239–260.

[16] G.W. Housner, The Dynamic Behavior of Water Tanks, Bull. Seismol. Soc. Am. 53 (1963) 381–387.

[17] G.W. Housner, Earthquake Pressures on Fluid Containers, Technical Report California Institute of Technology, Pasadena, California, NR-081-095, 1954.

[18] G.W. Housner, Dynamic Pressures on Accelerated Fluid Containers, Bull. Seismol. Soc. Am. 47 (1957) 15–35.

[19] P.K. Malhotra, T. Wenk, M. Wieland, Simple procedure for seismic analysis of liquid-storage tanks, Struct. Eng. Int. 10 (2000) 197–201.

[20] P.K. Malhotra, Practical nonlinear seismic analysis of tanks, Earthq. Spectra. 16 (2000) 473–492.

[21] A.S. Veletsos, Seismic Effects in Flexible Liquid Storage Tanks, 5th World Conf. Earthq. Eng. Rome, Italy. (1973).

[22] A.S. Veletsos, J.Y. Yang, Earthquake response of liquid-storage tanks, ASCE Adv. Civ. Eng. through Eng. Mech. Proceeding 2nd Annu. Eng. Mech. Div. Spec. Conf. (1977).

[23] A.S. Veletsos, Seismic response and design of liquid storage tanks, in: Guidel. Seism. Des. Oil Gas Pipelines Syst., ASCE, New York, 1984: pp. 255–370.

[24] M.A. Haroun, Dynamic Analyses of Liquid Storage Tanks, Research Report California Institute of Technology, Pasadena, California, EERL 80-04, 1980.

[25] M.A. Haroun, H.M. Ellaithy, Model for flexible tanks undergoing rocking, J. Eng. Mech. 111 (1985) 143–157.

[26] M.A. Haroun, G.W. Housner, Seismic Design of Liquid Storage Tanks, J. Tech. Counc. ASCE. 107 (1981) 191–207.

[27] A.S. Veletsos, Y. Tang, Soil-structure interaction effects for laterally excited liquid-storage tanks, J. Earthq. Eng. Struct. Dyn. 19 (1990) 473–496.

[28] A.S. Veletsos, Seismic response of anchored steel tanks, Proc. Third Symp. Curr. Issues Relat. to Nucl. Power Plant Struct. Equip. Piping, North Carolina State Univ. (1990) 2–15.

[29] D. Whittaker, D. Saunders, Revised NZSEE Recommendations for seismic design of storage tanks, 2008 NZSEE Conference, Paper Number 04, (2008).

[30] A.M. Haroun, G.W. Housner, EARTHQUAKE RESPONSE OF DEFORMABLE LIQUID STORAGE TANKS, J. Appl. Mech. 48 (1981) 411–418.

[31] G.M. Calvi, R. Nascimbene, Progettare i Gusci - Acciaio, cemento armato e precompresso. Piastre, serbatoi, cupole, paraboloidi e condotte, Gravità, instabilità e azioni sismiche, 2011.

[32] D.D. Kana, F.T. Dodge, Design support modeling of liquid slosh in storage tanks subjected to seismic excitation, 2nd ASCE Spec. Conf. Struct. Des. Nucl. Plant Facil. New Orleans, Louisiana. (n.d.).

[33] F.D. Fischer, F.G. Rammerstorfer, K. Scharf, Earthquake Resistant Design of Anchored and Unanchored Liquid Storage Tanks under Three-Dimensional Earthquake Excitation, G.I. Schuëller (Ed.), Springer Verlag, Berlin, 1991. (n.d.).

[34] F.D. Fischer, F.G. Rammerstorfer, Local instabilities of liquid filled cylindrical shells under earthquake excitation, SMiRT-7, Chicago, USA. (1983).

[35] F.D. Fischer, Dynamics fluid effects in liquid-filled flexible cylindrical tanks, Earthq. Eng. Struct. Dyn. (1979).

[36] F.D. Fischer, F.G. Rammerstorfer, Stability of liquid storage tanks under earthquake excitation, Proceeding 8th World Conf. Earthq. Eng. (1984).

[37] A.S. Veletsos, Y. Tang, Dynamics of vertically excitated luquid storage tanks, ASCE J. Eng. Mech. Div. (1986).

[38] M.A. Haroun, M.A. Tayler, Axisymmetrical vibrations of tanks - Numerical, J. Eng. Mech. (1985).

[39] P.K. Malhotra, Eartquake induced sloshing in tanks with insufficient freeboard, Struct. Eng. Int. 3 (2006) 222–225.

[40] J. Bielak, Dynamic behaviour of structures with embedded foundation, Earthq. Eng. Struct. Dyn. 3 (1975) 259–274.

[41] Jennings P.C., J. Bielak, Dynamics of building-soil interaction, Bull. Seismol. Soc. Am. 63 (1973) 9–48.

[42] A.S. Veletsos, Dynamics of structure-foundation systems-structural and geotechnical mechanics, Prentice Hall. (1977).

[43] A.S. Veletsos, Y. Tang, Soil-structural interaction effects for laterally excited liquid-tank system, Am. Soc. Mech. Eng. Press. Vessel. Pip. Conf. New Orleans. (1992).

[44] A.S. Veletsos, Y. Tang, Soil-Structure interaction effects for vertically ecited liquid storage tanks, Proceeding 9th World Conf. Earthq. Eng. Tokyo-Kyoto. (1988).

[45] J. Habenberger, J. Schwarz, Seismic response of flexibly supported anchored liquid storage tanks, 12th Conf. Earthq. Eng. London. (2002).

[46] J. Bielak, Modal analysis fot building-soil interaction, ASCE J. Eng. Mech. Div. 102 (1976) 771–786.

[47] M.A. Haroun, H.S. Badawi, Seismic behaviour of unanchored ground-based cylindrical tanks, Proceeding 9th World Conf. Earthq. Eng. Tokyo-Kyoto. (1988).

[48] T. Taniguchi, Rocking behavior of unanchored flat-bottom cylindrical shell tanks under action of horizontal base excitation, Eng. Struct. 26 (2004) 415–426.

[49] D.P. Clough, Experimental evaluation of seismic design methods for broad cylindrical tanks, UCB/EERC-77/10. (1977).

[50] R.W. Clough, N. A., Static tilt tests of a tall cylinder liquid storage tank, UCB/EERC-79/06. (1979) PB-272 280.

[51] R.S. Wozniak, W.. Mitchell, Basis of Seismic Design Provisions for Welded Steel Oil Storage Tanks, Sess. Adv. Storage Tank Des. Am. Pet. Institute, Washington, USA. (1978).

[52] K. Scharf, Contribution to the behaviour of earthquake excited above-ground liquid storage tanks, PhD. Thesis. (1989).

[53] F. Sakai, A. Isoe, H. Hirakawa, Y. Mentani, Experimental study on uplifting behaviour of flat-based liquid storage tank without anchors, Proceeding 9th World Conf. Earthq. Eng. Tokyo-Kyoto. (1988).

[54] M.G. Koller, P.K. Malhotra, Seismic evaluation of unanchored cylindrical tanks, Proceeding 13th World Conf. Earthq. Eng. Vancouver, Canada. (2004).

[55] P.K. Malhotra, A.S. Veletsos, Uplifting response of unanchored liquid storage tanks, J. Struct. Div. ASCE1. 120 (1994) 3525–3547.

[56] R. Peek, Analysis of unanchored liquid storage tanks under seismic loads, PhD. Thesis, Earthq. Eng. Res. Lab. Calif. Inst. Technol. Pasadena, Calif. (1986).

[57] R. Peek, Jennings P.C., Simplified analysis of unanchored tanks, Earthq. Eng. Struct. Dyn. (1988).

[58] M. Anghileri, L. Castelletti, M. Tirelli, Fluid structure interaction of wate filled tanks during the impact with the ground, Int. J. Impact Eng. (2005).

[59] M. Arafa, Finite element analysis of sloshing in rectangular liquid-filled tanks, J. Vib. Control. 13 (2007) 883–903.

[60] F.J. Cambra, Earthquake response considerations of broad liquid storage tanks, Res. Rep. Calif. Inst. Technol. , Pasadena, California, EERL 82-25. (1982).

[61] D. Lallemant, A. Kiremidjian, H. Burton, Statistical procedures for developing earthquake damage fragility curves, (2015). doi:10.1002/eqe.

[62] F.D. Fischer, F.G. Rammerstorfer, K. Scharf, Storage tanks under earthquake loading, ASME Appl. Mech. Rev. 43 (1990) 261–499.

[63] L. Yang, Z. Chen, G. Cao, C. Yu, W. Guo, An analytical formula for elastic–plastic instability of large oil storage tanks, Int. J. Press. Vessel. Pip. 101 (2013) 72–80. doi:10.1016/j.ijpvp.2012.10.006.

[64] T. Watabene, DAMAGE TO OIL REFINERY PLANTS AND A BUILDING COMPACTED BY THE NIIGATA EARTHQUAKE AND THEIR RESTORATION, Soil Found. 6 (1966).

[65] K. Kawano, T. Oda, K. Yoshida, S. Yamamoto, T. Shibuva, S. Yamada, Damage of Oil Storage Tanks for Off Miyagi Prefecture Earthquake of June 12, 1978, 1978.

[66] American Lifelines Alliance, Seismic Fragility Formulation for Water Systems, Part 2 - Appendices, (2001).

[67] F. Berahman, F. Behnamfar, Seismic Fragility Curves for Un-Anchored On-Grade Steel Storage Tanks: Bayesian Approach, J. Earthq. Eng. 11 (2007) 166–192. doi:10.1080/13632460601125722.

[68] K. Steinbrugge, D. Moran, An Engineering Study of the Southern California Earthquake of July 21, 1952 and its Aftershocks, Bull. Seismol. Soc. Am. 44 (1954).

[69] R. Hanson, Behavior of Liquid-Storage Tanks, in: Gt. Alaska Earthq. 1964, Washington D.C, 1973: pp. 331–339.

[70] D.P. Belanger, Port of Whittier, in: Gt. Alaska Earthq. 1964, Washington D.C, 1973: pp. 1074–1107.

[71] E. Hausler, N. Sitar, Performance of Soil Improvement Techniques in Earthquakes_Showa Oil Co . Niigata Refinery Oil Tanks, n.d.

[72] E. Hausler, N. Sitar, Performance of Soil Improvement Techniques in Earthquakes_Nippon Oil Co . Ose Oil Tank Yard, n.d.

[73] Miyagi, Japan 1978.pdf, (n.d.).

[74] Reconnaissance Report, Imperial County, California, Earthquake, October 15, 1979, EERI, Febr. 1980. (n.d.).

[75] M. Haroun, Behavior of Unanchored Oil Storage Tank: Imperial Valley Earthquake, J. Tech. Top. Civ. Eng. ASCE. 109 (1983) 23–40.

[76] J. Stratta, Reconnaissance Report: Greenville (Diablo/Livermore), California Earthquake Sequence January 1980, n.d.

[77] EERI, R. Scholl, J. Stratta, The Coalinga, California, Earthquake of May 2, 1983: A Reconnaissance Report, 1984.

[78] A. Kiremidjian, K. Ortiz, R. Nielsen, Seismic Risk to Major Industrial Facilities, Stanford, 1985.

[79] G.M. Mavko, S. Schulz, B.D. Brown, Effects of the 1983 Coalinga, California, earthquake on creep along the San Andreas fault, Bull. Seismol. Soc. Am. . 75 (1985) 475–489. http://www.bssaonline.org/content/75/2/475.abstract.

[80] P. Pineda, G.R. Saragoni, E. Arze L, Performance of steel tanks in Chile 2010 and 1985 earthquakes, Behav. Steel Struct. Seism. Areas. (2011) 337–342. doi:doi:10.1201/b11396-52.

[81] EERI, The Chile Earthquake of March 3, 1985 - Industrial Facilities, Earthq. Spectra. 2 (1986) 373–409.

[82] I.N. Connor, The San Antonio, Chile, Earthquake of 3 March 1985, San Antonio, Chile, Earthq. 3 March 1985. 18 (1985) 128–138.

[83] E. Booth, C. Taylor, The Chilean Earthquake of 3 March 1985 - A Field Report By EEFIT, 1988.

[84] P. Hashimoto, L. Tiong, Earthquake Experience Data on Anchored, Ground-Mounted Vertical Storage Tanks, Costa Mesa, California, 1989.

[85] D. Mitchell, R. Tinawi, Structural damage due to the April 22, 1991, Costa Rican earthquake, Can. J. Civ. Eng. 19 (1992) 586–605. doi:10.1139/l92-069.

[86] EERI, Costa Rica Earthquake Reconnaissance Report, Earthq. Spectra. Supplement (1991).

[87] G. Santana, The April 22, 1991 Limon (Costa Rica) Earthquake, in: Earthq. Eng. Tenth World Conf., Balkema, Rotterdam, 1994: pp. 7033–7038.

[88] EERI, Loma Prieta Earthquake October 17, 1989, Preliminary Reconnaissance Report, (1989).

[89] EEFIT, The Loma Prieta earthquake of 17 October 1989, 1993.

[90] A. Schiff, The Loma Prieta, California, Earthquake of October 17, 1989-Lifelines, USGS, 1998.

[91] I. EQE Engineering, The October 17, 1989 Loma Prieta Earthquake, San Francisco, California, 1989.

[92] EPRI, LANDERS AND BIG BEAR EARTHQUAKE 1992, (n.d.).

[93] EQE, The Landers and Big Bear Earthquakes of June 28,1992, (n.d.).

[94] P.A. Merriman, M.S. Williams, The magnitude 6.7 northridge, california, earthquake of 17 january 1994., Science. 266 (1994) 389–397. doi:10.1126/science.266.5184.389.

[95] T. Cooper, T. Wachholz, The Effects of the 1994 Northridge Earthquake on Storage Tanks, in: Proceeding NEHRP Conf. Work. Res. Northridge, Calif. Earthq. January 17, 1994, n.d.: pp. 751–764.

[96] EERI, Northridge Earthquake Reconnaissance Report, Earthq. Spectra. Supplement (1995).

[97] EQE, The January 17, 1995 Kobe Earthquake, An EQE Summary Report, 1995.

[98] R.P. Tritton, S.W. Kirkpatick, T. Woodrow, THE HYOGO-KEN NANBU (KOBE) EARTHQUAKE OF 17 JANUARY 1995 A FIELD REPORT BY EEFIT, (1997).

[99] Y. Kitagawa, H. Hiraishi, OVERVIEW OF THE 1995 HYOGO-KEN NANBU EARTHQUAKE AND PROPOSALS FOR, 4 (2004) 1–29.

[100] K. Hatayama, Lessons from the 2003 Tokachi-oki, Japan, earthquake for prediction of long-period strong ground motions and sloshing damage to oil storage tanks, J. Seismol. 12 (2008) 255–263. doi:10.1007/s10950-007-9066-y.

[101] S. Eshghi, M.S. Razzaghi, Performance of Industrial Facilities in the 2003 Bam, Iran, Earthquake, Earthq. Spectra. 21 (2005) 395–410. doi:10.1193/1.2098810.

[102] JSEE, Bam Earthquake of 05:26:26 of 26 December 2003, Ms6.5, (2003).

[103] S. Eshghi, M.S. Razzaghi, The Behavior of Special Structures During the Bam Earthquake of 26 December 2003, (2003) 197–207.

[104] F. Taucer, J. Alarcon, E. So, 2007 August 15 Magnitude 7.9 Earthquake near the Coast of Central Peru, EEFIT Field Mission, Final Report, 2007.

[105] D. Hopkins, R. Benites, J. Burr, C. Hamilton, R. Kotze, The Pisco (Peru) Earthquake of 15 August 2007, NZSEE Reconnaissance Report, Bull. New Zeal. Soc. Earthq. Eng. 41 (2008) 109–192. doi:11749857.

[106] R. Herrera, J.F. Beltran, Performance of steel structures during the February 27, 2010, Chile Eathquake, in: 15 WCEE, Lisboa, 2012.

[107] J. Moehle, R. Riddell, R. Boroschek, The Mw 8.8 Chile Earthquake of February 27, 2010, 2010.

[108] E. Krausmann, A.M. Cruz, Impact of the 11 March 2011, Great East Japan earthquake and tsunami on the chemical industry, Nat. Hazards. 67 (2013) 811–828. doi:10.1007/s11069-013-0607-0.

[109] EEFIT, EARTHQUAKE AND TSUNAMI OF 11 TH MARCH 2011 A FIELD REPORT BY EEFIT AND TSUNAMI OF 11 TH MARCH 2011, (2011).

[110] E. Fischer, Learning from Earthquakes : 2014 Napa Valley Earthquake Reconnaissance Report, 2014.

[111] I. Almutfi, A. Barbosa, J. Bray, T. Dawson, J. Marrow, M. Mieler, M 6.0 South Napa Earthquake of August 24, 2014 - EERI Special Earthquake Report, 2014.

[112] EERI, Earthquake Engineering Research Institute, (2016). https://www.eeri.org/.

[113] NIST, National Institute of Standard and Technology, (2016). http://www.nist.gov/.

[114] PEER, Pacific Earthquake Engineering Research Center, (2016). http://peer.berkeley.edu/.

[115] JSCE, Japan Society of Civil Engineers, (2016). http://www.jsce-int.org/.

[116] JSME, The Japan Society of Mechanical Engineers, (2016). http://www.jsme.or.jp/English/.

[117] MCEER, Earthquake Engineering to Extreme Events, (2016). http://www.buffalo.edu/mceer.html.

[118] NICEE, National Information Centre of Earthquake Engineering, (2005). http://www.nicee.org/.

[119] Stanford University, John A. Blume Earthquake Engineering Center, (2015). https://blume.stanford.edu/.

[120] D.M. Boore, J.P. Stewart, E. Seyhan, G.M. Atkinson, NGA-West2 Equations for Predicting Response Spectral Accelerations for Shallow Crustal Earthquakes, (2013).

[121] D.J. Wald, V. Quitoriano, T.H. Heaton, H. Kanamori, C.W. Scrivner, C.B. Worden, TriNet "Shakemaps": Rapid Generation of Peak Ground Motion and Intensity Maps for Earthquakes in Southern California, Earthq. Spectra. (1998).

[122] J.A. Blume, Preliminary Report (as of June 30, 1978) on the Japan Earthquake of June 12, 1978 and its effects, 1978.

[123] G.A. Brady, Preliminary Report in Investigations of Japanese Earthquake June 12, 1978, Menlo Park, California, 1978.

[124] EERI, Imperial County, California Earthquake Reconnaissance Report, 1980.

[125] T.K. Chan, J.D. Lichterman, S.W. Swan, P.I. Yanev, I. EQE Engineering, Effects of the Earthquake on Industrial Facilities: a Preliminary Summary, in: M.J. Rymer, W.L. Ellsworth (Eds.), Coalinga, California, Earthq. May 2, 1983, USGS, 1990: pp. 381–398. doi:10.1029/92GL00258.

[126] D.B. Ballantyne, C. Crouse, Reliability and Restoration of Water Supply Systems for Fire Suppression and Drinking Following Earthquakes, 1997.

[127] K. Brown, P. Rugar, C. Davis, T. Rulla, Seismic Performance of Los Angeles Water Tanks, Lifeline Earthquake Engineering, in: Proceedings, 4th US Conf. ASCE, TCLEE, San Francisco, California, 1995.

[128] H. Nishi, DAMAGE ON HAZARDOUS MATERIALS FACILITIES, in: Proc. Int. Symp. Eng. Lessons Learn. 2011 Gt. East Japan Earthq., Tokyo, 2012: pp. 903–912.

[129] USGS, ShakeMap - A Tool for Earthquake Response, (2003).

[130] ShakeMap Archives and Manual, USGS Earthq. Hazard Progr. (2017). https://earthquake.usgs.gov/data/shakemap/.

[131] T.D. Ancheta, R.B. Darragh, J.P. Stewart, E. Seyhan, W.J. Silva, B.S.J. Chiou, K.E.

Wooddell, R.W. Graves, A.R. Kottke, D.M. Boore, T. Kishida, J.L. Donahue, Pacific Eartquake Engineering PEER NGA-West2 Database, PEER Rep. 201303/, Pacific Earthq. Eng. Res. Center, Univ. California, Berkeley, CA. (2013).

[132] J. Douglas, Earthquake ground motion estimation using strong-motion records: A review of equations for the estimation of peak ground acceleration and response spectral ordinates, Earth-Science Rev. 61 (2003) 43–104.

[133] Applied Technology Council, Earthquake Damage Evaluation Data for CAlifornia, ATC 13, (1985).

[134] Applied Technology Council, Seismic Vulnerability and Inpact of Disruption of Lifelines in the Conterminous United States, ATC 25, (1991).

[135] ALA, American Lifeline Alliance, (2009). http://www.americanlifelinesalliance.org/.

[136] K. Porter, A Beginner's Guide to Fragility, Vulnerability, and Risk, Univ. Color. Boulder SPA Risk LLC, Denver CO USA. (2017).

[137] M. Colombi, B. Borzi, H. Crowley, M. Onida, F. Meroni, R. Pinho, Deriving vulnerability curves using Italian earthquake damage data, Bull. Earthq. Eng. 6 (2008) 485–504. doi:10.1007/s10518-008-9073-6.

[138] N. Lantada, J. Irizarry, A.H. Barbat, X. Goula, A. Roca, T. Susagna, L.G. Pujades, Seismic hazard and risk scenarios for Barcelona, Spain, using the Risk-UE vulnerability index method, Bull. Earthq. Eng. 8 (2010) 201–229. doi:10.1007/s10518-009-9148-z.

[139] H. Nam Phan, F. Paolacci, S.O. Bursi, N. Tondini, Seismic fragility analysis of elevated steel storage tanks supported by reinforced concrete columns, J. Loss Prev. Process Ind. 47 (2017) 57–65. doi:doi.org/10.1016/j.jlp.2017.02.017.

[140] A. Singhal, A.S. Kiremidjian, Method for probabilistic evaluation of seismic structural damage, J Struct. Eng. 122 (1996) 1459–1467.

[141] T. Rossetto, A. Elnashai, A new analytical procedure for the derivation of displacement-based vulnerability curves for populations of RC structures, Eng. Struct. 27 (2005) 397–409. doi:10.1016/j.engstruct.2004.11.002.

[142] K. Jaiswal, W. Aspinall, D. Perkins, D.J. Wald, K.A. Porter, Use of expert judgment elicitation to estimate seismic vulnerability of selected building types, Proc 15th Conf. Earthq. Eng. (2012) 1–10.

[143] Applied Technology Council (ATC), in: Earthq. Damage Eval. Data CAlifornia, ATC 13, Redwood City, CA, 1985.

[144] M. D'Amico, T. Taniguchi, T. Nakashima, Simplified analysis of the rocking motion of a cylindrical tank focusing on the role of dynamic forces, Proc. ASME 2017 Press. Vessel. Pip. Conf. July 16-20, 2017, Waikoloa, Hawaii, United State. (2017).

[145] F. Lees, Lees' Loss Prevention in the Process Industries - Hazard Identification, Assessment and Control, 3rd Editio, n.d.

[146] N. Buratti, F. Minghini, E. Ongaretto, M. Savoia, N. Tullini, Empirical seismic fragility for the precast RC industrial buildings damaged by the 2012 Emilia (Italy) earthquakes, Earthq. Engng Struct. Dyn. 46 (2017) 2317–2335.

[147] A.B. Gelman, J.B. Carlin, H.S. Stern, D.B. Rubin, Bayesian data analysis, 3rd ed., Chapman & Hall/CRC Press, 2013.

[148] L.E. Miller, J.T. Kunce, Prediction and statistical overkill revisited, Meas. Eval. Guid. 6 (1973) 157–163.

[149] F.E. Harrell, L.K. Lee, D.B. Matchar, T.A. Reichert, Regression models for prognostic prediction: Advantages, problems and suggested solutions, Cancer Treat. Rep. 69 (1985) 1071–1077.

[150] J.E. Barlett, J.W. Kortlik, C.C. Higgins, Organizational research: determining appropriate sample size in survey research, Inf. Technol. Learn. Perform. J. 19 (2001) 43–50.

[151] M.A. Babyak, What you see may not be what you get: a brief, nontechnical introduction to overfitting in regression-type models, Psycosomatic Med. 66 (2004) 411–421.

[152] R.J. Harris, A primer of multivariate statistics, Acad. Press. New York, USA. (1975).

[153] S.B. Green, How many subjects does it take to do a regression analysis?, Multivariate Behav. Res. 26 (1991) 499–510.

[154] E. Guadagnoli, F.V. Wayne, Relation to sample size to the stability of component patterns, Pcychological Bull. 103 (1988) 265–275.

[155] T. Rossetto, I. Ioannou, D.N. Grant, T. Maqsood, Guidelines for Empirical Vulnerability Assessment Report produced in the context of the Vulnerability Global Component project, GEM, Glob. Earthq. Model. (2014).

[156] K.A. Porter, K. Farokhnia, I.H. Cho, T. Rossetto, I. Ioannou, D. Grant, K. Jaiswal, D. Wald, D. D'Ayala, A. Meslem, E. So, A.S. Kiremidjian, H.Y. Noh, Global vulnerability estimation methods for the global earthquake model, Proc. 15th World Conf. Earthq. Eng. (2012).

[157] P.S. Koutsourelakis, H.J. Pradlwarter, G.I. Schueller, Reliability of Structures in High Dimensions, in: Proc. Appl. Math. Mech., 2003: pp. 495–496. doi:10.1002/pamm.200310.

[158] M. Shinozuka, M.Q. Feng, L. Lee, T. Naganuma, Statistical Analysis of Fragility Curves, J. Eng. Mech. 126 (2000) 1224–1231.

[159] R Development Core Team. R: A Language and Environment for Statistical Computing. Vienna, Austria. R Foundation for Statistical Computing, (2008).

[160] M. Plummer, JAGS : A Program for Analysis of Bayesian Graphical Models Using Gibbs

Sampling, in: Proc. 3rd Int. Work. Distrib. Stat. Comput. Wien, Austia, 20-22 March, 2003.

[161] T. Taniguchi, Rocking Mechanics of Flat-Bottom Cylindrical Shell Model Tanks Subjected to Harmonic Excitation, J. Press. Vessel Technol. ASME. 127 (2005) 373–386. doi:10.1115/1.2042473.

[162] T. Taniguchi, Y. Katayama, Masses of Fluid for Cylindrical Tanks in Rock with Partial Uplift of Bottom Plate, J. Press. Vessel Technol. ASME. 138 (2016) 51301-1–13. doi:10.1115/1.4032784.

[163] T. Taniguchi, D. Okui, A Case Study of Evaluation of Tank Rock Motion with Simplified Analysis Procedure, Proceeding Seism. Eng. ASME. 8 (2014). doi:10.1115/PVP2014-28635.

[164] F. Sakai, H. Ogawa, Seismic resistant design of liquid storage tanks in Japan, Sino-American Symp. Bridg. Struct. Eng. (1982).

[165] A. Isoe, Investigation on the uplift and slip behavior of flat-bottom cylindrical shell tank during earthquake, Dr. Eng. Thesis, Tokyo Univ. (in Japanese). (1994).

[166] R. Peek, Analysis of unanchored liquid storage tanks under lateral loads, Earthq. Eng. Struct. Dyn. 16 (1988) 1089–1100.

[167] A.S. Veletsos, Y. Tang, Rocking response of liquid storage tanks, J. Eng. Mech. 113 (1987).

[168] P.K. Malhotra, A.S. Velestos, Beam model for base uplifting analysis of cylindrical tanks, J. Struct. Div. ASCE. 120 (1994) 3471–3488.

[169] P.K. Malhotra, A.S. Velestos, Uplifting analysis of base plates in cylindrical tanks, J. Struct. Div. ASCE. 120 (1994) 3489–3505.

[170] G.W. Housner, The behavior of inverted pendulum structures during earthquakes, Bull. Seismol. Soc. Am. 53 (1963) 403–417.

[171] P.D. Spanos, A.S. Koh, Rocking of rigid blocks due to harmonic shaking, J. Eng. Mech. Div., ASCE. 117 (1991) 1627–1642.

[172] A. Anooshehpoor, T.H. Heaton, B. Shi, J.N. Brune, Estimates of the ground acceleration at Point Reyes station during the 1906 San Francisco earthquake, Bull. Seismol. Soc. Am. 89 (1999) 843–583.

[173] H.W. Shenton, Criteria for initiation of slide, rock, and slide-rock rigid body modes, J. Eng. Mech. Div., ASCE. 122 (1996) 690–693.

[174] A. Pompei, A. Scalia, M.A. Sumbatyan, Dynamics of rigid block due to horizontal ground motion, J. Eng. Mech. ASCE. 124 (1998) 713–717.

[175] J. Zhang, N. Makris, Rocking response of free-standing blocks under cycloidal pulses, J. Eng. Mech. ASCE. 127 (2001) 473–483.

[176] T. Taniguchi, Y. Mentani, H. Komori, The lift-off response of unanchored flat-bottom cylindrical shell tank subjected to horizontal excitation and its slip criteria, Proc. Seism. Eng. ASME. 402 (2000) 159–165.

[177] T. Taniguchi, T. Murayama, Study of free liftoff induced slip behavior of rectangular rigid body, Proc. Seism. Eng. ASME. 428 (2001) 123–130.

[178] T. Taniguchi, Nonlinear response analysis of rectangular rigid bodies subjected to horizontal and vertical ground motion, Earthq. Eng. Struct. Dyn. 31 (2002) 1481–1500.

[179] T. Taniguchi, Rocking response of unanchored flat-bottom cylindrical shell tanks subjected to horizontal base excitation, Part I: Rigid bottom plate, Proc. Seism. Eng. ASME. 466 (2003) 211–219.

[180] T. Taniguchi, Rocking response of unanchored flat-bottom cylindrical shell tanks subjected to horizontal base excitation, Part II: Flexible bottom plate, Proc. Seism. Eng. ASME. 466 (2003) 253–260.

[181] MITI Notification No.515, issued Oct. 26,1981, (n.d.).

[182] Vibration Handbook for Civil Engineers, JSCE (Japanese), (1985) 414–415.

[183] M. D'Amico, T. Taniguchi, T. Nakashima, Simplified analysis of the rocking motion of a cylindrical tank focusing on the role of dynamic forces, Proc. ASME 2017 Press. Vessel. Pip. Conf. July 16-20, 2017, Waikoloa, Hawaii, United State. (n.d.).

[184] T. Taniguchi, K. Imai, Governing Equation of Motion of Walking Behaviour Of Unanchored Flat-Bottom Cylindrical Shell Tanks During Free Rocking Motion, Proceeding Seism. Eng. ASME. (2005).

8. Appendix A

(Tank Damage Database)

Earthquake name	Year	Mw	Name of the tank site	Epicentral distance (km)	Notes about ep. Distance	Other distances	PGA (g) selected for analysis	PGA (g) from shape file	PGA (g) from Ballantyne & Crouse	PGA (g) from other report	PGA H1 (g)	PGA H2 (g)	PGA V (g)	Sv	Notes on PGA	Soil type	Soil type (EC8)	N° tanks	Note about N° tanks	Tank name	Dia (m)	H (m)	H/D	Note about H/D	Roof type	Fnd type	Shell junction	Shell plate	Anchorage	Fluid type	Fluid level	Comments
Alaska	1964	9.2	Nikiska Refinery	210		180 km from the fault	0.2	0.2							from shake map			1		R200	9.1	14.6	1.60		cone fixed					water	1	Collapse due to buckling, the bottom shell ripped loose from the tank wall on the side opposite the buckle, the cone roof was ripped off completely. (Bottom shell sta per piastra di base)
Alaska	1964	9.2	Nikiska Refinery	210		181 km from the fault	0.2	0.2							from shake map			1		R140	14.9	14.6	0.98								0.5	EFB, no leak
Alaska	1964	9.2	Nikiska Refinery	210		180 km from the fault	0.2	0.2							from shake map			1		R120	21.3	14.6	0.69		floating					crude oil	0.33	Roof rotated, damaged roof seal, and gage well
Alaska	1964	9.2	Anchorage area	130		180 km from the fault	0.21	0.21		0.2				2	It is taken to be the estimated maximum ground acceleration in Anchorage calculations made on an oil tank damaged	silts and a thick lens of bootlegger clay		1		P	43.9	17.1	0.39		floating					crude oil	0.95	Floating roof buckled, large waves
Alaska	1964	9.2	Anchorage area	130		180 km from the fault	0.21	0.21		0.2				2	It is taken to be the estimated maximum ground acceleration in Anchorage calculations made on an oil tank damaged	silts and a thick lens of bootlegger clay		1			27.4	14.6	0.53							oil	0.75	Roof buckled
Alaska	1964	9.2	Anchorage area	130		180 km from the fault	0.21	0.21		0.2				2	It is taken to be the estimated maximum ground acceleration in Anchoragecalculations made on an oil tank damaged during the	silts and a thick lens of bootlegger clay		1		S	27.4	14.6	0.53							oil	0.75	Roof-top wall connection and roof structural steel damaged
Alaska	1964	9.2	Anchorage area	130		180 km from the fault	0.21	0.21		0.2				2	It is taken to be the estimated maximum ground acceleration in Anchoragecalculations made on an oil tank damaged during the	silts and a thick lens of bootlegger clay		1			19.5	14.6	0.75		fixed						1	Elephant foot and uplift of foundation
Alaska	1964	9.2	Anchorage Airport	130		180 km from the fault	0.21	0.21		0.2				2	It is taken to be the estimated maximum ground acceleration in Anchoragecalculations made on an oil tank damaged during the	soils away from the shorline were more stable than those close		1		AA5	8.5	12.2	1.43								1	Collapse due to buckling. Leaking at wall-bottom junction
Alaska	1964	9.2	Anchorage area	130		180 km from the fault	0.21	0.21		0.2				2	ground acceleration in Anchoragecalculations made on an oil tank damaged during the earthquake showed that a maximum ground	silts and a thick lens of bootlegger clay		1		N	12.8	12.2	0.95							oil	0.95	Buckling and failure at pad, Leaking at wall-bottom junction (buckled bottom wall)
Alaska	1964	9.2	Anchorage area	130		180 km from the fault	0.21	0.21		0.2				2	It is taken to be the estimated maximum ground acceleration in Anchoragecalculations made on an oil tank damaged during the	silts and a thick lens of bootlegger clay		1		J	9.1	12.2	1.33							oil	1	Extensive Bottom shell buckling, loss of contents (in questo caso per bottom shell si intende forse la parete)
Alaska	1964	9.2	Anchorage area	130		180 km from the fault	0.21	0.21		0.2				2	It is taken to be the estimated maximum ground acceleration in Anchoragecalculations made on an oil tank damaged during the	silts and a thick lens of bootlegger clay		1		K	9.1	12.2	1.33							oil	1	Extensive Bottom shell buckling, loss of contents (in questo caso per bottom shell si intende forse la parete)
Alaska	1964	9.2	Anchorage area	130		180 km from the fault	0.21	0.21		0.2				2	It is taken to be the estimated maximum ground acceleration in Anchoragecalculations made on an oil tank damaged during the	silts and a thick lens of bootlegger clay		1		L	9.1	12.2	1.33							oil	1	Extensive Bottom shell buckling, loss of contents (in questo caso per bottom shell si intende forse la parete)
Alaska	1964	9.2	Anchorage area	130		180 km from the fault	0.21	0.21		0.2				2	It is taken to be the estimated maximum ground acceleration in Anchoragecalculations made on an oil tank damaged during the	silts and a thick lens of bootlegger clay		1		B	30.5	9.8	0.32							oil	1	Damage to roof, top of shell and roof columms
Alaska	1964	9.2	Anchorage Airport	130		180 km from the fault	0.21	0.21		0.2				2	It is taken to be the estimated maximum ground acceleration in Anchoragecalculations made on an oil tank damaged during the	soils away from the shorline were more stable than those close		1		C	13.7	9.8	0.71		fixed flat plate					fuel	1	Damage to roof, top of shell and roof rafters, Elephant foot and bottom wall buckled
Alaska	1964	9.2	Anchorage Airport	130		180 km from the fault	0.21	0.21		0.2				2	It is taken to be the estimated maximum ground acceleration in Anchoragecalculations made on an oil tank damaged during the	silts and a thick lens of bootlegger clay		1		D	36.6	9.8	0.27		fixed flat plate					oil	1	Damage to roof, top of shell and roof columms
Alaska	1964	9.2	Anchorage area	130		180 km from the fault	0.21	0.21		0.2				2	It is taken to be the estimated maximum ground acceleration in Anchoragecalculations made on an oil tank damaged during the	silts and a thick lens of bootlegger clay		1		I	16.8	7.0	0.42							fuel oil	1	Damage to roof rafters and top wall
Alaska	1964	9.2	Anchorage Airport	130		180 km from the fault	0.21	0.21		0.2				2	It is taken to be the estimated maximum ground acceleration in Anchoragecalculations made on an oil tank damaged during the	soils away from the shorline were more stable than those close		1		O	6.1	12.2	2.00								1	Bottom wall buckled and and broke the wall-to-bottom-plate weld, leaking at wall-bottom junction
Alaska	1964	9.2	Anchorage area	130		180 km from the fault	0.21	0.21		0.2				2	It is taken to be the estimated maximum ground acceleration in Anchoragecalculations made on an oil tank damaged during the	silts and a thick lens of bootlegger clay		1		Q	34.1	17.1	0.50		floating						1	Floating roof pontoon damaged
Alaska	1964	9.2	Anchorage area	130		180 km from the fault	0.21	0.21		0.2				2	It is taken to be the estimated maximum ground acceleration in Anchoragecalculations made on an oil tank damaged during the	silts and a thick lens of bootlegger clay		1		R	14.9	14.6	0.98								1	Bottom buckled, 12 inch uplift
Alaska	1964	9.2	Anchorage Airport	130		180 km from the fault	0.21	0.21		0.2				2	It is taken to be the estimated maximum ground acceleration in Anchoragecalculations made on an oil tank damaged during the	soils away from the shorline were more stable than those close		1		AA4	3.2	9.1	2.86								0.33	No damage
Alaska	1964	9.2	Anchorage Airport	130		180 km from the fault	0.21	0.21		0.2				2	It is taken to be the estimated maximum ground acceleration in Anchoragecalculations made on an oil tank damaged during the	soils away from the shorline were more stable than those close		1		AA7	12.2	13.0	1.06								0.75	Severe elephant foot buckling, failed
Alaska	1964	9.2	Anchorage area	130		180 km from the fault	0.21	0.21		0.2				2	It is taken to be the estimated maximum ground acceleration in Anchoragecalculations made on an oil tank damaged during the	silts and a thick lens of bootlegger clay		1		T	48.8	17.1	0.35								0.5	Support columms twisted and rafters damaged.
Alaska	1964	9.2	Anchorage area	130		180 km from the fault	0.21	0.21		0.2				2	It is taken to be the estimated maximum ground acceleration in Anchoragecalculations made on an oil tank damaged during the	silts and a thick lens of bootlegger clay		1		E	36.6	9.8	0.27								0.1	No damage
Alaska	1964	9.2	Anchorage area	130		180 km from the fault	0.21	0.21		0.2				2	It is taken to be the estimated maximum ground acceleration in Anchoragecalculations made on an oil tank damaged during the	silts and a thick lens of bootlegger clay		1		F	36.6	9.8	0.27								0.1	No damage
Alaska	1964	9.2	Anchorage area	130		180 km from the fault	0.21	0.21		0.2				2	It is taken to be the estimated maximum ground acceleration in Anchoragecalculations made on an oil tank damaged during the	silts and a thick lens of bootlegger clay		1		G-1	33.5	9.8	0.29								0.1	No damage
Alaska	1964	9.2	Anchorage area	130		180 km from the fault	0.21	0.21		0.2				2	It is taken to be the estimated maximum ground acceleration in Anchoragecalculations made on an oil tank damaged during the	silts and a thick lens of bootlegger clay		1		G-1	33.5	9.8	0.29								0.1	No damage
Alaska	1964	9.2	Anchorage area	130		180 km from the fault	0.21	0.21		0.2				2	It is taken to be the estimated maximum ground acceleration in Anchoragecalculations made on an oil tank damaged during the	silts and a thick lens of bootlegger clay		1		H	27.4	9.8	0.36		floating						0.66	No damage, except to the swing joint in the floating section
Alaska	1964	9.2					0.2			0.2				2	It is taken to be the estimated maximum ground acceleration in Anchoragecalculations made on an oil tank damaged during the			1		U	48.8	17.1	0.35								0.5	No damage
Alaska	1964	9.2	Nikiska Refinery	210		180 km from the fault	0.2	0.2							from shake map			1		R162	9.1	14.6	1.60		cone					crude oil	1	Cone roof damage, No elephant foot buckling
Alaska	1964	9.2	Nikiska Refinery	210		180 km from the fault	0.2	0.2							from shake map			1		R163	9.1	14.6	1.60		cone					crude oil	1	Cone roof damage, No elephant foot buckling
Alaska	1964	9.2	Nikiska Refinery	210		180 km from the fault	0.2	0.2							from shake map			1		R100	34.1	17.1	0.50		floating					crude oil	0.17	Roof damage
Alaska	1964	9.2	Nikiska Refinery	210		180 km from the fault	0.2	0.2							from shake map			1		R110	43.9	17.1	0.39		floating					crude oil	0.7	Roof damage
Alaska	1964	9.2	Port of Whittier (U.S Army Petroleum Distribution tank farm)	60		100 km from the fault	0.384	0.384		0.3					0,30 is PGA inferred from MMI VII-VIII (Belanger)	soils close to the shorline		1		Army 1	93.0	27.7	0.30		floating				0	fuel	0.7	Circumferential bulge around the base. This pronounced bulge occurred only in tanks not completely full, presumably because of the sloshing of the fluid. The floor plate also bulged and rippled. Engineers revealed that structural damage was not serious and the tank shell was completely secure.
Alaska	1964	9.2	Port of Whittier (U.S Army Petroleum Distribution tank farm)	60		100 km from the fault	0.384	0.384		0.3					0,30 is PGA inferred from MMI VII-VIII (Belanger)	soils close to the shorline		1		Army 2	93.0	27.7	0.30		floating				0	fuel	0.7	Circumferential bulge around the base. This pronounced bulge occurred only in tanks not completely full, presumably because of the sloshing of the fluid. The floor plate also bulged and rippled. Engineers revealed that structural damage was not serious and the tank shell was completely secure.
Alaska	1964	9.2	Port of Whittier (U.S Army Petroleum Distribution tank farm)	60		100 km from the fault	0.384	0.384		0.3					0,30 is PGA inferred from MMI VII-VIII (Belanger)	soils close to the shorline		1		Army 3	93.0	27.7	0.30		floating				0	fuel	0.7	Circumferential bulge around the base. This pronounced bulge occurred only in tanks not completely full, presumably because of the sloshing of the fluid. The floor plate also bulged and rippled. Engineers revealed that structural damage was not serious and the tank shell was completely secure.
Alaska	1964	9.2	Port of Whittier (U.S Army Petroleum Distribution tank farm)	60		100 km from the fault	0.384	0.384		0.3					0,30 is PGA inferred from MMI VII-VIII (Belanger)	soils close to the shorline		1		Army 4	93.0	27.7	0.30		floating				0	fuel	0.7	Circumferential bulge around the base. This pronounced bulge occurred only in tanks not completely full, presumably because of the sloshing of the fluid. The floor plate also bulged and rippled. Engineers revealed that structural damage was not serious and the tank shell was completely secure.
Alaska	1964	9.2	Port of Whittier (U.S Army Petroleum Distribution tank farm)	60		100 km from the fault	0.384	0.384		0.3					0,30 is PGA inferred from MMI VII-VIII (Belanger)	soils close to the shorline		1		Army 5	93.0	27.7	0.30		floating				0	fuel	0.95	Damage to pipe and pressure relief lines at the base of the tanks. Loss of contents (3000 barrels of leakage)
Alaska	1964	9.2	Port of Whittier (U.S Army Petroleum Distribution tank farm)	60		100 km from the fault	0.384	0.384		0.3					0,30 is PGA inferred from MMI VII-VIII (Belanger)	soils close to the shorline		1		Army 6	93.0	27.7	0.30		floating				0	fuel	0.95	Damage to pipe and pressure relief lines at the base of the tanks
Alaska	1964	9.2	Port of Whittier (U.S Army Petroleum Distribution tank farm)	60		100 km from the fault	0.384	0.384		0.3					0,30 is PGA inferred from MMI VII-VIII (Belanger)	soils close to the shorline		1		Army 7	93.0	27.7	0.30		floating				0	fuel	0.95	Damage to pipe and pressure relief lines at the base of the tanks
Alaska	1964	9.2	Port of Whittier (U.S Army Petroleum Distribution tank farm)	60		100 km from the fault	0.384	0.384		0.3					0,30 is PGA inferred from MMI VII-VIII (Belanger)	soils close to the shorline		1		Army 8	93.0	27.7	0.30		floating				0	fuel	0.95	Damage to pipe and pressure relief lines at the base of the tanks
Niigata	1964	7.6	Showa Oil Co. Niigata Refinery Oil Tanks (NIG002)	56							0.162	0.158	0.16		data from accelerometer located in the Kawagishicho apartment complex	coarse dune sand in the first 15 m, liquefaction potential			3		51.2	14.3	0.28		floating	Direct base on compacted sand mound by roller compaction (void ratio=0,7)			0	crude oil		Settlement of 20/30cm ==> Despite the fire (caused by sloshig and ignition in floating roof), little damage to the base tank
Niigata	1964	7.6	Showa Oil Co. Niigata Refinery Oil Tanks (NIG002)	56							0.162	0.158	0.16		data from accelerometer located in the Kawagishicho apartment complex	coarse dune sand in the first 15 m, liquefaction potential			2		61.9	16.5	0.27		floating	Direct base on compacted sand mound by roller compaction(void ratio=0,7)			0	crude oil		Settlement of 20/30cm ==> Despite the fire (caused by sloshig and ignition in floating roof), little damage to the base tank
Niigata	1964	7.6	Showa Oil Co. Niigata Refinery Oil Tanks (NIG002)	56							0.162	0.158	0.16		data from accelerometer located in the Kawagishicho apartment complex	coarse dune sand in the first 15 m, the sand below 15m consists of fine sea bed origin sand; liquefaction potential			9		25.0	10.7	0.43			Direct base on thinner (30 cm) sand mound without compaction by roller compaction			0	crude oil		Unequal settlement of 50cm and tilt==> damage of tank attachment piping
Niigata	1964	7.6	Showa Oil Co. Niigata Refinery Oil Tanks (NIG002)	56							0.162	0.158	0.16		data from accelerometer located in the Kawagishicho apartment complex	coarse dune sand in the first 15 m, the sand below 15m consists of fine sea bed origin sand; liquefaction potential			27													Slight damage

Niigata	1964	7.6	Showa Oil Co. Niigata Refinery Oil Tanks (NIG002)	56							0.162	0.158	0.16		data from accelerometer located in the Kawagishicho apartment complex	coarse dune sand in the first 15 m, the sand below 15m consists of fine sea bed origin sand; liquefaction potential			35														Burned out
Niigata	1964	7.6	Nippon Oil Co. Ose Oil Yard (NIG003)	56							0.162	0.158	0.16		data from accelerometer located in the Kawagishicho apartment complex	medium sand: 1m very loose sand, 1m silty sand, 5m medium sand grading from loose to dense; liquefaction potential			1		44.5	13.7	0.31		cone roof	Direct base on ground improved using vibroflotation				crude oil	0.95	no damage thanks to the vibroflotation improving of the ground (it settled about 2-3cm uniformly)
Niigata	1964	7.6	Nippon Oil Co. Ose Oil Yard (NIG003)	56							0.162	0.158	0.16		data from accelerometer located in the Kawagishicho apartment complex	medium sand: 1m very loose sand, 1m silty sand, 5m medium sand grading from loose to dense; liquefaction potential			1		44.5	13.7	0.31		cone roof	Direct base on ground improved using vibroflotation				crude oil		no damage thanks to the vibroflotation improving of the ground (very little damage the foundation)
Niigata	1964	7.6	Nippon Oil Co. Ose Oil Yard (NIG003)	56							0.162	0.158	0.16		data from accelerometer located in the Kawagishicho apartment complex	medium sand: 1m very loose sand, 1m silty sand, 5m medium sand grading from loose to dense; liquefaction potential			1		52.7	13.7	0.26		cone roof	Direct base on ground improved using vibroflotation				crude oil		no damage thanks to the vibroflotation improving of the ground (very little damage the foundation)
Niigata	1964	7.6	Nippon Oil Co. Ose Oil Yard (NIG003)	56							0.162	0.158	0.16		data from accelerometer located in the Kawagishicho apartment complex	medium sand: 1m very loose sand, 1m silty sand, 5m medium sand grading from loose to dense; liquefaction potential			3													Slight damage
Niigata	1964	7.6	Nippon Oil Co. Ose Oil Yard (NIG003)	56							0.162	0.158	0.16		data from accelerometer located in the Kawagishicho apartment complex	medium sand: 1m very loose sand, 1m silty sand, 5m medium sand grading from loose to dense; liquefaction potential			40													Settlement over 10 cm; most of the tanks got some trobles such as leakage
Niigata	1964	7.6	Nippon Oil Co. Ose Oil Yard (NIG003)	56							0.162	0.158	0.16		data from accelerometer located in the Kawagishicho apartment complex	medium sand: 1m very loose sand, 1m silty sand, 5m medium sand grading from loose to dense; liquefaction potential			11													Tilt over
Niigata	1964	7.6	Nippon Oil Co. Ose Oil Yard (NIG003)	56							0.162	0.158	0.16		data from accelerometer located in the Kawagishicho apartment complex	medium sand: 1m very loose sand, 1m silty sand, 5m medium sand grading from loose to dense; liquefaction potential			19													Mostly leakage
Niigata	1964	7.6	Nippon Oil Co. Ose Oil Yard (NIG003)	56							0.162	0.158	0.16		data from accelerometer located in the Kawagishicho apartment complex	medium sand: 1m very loose sand, 1m silty sand, 5m medium sand grading from loose to dense; liquefaction potential			37													No damage
Long Beach	1933	6.4	Huntington Beach	3.5		2 km to the fault	0.437114745			0.17					PGA from ASA2001: The ground motion is from an instrument in Long Beach (location unknown), 29 km from the epicenter with 0.2g vertical and 0,17g in the 270° horizontal direction; PGA selezionata viene da ATTENUATION CURVES (lla fine del file)_ strike-slip faulting		C	1		A	29.1	8.9	0.30		galvanized iron roof on wooden support		Riveted				0.98	oil splashed to the top of the shell. Damage to roof (galvanized iron roof on wooden support)
Long Beach	1933	6.4	Huntington Beach	3.5		2 km to the fault	0.437114745			0.17					PGA from AIA2001: The ground motion is from an instrument in Long Beach (location unknown), 29 km from the epicenter with 0.2g vertical and 0,17g in the 270° horizontal direction; PGA selezionata viene da ATTENUATION CURVES (lla fine del file)_ strike-slip faulting		C	3		A	29.1	8.9	0.30	<1	galvanized iron roof on wooden support		Riveted				0.5	No damage
Long Beach	1933	6.4		15		5 km to the fault	0.357645507			0.17					PGA from AIA2001: The ground motion is from an instrument in Long Beach (location unknown), 29 km from the epicenter with 0.2g vertical and 0,17g in the 270° horizontal direction; PGA selezionata viene da ATTENUATION CURVES (lla fine del file)_ strike-slip faulting		C	1		B			0.3	<1			Riveted					Total failure with both shell and roof sustaining damage
Long Beach	1933	6.4		15		5 km to the fault	0.357645507			0.17					PGA from ALA2001: The ground motion is from an instrument in Long Beach (location unknown), 29 km from the epicenter with 0.2g vertical and 0,17g in the 270° horizontal direction; PGA selezionata viene da ATTENUATION CURVES (lla fine del file)_ strike-slip faulting		C	43					0.3	<1							No damage
Long Beach	1933	6.4		45		1-2 km to the fault	0.447584769			0.17					PGA from ALA2001: The ground motion is from an instrument in Long Beach (location unknown), 29 km from the epicenter with 0.2g vertical and 0,17g in the 270° horizontal direction; PGA selezionata viene da ATTENUATION CURVES (lla fine del file)_ strike-slip faulting		C	1		C	45.7	19.2	0.42				Riveted			water	0.76	Failure of the fourth shell course (the upper)
Long Beach	1933	6.4															C		sono 13				0.30									tank separated from water draw-off drain; Oil lost down water draw-off drain
Long Beach	1933	6.4															C		a number				0.3									Tanks with diameter greater than 50 ft : damage to the roof/shell or floating roof
Long Beach	1933	6.4															C		a number				0.3									rivet damage and sweating at the seams
Long Beach	1933	6.4	Huntington Beach	3.5		2 km to the fault	0.437114745			0.17					PGA from AIA2001: The ground motion is from an instrument in Long Beach (location unknown), 29 km from the epicenter with 0.2g vertical and 0,17g in the 270° horizontal direction; PGA selezionata viene da ATTENUATION CURVES (lla fine del file)_ strike-slip faulting		C	2					0.3							0.95	Riveted joint failed, tank leaked
Long Beach	1933	6.4	Huntington Beach	3.5		2 km to the fault	0.437114745			0.17					PGA from ALA2001: The ground motion is from an instrument in Long Beach (location unknown), 29 km from the epicenter with 0.2g vertical and 0,17g in the 270° horizontal direction; PGA selezionata viene da ATTENUATION CURVES (lla fine del file)_ strike-slip faulting		C	1					0.3							0.95	Floating roof damaged.
Coalinga	1983	6.36		4.8			0.351654								FROM ATTENUATION CURVES (ultimo foglio del file)_ reverse slip faulting	primarily alluvial soils which are considered good foundation sois	C	1			14.6	9.1	0.63		fixed	gravel	Riveted				0.82	Bulging and rapture of shell at fluid level
Coalinga	1983	6.36		4.8			0.351654								FROM ATTENUATION CURVES (ultimo foglio del file)_ reverse slip faulting	primarily alluvial soils which are considered good foundation sois	C	1			14.6	9.1	0.63		fixed	gravel						Outflow pipe disconnected from tank
Coalinga	1983	6.36	Site A	6	Cooper da distanze un po diverse		0.387	0.387		0.47					ALA2001: O'Rourke and So [1999] use PGA=0,71g which is the average of the peak accelerations given in Cooper (0,6g to 0,82g). In this work (ASA2001) PGAs based on attenuation and to be consistent with Hashimoto [1989]	primarily alluvial soils which are considered good foundation sois		2	2 of 19				0.3		floating		Riveted				0.95	Floating roof damage; they are the largest tanks of the 19

Coalinga	1983	6.36	Site A	6	Cooper da distanze un po diverse		0.387	0.387		0.47					ALA2001: O'Rourke and So [1999] use PGA=0,71g which is the average of the peak accelerations given in Cooper (0,6g to 0,82g). In this work (ASA2001) PGAs based on attenuation and to be consistent with Hashimoto [1989]	primarily alluvial soils which are considered good foundation sois		17	17 of 19				0.3				Riveted					0.5	No apparent damage
Coalinga	1983	6.36	Site B	3.5	Cooper da distanze un po diverse		0.42	0.42		0.57					ALA2001: O'Rourke and So [1999] use PGA=0,71g which is the average of the peak accelerations given in Cooper (0,6g to 0,82g). In this work (ASA2001) PGAs based on attenuation and to be consistent with Hashimoto [1989]	primarily alluvial soils which are considered good foundation sois		2	50		36.6	14.6	0.40		floating	concrete foundation ring	Welded	1/4 in. bottom plate	0	oil	1	1/4 inch bottom plates; splashing or top spillage from the full tanks and some roof secondary seal damage.
Coalinga	1983	6.36	Site B	3.5	Cooper da distanze un po diverse		0.42	0.42		0.57					ASA2001: O'Rourke and So [1999] use PGA=0,71g which is the average of the peak accelerations given in Cooper (0,6g to 0,82g). In this work (ASA2001) PGAs based on attenuation and to be consistent with Hashimoto [1989]	primarily alluvial soils which are considered good foundation sois		1			36.6	14.6	0.40		floating	concrete foundation ring	Welded		0	oil	0.1	roof seal damage
Coalinga	1983	6.36	Site B	3.5	Cooper da distanze un po diverse		0.42	0.42		0.57					ASA 2001: O'Rourke and So [1999] use PGA=0,71g which is the average of the peak accelerations given in Cooper (0,6g to 0,82g). In this work (ASA2001) PGAs based on attenuation and to be consistent with Hashimoto [1989]	primarily alluvial soils which are considered good foundation sois		3			36.6	14.6	0.40		floating	concrete foundation ring	Welded		0	oil	0.5	No apparent damage
Coalinga	1983	6.36	Site B	3.5	Cooper da distanze un po diverse		0.42	0.42		0.57					ASA2001: O'Rourke and So [1999] use PGA=0,71g which is the average of the peak accelerations given in Cooper (0,6g to 0,82g). In this work (ASA2001) PGAs based on attenuation and to be consistent with Hashimoto [1989]	primarily alluvial soils which are considered good foundation sois		1		firewater tank	18.6	12.2	0.66							water	1	settled uniformly about 2 inches, but no visible damage
Coalinga	1983	6.36	Site C	5.5	Cooper da distanze un po diverse		0.39	0.39		0.39					ASA2001: O'Rourke and So [1999] use PGA=0,71g which is the average of the peak accelerations given in Cooper (0,6g to 0,82g). In this work (ASA2001) PGAs based on attenuation and to be consistent with Hashimoto [1989]	primarily alluvial soils which are considered good foundation sois		1		7	61.0	14.6	0.24		floating	No concrete ring foundation but tanks are set on gravel pad	Welded		0	crude oil	0.73	roof seal damage on a NE-SW axis; the seal, which are normally straight, had been bent at some locations 90° or more; Tank spilled/splashed oil over the top of the tank; it pounded into the foundation soil about 100mm (4in), again on a NE-SW axis, with no pounding on the NW-SE axis. On the west side, the tank lifted sufficiently to break a water-draw/bottom plate weld which allowed significant leakage of crude oil. A pipe support on the west side was also bent, and showed movement of about 100mm (4in) each side of the pipe centerline.
Coalinga	1983	6.36	Site C	5.5	Cooper da distanze un po diverse		0.39	0.39		0.39					ASA2001: O'Rourke and So [1999] use PGA=0,71g which is the average of the peak accelerations given in Cooper (0,6g to 0,82g). In this work (ASA2001) PGAs based on attenuation and to be consistent with Hashimoto [1989]	primarily alluvial soils which are considered good foundation sois		1		8	61.0	14.6	0.24		floating	No concrete ring foundation but tanks are set on gravel pad	Welded		0	crude oil	0.21	roof seal damage on a NE-SW axis; the seal, which are normally straight, had been bent at some locations 90° or more. The flange of the wind girder buckled on south side.
Coalinga	1983	6.36	Site C	5.5	Cooper da distanze un po diverse		0.39	0.39		0.39					ASA2001: O'Rourke and So [1999] use PGA=0,71g which is the average of the peak accelerations given in Cooper (0,6g to 0,82g). In this work (ASA2001) PGAs based on attenuation and to be consistent with Hashimoto [1989]	primarily alluvial soils which are considered good foundation sois		1		13	61.0	14.6	0.24		floating	No concrete ring foundation but tanks are set on gravel pad	Welded		0	crude oil	0.2	roof seal damage on a NE-SW axis; the seal, which are normally straight, had been bent at some locations 90° or more
Coalinga	1983	6.36	Site C	5.5	Cooper da distanze un po diverse		0.39	0.39		0.39					ASA2001: O'Rourke and So [1999] use PGA=0,71g which is the average of the peak accelerations given in Cooper (0,6g to 0,82g). In this work (ASA2001) PGAs based on attenuation and to be consistent with Hashimoto [1989]	primarily alluvial soils which are considered good foundation sois		1		14	61.0	14.6	0.24		floating	No concrete ring foundation but tanks are set on gravel pad	Welded		0	crude oil	0.2	roof seal damage on a NE-SW axis; the seal, which are normally straight, had been bent at some locations 90° or more
Coalinga	1983	6.36	Site C	5.5	Cooper da distanze un po diverse		0.39	0.39		0.39					ASA2001: O'Rourke and So [1999] use PGA=0,71g which is the average of the peak accelerations given in Cooper (0,6g to 0,82g). In this work (ASA2001) PGAs based on attenuation and to be consistent with Hashimoto [1989]	primarily alluvial soils which are considered good foundation sois		1		firewater tank	36.6	12.2	0.33		open top		Riveted		0	water		Welded bottom (the old shell was welded to a new bottom); Slight bulge in bottom course but not elephant foot buckling
Coalinga	1983	6.36	Site D	1.5	Cooper da distanze un po diverse		0.44	0.44		0.7					ASA2001: O'Rourke and So [1999] use PGA=0,71g which is the average of the peak accelerations given in Cooper (0,6g to 0,82g). In this work (ASA2001) PGAs based on attenuation and to be consistent with Hashimoto [1989]	primarily alluvial soils which are considered good foundation sois		1					0.3				Riveted					Top riveted ring failed by buckling
Coalinga	1983	6.36	Site D	1.5	Cooper da distanze un po diverse		0.44	0.44		0.7					ASA2001: O'Rourke and So [1999] use PGA=0,71g which is the average of the peak accelerations given in Cooper (0,6g to 0,82g). In this work (ASA2001) PGAs based on attenuation and to be consistent with Hashimoto [1989]	primarily alluvial soils which are considered good foundation sois		1					1.1				Bolted					Tank pounded into the ground
Coalinga	1983	6.36	Site D	1.5	Cooper da distanze un po diverse		0.44	0.44		0.7					ASA2001: O'Rourke and So [1999] use PGA=0,71g which is the average of the peak accelerations given in Cooper (0,6g to 0,82g). In this work (ASA2001) PGAs based on attenuation and to be consistent with Hashimoto [1989]	primarily alluvial soils which are considered good foundation sois		1					0.3	<1								broken valves/fittings
Coalinga	1983	6.36	Shell Oil. Co. Tank Farm 29	1.5			0.44	0.44								primarily alluvial soils which are considered good foundation sois		1					0.3	<1					oil	0.75	Buckled at its wall and lost some of its contents. This tank burst its walls
Coalinga	1983	6.36	Shell Oil. Co. Tank Farm 29	1.5			0.44	0.44								primarily alluvial soils which are considered good foundation sois		3					0.3	<1					oil	0.75	Buckled at their wall and lost some of their contents
Coalinga	1983	6.36	Shell Oil. Co. Tank Farm 29	1.5			0.44	0.44								primarily alluvial soils which are considered good foundation sois		2					0.3	<1					oil	0	No Damage
Coalinga	1983	6.36		16			0.187449051									primarily alluvial soils which are considered good foundation sois	C	1					0.3				Bolted				Roof spillage
Coalinga	1983	6.36	Site E	2			0.43	0.43		0.62					ASA2001: O'Rourke and So [1999] use PGA=0,71g which is the average of the peak accelerations given in Cooper (0,6g to 0,82g). In this work (ASA2001) PGAs based on attenuation and to be consistent with Hashimoto [1989]	primarily alluvial soils which are considered good foundation sois		1					1.1	>1		crushed rock foundation	Bolted					broken cast iron valves and fittings, pulled Dresser Couplings, and minor soil settlement
Coalinga	1983	6.36	Site E	2			0.43	0.43		0.62					ASA2001: O'Rourke and So [1999] use PGA=0,71g which is the average of the peak accelerations given in Cooper (0,6g to 0,82g). In this work (ASA2001) PGAs based on attenuation and to be consistent with Hashimoto [1989]	primarily alluvial soils which are considered good foundation sois		1					1.1	>1		crushed rock foundation	Bolted					broken cast iron valves and fittings, pulled Dresser Couplings, and minor soil settlement
Coalinga	1983	6.36	Site F	3.4			0.42	0.42		0.57					ASA2001: O'Rourke and So [1999] use PGA=0,71g which is the average of the peak accelerations given in Cooper (0,6g to 0,82g). In this work (ASA2001) PGAs based on attenuation and to be consistent with Hashimoto [1989]	primarily alluvial soils which are considered good foundation sois		1			33.5	12.2	0.36								0.65	Evidence of rocking of tank on concrete pad and spalling of concrete pad. No loss of water from tank or piping.
Coalinga	1983	6.36	Site G	6			0.37	0.37		0.43					ASA2001: O'Rourke and So [1999] use PGA=0,71g which is the average of the peak accelerations given in Cooper (0,6g to 0,82g). In this work (ASA2001) PGAs based on attenuation and to be consistent with Hashimoto [1989]	primarily alluvial soils which are considered good foundation sois		2			16.8	9.8	0.58				Bolted				0.75	Elephant foot buckling
Coalinga	1983	6.36	Site G	6				0.37		0.43					ASA2001: O'Rourke and So [1999] use PGA=0,71g which is the average of the peak accelerations given in Cooper (0,6g to 0,82g). In this work (ASA2001) PGAs based on attenuation and to be consistent with Hashimoto [1989]	primarily alluvial soils which are considered good foundation sois			other tanks							Bolted				0.40	Leakage at bolt holes
Coalinga	1983	6.36					0.39			0.39					ASA2001: O'Rourke and So [1999] use PGA=0,71g which is the average of the peak accelerations given in Cooper (0,6g to 0,82g). In this work (ASA2001) PGAs based on attenuation and to be consistent with Hashimoto [1989]	primarily alluvial soils which are considered good foundation sois		1		Filter Plant Backwash	9.14	18.3	2.0				Bolted		1		0.75	Minor leaks at outlet pipe due to rocking of tank (possibly not from EQ). Stretched anchor bolts
Coalinga	1983	6.36					0.23			0.23					ASA2001: O'Rourke and So [1999] use PGA=0,71g which is the average of the peak accelerations given in Cooper (0,6g to 0,82g). In this work (ASA2001) PGAs based on attenuation and to be consistent with Hashimoto [1989]	primarily alluvial soils which are considered good foundation sois		1		Main tank			1.1								0.5	Slight damage

Coalinga	1983	6.36	Chevron Oil Plant	10				0.368								primarily alluvial soils which are considered good foundation sois			Several tanks (non è un impianto con tantissimi tank). Dato che ho detto che si sono rotti 3 tank, che secondo il report sono il 20% del totale, assumo che 15 sono i tank del sito e 12 (=15-3) non si sono rotti.	12			0.3								oil	0.5	No Damage
Coalinga	1983	6.36	Chevron Oil Plant	10				0.368								primarily alluvial soils which are considered good foundation sois			all the full tanks sustained some loss of oil....(io metterei 1)	1			0.3								oil	1	some loss of oil due to sloshing of their contents through vents,
Coalinga	1983	6.36	Chevron Oil Plant	10				0.368								primarily alluvial soils which are considered good foundation sois			all the full tanks sustained some loss of oil....(io metterei 1)	1			0.3								oil	1	some loss of oil due to rupture of the tank
Coalinga	1983	6.36	Chevron Oil Plant	10				0.368								primarily alluvial soils which are considered good foundation sois			all the full tanks sustained some loss of oil....(io metterei 1)	1			0.3								oil	1	some loss of oil due to breakage of the connected piping
Coalinga	1983	6.36		12			0.3	0.3								primarily alluvial soils which are considered good foundation sois		1		Water storage tank			1.1			concrete pad					water	0.9	Evidence of rocking of tank on concrete pad; spalling of concrete-pad grout. No loss of water from tank or piping
Coalinga	1983	6.36					0.45			0.45					ASA2001: O'Rourke and So [1999] use PGA=0,71g which is the average of the peak accelerations given in Cooper (0,6g to 0,82g). In this work (ASA2001) PGAs based on attenuation and to be consistent with Hashimoto [1989]	primarily alluvial soils which are considered good foundation sois		1		East tank			0.3									0.5	Broken Cl inlet/outlet pipe
Greenville	1980	5.8	Concannon Winery	19	circa	Si trova proprio sulla faglia Las Positas Fault		0.175		0,2-0,3					Sandia Laboratories is located about 3 km from the two wineries and near the Greenville Fault. At this site, the Peak Ground Acceleration has been estimated in the 0,2-0,3g range, though the nearest strong motion record was taken 15 km away				N° tanks:37 (non so se utilizzare questi dati o meno perché il numero dei serbatoi l'ho ricavato da google maps adesso mentre il terremoto è avvenuto nel 1980)			1.1	>1									No Damage
Greenville	1980	5.8	Wente Bros. Winery	19	circa	Si trova proprio sulla faglia Las Positas Fault		0.172		0,2-0,3					Sandia Laboratories is located about 3 km from the two wineries and near the Greenville Fault. At this site, the Peak Ground Acceleration has been estimated in the 0,2-0,3g range, though the nearest strong motion record was taken 15 km away				40			1.1			tanks are seated on elevated concrete pads 2 to 4 feet above the ground			1	wine	0.3	No damage or minor damage
Greenville	1980	5.8	Wente Bros. Winery	19	circa	Si trova proprio sulla faglia Las Positas Fault		0.172		0,2-0,3					Sandia Laboratories is located about 3 km from the two wineries and near the Greenville Fault. At this site, the Peak Ground Acceleration has been estimated in the 0,2-0,3g range, though the nearest strong motion record was taken 15 km away				10			1.1	>2		tanks are seated on elevated concrete pads 2 to 4 feet above the ground			1	wine	1	No damage
Greenville	1980	5.8	Wente Bros. Winery	19	circa	Si trova proprio sulla faglia Las Positas Fault		0.172		0,2-0,3					Sandia Laboratories is located about 3 km from the two wineries and near the Greenville Fault. At this site, the Peak Ground Acceleration has been estimated in the 0,2-0,3g range, though the nearest strong motion record was taken 15 km away				24			1.1	>2		tanks are seated on elevated concrete pads 2 to 4 feet above the ground			1	wine	1	Light damage: minor spalling of concrete pad, failed anchorage welds, minor local buckling.
Greenville	1980	5.8	Wente Bros. Winery	19	circa	Si trova proprio sulla faglia Las Positas Fault		0.172		0,2-0,3					Sandia Laboratories is located about 3 km from the two wineries and near the Greenville Fault. At this site, the Peak Ground Acceleration has been estimated in the 0,2-0,3g range, though the nearest strong motion record was taken 15 km away				70			1.1	>1,5 & <=2		tanks are seated on elevated concrete pads 2 to 4 feet above the ground			1	wine	1	Medium damage: concrete spalling of pads, failed anchorage welds and bolts, some shell buckling with peak to peak buckle amplitudes of less than 2 inches.)
Greenville	1980	5.8	Wente Bros. Winery	19	circa	Si trova proprio sulla faglia Las Positas Fault		0.172		0,2-0,3					Sandia Laboratories is located about 3 km from the two wineries and near the Greenville Fault. At this site, the Peak Ground Acceleration has been estimated in the 0,2-0,3g range, though the nearest strong motion record was taken 15 km away				26			1.1	<1,5		tanks are seated on elevated concrete pads 2 to 4 feet above the ground			1	wine	1	Severe damage: anchors failed, the shell were buckled extensively with buckle amplitudes exceeding 2 inches peak to peak. Most of the severely damaged tanks had permanent overall deformations such as uplift at the base by as much as 3 inches and visible tilting from the vertical.
Greenville	1980	5.8	Sandia Laboratories	19		Si trova proprio sulla faglia Las Positas Fault	0.167	0.167		0,2-0,3					Sandia Laboratories is located about 3 km from the two wineries and near the Greenville Fault. At this site, the Peak Ground Acceleration has been estimated in the 0,2-0,3g range, though the nearest strong motion record was taken 15 km away			1			7.6	15.2	1.1	2.00	fixed	concrete mat foundation	Welded		1	oil	1	A continuous EFB developed during the earthquake. The tank did not overturn, rupture, o otherwise spill its contents save a small amount that was forced out of the vent at the top of the tank
Imperial Valley	1979	6.53	Imperial Irrigation District (IID) power plant	26.5	è un epicentro diverso da quello che ho preso da USGS	5 km from the Imperial Fault	0.45	0.45		0.49					ALA2001: PGA from Haroun			1		1 of 6	41.1	13.7	0.33		fixed	asphalt base and ringwall foundation	Welded		0	oil	1	Buckling of roof plate, roof stringers collapsed; separation of roof and wall at the perimeter weld; some fuel spilled due to the sloshing. Uplift from the ground
Imperial Valley	1979	6.53	Imperial Irrigation District (IID) power plant	26.5	è un epicentro diverso da quello che ho preso da USGS	5 km from the Imperial Fault	0.45	0.45		0.49					ALA2001: PGA from Haroun			1		2 of 6	22.3	6.1	0.27		fixed	asphalt base and ringwall foundation	Welded		0	oil	1	Some buckling of roof plate.
Imperial Valley	1979	6.53	Imperial Irrigation District (IID) power plant	26.5	è un epicentro diverso da quello che ho preso da USGS	5 km from the Imperial Fault	0.45	0.45		0.49					ALA2001: PGA from Haroun			1		3 of 6			0.3		fixed	asphalt base and ringwall foundation	Welded		0	oil		No apparent damage
Imperial Valley	1979	6.53	Imperial Irrigation District (IID) power plant	26.5	è un epicentro diverso da quello che ho preso da USGS	5 km from the Imperial Fault	0.45	0.45		0.49					ALA2001: PGA from Haroun			1		4 of 6			0.3		fixed	asphalt base and ringwall foundation	Welded		0	oil		A cracked weld at roof/wall allowed some oil sloshing to leak out
Imperial Valley	1979	6.53	Imperial Irrigation District (IID) power plant	26.5	è un epicentro diverso da quello che ho preso da USGS	5 km from the Imperial Fault	0.45	0.45		0.49					ALA2001: PGA from Haroun			1		5 of 6			0.3		fixed	asphalt base and ringwall foundation	Welded		0	oil		No apparent damage
Imperial Valley	1979	6.53	Imperial Irrigation District (IID) power plant	26.5	è un epicentro diverso da quello che ho preso da USGS	5 km from the Imperial Fault	0.45	0.45		0.49					ALA2001: PGA from Haroun			1		6 of 6			0.3		fixed	asphalt base and ringwall foundation	Welded		0	oil		No apparent damage
Imperial Valley	1979	6.53	SPPL terminal	32	è un epicentro diverso da quello che ho preso da USGS	6 km to the Imperial Fault	0.467	0.467		0.24					ALA2001: PGA from Haroun			1		IP 1	24.4	14.6	0.60		Floating	On earth (rock base)			0	gasoline	0.43	Roof seal damage, broken antirotation devices, relief piping damage, settlement.
Imperial Valley	1979	6.53	SPPL terminal	32	è un epicentro diverso da quello che ho preso da USGS	6 km to the Imperial Fault	0.467	0.467		0.24					ALA2001: PGA from Haroun			1		IP 2	24.4	14.6	0.60		Floating	On earth (rock base)			0	gasoline	0.49	Roof seal damage, broken antirotation devices, relief piping damage, settlement.
Imperial Valley	1979	6.53	SPPL terminal	32	è un epicentro diverso da quello che ho preso da USGS	6 km to the Imperial Fault	0.467	0.467		0.24					ALA2001: PGA from Haroun			1		IP 3	20.4	12.3	0.60		cone	On earth (rock base)			0	gasoline	0.39	No apparent damage
Imperial Valley	1979	6.53	SPPL terminal	32	è un epicentro diverso da quello che ho preso da USGS	6 km to the Imperial Fault	0.467	0.467		0.24					ALA2001: PGA from Haroun			1		IP 4	14.6	14.6	1		Floating	On earth (rock base)			0	gasoline	0.53	Dents in shell from roof, Roof seal damage, broken antirotation devices, relief piping damage, settlement 1 in; Small Elephant foot buckling with no leak
Imperial Valley	1979	6.53	SPPL terminal	32	è un epicentro diverso da quello che ho preso da USGS	6 km to the Imperial Fault	0.467	0.467		0.24					ALA2001: PGA from Haroun			1		IP 5	14.6	14.6	1		Floating	On earth (rock base)			0	gasoline	0.73	Dents in shell from roof; small elephant foot buckling no leak, settlement of tank 1 in. No significant damage to connecting pipes from the tanks was observed (*major damage)
Imperial Valley	1979	6.53	SPPL terminal	32	è un epicentro diverso da quello che ho preso da USGS	6 km to the Imperial Fault	0.467	0.467		0.24					ALA2001: PGA from Haroun			1		IP 6	13	12.2	0.94		Floating	Concrete ringwall			0	gasoline	0.38	Primary seal on floating roof damaged
Imperial Valley	1979	6.53	SPPL terminal	32	è un epicentro diverso da quello che ho preso da USGS	6 km to the Imperial Fault	0.467	0.467		0.24					ALA2001: PGA from Haroun			1		IP 7	13	12.2	0.94		cone	Concrete ringwall			0	gasoline	0.4	No apparent damage

Imperial Valley	1979	6.53	SPPL terminal	32	è un epicentro diverso da quello che ho preso da USGS	6 km to the Imperial Fault	0.467	0.467		0.24					ALA2001: PGA from Haroun			1		IP 8	24.7	14.6	0.59		Floating	Concrete ringwall			0	gasoline	0.82	Primary seal on floating roof damaged; settlement of tank 1 in., roof drain leaks, leak in tank where floor plates overlap and joint shell. Stair platform damage
Imperial Valley	1979	6.53	SPPL terminal	32	è un epicentro diverso da quello che ho preso da USGS	6 km to the Imperial Fault	0.467	0.467		0.24					ALA2001: PGA from Haroun			1		IP 9	13	12.2	0.94		Floating	Concrete ringwall			0	gasoline	0.65	roof drain leaks, swingline cable broke
Imperial Valley	1979	6.53	SPPL terminal	32	è un epicentro diverso da quello che ho preso da USGS	6 km to the Imperial Fault	0.467	0.467		0.24					ALA2001: PGA from Haroun			1		IP 10	13	12.2	0.94		Floating	Concrete ringwall			0	gasoline	0.76	roof drain leaks
Imperial Valley	1979	6.53	SPPL terminal	32	è un epicentro diverso da quello che ho preso da USGS	6 km to the Imperial Fault	0.467	0.467		0.24					ALA2001: PGA from Haroun			1		IP 11	14.2	12.2	0.86		cone	Concrete ringwall			0	gasoline	0.86	Relief piping damaged, grounding cable disconnected, Settlement of tank1-2 in. on S.W side, swingline leaking
Imperial Valley	1979	6.53	SPPL terminal	32	è un epicentro diverso da quello che ho preso da USGS	6 km to the Imperial Fault	0.467	0.467		0.24					ALA2001: PGA from Haroun			1		IP 12	13	12.2	0.94		Floating	Concrete ringwall			0	gasoline	0.86	swingline cable broke, swingline jumped track can caused floating roof to hang, gauge-antirotation pipe broke from floor and bent severely, roof drain leaks
Imperial Valley	1979	6.53	SPPL terminal	32	è un epicentro diverso da quello che ho preso da USGS	6 km to the Imperial Fault	0.467	0.467		0.24					ALA2001: PGA from Haroun			1		IP 13	12.6	14.9	1.18		fixed cone with internal pan	Concrete ringwall			0	gasoline	0.7	"elephant's foot buckling" 6 inches outward, at the base of the tank that extended over a 90° arc and bulged out a maximum of 6 in. over a 2-ft height and in opposite side leak in tank at floor- wall junction (10cm (4in) weld separation at the shell-bottom plate joint. Crack in floor coating, no leak. (*major damagr)
Imperial Valley	1979	6.53	SPPL terminal	32	è un epicentro diverso da quello che ho preso da USGS	6 km to the Imperial Fault	0.467	0.467		0.24					ALA2001: PGA from Haroun			1		IP 14	14.7	14.9	1.01		fixed cone with internal pan	Concrete ringwall			0	gasoline	0.61	Ringwall cracked
Imperial Valley	1979	6.53	SPPL terminal	32	è un epicentro diverso da quello che ho preso da USGS	6 km to the Imperial Fault	0.467	0.467		0.24					ALA2001: PGA from Haroun			1		IP 15	15.2	14.9	0.98		fixed cone with internal pan	Concrete ringwall			0	gasoline	0.61	Ringwall cracked
Imperial Valley	1979	6.53	SPPL terminal	32	è un epicentro diverso da quello che ho preso da USGS	6 km to the Imperial Fault	0.467	0.467		0.24					ALA2001: PGA from Haroun			1		IP 16	14.6	14.6	1		fixed cone with internal pan	Concrete ringwall			0	gasoline	0.83	Elephant foot with no shell-bottom separation, 6 in. bulge, ringwall cracked, a minor leak in a 1-in.-diameter connecting pipeline. (*major damage)
Imperial Valley	1979	6.53	SPPL terminal	32	è un epicentro diverso da quello che ho preso da USGS	6 km to the Imperial Fault	0.467	0.467		0.24					ALA2001: PGA from Haroun			1		IPC-1	6.5	7.3	1.12		fixed cone with internal pan	On earth (rock base)			0	gasoline	0.3	No apparent damage
Imperial Valley	1979	6.53	SPPL terminal	32	è un epicentro diverso da quello che ho preso da USGS	6 km to the Imperial Fault	0.467	0.467		0.24					ALA2001: PGA from Haroun			1		IPC-2	6.5	7.3	1.12		Floating	On earth (rock base)			0	gasoline	0.39	No apparent damage
Imperial Valley	1979	6.53	Valley Nitrogen	20	è un epicentro diverso da quello che ho preso da USGS	12 km to fault displacement	0.378	0.378										3					0.3	<<1							No apparent significant damage
Imperial Valley	1979	6.53	Valley Nitrogen	20	è un epicentro diverso da quello che ho preso da USGS	12 km to fault displacement	0.378	0.378										1					0.3	<1							No apparent significant damage
Imperial Valley	1979	6.53	Valley Nitrogen	20	è un epicentro diverso da quello che ho preso da USGS	12 km to fault displacement	0.378	0.378										1					1	>=1							No apparent significant damage
Miyagi	1978		Tohoku Oil Sendai Refinery	100			0.285	0.285			0.27	0.29	0.17		At the Shiogama Port the strong motion seismogram showed maximum acceleration on the ground surface to be 266 gals in the NS direction, 288 gals in the EW direction, and 166 gals in the vertical direction.	surface soils are sandy		1		T-1			0.3	<<1	Floating	concrete block on sand mound			1	oil		Settlement 20-60 mm; The rolling lader on the floating roof was buckled or deformed and oil flushed out on the floating roof
Miyagi	1978		Tohoku Oil Sendai Refinery	100			0.285	0.285			0.27	0.29	0.17		At the Shiogama Port the strong motion seismogram showed maximum acceleration on the ground surface to be 266 gals in the NS direction, 288 gals in the EW direction, and 166 gals in the vertical direction.	surface soils are sandy		1		T-2			0.3	<<1	Floating	concrete block on sand mound			1	oil		Settlement 60-100 mm; The rolling lader on the floating roof was buckled or deformed and oil flushed out on the floating roof
Miyagi	1978		Tohoku Oil Sendai Refinery	100			0.285	0.285			0.27	0.29	0.17		At the Shiogama Port the strong motion seismogram showed maximum acceleration on the ground surface to be 266 gals in the NS direction, 288 gals in the EW direction, and 166 gals in the vertical direction.	surface soils are sandy		1		T-3			0.3	<<1	Floating	concrete block on sand mound			1	oil		Settlement 60-100 mm; The rolling lader on the floating roof was buckled or deformed and oil flushed out on the floating roof
Miyagi	1978		Tohoku Oil Sendai Refinery	100			0.285	0.285			0.27	0.29	0.17		At the Shiogama Port the strong motion seismogram showed maximum acceleration on the ground surface to be 266 gals in the NS direction, 288 gals in the EW direction, and 166 gals in the vertical direction.	surface soils are sandy		1		T-4			0.3	<<1	Floating	concrete block on sand mound			1	oil		Settlement 20-60 mm
Miyagi	1978		Tohoku Oil Sendai Refinery	100			0.285	0.285			0.27	0.29	0.17		At the Shiogama Port the strong motion seismogram showed maximum acceleration on the ground surface to be 266 gals in the NS direction, 288 gals in the EW direction, and 166 gals in the vertical direction.	surface soils are sandy		1		T-5			0.3	<<1	Floating	concrete block on sand mound			1	oil		Settlement 20-60 mm; The rolling lader on the floating roof was buckled or deformed and oil flushed out on the floating roof
Miyagi	1978		Tohoku Oil Sendai Refinery	100			0.285	0.285			0.27	0.29	0.17		At the Shiogama Port the strong motion seismogram showed maximum acceleration on the ground surface to be 266 gals in the NS direction, 288 gals in the EW direction, and 166 gals in the vertical direction.	surface soils are sandy		1		T-6			0.3	<<1	Floating	concrete block on sand mound			1	oil		Settlement 20-60 mm; The rolling lader on the floating roof was buckled or deformed and oil flushed out on the floating roof
Miyagi	1978		Tohoku Oil Sendai Refinery	100			0.285	0.285			0.27	0.29	0.17		At the Shiogama Port the strong motion seismogram showed maximum acceleration on the ground surface to be 266 gals in the NS direction, 288 gals in the EW direction, and 166 gals in the vertical direction.	surface soils are sandy		1		T-7			0.3	<<1	Floating	concrete block on sand mound			1	oil		Settlement 20-60 mm; The rolling lader on the floating roof was buckled or deformed and oil flushed out on the floating roof
Miyagi	1978		Tohoku Oil Sendai Refinery	100			0.285	0.285			0.27	0.29	0.17		At the Shiogama Port the strong motion seismogram showed maximum acceleration on the ground surface to be 266 gals in the NS direction, 288 gals in the EW direction, and 166 gals in the vertical direction.	surface soils are sandy		1		T-8			0.3	<<1	Floating	concrete block on sand mound			1	oil		Settlement 60-100 mm; The rolling lader on the floating roof was buckled or deformed and oil flushed out on the floating roof
Miyagi	1978		Tohoku Oil Sendai Refinery	100			0.285	0.285			0.27	0.29	0.17		At the Shiogama Port the strong motion seismogram showed maximum acceleration on the ground surface to be 266 gals in the NS direction, 288 gals in the EW direction, and 166 gals in the vertical direction.	surface soils are sandy		1		T-9			0.3	<<1	Floating	concrete block on sand mound			1	oil		Settlement 60-100 mm; The rolling lader on the floating roof was buckled or deformed and oil flushed out on the floating roof
Miyagi	1978		Tohoku Oil Sendai Refinery	100			0.285	0.285			0.27	0.29	0.17		At the Shiogama Port the strong motion seismogram showed maximum acceleration on the ground surface to be 266 gals in the NS direction, 288 gals in the EW direction, and 166 gals in the vertical direction.	surface soils are sandy		1		T-10			0.3	<<1	Floating	concrete block on sand mound			1	oil		No damage
Miyagi	1978		Tohoku Oil Sendai Refinery	100			0.285	0.285			0.27	0.29	0.17		At the Shiogama Port the strong motion seismogram showed maximum acceleration on the ground surface to be 266 gals in the NS direction, 288 gals in the EW direction, and 166 gals in the vertical direction.	surface soils are sandy		1		T-101			1.1	>1		concrete block on sand mound			1			No damage
Miyagi	1978		Tohoku Oil Sendai Refinery	100			0.285	0.285			0.27	0.29	0.17		At the Shiogama Port the strong motion seismogram showed maximum acceleration on the ground surface to be 266 gals in the NS direction, 288 gals in the EW direction, and 166 gals in the vertical direction.	surface soils are sandy		1		T-102			1.1	>1		concrete block on sand mound			1			No damage
Miyagi	1978		Tohoku Oil Sendai Refinery	100			0.285	0.285			0.27	0.29	0.17		At the Shiogama Port the strong motion seismogram showed maximum acceleration on the ground surface to be 266 gals in the NS direction, 288 gals in the EW direction, and 166 gals in the vertical direction.	surface soils are sandy		1		T-103			0.3	<1	fixed flat	concrete block on sand mound			1	oil		No damage
Miyagi	1978		Tohoku Oil Sendai Refinery	100			0.285	0.285			0.27	0.29	0.17		At the Shiogama Port the strong motion seismogram showed maximum acceleration on the ground surface to be 266 gals in the NS direction, 288 gals in the EW direction, and 166 gals in the vertical direction.	surface soils are sandy		1		T-104			0.3	<1	fixed flat	concrete block on sand mound			1	oil		No damage
Miyagi	1978		Tohoku Oil Sendai Refinery	100			0.285	0.285			0.27	0.29	0.17		At the Shiogama Port the strong motion seismogram showed maximum acceleration on the ground surface to be 266 gals in the NS direction, 288 gals in the EW direction, and 166 gals in the vertical direction.	surface soils are sandy		1		T-301			1.1	>1	fixed flat	concrete block on sand mound			1	water		Have experienced significant rocking. Anchor bolts were pulled out

Miyagi	1978		Tohoku Oil Sendai Refinery	100			0.285	0.285			0.27	0.29	0.17		At the Shiogama Port the strong motion seismogram showed maximum acceleration on the ground surface to be 266 gals in the NS direction, 288 gals in the EW direction, and 166 gals in the vertical direction.	surface soils are sandy		1		T-302			1.1	>1	fixed flat	concrete block on sand mound			1	water		Have experienced significant rocking. Anchor bolts were pulled out
Miyagi	1978		Tohoku Oil Sendai Refinery	100			0.285	0.285			0.27	0.29	0.17		At the Shiogama Port the strong motion seismogram showed maximum acceleration on the ground surface to be 266 gals in the NS direction, 288 gals in the EW direction, and 166 gals in the vertical direction.	surface soils are sandy		1		T-355			1.1	>1	fixed flat	concrete block on sand mound			1	water		Have experienced significant rocking. Anchor bolts were pulled out
Miyagi	1978		Tohoku Oil Sendai Refinery	100			0.285	0.285			0.27	0.29	0.17		At the Shiogama Port the strong motion seismogram showed maximum acceleration on the ground surface to be 266 gals in the NS direction, 288 gals in the EW direction, and 166 gals in the vertical direction.	surface soils are sandy		1		T-105			1	>=1	fixed flat	concrete block on sand mound			1	oil		No damage
Miyagi	1978		Tohoku Oil Sendai Refinery	100			0.285	0.285			0.27	0.29	0.17		At the Shiogama Port the strong motion seismogram showed maximum acceleration on the ground surface to be 266 gals in the NS direction, 288 gals in the EW direction, and 166 gals in the vertical direction.	surface soils are sandy		1		T-106			1.1	>1	fixed flat	concrete block on sand mound			1			No damage
Miyagi	1978		Tohoku Oil Sendai Refinery	100			0.285	0.285			0.27	0.29	0.17		At the Shiogama Port the strong motion seismogram showed maximum acceleration on the ground surface to be 266 gals in the NS direction, 288 gals in the EW direction, and 166 gals in the vertical direction.	surface soils are sandy		1		T-107			0.3			concrete block on sand mound			1			No damage
Miyagi	1978		Tohoku Oil Sendai Refinery	100			0.285	0.285			0.27	0.29	0.17		At the Shiogama Port the strong motion seismogram showed maximum acceleration on the ground surface to be 266 gals in the NS direction, 288 gals in the EW direction, and 166 gals in the vertical direction.	surface soils are sandy		1		T-108			1	<=1 piu tozzo che snello	floating	concrete block on sand mound			1	oil		No damage
Miyagi	1978		Tohoku Oil Sendai Refinery	100			0.285	0.285			0.27	0.29	0.17		At the Shiogama Port the strong motion seismogram showed maximum acceleration on the ground surface to be 266 gals in the NS direction, 288 gals in the EW direction, and 166 gals in the vertical direction.	surface soils are sandy		1		T-109			1	<=1 piu tozzo che snello	floating	concrete block on sand mound			1	oil		No damage
Miyagi	1978		Tohoku Oil Sendai Refinery	100			0.285	0.285			0.27	0.29	0.17		At the Shiogama Port the strong motion seismogram showed maximum acceleration on the ground surface to be 266 gals in the NS direction, 288 gals in the EW direction, and 166 gals in the vertical direction.	surface soils are sandy		1		T-110			1	<=1 piu tozzo che snello	floating	concrete block on sand mound			1	oil		Settlement 20-60 mm
Miyagi	1978		Tohoku Oil Sendai Refinery	100			0.285	0.285			0.27	0.29	0.17		At the Shiogama Port the strong motion seismogram showed maximum acceleration on the ground surface to be 266 gals in the NS direction, 288 gals in the EW direction, and 166 gals in the vertical direction.	surface soils are sandy		1		T-111			0.3	<1	fixed flat	concrete block on sand mound			1	oil		No damage
Miyagi	1978		Tohoku Oil Sendai Refinery	100			0.285	0.285			0.27	0.29	0.17		At the Shiogama Port the strong motion seismogram showed maximum acceleration on the ground surface to be 266 gals in the NS direction, 288 gals in the EW direction, and 166 gals in the vertical direction.	surface soils are sandy		1		T-112			0.3	<1	floating	concrete block on sand mound			1	oil		No damage
Miyagi	1978		Tohoku Oil Sendai Refinery	100			0.285	0.285			0.27	0.29	0.17		At the Shiogama Port the strong motion seismogram showed maximum acceleration on the ground surface to be 266 gals in the NS direction, 288 gals in the EW direction, and 166 gals in the vertical direction.	surface soils are sandy		1		T-113			1.1	>1	fixed flat	concrete block on sand mound			1			No damage
Miyagi	1978		Tohoku Oil Sendai Refinery	100			0.285	0.285			0.27	0.29	0.17		At the Shiogama Port the strong motion seismogram showed maximum acceleration on the ground surface to be 266 gals in the NS direction, 288 gals in the EW direction, and 166 gals in the vertical direction.	surface soils are sandy		1		T-114			1.1	>1	fixed flat	concrete block on sand mound			1			Settlement 20-60 mm
Miyagi	1978		Tohoku Oil Sendai Refinery	100			0.285	0.285			0.27	0.29	0.17		At the Shiogama Port the strong motion seismogram showed maximum acceleration on the ground surface to be 266 gals in the NS direction, 288 gals in the EW direction, and 166 gals in the vertical direction.	surface soils are sandy		1		T-115			1	>=1 Piu snello che tozzo	fixed flat	concrete block on sand mound			1	oil		No damage
Miyagi	1978		Tohoku Oil Sendai Refinery	100			0.285	0.285			0.27	0.29	0.17		At the Shiogama Port the strong motion seismogram showed maximum acceleration on the ground surface to be 266 gals in the NS direction, 288 gals in the EW direction, and 166 gals in the vertical direction.	surface soils are sandy		1		T-116			1.1	>1	fixed flat	concrete block on sand mound			1			No damage
Miyagi	1978		Tohoku Oil Sendai Refinery	100			0.285	0.285			0.27	0.29	0.17		At the Shiogama Port the strong motion seismogram showed maximum acceleration on the ground surface to be 266 gals in the NS direction, 288 gals in the EW direction, and 166 gals in the vertical direction.	surface soils are sandy		1		T-117			1.1	>1	fixed flat	concrete block on sand mound			1			No damage
Miyagi	1978		Tohoku Oil Sendai Refinery	100			0.285	0.285			0.27	0.29	0.17		At the Shiogama Port the strong motion seismogram showed maximum acceleration on the ground surface to be 266 gals in the NS direction, 288 gals in the EW direction, and 166 gals in the vertical direction.	surface soils are sandy		1		T-118			1	>=1 piu snello che tozzo	fixed flat	concrete block on sand mound			1	oil		Settlement of more than 100 mm
Miyagi	1978		Tohoku Oil Sendai Refinery	100			0.285	0.285			0.27	0.29	0.17		At the Shiogama Port the strong motion seismogram showed maximum acceleration on the ground surface to be 266 gals in the NS direction, 288 gals in the EW direction, and 166 gals in the vertical direction.	surface soils are sandy		1		T-119			0.3	<1	fixed flat	concrete block on sand mound			1	oil		No damage
Miyagi	1978		Tohoku Oil Sendai Refinery	100			0.285	0.285			0.27	0.29	0.17		At the Shiogama Port the strong motion seismogram showed maximum acceleration on the ground surface to be 266 gals in the NS direction, 288 gals in the EW direction, and 166 gals in the vertical direction.	surface soils are sandy		1		T-120			0.3	<1	fixed flat	concrete block on sand mound			1	oil		No damage
Miyagi	1978		Tohoku Oil Sendai Refinery	100			0.285	0.285			0.27	0.29	0.17		At the Shiogama Port the strong motion seismogram showed maximum acceleration on the ground surface to be 266 gals in the NS direction, 288 gals in the EW direction, and 166 gals in the vertical direction.	surface soils are sandy		1		T-121			0.3	<1	floating	concrete block on sand mound			1	oil		Settlement 20-60 mm
Miyagi	1978		Tohoku Oil Sendai Refinery	100			0.285	0.285			0.27	0.29	0.17		At the Shiogama Port the strong motion seismogram showed maximum acceleration on the ground surface to be 266 gals in the NS direction, 288 gals in the EW direction, and 166 gals in the vertical direction.	surface soils are sandy		1		T-122			1	1	fixed flat	concrete block on sand mound			1			No damage
Miyagi	1978		Tohoku Oil Sendai Refinery	100			0.285	0.285			0.27	0.29	0.17		At the Shiogama Port the strong motion seismogram showed maximum acceleration on the ground surface to be 266 gals in the NS direction, 288 gals in the EW direction, and 166 gals in the vertical direction.	surface soils are sandy		1		T-123			1.1	>1	fixed flat	concrete block on sand mound			1			No damage
Miyagi	1978		Tohoku Oil Sendai Refinery	100			0.285	0.285			0.27	0.29	0.17		At the Shiogama Port the strong motion seismogram showed maximum acceleration on the ground surface to be 266 gals in the NS direction, 288 gals in the EW direction, and 166 gals in the vertical direction.	surface soils are sandy		1		T-124			0.3	<1	fixed flat	concrete block on sand mound			1	oil		No damage
Miyagi	1978		Tohoku Oil Sendai Refinery	100			0.285	0.285			0.27	0.29	0.17		At the Shiogama Port the strong motion seismogram showed maximum acceleration on the ground surface to be 266 gals in the NS direction, 288 gals in the EW direction, and 166 gals in the vertical direction.	surface soils are sandy		1		T-125			0.3	<1	fixed flat	concrete block on sand mound			1	oil		No damage
Miyagi	1978		Tohoku Oil Sendai Refinery	100			0.285	0.285			0.27	0.29	0.17		At the Shiogama Port the strong motion seismogram showed maximum acceleration on the ground surface to be 266 gals in the NS direction, 288 gals in the EW direction, and 166 gals in the vertical direction.	surface soils are sandy		1		T-126			0.3	<1	fixed flat	concrete block on sand mound			1	oil		No damage

Miyagi	1978		Tohoku Oil Sendai Refinery	100			0.285	0.285			0.27	0.29	0.17		At the Shiogama Port the strong motion seismogram showed maximum acceleration on the ground surface to be 266 gals in the NS direction, 288 gals in the EW direction, and 166 gals in the vertical direction.	surface soils are sandy		1		T-127			0.3	<1	fixed flat	concrete block on sand mound			1	oil		Settlement 20-60 mm
Miyagi	1978		Tohoku Oil Sendai Refinery	100			0.285	0.285			0.27	0.29	0.17		At the Shiogama Port the strong motion seismogram showed maximum acceleration on the ground surface to be 266 gals in the NS direction, 288 gals in the EW direction, and 166 gals in the vertical direction.	surface soils are sandy		1		T-128			1	1	floating	concrete block on sand mound			1	oil		No damage
Miyagi	1978		Tohoku Oil Sendai Refinery	100			0.285	0.285			0.27	0.29	0.17		At the Shiogama Port the strong motion seismogram showed maximum acceleration on the ground surface to be 266 gals in the NS direction, 288 gals in the EW direction, and 166 gals in the vertical direction.	surface soils are sandy		1		T-129			0.3	<1	floating	concrete block on sand mound			1	oil		Settlement 20-60 mm
Miyagi	1978		Tohoku Oil Sendai Refinery	100			0.285	0.285			0.27	0.29	0.17		At the Shiogama Port the strong motion seismogram showed maximum acceleration on the ground surface to be 266 gals in the NS direction, 288 gals in the EW direction, and 166 gals in the vertical direction.	surface soils are sandy		1		T-130			0.3	circa 0,3	fixed flat	concrete block on sand mound			1	oil		Settlement from 100 mm to 140 mm. Also, because of the settlement, the annular bottom plate deformed so much that an acute angle was formed with the shell plate
Miyagi	1978		Tohoku Oil Sendai Refinery	100			0.285	0.285			0.27	0.29	0.17		At the Shiogama Port the strong motion seismogram showed maximum acceleration on the ground surface to be 266 gals in the NS direction, 288 gals in the EW direction, and 166 gals in the vertical direction.	surface soils are sandy		1		T-131			0.3	circa 0,3	fixed flat	concrete block on sand mound			1	oil		Settlement from 100 mm to 140 mm. Also, because of the settlement, the annular bottom plate deformed so much that an acute angle was formed with the shell plate. Crack of anular bottom plate, oil leak
Miyagi	1978		Tohoku Oil Sendai Refinery	100			0.285	0.285			0.27	0.29	0.17		At the Shiogama Port the strong motion seismogram showed maximum acceleration on the ground surface to be 266 gals in the NS direction, 288 gals in the EW direction, and 166 gals in the vertical direction.	surface soils are sandy		1		T-132			0.3	<1	fixed flat	concrete block on sand mound			1	oil		No damage
Miyagi	1978		Tohoku Oil Sendai Refinery	100			0.285	0.285			0.27	0.29	0.17		At the Shiogama Port the strong motion seismogram showed maximum acceleration on the ground surface to be 266 gals in the NS direction, 288 gals in the EW direction, and 166 gals in the vertical direction.	surface soils are sandy		1		T-133			0.3	<1	fixed flat	concrete block on sand mound			1	oil		No damage
Miyagi	1978		Tohoku Oil Sendai Refinery	100			0.285	0.285			0.27	0.29	0.17		At the Shiogama Port the strong motion seismogram showed maximum acceleration on the ground surface to be 266 gals in the NS direction, 288 gals in the EW direction, and 166 gals in the vertical direction.	surface soils are sandy		1		T-201			1.1	>1	fixed flat	concrete block on sand mound			1			No damage
Miyagi	1978		Tohoku Oil Sendai Refinery	100			0.285	0.285			0.27	0.29	0.17		At the Shiogama Port the strong motion seismogram showed maximum acceleration on the ground surface to be 266 gals in the NS direction, 288 gals in the EW direction, and 166 gals in the vertical direction.	surface soils are sandy		1		T-202			0.3	<1	floating	concrete block on sand mound			1	oil		Settlement 20-60 mm
Miyagi	1978		Tohoku Oil Sendai Refinery	100			0.285	0.285			0.27	0.29	0.17		At the Shiogama Port the strong motion seismogram showed maximum acceleration on the ground surface to be 266 gals in the NS direction, 288 gals in the EW direction, and 166 gals in the vertical direction.	surface soils are sandy		1		T-203			0.3	<1	fixed flat	concrete block on sand mound			1	oil		Settlement of more than 100 mm
Miyagi	1978		Tohoku Oil Sendai Refinery	100			0.285	0.285			0.27	0.29	0.17		At the Shiogama Port the strong motion seismogram showed maximum acceleration on the ground surface to be 266 gals in the NS direction, 288 gals in the EW direction, and 166 gals in the vertical direction.	surface soils are sandy		1		T-204			0.3	<1	floating	concrete block on sand mound			1	oil		No damage
Miyagi	1978		Tohoku Oil Sendai Refinery	100			0.285	0.285			0.27	0.29	0.17		At the Shiogama Port the strong motion seismogram showed maximum acceleration on the ground surface to be 266 gals in the NS direction, 288 gals in the EW direction, and 166 gals in the vertical direction.	surface soils are sandy		1		T-205			0.3	<1	floating	concrete block on sand mound			1	oil		No damage
Miyagi	1978		Tohoku Oil Sendai Refinery	100			0.285	0.285			0.27	0.29	0.17		At the Shiogama Port the strong motion seismogram showed maximum acceleration on the ground surface to be 266 gals in the NS direction, 288 gals in the EW direction, and 166 gals in the vertical direction.	surface soils are sandy		1		T-206			0.3	<1	floating	concrete block on sand mound			1	oil		Settlement 20-60 mm
Miyagi	1978		Tohoku Oil Sendai Refinery	100			0.285	0.285			0.27	0.29	0.17		At the Shiogama Port the strong motion seismogram showed maximum acceleration on the ground surface to be 266 gals in the NS direction, 288 gals in the EW direction, and 166 gals in the vertical direction.	surface soils are sandy		1		T-207			0.3	<1	floating	concrete block on sand mound			1	oil		Settlement 20-60 mm
Miyagi	1978		Tohoku Oil Sendai Refinery	100			0.285	0.285			0.27	0.29	0.17		At the Shiogama Port the strong motion seismogram showed maximum acceleration on the ground surface to be 266 gals in the NS direction, 288 gals in the EW direction, and 166 gals in the vertical direction.	surface soils are sandy		1		T-208			1	>=1 piu snello che tozzo	fixed flat	concrete block on sand mound			1	oil		Settlement 20-60 mm
Miyagi	1978		Tohoku Oil Sendai Refinery	100			0.285	0.285			0.27	0.29	0.17		At the Shiogama Port the strong motion seismogram showed maximum acceleration on the ground surface to be 266 gals in the NS direction, 288 gals in the EW direction, and 166 gals in the vertical direction.	surface soils are sandy		1		T-209			1	>=1 piu snello che tozzo	fixed flat	concrete block on sand mound			1	oil		No damage
Miyagi	1978		Tohoku Oil Sendai Refinery	100			0.285	0.285			0.27	0.29	0.17		At the Shiogama Port the strong motion seismogram showed maximum acceleration on the ground surface to be 266 gals in the NS direction, 288 gals in the EW direction, and 166 gals in the vertical direction.	surface soils are sandy		1		T-210			0.3	<1	fixed flat	concrete block on sand mound			1	oil		No damage
Miyagi	1978		Tohoku Oil Sendai Refinery	100			0.285	0.285			0.27	0.29	0.17		At the Shiogama Port the strong motion seismogram showed maximum acceleration on the ground surface to be 266 gals in the NS direction, 288 gals in the EW direction, and 166 gals in the vertical direction.	surface soils are sandy		1		T-211			0.3	<1	fixed flat	concrete block on sand mound			1	oil		No damage
Miyagi	1978		Tohoku Oil Sendai Refinery	100			0.285	0.285			0.27	0.29	0.17		At the Shiogama Port the strong motion seismogram showed maximum acceleration on the ground surface to be 266 gals in the NS direction, 288 gals in the EW direction, and 166 gals in the vertical direction.	surface soils are sandy		1		T-212			0.3	<1	fixed flat	concrete block on sand mound			1	oil		Settlement 60-100 mm
Miyagi	1978		Tohoku Oil Sendai Refinery	100			0.285	0.285			0.27	0.29	0.17		At the Shiogama Port the strong motion seismogram showed maximum acceleration on the ground surface to be 266 gals in the NS direction, 288 gals in the EW direction, and 166 gals in the vertical direction.	surface soils are sandy		1		T-213			0.3	<1	floating	concrete block on sand mound			1	oil		Settlement 20-60 mm
Miyagi	1978		Tohoku Oil Sendai Refinery	100			0.285	0.285			0.27	0.29	0.17		At the Shiogama Port the strong motion seismogram showed maximum acceleration on the ground surface to be 266 gals in the NS direction, 288 gals in the EW direction, and 166 gals in the vertical direction.	surface soils are sandy		1		T-214			1	<=1 piu tozzo che snello	floating	concrete block on sand mound			1	oil		No damage
Miyagi	1978		Tohoku Oil Sendai Refinery	100			0.285	0.285			0.27	0.29	0.17		At the Shiogama Port the strong motion seismogram showed maximum acceleration on the ground surface to be 266 gals in the NS direction, 288 gals in the EW direction, and 166 gals in the vertical direction.	surface soils are sandy		1		T-215			0.3	circa 0,3	fixed flat	concrete block on sand mound			1	oil		Settlement 20-60 mm
Miyagi	1978		Tohoku Oil Sendai Refinery	100			0.285	0.285			0.27	0.29	0.17		At the Shiogama Port the strong motion seismogram showed maximum acceleration on the ground surface to be 266 gals in the NS direction, 288 gals in the EW direction, and 166 gals in the vertical direction.	surface soils are sandy		1		T-216			0.3	circa 0,3	fixed flat	concrete block on sand mound			1	oil		Settlement 20-60 mm
Miyagi	1978		Tohoku Oil Sendai Refinery	100			0.285	0.285			0.27	0.29	0.17		At the Shiogama Port the strong motion seismogram showed maximum acceleration on the ground surface to be 266 gals in the NS direction, 288 gals in the EW direction, and 166 gals in the vertical direction.	surface soils are sandy		1		T-217			0.3	circa 0,3	fixed flat	concrete block on sand mound			1	oil		This tank failed at the annulat bottom plate along the inside fillet weld toe at the corner joint with the shell plate, and the content flowed out. Measurements of the annular bottom plate thickness after the earthquake revealed that the thickness of the annular bottom plates in these tanks decreased by corrosion. Subsequent partial vacuum collapse of the top

Miyagi	1978		Tohoku Oil Sendai Refinery	100			0.285	0.285			0.27	0.29	0.17		At the Shiogama Port the strong motion seismogram showed maximum acceleration on the ground surface to be 266 gals in the NS direction, 288 gals in the EW direction, and 166 gals in the vertical direction.	surface soils are sandy		1		T-218			0.3	circa 0,3	fixed flat	concrete block on sand mound			1	oil		This tank failed at the annulat bottom plate along the inside fillet weld toe at the corner joint with the shell plate, and the content flowed out. Measurements of the annular bottom plate thickness after the earthquake revealed that the thickness of the annular bottom plates in these tanks decreased by corrosion. Subsequent partial vacuum collapse of the top
Miyagi	1978		Tohoku Oil Sendai Refinery	100			0.285	0.285			0.27	0.29	0.17		At the Shiogama Port the strong motion seismogram showed maximum acceleration on the ground surface to be 266 gals in the NS direction, 288 gals in the EW direction, and 166 gals in the vertical direction.	surface soils are sandy		1		T-219			1	<=1	fixed flat	concrete block on sand mound			1	oil		Settlement 20-60 mm
Miyagi	1978		Tohoku Oil Sendai Refinery	100			0.285	0.285			0.27	0.29	0.17		At the Shiogama Port the strong motion seismogram showed maximum acceleration on the ground surface to be 266 gals in the NS direction, 288 gals in the EW direction, and 166 gals in the vertical direction.	surface soils are sandy		1		T-220			1	>=1 piu snello che tozzo	fixed flat	concrete block on sand mound			1	oil		Settlement 60-100 mm
Miyagi	1978		Tohoku Oil Sendai Refinery	100			0.285	0.285			0.27	0.29	0.17		At the Shiogama Port the strong motion seismogram showed maximum acceleration on the ground surface to be 266 gals in the NS direction, 288 gals in the EW direction, and 166 gals in the vertical direction.	surface soils are sandy		1		T-221			0.3	<1	fixed flat	concrete block on sand mound			1	oil		Settlement 20-60 mm; Crack of annular bottom plate, oil leak
Miyagi	1978		Tohoku Oil Sendai Refinery	100			0.285	0.285			0.27	0.29	0.17		At the Shiogama Port the strong motion seismogram showed maximum acceleration on the ground surface to be 266 gals in the NS direction, 288 gals in the EW direction, and 166 gals in the vertical direction.	surface soils are sandy		1		T-222			0.3	<1	fixed flat	concrete block on sand mound			1	oil		No damage
Miyagi	1978		Tohoku Oil Sendai Refinery	100			0.285	0.285			0.27	0.29	0.17		At the Shiogama Port the strong motion seismogram showed maximum acceleration on the ground surface to be 266 gals in the NS direction, 288 gals in the EW direction, and 166 gals in the vertical direction.	surface soils are sandy		1		T-223			0.3	<1	fixed flat	concrete block on sand mound			1	oil		No damage
Miyagi	1978		Tohoku Oil Sendai Refinery	100			0.285	0.285			0.27	0.29	0.17		At the Shiogama Port the strong motion seismogram showed maximum acceleration on the ground surface to be 266 gals in the NS direction, 288 gals in the EW direction, and 166 gals in the vertical direction.	surface soils are sandy		1		T-224			0.3	<1	fixed flat	concrete block on sand mound			1	oil		This tank failed at the annulat bottom plate along the inside fillet weld toe at the corner joint with the shell plate, and the content flowed out. Measurements of the annular bottom plate thickness after the earthquake revealed that the thickness of the annular bottom plates in these tanks decreased by corrosion. Subsequent partial vacuum collapse of the top
Miyagi	1978		Tohoku Oil Sendai Refinery	100			0.285	0.285			0.27	0.29	0.17		At the Shiogama Port the strong motion seismogram showed maximum acceleration on the ground surface to be 266 gals in the NS direction, 288 gals in the EW direction, and 166 gals in the vertical direction.	surface soils are sandy		1		T-401			1	1	fixed flat	concrete block on sand mound			1			No damage
Miyagi	1978		Tohoku Oil Sendai Refinery	100			0.285	0.285			0.27	0.29	0.17		At the Shiogama Port the strong motion seismogram showed maximum acceleration on the ground surface to be 266 gals in the NS direction, 288 gals in the EW direction, and 166 gals in the vertical direction.	surface soils are sandy		1		T-402			1	1	fixed flat	concrete block on sand mound			1			No damage
Miyagi	1978		Tohoku Oil Sendai Refinery	100			0.285	0.285			0.27	0.29	0.17		At the Shiogama Port the strong motion seismogram showed maximum acceleration on the ground surface to be 266 gals in the NS direction, 288 gals in the EW direction, and 166 gals in the vertical direction.	surface soils are sandy		1		T-403			1	1	fixed flat	concrete block on sand mound			1			No damage
Managua	1972	6.24		50			0.39				0.34	0.39	0.33					3					1.1						water		Elephant foot buckling, but the tanks were left in service (no leak?
San Fernando	1971	6.61	Metropolitan Water District Jensen Plant	14.5		near or on the falted zone	0.469	0.469		0.6					ASA2001: PGA from Wald	bluff		1		FP Washwater	30.5	11.0	0.36		fixed (knuckle joint)	ring foundation	welded	The lowest shell course was 17,5 mm (11/16 in.); the upper course	1	water	0.58	Roof and upper shell damage (buckling). Uplifted 0,33m (13in.) based on the observed anchor bolt stretch; No EFB
San Fernando	1971	6.61	Olive View Hospital	10			0.68	0.68		0.6					ASA2001: PGA from Wald			1		Olive View TK	16.8	12.2	0.73		fixed		welded	The bottom course 11,4mm (0,45 in.) and the top course 6,4 mm (0,25 in.)			0.9	Elephant foot buckling and also a 3m (10ft) floor/shell tear. The inlet/outlet piping was also damaged, allowing the tank to lose its contents. Inside the tank roof rafters buckled and vertical buckling of the floor occurred in several places.
San Fernando	1971	6.61	Veterans Hospital	9.5			0.86	0.86		1.2					ASA2001: Location of Mutual Water Co is unknown. Why PGA=1,2g not verified			1		Vet Hosp 1			0.3				riveted		1		0.9	the anchor bolts stretched or displaced and the inlet/outlet piping sheared. Buckled anchorage sistem made of steel beam
San Fernando	1971	6.61	Veterans Hospital	9.5			0.86	0.86		1.2					ASA2001: Location of Mutual Water Co is unknown. Why PGA=1,2g not verified			1		Vet Hosp 2			0.3				welded				0.9	No significant damage
San Fernando	1971	6.61	City of Los Angeles Department of Water Plant (CLADWP)	9.3			0.827	0.827		1.2					ASA2001: Location of Mutual Water Co is unknown. Why PGA=1,2g not verified			1		Alta Vista 1	16.5	8.5	0.52				riveted	bottom shell course: 9,5mm (0,375in.)			0.9	damage to cast-iron inlet/outlet fittings, with no damage to tank shell or bottom.
San Fernando	1971	6.61	City of Los Angeles Department of Water Plant (CLADWP)	9.3			0.827	0.827		1.2					ASA2001: Location of Mutual Water Co is unknown. Why PGA=1,2g not verified			1		Alta Vista 2	29.0	11.1	0.38				welded				0.9	damage to cast-iron inlet/outlet fittings, with no damage to tank shell or bottom.
San Fernando	1971	6.61	Newhall County Water District	13		8-10 km of the surface faulting	0.44	0.44		1.2					ASA2001: Location of Mutual Water Co is unknown. Why PGA=1,2g not verified			1		Newhall CWD 1			0.3								0.9	floor plate ruptures and shell buckling.
San Fernando	1971	6.61	Newhall County Water District	13		8-10 km of the surface faulting	0.44	0.44		1.2					ASA2001: Location of Mutual Water Co is unknown. Why PGA=1,2g not verified			1		Newhall CWD 2			0.3								0.9	floor plate ruptures and shell buckling.
San Fernando	1971	6.61	Mutual Water Company (Kagel Canyon area)				0.68	0,66-0,70		1.2					ASA2001: Location of Mutual Water Co is unknown. Why PGA=1,2g not verified			5		Mutual Water Co	6.1	6.1	1.00				bolted				0.9	Failed
San Fernando	1971	6.61	CLADWP Sesnon Tank	20			0.33	0.33		0.3					ALA2001			1		Sesnon Tank	29.0	12.8	0.44		Roof beams with a wooden roof	12,7 mm (1 in.) by 0,9 m (36 in.) sketch plate (annular ring)	welded	Bottom course 25,4 mm (1 in.) and top course 8 mm (5/16 in.)	0		0.95	Buckle 7,4m (24ft) above the bottom on a 150° arc. Uplifted. Damage to wood roof
San Fernando	1971	6.61	CLADWP Granada High Tank	18			0.36	0.36		0.4					ALA2001			1		Granada High Tank	16.8	13.7	0.82		wooden roof		riveted				0.9	Roof collapse and shifting of wooden roof
San Fernando	1971	6.61	Newhall Refinery	12		4-5 km from the surface faulting	0.49	0.49		0.6					ALA2001			1		Newhall 1	18.3	12.2	0.67							Jet Fuel	1	Elephant foot buckling on one side
San Fernando	1971	6.61	Newhall Refinery	12		4-5 km from the surface faulting	0.49	0.49		0.6					ALA2001			1		Newhall 2	18.3	12.2	0.67							Jet Fuel	1	Elephant foot buckling on one side
San Fernando	1971	6.61	Newhall Refinery	12		4-5 km from the surface faulting	0.49	0.49		0.6					ALA2001			1		Newhall 3	18.3	12.2	0.67							Jet Fuel	1	Elephant foot buckling on one side
San Fernando	1971	6.61	Newhall Refinery	12		4-5 km from the surface faulting	0.49	0.49		0.6					ALA2001			1		Newhall 4	36.6	12.2	0.33								0.9	Minor piping damage
San Fernando	1971	6.61	Newhall Refinery	12		4-5 km from the surface faulting	0.49	0.49		0.6					ALA2001			1		Newhall 5	36.6	12.2	0.33								0.9	Minor piping damage
San Fernando	1971	6.61	El Segundo	55			0.12	0.12										1			18.3	9.1	0.5		floating						0.94	roof seals caught on tank rim
San Fernando	1971	6.61	El Segundo	55			0.12	0.12										1			24.4	14.6	0.6		floating						0.93	roof seals caught on tank rim
San Fernando	1971	6.61	El Segundo	55			0.12	0.12										1			33.5	14.6	0.44		floating						0.97	roof seals caught on tank rim
San Fernando	1971	6.61	El Segundo	55			0.12	0.12										1			23.8	10.7	0.45		floating							Buckled roof plate
San Fernando	1971	6.61	El Segundo	55			0.12	0.12										1					0.3									Cracked deck plate
San Fernando	1971	6.61	El Segundo	55			0.12	0.12										1					0.3									Cracked rim plate??
San Fernando	1971	6.61	El Segundo	55			0.12	0.12										2			34.7	9.1	0.26		floating						0.93	Oil spolled out of the roof
Northridge	1994	6.69	Van Nuys	8			0.46	0.46		0.55					PGA from ALA 2001 (confrontata poi nella mappa di figura 2.4 di EEFIT Report)			1		Van Nuys 1	8.8	14.6	1.65		cone roof with internal pan	set on a rock base with no concrete foundations			0	fuel	0.5	bolt shearing on the walkway between two tanks:
Northridge	1994	6.69	Van Nuys	8			0.46	0.46		0.55					PGA from ALA 2001 (confrontata poi nella mappa di figura 2.4 di EEFIT Report)			1		Van Nuys 2	11.0	13.7	1.25		cone roof with internal pan	set on a rock base with no concrete foundations			0	fuel	0.5	bolt shearing on the walkway between two tanks:
Northridge	1994	6.69	Van Nuys	8			0.46	0.46		0.55					PGA from ALA 2001 (confrontata poi nella mappa di figura 2.4 di EEFIT Report)			1		Van Nuys 3	20.4	14.6	0.72		cone roof with internal pan	set on a rock base with no concrete foundations			0	fuel	0.5	bolt shearing on the walkway between two tanks:
Northridge	1994	6.69	Van Nuys	8			0.46	0.46		0.55					PGA from ALA 2001 (confrontata poi nella mappa di figura 2.4 di EEFIT Report)			1		Van Nuys 4	21.9	14.6	0.67		cone roof with internal pan	set on a rock base with no concrete foundations			0	fuel	0.5	bolt shearing on the walkway between two tanks:
Northridge	1994	6.69	Van Nuys	8			0.46	0.46		0.55					PGA from ALA 2001 (confrontata poi nella mappa di figura 2.4 di EEFIT Report)			1		Van Nuys 5	4.6	9.1	2.00		cone roof	set on a rock base with no concrete foundations			0	wastewater	0.5	bolt shearing on the walkway between two tanks:
Northridge	1994	6.69	Van Nuys	8			0.46	0.46		0.55					PGA from ALA 2001 (confrontata poi nella mappa di figura 2.4 di EEFIT Report)			3			3.20044	10.1	3.14			concrete pad foundation			0	water		No damage
Northridge	1994	6.69	Van Nuys	8			0.46	0.46		0.55					PGA from ALA 2001 (confrontata poi nella mappa di figura 2.4 di EEFIT Report)			2			3.20044	10.1	3.14						0	water	0.95	No damage

Northridge	1994	6.69	Sepulveda	7			0.59	0.59		0.9					PGA from ALA 2001 (confrontata poi nella mappa di figura 2.4 di EEFIT Report)			1		A	19.8	11.0	0.55		cone roof with internal pan	Not on concrete ring foundation			0	fuel	0.67	No shell buckling was evident. However sloshing did occur; some product ended up on top of the pans, but did not sink them. The spillage was removed
Northridge	1994	6.69	Sepulveda	7			0.59	0.59		0.9					PGA from ALA 2001 (confrontata poi nella mappa di figura 2.4 di EEFIT Report)			1		B	21.9	11.0	0.5		cone roof with internal pan	Not on concrete ring foundation			0	fuel	0.33	No shell buckling was evident. However sloshing did occur; some product ended up on top of the pans, but did not sink them. The spillage was removed
Northridge	1994	6.69	Sepulveda	7			0.59	0.59		0.9					PGA from ALA 2001 (confrontata poi nella mappa di figura 2.4 di EEFIT Report)			1		C	18.3	11.0	0.6		cone roof with internal pan	Not on concrete ring foundation			0	fuel	0.33	No shell buckling was evident. However sloshing did occur; some product ended up on top of the pans, but did not sink them. The spillage was removed
Northridge	1994	6.69	Sepulveda	7			0.59	0.59		0.9					PGA from ALA 2001 (confrontata poi nella mappa di figura 2.4 di EEFIT Report)			1		AG 1	3.7	7.3	2			common foundation			1	wastewater	1	it was evident that the paint between the nut and the chair plate had parted on all 16 bolts. This paint crack is taken as an indication that the anchored bolts worked. No buckling on shell
Northridge	1994	6.69	Sepulveda	7			0.59	0.59		0.9					PGA from ALA 2001 (confrontata poi nella mappa di figura 2.4 di EEFIT Report)			1		AG 2	3.7	7.3	2			common foundation			1	wastewater	0	the tank did not have paint cracks. No buckling on shell
Northridge	1994	6.69	Alison Canyon	10			0.67	0,66-0,68		0.7					PGA from ALA 2001 (confrontata poi nella mappa di figura 2.4 di EEFIT Report)			1		Aliso 1	12.2	7.3	0.6				bolted			crude oil	0.75	totally collapsed
Northridge	1994	6.69	Alison Canyon	10			0.67	0,66-0,68		0.7					PGA from ALA 2001 (confrontata poi nella mappa di figura 2.4 di EEFIT Report)			1		Aliso 2	12.2	7.3	0.6				bolted			crude oil		Photo showe some shell damage
Northridge	1994	6.69	Alison Canyon	10			0.67	0,66-0,68		0.7					PGA from ALA 2001 (confrontata poi nella mappa di figura 2.4 di EEFIT Report)			1		Aliso 3	12.2	7.3	0.6				bolted			crude oil		No significant damage
Northridge	1994	6.69	Alison Canyon	10			0.67	0,66-0,68		0.7					PGA from ALA 2001 (confrontata poi nella mappa di figura 2.4 di EEFIT Report)			1		Aliso 4	12.2	7.3	0.6				bolted			crude oil		No significant damage
Northridge	1994	6.69	City of Simi (Water District 8)	21.5			0.38	0,36-0,40										24					0.3								No damage
Northridge	1994	6.69	City of Simi (Water District 8)	21.5		close to fault	0.38	0,36-0,40										9					0.3								Principal problems were broken valves and fittings at the tanks, with some movement (sliding)
Northridge	1994	6.69	City of Simi (Water District 8)	21.5		close to fault	0.38	0,36-0,40		0,3-0,4					PHGA contour map (Fig. 2,4 of EEFIT report)			1					1.1								tank with a buried drain, the piping came off the bottom of the tank. Loss of content.
Northridge	1994	6.69	Southern California Water Company (SCWC), Simi Valley				0.9			0.9					PGA from ALA 2001			1		Armin	12.8	9.09	0.71									EFB
Northridge	1994	6.69	Southern California Water Company (SCWC), Simi Valley	11			0.794	0.794		0.9					PGA from ALA 2001			1		Lautenschlager 1	19.5	6.7	0.34				welded			water	0.89	No significant damage
Northridge	1994	6.69	Southern California Water Company (SCWC), Simi Valley	11			0.794	0.794		0.9					PGA from ALA 2001			1		Lautenschlager 2	19.5	7.3	0.38				welded			water	0.81	No significant damage
Northridge	1994	6.69	Southern California Water Company (SCWC), Simi Valley	16			0.555	0.555	0.32	0.9					PGA from ALA 2001			1		Tapo	39.6	9.8	0.25				welded			water	0.89	No significant damage
Northridge	1994	6.69	Southern California Water Company (SCWC), Simi Valley	18			0.46	0.46	0.3	0.75					PGA from ALA 2001			1		Crater East	18.3	7.3	0.40				bolted			water	0.84	No significant damage
Northridge	1994	6.69	Southern California Water Company (SCWC), Simi Valley	18			0.46	0.46	0.3	0.75					PGA from ALA 2001			1		Crater West	11.9	7.3	0.62				bolted			water	0.84	No significant damage
Northridge	1994	6.69	Southern California Water Company (SCWC), Simi Valley	20.7			0.42	0.42	0.3	0.7					PGA from ALA 2001			1		Alamo	30.5	6.2	0.21				welded			water	0.99	No significant damage
Northridge	1994	6.69	Southern California Water Company (SCWC), Simi Valley	12.1			0.9	0.9	0.75	0.9					PGA from ALA 2001			1		Katerine	11.9	7.3	0.62				bolted			water	0.86	Failed by EFB with loss of contents
Northridge	1994	6.69	Southern California Water Company (SCWC), Simi Valley	17			0.52	0.516	0.32	0.85					PGA from ALA 2001			1		Rebecca North	11.9	7.3	0.62				bolted			water	0.94	Failed by EFB with loss of contents
Northridge	1994	6.69	Southern California Water Company (SCWC), Simi Valley	17			0.52	0.516	0.32	0.85					PGA from ALA 2001			1		Rebecca South	11.9	7.3	0.62				bolted			water	0.94	Failed by EFB with loss of contents
Northridge	1994	6.69	Southern California Water Company (SCWC), Simi Valley	19.3			0.44	0.435	0.3	0.7					PGA from ALA 2001			1		Sycamore North	9.1	7.3	0.8				bolted			water	0.69	Failed by EFB with loss of contents
Northridge	1994	6.69	Southern California Water Company (SCWC), Simi Valley	19.3			0.435	0.435	0.3	0.7					PGA from ALA 2001			1		Sycamore South	9.1	7.3	0.8				bolted			water	0.69	Failed by EFB with loss of contents
Northridge	1994	6.69	Southern California Water Company (SCWC), Simi Valley			general area of the other (riferito a SCWC, Simi Valley)	0.571363636	0.571363636		0.7					PGA from ALA 2001; il valore che ho messo nella colonna Shape file viene da una media che ho calcolato sulle PGA dei tanks del SCWC			1		SCWC 1	15.8	9.8	0.62				welded			water		Survived
Northridge	1994	6.69	Southern California Water Company (SCWC), Simi Valley			general area of the other (riferito a SCWC, Simi Valley)	0.571363636	0.571363636		0.7					PGA from ALA 2001; il valore che ho messo nella colonna Shape file viene da una media che ho calcolato sulle PGA dei tanks del SCWC			1		SCWC 2	15.8	9.8	0.62				welded			water		Survived
Northridge	1994	6.69	Southern California Water Company (SCWC), Simi Valley			general area of the other (riferito a SCWC, Simi Valley)	0.571363636	0.571363636		0.7					PGA from ALA 2001; il valore che ho messo nella colonna Shape file viene da una media che ho calcolato sulle PGA dei tanks del SCWC			1		SCWC 3	27.4	9.8	0.36				welded			water		Survived
Northridge	1994	6.69	Southern California Water Company (SCWC), Simi Valley			general area of the other (riferito a SCWC, Simi Valley)	0.571363636	0.571363636		0.7					PGA from ALA 2001; il valore che ho messo nella colonna Shape file viene da una media che ho calcolato sulle PGA dei tanks del SCWC			1		SCWC 4	39.0	9.8	0.25				welded			water		Survived
Northridge	1994	6.69	City of Los Angeles, Department of Water and Power (CLADWP); San Fernando Valley	14		circa (cercando il nome del tank su google viene fuori una località)	0.38	0,36-0,40	0.38	0.4					PGA from ALA 2001			1		Topanga	11.0	9.0	0.82		wood		welded		0	water	0.9	No tank damage, replaced broken inlet/outlet valve. Loss of contents
Northridge	1994	6.69	City of Los Angeles, Department of Water and Power (CLADWP); San Fernando Valley				0.36		0.22	0.5					PGA from ALA 2001			1		Zelzah	21.3	12.2	0.57		wood		welded		0	water	0.81	Wood roof collapsed, local buckling at top, broken valve. Loss of contents
Northridge	1994	6.69	City of Los Angeles, Department of Water and Power (CLADWP); San Fernando Valley				0.315		0.23	0.4					PGA from ALA 2001			1		Mulholland	15.8	10.2	0.64		wood		welded		0	water	0	Overflow pipe pulled away. Loss of contents
Northridge	1994	6.69	City of Los Angeles, Department of Water and Power (CLADWP); San Fernando Valley	13		circa (cercando il nome del tank su google viene fuori una località)	0.48	0.48	0.28	0.5					PGA from ALA 2001			1		Beverly Glen	30.5	12.3	0.41		wood		riveted		0	water		Wood roof collapsed, local buckling, dressed coupling pulled out. Loss of contents
Northridge	1994	6.69	City of Los Angeles, Department of Water and Power (CLADWP); San Fernando Valley				0.83		0.96	0.7					PGA from ALA 2001			1		Jensen Clearwell	42.7	12.2	0.29						0	water	0.96	No tank damage
Northridge	1994	6.69	City of Los Angeles, Department of Water and Power (CLADWP); San Fernando Valley	15		circa (cercando il nome del tank su google viene fuori una località)	0.23		0.16	0.3					PGA from ALA 2001			1		Coldwater	30.4804	12.34455	0.405		wood		riveted		0	water		Wood roof shifted and collapsed, piping failure. Loss of contents

Northridge	1994	6.69	City of Los Angeles, Department of Water and Power (CLADWP); San Fernando Valley				0.68	0.68	0.46	1				PGA from ALA 2001			1		Granada High	16.8	10.7	0.64		wood		riveted		0	water	0.9	Tank collapsed and removed. This tank had also suffered damage in the San Fernando EQ
Northridge	1994	6.69	City of Los Angeles, Department of Water and Power (CLADWP); San Fernando Valley	17			0.66	0.66	0.9	0.6				PGA from ALA 2001			1		Alta Vista 1	16.5	8.8	0.54		wood		riveted		0	water	1	No tank damage
Northridge	1994	6.69	City of Los Angeles, Department of Water and Power (CLADWP); San Fernando Valley	17			0.66	0.66	0.9	0.6				PGA from ALA 2001			1		Alta Vista 2	29.0	11.1	0.38		wood		welded		0	water	0.84	No tank damage
Northridge	1994	6.69	City of Los Angeles, Department of Water and Power (CLADWP); San Fernando Valley				0.275		0.25	0.3				PGA from ALA 2001			1		Altaview	19.8	13.0	0.65						0	water	0.97	Settlement
Northridge	1994	6.69	City of Los Angeles, Department of Water and Power (CLADWP); San Fernando Valley				0.44	0.44	0.4	0.3				PGA from ALA 2001			1		Kittridge 3	57.9	15.5	0.27		wood		welded		0	water		No damage
Northridge	1994	6.69	City of Los Angeles, Department of Water and Power (CLADWP); San Fernando Valley				0.44	0.44	0.4	0.3				PGA from ALA 2001			1		Kittridge 4	57.9	15.5	0.27		wood		welded		0	water		No damage
Northridge	1994	6.69	City of Los Angeles, Department of Water and Power (CLADWP); San Fernando Valley				0.38	0.38	0.38	0.43				PGA from ALA 2001			1		Corbin	47.5	9.1	0.19		wood		welded		0	water	0.84	Minor draw line damage, partially buried
Northridge	1994	6.69	City of Los Angeles, Department of Water and Power (CLADWP); San Fernando Valley				0.34		0.38	0.3				PGA from ALA 2001			1		Donick	37.4	7.3	0.20				welded		0		0.94	No tank damage
Northridge	1994	6.69	City of Los Angeles, Department of Water and Power (CLADWP)				0.62	0.62		0.56				PGA from ALA 2001 (Assumed same PGA as Magic Mountain tanks (also located at Valencia))			1		Santa Clarita	24.38	12.19	0.50				welded				0.98	EFB, Roof damage
Northridge	1994	6.69	Valencia Water Company; Valencia	23.2			0.56	0.56		0.56	0.56	0.34	0.39	PGA from ALA 2001 (Inoltre da cooper vedo che a 1,5 km c'è una Pardee Substation che registra 180= 0,56g; up=0,39; 090=0,34			1		Round Mountain	40.2	9.8	0.24				welded			water	0.93	No tank damage
Northridge	1994	6.69	Valencia Water Company; Valencia	27.2			0.45	0.45		0.5				PGA from ALA 2001			1		Hasley	36.6	12.2	0.33				welded			water	0.93	No tank damage
Northridge	1994	6.69	Valencia Water Company; Valencia	20.5				0,54-0,56		0.56				PGA from ALA 2001				1	Magic Mountain II	22.3	7.3	0.33				bolted			water	0.84	Failed, hit by Magic Mountain I
Northridge	1994	6.69	Valencia Water Company; Valencia	20.5			0.55	0,54-0,56		0.56				PGA from ALA 2001			1		Magic Mountain I	18.3	7.3	0.4				bolted			water	0.84	Complete failure, tearing of bottom shell course at base
Northridge	1994	6.69	Valencia Water Company; Valencia	20.5			0.55	0,54-0,56		0.56				PGA from ALA 2001			1		Magic Mountain III	24.4	9.8	0.40		external roof rafters		welded			water	0.93	No damage, this tank partially buried 2,5 feet
Northridge	1994	6.69	Valencia Water Company; Valencia	27.2			0.446	0.446		0.5				PGA from ALA 2001			1		Presley	21.3	9.7537186	0.46				welded			water	0.93	No damage
Northridge	1994	6.69	Valencia Water Company; Valencia	19			0.557	0.557		0.55				PGA from ALA 2001			1		4 Million	45.7	9.1	0.2				welded			water	0.93	No damage
Northridge	1994	6.69	Valencia Water Company; Valencia	26.4			0.465	0.465		0.43				PGA from ALA 2001			1		Seco	22.3	7.3	0.33				welded			water	0.92	No damage
Northridge	1994	6.69	Valencia Water Company; Valencia	17			0.58	0.58		0.55				PGA from ALA 2001			1		Larwin	18.3	12.2	0.67			concrete ring foundation	welded		1	water	0.8	Complete failure, EFB, broken piping connection, roof/shell joint failure
Northridge	1994	6.69	Valencia Water Company; Valencia	19			0.544	0.544		0.55				PGA from ALA 2001			1		Poe	27.4	9.8	0.36				welded			water	0.93	Roof rafter damage, sagging of the roof, NO LOC
Northridge	1994	6.69	Valencia Water Company; Valencia	26.4			0.465	0.465		0.43				PGA from ALA 2001			1		Paragon	22.3	9.8	0.44				welded			water	0.93	No damage
Northridge	1994	6.69	Newhall County Water District (NCWD); Newhall				0.63			0.63				PGA from ALA 2001 (Cooper: "a California Strong Motion Instrument Program (CSMIP) accelerometer was located at the Newhall Fire Station, near the center of the service area of the district; Its maximum reading were: 90°, 0,63g; 360°, 0,61g and 0,62g vertical			1		Newhall 1	18.3	9.1	0.50				welded		0	water	0.9	EFB, collapse, piping damage
Northridge	1994	6.69	Newhall County Water District (NCWD); Newhall	16.4			0.636	0.636		0.63	0.63	0.61	0.62	PGA from ALA 2001 (Cooper: "a California Strong Motion Instrument Program (CSMIP) accelerometer was located at the Newhall Fire Station, near the center of the service area of the district; Its maximum reading were: 90°, 0,63g; 360°, 0,61g and 0,62g vertical			1		Newhall 2	12.2	9.8	0.8			gravel pad	welded		0	water	0.9	Broken/pullout piping, EFB, foundation settling
Northridge	1994	6.69	Newhall County Water District (NCWD); Newhall	15.7			0.626	0.626		0.63	0.63	0.61	0.62	PGA from ALA 2001 (Cooper: "a California Strong Motion Instrument Program (CSMIP) accelerometer was located at the Newhall Fire Station, near the center of the service area of the district; Its maximum reading were: 90°, 0,63g; 360°, 0,61g and 0,62g vertical			1		Newhall 3	12.2	9.8	0.8			gravel pad	welded		0	water	0.9	Broken/pullout piping, EFB, foundation settling
Northridge	1994	6.69	Newhall County Water District (NCWD); Newhall	16.2			0.61	0.61		0.63	0.63	0.61	0.62	PGA from ALA 2001 (Cooper: "a California Strong Motion Instrument Program (CSMIP) accelerometer was located at the Newhall Fire Station, near the center of the service area of the district; Its maximum reading were: 90°, 0,63g; 360°, 0,61g and 0,62g vertical			1		Newhall 4	12.2	9.8	0.8			gravel pad	welded		0	water	0.9	Broken/pullout piping, EFB, foundation settling, roof rafters pulled out
Northridge	1994	6.69	Newhall County Water District (NCWD); Newhall	18			0.61	0.61		0.63	0.63	0.61	0.62	PGA from ALA 2001 (Cooper: "a California Strong Motion Instrument Program (CSMIP) accelerometer was located at the Newhall Fire Station, near the center of the service area of the district; Its maximum reading were: 90°, 0,63g; 360°, 0,61g and 0,62g vertical			1		Newhall 5	19.5	9.8	0.5				welded		0	water	0.9	Roof rafter damage, EFB, inlet/oulet piping sheared
Northridge	1994	6.69	Newhall County Water District (NCWD); Newhall	15.2			0.629	0.629		0.63	0.63	0.61	0.62	PGA from ALA 2001 (Cooper: "a California Strong Motion Instrument Program (CSMIP) accelerometer was located at the Newhall Fire Station, near the center of the service area of the district; Its maximum reading were: 90°, 0,63g; 360°, 0,61g and 0,62g vertical			1		Newhall 6	6.1	6.1	1				welded		0	water	0.9	EFB, piping failure, plate failure, tank replaced
Northridge	1994	6.69	Newhall County Water District (NCWD); Newhall	16.2			0.61	0.61		0.63	0.63	0.61	0.62	PGA from ALA 2001 (Cooper: "a California Strong Motion Instrument Program (CSMIP) accelerometer was located at the Newhall Fire Station, near the center of the service area of the district; Its maximum reading were: 90°, 0,63g; 360°, 0,61g and 0,62g vertical			1		Newhall 7	27.4	9.8	0.36		fixed	concrete ring foundation	welded		0	water	0.9	Roof shell seam opened, rafters fell, NO EFB

Northridge	1994	6.69	Newhall County Water District (NCWD); Newhall	14.3			0.64	0.64		0.63	0.63	0.61	0.62		PGA from ALA 2001 (Cooper: "a California Strong Motion Instrument Program (CSMIP) accelerometer was located at the Newhall Fire Station, near the center of the service area of the district; Its maximum reading were: 90°, 0,63g; 360°, 0,61g and 0,62g vertical			1		Newhall 8	18.3	7.3	0.4				welded		0	water	0.9	Roof rafters pulled away from the shell, roof damage
Northridge	1994	6.69	Newhall County Water District (NCWD); Newhall	18			0.626	0.626		0.63	0.63	0.61	0.62		PGA from ALA 2001 (Cooper: "a California Strong Motion Instrument Program (CSMIP) accelerometer was located at the Newhall Fire Station, near the center of the service area of the district; Its maximum reading were: 90°, 0,63g; 360°, 0,61g and 0,62g vertical			1		Newhall 10	24.4	12.2	0.5			concrete ring foundation	welded		0	water	0.9	No apparent damage
Northridge	1994	6.69	American National Can site in Northridge				0.344			0.344					Free field motion recorded at the Arleta site, which is fairly close the tank site			1			11.3	9.8	0.86			concrete pad foundation			0	water	0.9	Compression failure in its shell; tank uplifted about 30 cm and, when dropped, it severed the adjacent piping and release its content. it appears that the current American Water Works Association code is sufficiently conservative for the design of tank shells and baseplates, but flexibility in the adjacent piping must be emphasized. Numerous other tanks had damaged piping because of inadequate flexibility in the piping.
Loma Prieta	1989	6.93	Richmond Terminal	108			0.12	0.12		0,13 (ASA2001)	0.11	0.13	0.04		Accelerometers values from Cooper: 280°= 0,11g ; UP = 0,04; 190°=0,13	tidewater with no good soil conditions		1		Richmond 1	12.8	12.2	0.95			all tanks are on pile foundation with a continuous concrete pile cap					0.9	EFB, pipe supports pulled from tank shell
Loma Prieta	1989	6.93	Richmond Terminal	108			0.12	0.12		0,13 (ASA2001)	0.11	0.13	0.04		Accelerometers values from Cooper: 280°= 0,11g ; UP = 0,04; 190°=0,13	tidewater with no good soil conditions		1		Richmond 2	12.8	12.2	0.95			all tanks are on pile foundation with a continuous concrete pile cap					0.9	EFB, pipe supports pulled from tank shell
Loma Prieta	1989	6.93	Richmond Terminal	108			0.12	0.12		0,13 (ASA2001)	0.11	0.13	0.04		Accelerometers values from Cooper: 280°= 0,11g ; UP = 0,04; 190°=0,13	tidewater with no good soil conditions		1		Richmond 3			0.95			all tanks are on pile foundation with a continuous concrete pile cap					0.9	EFB, pipe supports pulled from tank shell
Loma Prieta	1989	6.93	Richmond Terminal	108			0.12	0.12		0,13 (ASA2001)	0.11	0.13	0.04		Accelerometers values from Cooper: 280°= 0,11g ; UP = 0,04; 190°=0,13	tidewater with no good soil conditions		1		Richmond 4			0.95			all tanks are on pile foundation with a continuous concrete pile cap					0.5	EFB, pipe supports pulled from tank shell
Loma Prieta	1989	6.93	Richmond Terminal	108			0.12	0.12		0,13 (ASA2001)	0.11	0.13	0.04		Accelerometers values from Cooper: 280°= 0,11g ; UP = 0,04; 190°=0,13	tidewater with no good soil conditions		1		Richmond 5			0.95			all tanks are on pile foundation with a continuous concrete pile cap					0.5	EFB, pipe supports pulled from tank shell
Loma Prieta	1989	6.93	Richmond Terminal	108			0.12	0.12		0,13 (ASA2001)	0.11	0.13	0.04		Accelerometers values from Cooper: 280°= 0,11g ; UP = 0,04; 190°=0,13	tidewater with no good soil conditions		15		Richmond 6-20			0.95			all tanks are on pile foundation with a continuous concrete pile cap					0.5	pipe supports pulled from tank shell
Loma Prieta	1989	6.93	Richmond Terminal	108			0.12	0.12		0,13 (ASA2001)	0.11	0.13	0.04		Accelerometers values from Cooper: 280°= 0,11g ; UP = 0,04; 190°=0,13	tidewater with no good soil conditions		12		Lube 1-12	3.7	7.3	2.00						0	lubricating oil	0.25	No apparent damage
Loma Prieta	1989	6.93	Richmond Terminal	108			0.12	0.12		0,13 (ASA2001)	0.11	0.13	0.04		Accelerometers values from Cooper: 280°= 0,11g ; UP = 0,04; 190°=0,13	tidewater with no good soil conditions		1		Lube 13	3.7	15.2	4.17						1	lubricating oil	0.25	Anchor bolt restraining and bending bottom plate
Loma Prieta	1989	6.93	Richmond Terminal	108			0.12	0.12		0,13 (ASA2001)	0.11	0.13	0.04		Accelerometers values from Cooper: 280°= 0,11g ; UP = 0,04; 190°=0,13	tidewater with no good soil conditions		1		Lube 14	3.7	15.2	4.17						1	lubricating oil	0.25	Anchor bolt restraining and bending bottom plate
Loma Prieta	1989	6.93	Richmond Terminal	108			0.12	0.12		0,13 (ASA2001)	0.11	0.13	0.04		Accelerometers values from Cooper: 280°= 0,11g ; UP = 0,04; 190°=0,13	tidewater with no good soil conditions		10		Lube 15-24	3.7	15.2	4.17						0	lubricating oil	0.25	No apparent damage
Loma Prieta	1989	6.93	Richmond Terminal	108			0.12	0.12		0,13 (ASA2001)	0.11	0.13	0.04		Accelerometers values from Cooper: 280°= 0,11g ; UP = 0,04; 190°=0,13	tidewater with no good soil conditions		12		Lube 25-36	3.7	11.0	3						0	lubricating oil	0.25	No apparent damage
Loma Prieta	1989	6.93	Richmond Terminal	108			0.12	0.12		0,13 (ASA2001)	0.11	0.13	0.04		Accelerometers values from Cooper: 280°= 0,11g ; UP = 0,04; 190°=0,13	tidewater with no good soil conditions		12		Lube 37-48	6.4	12.2	1.90						0	lubricating oil	0.25	No apparent damage
Loma Prieta	1989	6.93	Richmond Terminal	108			0.12	0.12		0,13 (ASA2001)	0.11	0.13	0.04		Accelerometers values from Cooper: 280°= 0,11g ; UP = 0,04; 190°=0,13	tidewater with no good soil conditions		11		Lube 49-59	9.1	12.2	1.33						0	lubricating oil	0.25	No apparent damage
Loma Prieta	1989	6.93	Richmond Terminal	108			0.12	0.12		0,13 (ASA2001)	0.11	0.13	0.04		Accelerometers values from Cooper: 280°= 0,11g ; UP = 0,04; 190°=0,13	tidewater with no good soil conditions		1		Lube 60	9.1	12.2	1.33		floating				0	lubricating oil	1	EFB; Walkway between this tank and another pulled loose and fell to ground
Loma Prieta	1989	6.93	San Jose Terminal	40			0.253	0.253		0,17 (ASA2001)	0.16	0.17	0.1		Accelerometers values from Cooper: 090°= 0,16g ; UP = 0,10; 360°=0,17. The station, called AGNEWS, is about 5 km from San Jose	alluvium soils= good foundation soils		1		San Jose 1	23.5	14.6	0.62			cone roof with an internal floating pan				gasoline	0.95	Severe bending and buckling of the internal pan. The pan sink after damage. NO LOC
Loma Prieta	1989	6.93	San Jose Terminal	40			0.253	0.253		0,17 (ASA2001)	0.16	0.17	0.1		Accelerometers values from Cooper: 090°= 0,16g ; UP = 0,10; 360°=0,17. The station, called AGNEWS, is about 5 km from San Jose	alluvium soils= good foundation soils		1		San Jose 2	26.8	14.6	0.55			cone roof with an internal floating pan				turbin fuel	0.95	Severe bending and buckling of the internal pan. The pan sink after damage. NO LOC
Loma Prieta	1989	6.93	San Jose Terminal	40			0.253	0.253		0,17 (ASA2001)	0.16	0.17	0.1		Accelerometers values from Cooper: 090°= 0,16g ; UP = 0,10; 360°=0,17. The station, called AGNEWS, is about 5 km from San Jose	alluvium soils= good foundation soils		30		San Jose 3-30	19.8122	14.630578	0.74			cone roof with an internal floating pan						No apparent damage
Loma Prieta	1989	6.93	Brismane Terminal	85			0.194	0.194		0,11 (ASA2001)	0.11	0.05	0.06		Accelerometers values from Cooper: 205°= 0,11g ; UP = 0,05; 115°=0,06. The station, called SSF SIERRA PT (2 km from Brismane terminal)	Hillside location with good foundation conditions		3		Brismane 1-3	30.5	9.1	0.3									No apparent damage
Loma Prieta	1989	6.93	Brismane Terminal	85			0.194	0.194		0,11 (ASA2001)	0.11	0.05	0.06		Accelerometers values from Cooper: 205°= 0,11g ; UP = 0,05; 115°=0,06. The station, called SSF SIERRA PT (2 km from Brismane terminal)	Hillside location with good foundation conditions		8		Brismane 4-11	19.8	13.4	0.68									No apparent damage
Loma Prieta	1989	6.93	Brismane Terminal	85			0.194	0.194		0,11 (ASA2001)	0.11	0.05	0.06		Accelerometers values from Cooper: 205°= 0,11g ; UP = 0,05; 115°=0,06. The station, called SSF SIERRA PT (2 km from Brismane terminal)	Hillside location with good foundation conditions		6		Brismane 12-17	12.2	14.6	1.2									No apparent damage
Loma Prieta	1989	6.93	Gilroy	28			0.5			0,50 (ASA2001)	0.5	0.43	0.22		Accelerometers values from Cooper: 090°= 0,50g ; UP = 0,22; 360°=0,43. The station is called Gilroy	sandstone		1		Gilroy	24.4	7.9	0.33							water	0.95	No apparent damage
Loma Prieta	1989	6.93	Moss landing	22			0.36	0.36		0.24					ASA2001 dice 0,24g (PGA based on attenuation)			1		PG&E Moss Landing 1	17.1	12.2	0.71			poorly founded on crushed rock	weld		0	water	0.9	Failed at floor/shell connection (junction possibly corroded) initiated by uplift of the tank at the bottom rupture location possibly combined with settlement of the aggregate on the opposite side from the rupture. The tank base then receiving insufficient support directly from the foundation, overloaded the shell to base plate connection. The roof/shell connection failure and buckling of the shell may have been caused by liquid sloshing effects or may be the result of the rapid emptying of the tank creating a partical vacuum within the ullage space. The observed evidence is consistent with either possible cause. Tank drained rapidly and shell in the top course buckled for vacuum. Roof/shell connection damage
Loma Prieta	1989	6.93	Moss landing	22			0.36	0.36		0.24					ASA2001 dice 0,24g (PGA based on attenuation)			1		PG&E Moss Landing 2	17.1	12.2	0.71	USGS1998 dice solo che è un tenak da 750,000gal ma io , come anche ALA2001, abbiamo supposto le stesse dimensioni			weld			water	0.9	Piping failure with loss of contents
Loma Prieta	1989	6.93	Moss landing	22			0.36	0.36		0.24					ASA2001 dice 0,24g (PGA based on attenuation)			1		PG&E Moss Landing 3	17.1	12.2	0.71	USGS1998 dice solo che è un tenak da 750,000gal ma io , come anche ALA2001, abbiamo supposto le stesse dimensioni			weld			water	0.9	Piping failure with loss of contents
Loma Prieta	1989	6.93	Los Gatos, San Jose	23			0.5	0,44-0,56		0.28					ASA2001 dice 0,28g (PGA based on attenuation)			1		Los Gatos SJ 1			1.1				bolted		0	water	0.95	EFB
Loma Prieta	1989	6.93	Los Gatos, San Jose	23			0.5	0,44-0,56		0.28					ASA2001 dice 0,28g (PGA based on attenuation)			1		Los Gatos SJ 2			0.3				welded					The inlet/outlet underneath separeted from the floor plate
Loma Prieta	1989	6.93	Wastonville	18			0.4175	0,395-0,44		0.54					ASA2001 dice 0,54g			1		Wastonville 1			0.3						water	0.95	Buckled on one side at the roof/shell joint but NO LOC. Also at this tank, the pilot line on the altitude valve broke, causing a minor leak. In spite of this damage, the tank did not leak and continued to operate
Loma Prieta	1989	6.93	Wastonville	18			0.4175	0,395-0,45		0.54					ASA2001 dice 0,54g			1		Wastonville 2			0.3						water	0.95	No damage
Loma Prieta	1989	6.93	Santa Cruz, Scotts Valley	12			0.55	0,46-0,64		0.47		0.44	0.4		ASA2001 dice 0,47g . Santa Cruz Station 090°=0,44; UP=0,40; 360°=0,47			1		Santa Cruz 1/ Scotts Valley			0.3		wood	concrete ringwall	welded		0		0.95	Tank damaged at the wood roof connection to the tank shell. The tank drained because its inflow and outflow pipes broke
Loma Prieta	1989	6.93	Santa Cruz, Scotts Valley	12			0.55	0,46-0,64		0.47		0.44	0.4		ASA2001 dice 0,47g . Santa Cruz Station 090°=0,44; UP=0,40; 360°=0,47			1		Santa Cruz 2/ Scotts Valley			1.1		wood	concrete ringwall	welded		0		0.95	Tank damaged at the wood roof connection to the tank shell. The tank drained because its inflow and outflow pipes broke
Loma Prieta	1989	6.93	Santa Cruz, Scotts Valley	12			0.55	0,46-0,64		0.47		0.44	0.4		ASA2001 dice 0,47g . Santa Cruz Station 090°=0,44; UP=0,40; 360°=0,47	bedrock		1		Santa Cruz 3			0.3			concrete ring	welded		0	water	0.95	No damage
Loma Prieta	1989	6.93	Hollister	46			0.32	0,28-0,36		0.1					ASA2001 dice 0,1g (PGA based on attenuation)			1		Hollister 1			0.3				welded				0.95	No damage

Loma Prieta	1989	6.93	Pajaro	19			0.395	0.395								river bottom, a potentially liquefiable area		1		Pajaro 1			0.3			wick (vertical gravel) drains foundation	welded		0	water		No damage
Loma Prieta	1989	6.93	Sunny Mesa	19			0.395	0.395										1					1.1				welded					was tilted with its base lifted off its foundation on one side and settled as much as 2 in. on the other side; however, it did not leak. An 8 -in.-diameter tee on the inlet/outlet broke and released all but 4 ft of water in the tank before the tank outlet valve was closed
Loma Prieta	1989	6.93	Moss landing	22			0.36	0.36		0.24					ASA2001 dice 0,24g (PGA based on attenuation)			4	ne vedo 4 in foto ma saranno di più		50	12	0.24							oil		No damage
Loma Prieta	1989	6.93	Gonzales	72				0.2											10	10 of 100	6	10	1.66667			concrete plinth of 0,8 m high		stainless steel	1	wine	0.26	The tanks are also fixed to the base through a bottom exit pipe nozzle which is connected to a trough embedded in the concrete (Figure 6.2). The leakage failure occurred at the weld of the trough section to the tank shell wall. The connection, on rocking movement of the tank, and the uplift of the tank wall, was unable to deform sufficiently to accommodate the relative movement between tank wall and the fixed trough.
Loma Prieta	1989	6.93	Gonzales	72				0.2											90	90 of 100			1.1	>1		concrete plinth of 0,8 m high		stainless steel	1	wine		No damage
Loma Prieta	1989	6.93	Unocal Terminal	108				0.12			0.11	0.13	0.04		Accelerometers values from Cooper: 280°= 0,11g ; UP = 0,04; 190°=0,13	tidewater with no good soil conditions				1			0.3			tank foundations were pads on piles			0	gasoline or lube oil	0.9	(damage was associated with uplift and overturning of tank walls; uplift was measured at between 6 in. and 8 in) this tank was cracked vertically at the bottom plate
Loma Prieta	1989	6.93	Unocal Terminal	108				0.12			0.11	0.13	0.04		Accelerometers values from Cooper: 280°= 0,11g ; UP = 0,04; 190°=0,13	tidewater with no good soil conditions				1			0.3			tank foundations were pads on piles			0	gasoline or lube oil	0.9	(damage was associated with uplift and overturning of tank walls; uplift was measured at between 6 in. and 8 in) This tank ruptured when a lateral pipe support, attached to the tank side wall and to a restrained foam line, tore a hole in the sidewall when the tank wall moved up.
Loma Prieta	1989	6.93	Unocal Terminal	108				0.12			0.11	0.13	0.04		Accelerometers values from Cooper: 280°= 0,11g ; UP = 0,04; 190°=0,13	tidewater with no good soil conditions				1			0.3			tank foundations were pads on piles			0	gasoline or lube oil	0.9	(damage was associated with uplift and overturning of tank walls; uplift was measured at between 6 in. and 8 in) This tank had a classic elephant-foot buckle near the bottom and ruptured at the side wall-bottom plate connection.
Loma Prieta	1989	6.93	Unocal Terminal	108				0.12			0.11	0.13	0.04		Accelerometers values from Cooper: 280°= 0,11g ; UP = 0,04; 190°=0,13	tidewater with no good soil conditions				1			0.3			tank foundations were pads on piles			0	gasoline or lube oil	0.9	(damage was associated with uplift and overturning of tank walls; uplift was measured at between 6 in. and 8 in) This tank had a classic elephant-foot buckle near the bottom
Loma Prieta	1989	6.93	Unocal Terminal	108				0.12			0.11	0.13	0.04		Accelerometers values from Cooper: 280°= 0,11g ; UP = 0,04; 190°=0,13	tidewater with no good soil conditions				1			0.3			tank foundations were pads on piles			0	gasoline or lube oil	0.9	(damage was associated with uplift and overturning of tank walls; uplift was measured at between 6 in. and 8 in) This tank had a classic elephant-foot buckle near the bottom
Loma Prieta	1989	6.93	Unocal Terminal	108				0.12			0.11	0.13	0.04		Accelerometers values from Cooper: 280°= 0,11g ; UP = 0,04; 190°=0,13	tidewater with no good soil conditions				1			0.3			tank foundations were pads on piles			0	gasoline or lube oil	0.9	(damage was associated with uplift and overturning of tank walls; uplift was measured at between 6 in. and 8 in)
Loma Prieta	1989	6.93	Unocal Terminal	108				0.12			0.11	0.13	0.04		Accelerometers values from Cooper: 280°= 0,11g ; UP = 0,04; 190°=0,13	tidewater with no good soil conditions			other similar tanks that were undamaged were either partially full or empty.	6			0.3			tank foundations were pads on piles				gasoline or lube oil	0.4	No damage
Loma Prieta	1989	6.93	Texaco Terminal	108			0.12	0.12			0.11	0.13	0.04		Accelerometers values from Cooper: 280°= 0,11g ; UP = 0,04; 190°=0,13	tidewater with no good soil conditions		1		20002/Texaco	16.8	14.6	0.87			concrete ringwall	welded			gasoline	0.85	Failure of overconstrained piping_bottom penetration
Loma Prieta	1989	6.93	Texaco Terminal	108			0.12	0.12			0.11	0.13	0.04		Accelerometers values from Cooper: 280°= 0,11g ; UP = 0,04; 190°=0,13	tidewater with no good soil conditions		1		20001/Texaco	16.8	14.6	0.87				welded			diesel	0.39	No damage
Loma Prieta	1989	6.93	Texaco Terminal	108			0.12	0.12			0.11	0.13	0.04		Accelerometers values from Cooper: 280°= 0,11g ; UP = 0,04; 190°=0,13	tidewater with no good soil conditions		1		20003/Texaco	16.8	14.6	0.87				welded			gasoline	0.54	No damage
Loma Prieta	1989	6.93	Texaco Terminal	108			0.12	0.12			0.11	0.13	0.04		Accelerometers values from Cooper: 280°= 0,11g ; UP = 0,04; 190°=0,13	tidewater with no good soil conditions		1		20008/Texaco	16.5	14.9	0.91				welded			gasoline	0.77	Roof walkways jumped off rails
Loma Prieta	1989	6.93	Texaco Terminal	108			0.12	0.12			0.11	0.13	0.04		Accelerometers values from Cooper: 280°= 0,11g ; UP = 0,04; 190°=0,13	tidewater with no good soil conditions		1		20009/Texaco	16.5	14.9	0.91				welded			gasoline	0.46	No damage
Loma Prieta	1989	6.93	Texaco Terminal	108			0.12	0.12			0.11	0.13	0.04		Accelerometers values from Cooper: 280°= 0,11g ; UP = 0,04; 190°=0,13	tidewater with no good soil conditions		1		20010/Texaco	16.5	14.9	0.91				welded			gasoline	0.25	Roof walkways jumped off rails
Loma Prieta	1989	6.93	Texaco Terminal	108			0.12	0.12			0.11	0.13	0.04		Accelerometers values from Cooper: 280°= 0,11g ; UP = 0,04; 190°=0,13	tidewater with no good soil conditions		1					0.3						0	water	0.9	The damage was associated with uplift and overturning. The bottom pipe outlet was allowed 2-1/2 in. of uplift before it was constrained. Because the uplift was greater than 2 1/2 in., the outlet yanked on the bottom causing a leak.
Kern County	1952	7.36	Pentland Station	25			0.190852678	Modified Mercalli Intensity Scale: VII (-VIII)		0,19 (ASA2001)	0.17	0.19	0.11		Accelerometers values from Cooper: 021°=0,17, up=0,11. 111°=0,19; (Taft instrument is not at the site of tanks and it is at 41 km NW of the epicenter). La PGA selezionata viene da ATTENUATION CURVES (foglio alla fine del file excel)_reverse faulting	alluvium soil	C	1		550x81	34.9	9.1	0.26		fixed		riveted			petroleum prodacts	0.13	Bottom ring bulged 1/4''
Kern County	1952	7.36	Pentland Station	25			0.190852678	Modified Mercalli Intensity Scale: VII (-VIII)		0,19 (ASA2001)	0.17	0.19	0.11		Accelerometers values from Cooper: 021°=0,17, up=0,11. 111°=0,19; (Taft instrument is not at the site of tanks and it is at 41 km NW of the epicenter). La PGA selezionata viene da ATTENUATION CURVES (foglio alla fine del file excel)_reverse faulting	alluvium soil	C	1		550x82	34.9	9.1	0.26		floating		riveted			petroleum prodacts	0.63	No damage
Kern County	1952	7.36	Pentland Station	25			0.190852678	Modified Mercalli Intensity Scale: VII (-VIII)		0,19 (ASA2001)	0.17	0.19	0.11		Accelerometers values from Cooper: 021°=0,17, up=0,11. 111°=0,19; (Taft instrument is not at the site of tanks and it is at 41 km NW of the epicenter). La PGA selezionata viene da ATTENUATION CURVES (foglio alla fine del file excel)_reverse faulting	alluvium soil	C	1		550x83	34.9	9.1	0.26		fixed		riveted			petroleum prodacts	0.09	Earth imprints by bottom edge
Kern County	1952	7.36	Pentland Station	25			0.190852678	Modified Mercalli Intensity Scale: VII (-VIII)		0,19 (ASA2001)	0.17	0.19	0.11		Accelerometers values from Cooper: 021°=0,17, up=0,11. 111°=0,19; (Taft instrument is not at the site of tanks and it is at 41 km NW of the epicenter). La PGA selezionata viene da ATTENUATION CURVES (foglio alla fine del file excel)_reverse faulting	alluvium soil	C	1		550x84	34.9	9.1	0.26		floating		riveted			petroleum prodacts	0.6	some oil splashed onto top
Kern County	1952	7.36	Pentland Station	25			0.190852678	Modified Mercalli Intensity Scale: VII (-VIII)		0,19 (ASA2001)	0.17	0.19	0.11		Accelerometers values from Cooper: 021°=0,17, up=0,11. 111°=0,19; (Taft instrument is not at the site of tanks and it is at 41 km NW of the epicenter). La PGA selezionata viene da ATTENUATION CURVES (foglio alla fine del file excel)_reverse faulting	alluvium soil	C	1		550x85	35.0	9.1	0.26		fixed		riveted			petroleum prodacts	0.31	No damage
Kern County	1952	7.36	Pentland Station	25			0.190852678	Modified Mercalli Intensity Scale: VII (-VIII)		0,19 (ASA2001)	0.17	0.19	0.11		Accelerometers values from Cooper: 021°=0,17, up=0,11. 111°=0,19; (Taft instrument is not at the site of tanks and it is at 41 km NW of the epicenter). La PGA selezionata viene da ATTENUATION CURVES (foglio alla fine del file excel)_reverse faulting	alluvium soil	C	1		550x86	34.9	9.1	0.26		floating		riveted			petroleum prodacts	0.91	Approx. 15 seals damaged, oil splashed over side, earth imprints by bottom edge
Kern County	1952	7.36	Emidio Station	7.7			0.351058278	Modified Mercalli Intensity Scale: VIII		0,19 (ASA2001)	0.17	0.19	0.11		Accelerometers values from Cooper: 021°=0,17, up=0,11. 111°=0,19; (Taft instrument is not at the site of tanks and it is at 41 km NW of the epicenter). La PGA selezionata viene da ATTENUATION CURVES (foglio alla fine del file excel)_reverse faulting	alluvium soil	C	1		37003	28.7	9.2	0.32		floating		riveted			petroleum prodacts	0.29	Oil splashed onto roof
Kern County	1952	7.36	Emidio Station	7.7			0.351058278	Modified Mercalli Intensity Scale: VIII		0,19 (ASA2001)	0.17	0.19	0.11		Accelerometers values from Cooper: 021°=0,17, up=0,11. 111°=0,19; (Taft instrument is not at the site of tanks and it is at 41 km NW of the epicenter). La PGA selezionata viene da ATTENUATION CURVES (foglio alla fine del file excel)_reverse faulting	alluvium soil	C	1		37014	28.7	9.1	0.32		fixed		riveted			petroleum prodacts	0.63	No damage
Kern County	1952	7.36	Emidio Station	7.7			0.351058278	Modified Mercalli Intensity Scale: VIII		0,19 (ASA2001)	0.17	0.19	0.11		Accelerometers values from Cooper: 021°=0,17, up=0,11. 111°=0,19; (Taft instrument is not at the site of tanks and it is at 41 km NW of the epicenter). La PGA selezionata viene da ATTENUATION CURVES (foglio alla fine del file excel)_reverse faulting	alluvium soil	C	1		550x79	35.0	9.1	0.26		floating		riveted			petroleum prodacts	0.15	No damage
Kern County	1952	7.36	Emidio Station	7.7			0.351058278	Modified Mercalli Intensity Scale: VIII		0,19 (ASA2001)	0.17	0.19	0.11		Accelerometers values from Cooper: 021°=0,17, up=0,11. 111°=0,19; (Taft instrument is not at the site of tanks and it is at 41 km NW of the epicenter). La PGA selezionata viene da ATTENUATION CURVES (foglio alla fine del file excel)_reverse faulting	alluvium soil	C	1		800x11	35.7	12.7	0.36		fixed		riveted			petroleum prodacts	0.24	No damage
Kern County	1952	7.36	Rose Station	7.7			0.351058278	Modified Mercalli Intensity Scale: VIII		0,19 (ASA2001)	0.17	0.19	0.11		Accelerometers values from Cooper: 021°=0,17, up=0,11. 111°=0,19; (Taft instrument is not at the site of tanks and it is at 41 km NW of the epicenter). La PGA selezionata viene da ATTENUATION CURVES (foglio alla fine del file excel)_reverse faulting	alluvium soil	C	1		37004	28.7	9.2	0.32		floating		riveted			petroleum prodacts	0.66	Tank settled, lower course bulged, oil splashed on shell

Kern County	1952	7.36	Rose Station	7.7			0.351058278	Modified Mercalli Intensity Scale: VIII		0,19 (ASA2001)	0.17	0.19	0.11		Accelerometers values from Cooper: 021°=0,17, up=0,11. 111°=0,19; (Taft instrument is not at the site of tanks and it is at 41 km NW of the epicenter). La PGA selezionata viene da ATTENUATION CURVES (foglio alla fine del file excel)_reverse faulting	alluvium soil	C	1		37015	28.7	9.2	0.32		fixed		riveted			petroleum prodacts	0.25	No damage
Kern County	1952	7.36	Grapevine Station	13			0.218628	Modified Mercalli Intensity Scale: VIII		0,19 (ASA2001)	0.17	0.19	0.11		Accelerometers values from Cooper: 021°=0,17, up=0,11. 111°=0,19; (Taft instrument is not at the site of tanks and it is at 41 km NW of the epicenter). La PGA selezionata viene da ATTENUATION CURVES (foglio alla fine del file excel)_reverse faulting	rock soil	A	1		37005	28.7	9.2	0.32		floating		riveted			petroleum prodacts	0.71	Bottom leaked, oil splashed over wind girder
Kern County	1952	7.36	Grapevine Station	13			0.218628	Modified Mercalli Intensity Scale: VIII		0,19 (ASA2001)	0.17	0.19	0.11		Accelerometers values from Cooper: 021°=0,17, up=0,11. 111°=0,19; (Taft instrument is not at the site of tanks and it is at 41 km NW of the epicenter). La PGA selezionata viene da ATTENUATION CURVES (foglio alla fine del file excel)_reverse faulting	rock soil	A	1		37016	28.7	9.2	0.32		fixed		riveted			petroleum prodacts	0.08	No damage
Kern County	1952	7.36	Lebec Station	20			0.163887	Modified Mercalli Intensity Scale: VII (-VIII)		0,19 (ASA2001)	0.17	0.19	0.11		Accelerometers values from Cooper: 021°=0,17, up=0,11. 111°=0,19; (Taft instrument is not at the site of tanks and it is at 41 km NW of the epicenter). La PGA selezionata viene da ATTENUATION CURVES (foglio alla fine del file excel)_reverse faulting	rock soil	A	1		37006	28.7	9.2	0.32		floating		riveted			petroleum prodacts	0.52	Oil splashed onto roof
Kern County	1952	7.36	Lebec Station	20			0.163887	Modified Mercalli Intensity Scale: VII (-VIII)		0,19 (ASA2001)	0.17	0.19	0.11		Accelerometers values from Cooper: 021°=0,17, up=0,11. 111°=0,19; (Taft instrument is not at the site of tanks and it is at 41 km NW of the epicenter). La PGA selezionata viene da ATTENUATION CURVES (foglio alla fine del file excel)_reverse faulting	rock soil	A	1		370x13	28.9	9.1	0.31		floating		riveted			petroleum prodacts	0.53	Earth imprints by bottom edge
Kern County	1952	7.36	Lebec Station	20			0.163887	Modified Mercalli Intensity Scale: VII (-VIII)		0,19 (ASA2001)	0.17	0.19	0.11		Accelerometers values from Cooper: 021°=0,17, up=0,11. 111°=0,19; (Taft instrument is not at the site of tanks and it is at 41 km NW of the epicenter). La PGA selezionata viene da ATTENUATION CURVES (foglio alla fine del file excel)_reverse faulting	rock soil	A	1		55021	34.9	9.1	0.26		fixed		riveted			petroleum prodacts	0.41	No damage
Kern County	1952	7.36	Lebec Station	20			0.163887	Modified Mercalli Intensity Scale: VII (-VIII)		0,19 (ASA2001)	0.17	0.19	0.11		Accelerometers values from Cooper: 021°=0,17, up=0,11. 111°=0,19; (Taft instrument is not at the site of tanks and it is at 41 km NW of the epicenter). La PGA selezionata viene da ATTENUATION CURVES (foglio alla fine del file excel)_reverse faulting	rock soil	A	1		55022	34.9	9.1	0.26		fixed		riveted			petroleum prodacts	0.18	No damage
Kern County	1952	7.36	Lebec Station	20			0.163887	Modified Mercalli Intensity Scale: VII (-VIII)		0,19 (ASA2001)	0.17	0.19	0.11		Accelerometers values from Cooper: 021°=0,17, up=0,11. 111°=0,19; (Taft instrument is not at the site of tanks and it is at 41 km NW of the epicenter). La PGA selezionata viene da ATTENUATION CURVES (foglio alla fine del file excel)_reverse faulting	rock soil	A	1		55047	34.9	9.1	0.26		fixed		riveted			petroleum prodacts	0.11	No damage
Kern County	1952	7.36	Lebec Station	20			0.163887	Modified Mercalli Intensity Scale: VII (-VIII)		0,19 (ASA2001)	0.17	0.19	0.11		Accelerometers values from Cooper: 021°=0,17, up=0,11. 111°=0,19; (Taft instrument is not at the site of tanks and it is at 41 km NW of the epicenter). La PGA selezionata viene da ATTENUATION CURVES (foglio alla fine del file excel)_reverse faulting	rock soil	A	1		80105	35.7	12.7	0.36		fixed		riveted			petroleum prodacts	0	No damage
Kern County	1952	7.36	Pacific Gas and Electric Kern Power House	42			0.131719864	Modified Mercalli Intensity Scale: VIII		0,19 (ASA2001)	0.17	0.19	0.11		Accelerometers values from Cooper: 021°=0,17, up=0,11. 111°=0,19; (Taft instrument is not at the site of tanks and it is at 41 km NW of the epicenter). La PGA selezionata viene da ATTENUATION CURVES (foglio alla fine del file excel)_reverse faulting	alluvium soil	C	1		PG&E 1	36.6	6.2	0.17		floating					oil		Damage to roof truss, accompanied by some sloshing and oil spillage
Kern County	1952	7.36	Pacific Gas and Electric Kern Power House	42			0.131719864	Modified Mercalli Intensity Scale: VIII		0,19 (ASA2001)	0.17	0.19	0.11		Accelerometers values from Cooper: 021°=0,17, up=0,11. 111°=0,19; (Taft instrument is not at the site of tanks and it is at 41 km NW of the epicenter). La PGA selezionata viene da ATTENUATION CURVES (foglio alla fine del file excel)_reverse faulting	alluvium soil	C	1		PG&E 2	23.8	8.9	0.38		floating					oil		Damage to roof truss, accompanied by some sloshing and oil spillage
Kern County	1952	7.36	Pacific Gas and Electric Kern Power House	42			0.131719864	Modified Mercalli Intensity Scale: VIII		0,19 (ASA2001)	0.17	0.19	0.11		Accelerometers values from Cooper: 021°=0,17, up=0,11. 111°=0,19; (Taft instrument is not at the site of tanks and it is at 41 km NW of the epicenter). La PGA selezionata viene da ATTENUATION CURVES (foglio alla fine del file excel)_reverse faulting	alluvium soil	C	1		PG&E 3	23.8	13.5	0.57		floating					oil		seal damage, accompanied by some sloshing and oil spillage
Kern County	1952	7.36	Pacific Gas and Electric Kern Power House	42			0.131719864	Modified Mercalli Intensity Scale: VIII		0,19 (ASA2001)	0.17	0.19	0.11		Accelerometers values from Cooper: 021°=0,17, up=0,11. 111°=0,19; (Taft instrument is not at the site of tanks and it is at 41 km NW of the epicenter). La PGA selezionata viene da ATTENUATION CURVES (foglio alla fine del file excel)_reverse faulting	alluvium soil	C	1		PG&E 4	36.6	8.9	0.24		floating					oil		Damage to roof truss, accompanied by some sloshing and oil spillage
Kern County	1952	7.36	Continental Station	38			0.142400968	Modified Mercalli Intensity Scale: VII (-VIII). Molto vicina alla stazione di registrazione TAFT quindi vale 0,19		0,19 (ASA2001)	0.17	0.19	0.11		Accelerometers values from Cooper: 021°=0,17, up=0,11. 111°=0,19; (Taft instrument is not at the site of tanks and it is at 41 km NW of the epicenter). La PGA selezionata viene da ATTENUATION CURVES (foglio alla fine del file excel)_reverse faulting	alluvium soil	C	4	non so quanti tank ci sono, ma so che non hanno subito danni; quindi ho calcolato il numer di tank che in media ci sono nelle stazioni precedenti		32.1	9.5	0.3							oil		No damage
Kern County	1952	7.36	Emidio Station	7.7			0.351058278	Modified Mercalli Intensity Scale: VIII		0,19 (ASA2001)	0.17	0.19	0.11		Accelerometers values from Cooper: 021°=0,17, up=0,11. 111°=0,19; (Taft instrument is not at the site of tanks and it is at 41 km NW of the epicenter). La PGA selezionata viene da ATTENUATION CURVES (foglio alla fine del file excel)_reverse faulting	alluvium soil	C	1					1.1				bolted			oil	0.9	EFB
Kern County	1952	7.36								0,19 (ASA2001)	0.17	0.19	0.11		Accelerometers values from Cooper: 021°=0,17, up=0,11. 111°=0,19; (Taft instrument is not at the site of tanks and it is at 41 km NW of the epicenter). La PGA selezionata viene da ATTENUATION CURVES (foglio alla fine del file excel)_reverse faulting	alluvium soil	C		è 1 ma non so a che distanza è.								bolted			oil	0.9	collapsed by EFB and fell over
Kern County	1952	7.36	Weed Patch Refinery	28			0.177148461	Modified Mercalli Intensity Scale: VIII		0,19 (ASA2001)	0.17	0.19	0.11		Accelerometers values from Cooper: 021°=0,17, up=0,11. 111°=0,19; (Taft instrument is not at the site of tanks and it is at 41 km NW of the epicenter). La PGA selezionata viene da ATTENUATION CURVES (foglio alla fine del file excel)_reverse faulting	alluvium soil	C	2	non so quanti tank ci sono, ma so che non hanno subito danni; quindi ho calcolato il numer di tank che in media ci sono nelle stazioni precedenti		32.1	9.5	0.3		cone fixed		welded			oil	0.9	sloshing, with the roof/shell weld being broken and consequent spillage of oil by sloshing
Kern County	1952	7.36	Weed Patch Refinery	28			0.177148461	Modified Mercalli Intensity Scale: VIII		0,19 (ASA2001)	0.17	0.19	0.11		Accelerometers values from Cooper: 021°=0,17, up=0,11. 111°=0,19; (Taft instrument is not at the site of tanks and it is at 41 km NW of the epicenter). La PGA selezionata viene da ATTENUATION CURVES (foglio alla fine del file excel)_reverse faulting	alluvium soil	C	2	non so quanti tank ci sono, ma so che non hanno subito danni; quindi ho calcolato il numer di tank che in media ci sono nelle stazioni precedenti		32.1	9.5	0.3		cone fixed		welded			oil	0.9	sloshing
Kern County	1952	7.36	Caliente	48			0.118023309	Modified Mercalli Intensity Scale: VII (-VIII)									1						1	<=1	wood	concrete base			0	water		Water sloshed within, breaking wood roof, and damaging parked car. Piping broke. Tank moved.
Kern County	1952	7.36	Woodford	48			0.118023309	Modified Mercalli Intensity Scale: VII									1				0.3		wood	concrete slab				water		collapse of wooden roofs. Pipe connections to 350,000 gal. tank broke off at tank

Kern County	1952	7.36	Woodford	48			0.118023309	Modified Mercalli Intensity Scale: VII									1					0.3		wood	gravel packed mound				water		collapse of wooden roofs.
Kern County	1952	7.36	Standard Oil Refinery, Oildale	50			0.113964137	Modified Mercalli Intensity Scale: VIII									1			15.2	16.2	1.06		floating					oil	1	the sloshing has been reported to have raised the roof momentarily 18 inches to 24 inches. In additien, the roof rotated counterclockwise. Guide broken and pulled out of sleeve when roof rotated to left.
Kern County	1952	7.36	Standard Oil Refinery, Oildale	50			0.113964137	Modified Mercalli Intensity Scale: VIII									9	8 or 10 other tanks		15.2	16.2	1.06							oil	0	No damage
Kern County	1952	7.36	Clear Creek	48			0.118023309										2			3.7	7.3	2.00		cone fixed					gasoline	0.5	No damage
Kern County	1952	7.36	Clear Creek	48			0.118023309										2					2		cone fixed					gasoline		No damage
Kern County	1952	7.36	Arvin	28			0.177148461	Modified Mercalli Intensity Scale: VIII		0,19 (ASA2001)	0.17	0.19	0.11		Accelerometers values from Cooper: 021°=0,17, up=0,11. 111°=0,19; (Taft instrument is not at the site of tanks and it is at 41 km NW of the epicenter). La PGA selezionata viene da ATTENUATION CURVES (foglio alla fine del file excel)_reverse faulting	alluvium soil	C	4	non so quanti tank ci sono, ma so che non hanno subito danni; quindi ho calcolato il numer di tank che in media ci sono nelle stazioni precedenti		3.7	7.3	2.00								No damage
Kern County	1952	7.36	Arvin	28			0.177148461	Modified Mercalli Intensity Scale: VIII		0,19 (ASA2001)	0.17	0.19	0.11		Accelerometers values from Cooper: 021°=0,17, up=0,11. 111°=0,19; (Taft instrument is not at the site of tanks and it is at 41 km NW of the epicenter). La PGA selezionata viene da ATTENUATION CURVES (foglio alla fine del file excel)_reverse faulting	alluvium soil	C	4	non so quanti tank ci sono, ma so che non hanno subito danni; quindi ho calcolato il numer di tank che in media ci sono nelle stazioni precedenti		3.7	7.3	2.00								No damage
Kern County	1952	7.36	Arvin	28			0.177148461	Modified Mercalli Intensity Scale: VIII		0,19 (ASA2001)	0.17	0.19	0.11		Accelerometers values from Cooper: 021°=0,17, up=0,11. 111°=0,19; (Taft instrument is not at the site of tanks and it is at 41 km NW of the epicenter). La PGA selezionata viene da ATTENUATION CURVES (foglio alla fine del file excel)_reverse faulting	alluvium soil	C	4	non so quanti tank ci sono, ma so che non hanno subito danni; quindi ho calcolato il numer di tank che in media ci sono nelle stazioni precedenti		3.7	7.3	2.00								No damage
Kern County	1952	7.36	Emidio Station	7.7			0.351058278	Modified Mercalli Intensity Scale: VIII		0,19 (ASA2001)	0.17	0.19	0.11		Accelerometers values from Cooper: 021°=0,17, up=0,11. 111°=0,19; (Taft instrument is not at the site of tanks and it is at 41 km NW of the epicenter). La PGA selezionata viene da ATTENUATION CURVES (foglio alla fine del file excel)_reverse faulting	alluvium soil	C	1					1.1					light gauge metal				Buckling along bottom
Kern County	1952	7.36	Emidio Station	7.7			0.351058278	Modified Mercalli Intensity Scale: VIII		0,19 (ASA2001)	0.17	0.19	0.11		Accelerometers values from Cooper: 021°=0,17, up=0,11. 111°=0,19; (Taft instrument is not at the site of tanks and it is at 41 km NW of the epicenter). La PGA selezionata viene da ATTENUATION CURVES (foglio alla fine del file excel)_reverse faulting	alluvium soil	C	1					1.1					light gauge metal				Buckling along bottom. Note broken piping.
Landers	1992	7.28	High Desert Water District (HDWD)	5			0.52	0.52		0.15					ASA2001 (che si rifà a Cooper 1997) da Pga=0,15	shallow alluvium or placed fill, which is underlain by firm soil or rock		1		2 M.G.	36.6	7.3	0.20			gravel base			0	water		No significant damage
Landers	1992	7.28	High Desert Water District (HDWD)	7.4			0.48	0.48		0.15					ASA2001 (che si rifà a Cooper 1997) da Pga=0,15	shallow alluvium or placed fill, which is underlain by firm soil or rock		1		R-7	25.9	7.3	0.28			gravel base			0	water		No significant damage
Landers	1992	7.28	High Desert Water District (HDWD)	7.4			0.48	0.48		0.15					ASA2001 (che si rifà a Cooper 1997) da Pga=0,15	shallow alluvium or placed fill, which is underlain by firm soil or rock		1		R-8	10.1	7.3	0.73			gravel base			0	water		No significant damage
Landers	1992	7.28	High Desert Water District (HDWD)	8.6			0.48	0.48		0.2					ASA2001 (che si rifà a Cooper 1997) da Pga=0,20	shallow alluvium or placed fill, which is underlain by firm soil or rock		1		R-14	21.3	5.5	0.26			gravel base			0	water		No significant damage
Landers	1992	7.28	High Desert Water District (HDWD)	6.5			0.43	0.43		0.19					ASA2001 (che si rifà a Cooper 1997) da Pga=0,19	shallow alluvium or placed fill, which is underlain by firm soil or rock		1		R-15	22.8603	7.315289	0.32			gravel base			0	water		No significant damage
Landers	1992	7.28	High Desert Water District (HDWD)	14.3			0.516	0.516		0.15					ASA2001 (che si rifà a Cooper 1997) da Pga=0,15	shallow alluvium or placed fill, which is underlain by firm soil or rock		1		R-2	25.9083	7.315289	0.28235			gravel base			0	water		No significant damage
Landers	1992	7.28	High Desert Water District (HDWD)	13			0.458	0.458		0.2					ASA2001 (che si rifà a Cooper 1997) da Pga=0,20	shallow alluvium or placed fill, which is underlain by firm soil or rock		1		R-3	25.9083	7.315289	0.28235			gravel base			0	water		No significant damage
Landers	1992	7.28	High Desert Water District (HDWD)	13			0.48	0.48		0.2					ASA2001 (che si rifà a Cooper 1997) da Pga=0,20	shallow alluvium or placed fill, which is underlain by firm soil or rock		1		R-4	9.14411	7.315289	0.8			gravel base			0	water		No significant damage
Landers	1992	7.28	High Desert Water District (HDWD)	16.4			0.429	0.429		0.2					ASA2001 (che si rifà a Cooper 1997) da Pga=0,20	shallow alluvium or placed fill, which is underlain by firm soil or rock		1		R-5	7.9249	7.315289	0.92308			gravel base			0	water		No significant damage
Landers	1992	7.28	High Desert Water District (HDWD)	12			0.43	0.43		0.1					ASA2001 (che si rifà a Cooper 1997) da Pga=0,10	shallow alluvium or placed fill, which is underlain by firm soil or rock		1		Upper Ridge	13.1066	7.315289	0.55814			gravel base			0	water		No significant damage
Landers	1992	7.28	High Desert Water District (HDWD)	12			0.44	0.44		0.1					ASA2001 (che si rifà a Cooper 1997) da Pga=0,10	shallow alluvium or placed fill, which is underlain by firm soil or rock		1		Lower Ridge	5.48647	4.8768593	0.88889			gravel base			0	water		No significant damage
Landers	1992	7.28	High Desert Water District (HDWD)	13			0.53	0.53		0.15					ASA2001 (che si rifà a Cooper 1997) da Pga=0,15	shallow alluvium or placed fill, which is underlain by firm soil or rock		1		Upper Fox	24.3843	12.192148	0.5			gravel base			0	water		No significant damage
Landers	1992	7.28	High Desert Water District (HDWD)	12			0.52	0.52		0.15					ASA2001 (che si rifà a Cooper 1997) da Pga=0,15	shallow alluvium or placed fill, which is underlain by firm soil or rock		1		Lower Fox	10.851	4.8768593	0.44944			gravel base			0	water		No significant damage
Landers	1992	7.28	High Desert Water District (HDWD)	13.7			0.553	0.553		0.15					ASA2001 (che si rifà a Cooper 1997) da Pga=0,15	shallow alluvium or placed fill, which is underlain by firm soil or rock		1		Golden Bee	14.4172	9.7537186	0.67653			gravel base			0	water		No significant damage
Landers	1992	7.28	High Desert Water District (HDWD)	13			0.448	0.448		0.1					ASA2001 (che si rifà a Cooper 1997) da Pga=0,10	shallow alluvium or placed fill, which is underlain by firm soil or rock		1		Homestead	11.7654	7.315289	0.62176			gravel base			0	water		No significant damage
Landers	1992	7.28	High Desert Water District (HDWD)	13			0.511	0.511		0.15					ASA2001 (che si rifà a Cooper 1997) da Pga=0,15	shallow alluvium or placed fill, which is underlain by firm soil or rock		1		Hospital Desert Gold	11.7654	7.315289	0.62176			gravel base			0	water		No significant damage
Landers	1992	7.28	San Bernardino County Service Area 70	6.7			0.477	0.477	0.47	0.47					ASA2001 (che si rifà a Cooper 1997) da Pga=0,47	rock		1		CSA-70-1	11.7654	7.315289	0.62176			rock foundation	bolted	segments of 3,4mm (10ga) shell and bottom plate thickness	0			EFB all around, and tearing of the shell at the clean-out door on the side west, and pulling loose of dresser coulpling on both inlet and outlet piping
Landers	1992	7.28	Bighorn Desert View Water Agency	7.3			0.533	0.533		0.56					ASA2001 (che si rifà a Cooper 1997) da Pga=0,56	rock		1		A	16.4594	7.315289	0.44444			rock base	welded	6,35 mm (,025 in.) shell and bottom, 4016 mm (0,1875 in.) rof	0	water	0.92	it failed at the shell bottom plate joint at two locations :2,75 m (9ft) rip on the north side of the tank. There was EFB around the entire tank. There was a 150mm (6 in.) riser pipe on the south side of the tank which lifted about 0,6m (2ft) out of the ground. This riser pipe was then bent and torn from the tank when the tank shell came back to grade. There appeared to be an 80 mm (3in.) horizontal movement of the tank to the north. (DS=4)
Landers	1992	7.28	Bighorn Desert View Water Agency	9.3			0.51	0.51	0.55	0.55					ASA2001 (che si rifà a Cooper 1997) da Pga=0,55			1		B	8.0773	7.315289	0.90566				welded		0	water	0.95	Minor damage
Landers	1992	7.28	Bighorn Desert View Water Agency	9.3			0.51	0.51	0.55	0.55					ASA2001 (che si rifà a Cooper 1997) da Pga=0,55			1		C	18.1358	7.315289	0.40336				welded		0	water	0.94	Minor damage
Landers	1992	7.28	Bighorn Desert View Water Agency	6.5			0.51	0.51	0.55	0.55					ASA2001 (che si rifà a Cooper 1997) da Pga=0,55			1		10	9.9366	4.8768593	0.4908						0	water	0.91	Minor damage
Landers	1992	7.28	Bighorn Desert View Water Agency	3.5			0.504	0.504	0.54	0.54					ASA2001 (che si rifà a Cooper 1997) da Pga=0,54			1		22-A	9.9366	4.8768593	0.4908						0	water	0.91	Minor damage
Landers	1992	7.28	Bighorn Desert View Water Agency	3.5			0.504	0.504	0.54	0.54					ASA2001 (che si rifà a Cooper 1997) da Pga=0,54			1		22-B	9.9366	4.8768593	0.4908						0	water	0.91	Minor damage
Landers	1992	7.28	Bighorn Desert View Water Agency	3.5			0.504	0.504	0.54	0.54					ASA2001 (che si rifà a Cooper 1997) da Pga=0,54			1		22-C	14.021	4.8768593	0.34783						0	water	0.91	Minor damage
Landers	1992	7.28	Bighorn Desert View Water Agency	3.5			0.504	0.504	0.54	0.54					ASA2001 (che si rifà a Cooper 1997) da Pga=0,54			1		22-D	22.2507	4.8768593	0.21918						0	water	0.9	Minor damage

Landers	1992	7.28	Bighorn Desert View Water Agency	2			0.53	0.53	0.55	0.55					ASA2001 (che si rifà a Cooper 1997) da Pga=0,55			1		34	6.40088	4.8768593	0.7619						0	water	0.91	Minor damage
Landers	1992	7.28	SCE Coolwater	90			0.53	0,26-0,28		0.53	0.34	0.53	0.21		ASA2001 (che si rifà a Cooper 1997) da Pga=0,53 e dice che è un "free field accelerometer at the site". Cooper riporta "Strong motion records" in corrispondenza dei tre Coldwater tanks SCE: 360°=0,34g; UP=0,21g; 270°=0,53g.	good alluvium		1		SCE Coolwater 1 of 3	83.2114	15.240185	0.18315		floating	concrete foundation				oil	1	No damage
Landers	1992	7.28	SCE Coolwater	90			0.53	0,26-0,28		0.53	0.34	0.53	0.21		ASA2001 (che si rifà a Cooper 1997) da Pga=0,53 e dice che è un "free field accelerometer at the site". Cooper riporta "Strong motion records" in corrispondenza dei tre Coldwater tanks SCE: 360°=0,34g; UP=0,21g; 270°=0,53g.	good alluvium		1		SCE Coolwater 2 of 3	83.2114	15.240185	0.18315		floating	concrete foundation				oil	0.5	No damage
Landers	1992	7.28	SCE Coolwater	90			0.53	0,26-0,28		0.53	0.34	0.53	0.21		ASA2001 (che si rifà a Cooper 1997) da Pga=0,53 e dice che è un "free field accelerometer at the site". Cooper riporta "Strong motion records" in corrispondenza dei tre Coldwater tanks SCE: 360°=0,34g; UP=0,21g; 270°=0,53g.	good alluvium		1		SCE Coolwater 3 of 3	67.6664	14.630578	0.21622		floating	concrete foundation				oil	0	No damage
Landers	1992	7.28	Barstow	91		30 km from the fault	0.19	0,14-0,24	0.14		0.15	0.14	0.07		ASA2001 (che si rifà a Ballentyne) da Pga=0,14 . Cooper riporta "Strong motion records" in corrispondenza di Barstow Vineyard &H st (CSMIP): 090°=0,15g; UP=0,07g; 360°=0,14g.			1		Beryl SCWC	9.14411	7.315289	0.8				bolted				0.88	Small leakage of bottom flange (small)
Landers	1992	7.28	Barstow	91		30 km from the fault	0.19	0,14-0,24	0.14						ASA2001 (che si rifà a Ballentyne) da Pga=0,14 . Cooper riporta "Strong motion records" in corrispondenza di Barstow Vineyard &H st (CSMIP): 090°=0,15g; UP=0,07g; 360°=0,14g.			1		Basalt SCWC	9.14411	7.315289	0.8				bolted				0.88	Failure of pipe through bottom penetration
Landers	1992	7.28	Barstow	91		30 km from the fault	0.19	0,14-0,24	0.14						ASA2001 (che si rifà a Ballentyne) da Pga=0,14 . Cooper riporta "Strong motion records" in corrispondenza di Barstow Vineyard &H st (CSMIP): 090°=0,15g; UP=0,07g; 360°=0,14g.			1		Arville-N SCWC	8.93075	12.649354	1.41638				welded (fillet)			0	0.89	Failure of pipe through bottom penetration
Landers	1992	7.28	Barstow	91		30 km from the fault	0.19	0,14-0,24	0.14						ASA2001 (che si rifà a Ballentyne) da Pga=0,14 . Cooper riporta "Strong motion records" in corrispondenza di Barstow Vineyard &H st (CSMIP): 090°=0,15g; UP=0,07g; 360°=0,14g.			1		Arville-S SCWC	8.93075	13.563765	1.51877				welded			0	0.90	Tank lateral movement
Kobe	1995	6.9		10		2-4 km from an active fault				0,6-0,8					PGA from Cooper 97	reclaimed ground, liquefaction damaged tanks		2					2	2 dalle foto							There was no loss of product from damaged tanks. The damage consists principaly of tank tilting, pipe support/piping loss of foundation supports, and walkway-platform loss of support.
Kobe	1995	6.9	Osaka and Sakai Refinery	35				0,28-0,44		0.2					From Cooper: PGA estimated to be 0,20g at these sites			275					0.3	<1 da google map						No major damage
Kobe	1995	6.9	Osaka and Sakai Refinery	35				0,28-0,44		0.2					From Cooper: PGA estimated to be 0,20g at these sites			145					1	>=1 da google map						No major damage
Kobe	1995	6.9	Higashinada	23				0,72-0,76		0.5					From EQE Summary Report (shape file non iterattive)			2							concrete foundation supported on 30 meter-long precast concrete piles			0	fuel		The ground settled near the tanks by as much as 70 centimeters. As a result of the settlement, the tops of the piles could easily be seen beneath the foundations. The foundations were observed to have tilted slightly, with no damaging effects to the tanks.
Kobe	1995	6.9	Higashinada	23				0,72-0,76		0.5					From EQE Summary Report (shape file non iterattive)			1							concrete foundation supported on 30 meter-long precast concrete piles			0	raw water		The ground settled near the tanks by as much as 70 centimeters. As a result of the settlement, the tops of the piles could easily be seen beneath the foundations. The foundations were observed to have tilted slightly, with no damaging effects to the tanks.
Kobe	1995	6.9	Higashinada	23				0,72-0,76		0.5					From EQE Summary Report (shape file non iterattive)			1							concrete foundation supported on 30 meter-long precast concrete piles			0	purified water		The ground settled near the tanks by as much as 70 centimeters. As a result of the settlement, the tops of the piles could easily be seen beneath the foundations. The foundations were observed to have tilted slightly, with no damaging effects to the tanks.
Costa Rica	1991	7.6	Recope Refinery, Moin	34			0.24	0.24		0,21 (shake map non interattive.. Forse troppo bassa)		0.35			From ALA 2001: Ground motion for Port of Moin , near Limon, was estimated based on mapped intensity MMI VIII=PGA0,35g			1		701	43.8917	9.4489149	0.21528				welded			0	light crude	0.93	it had lost some of its contents due to sloshing, roof damage, fire caused by tank 792
Costa Rica	1991	7.6	Recope Refinery, Moin	34			0.24	0.24		0,21 (shake map non interattive.. Forse troppo bassa)		0.35			From ALA 2001: Ground motion for Port of Moin , near Limon, was estimated based on mapped intensity MMI VIII=PGA0,35g			1		704	44.1965	11.887345	0.26897				welded			0	light crude	0.94	they suffered severe damage to the roof and the tops of the walls due to sloshing of the contents. The forces due to hydrodynamic effects caused rupturing of the joint in the stee plates at the roof-wall junction
Costa Rica	1991	7.6	Recope Refinery, Moin	34			0.24	0.24		0,21 (shake map non interattive.. Forse troppo bassa)		0.35			From ALA 2001: Ground motion for Port of Moin , near Limon, was estimated based on mapped intensity MMI VIII=PGA0,35g			1		705	44.1965	11.887345	0.26897				welded			0	light crude	0.94	they suffered severe damage to the roof and the tops of the walls due to sloshing of the contents. The forces due to hydrodynamic effects caused rupturing of the joint in the stee plates at the roof-wall junction
Costa Rica	1991	7.6	Recope Refinery, Moin	34			0.24	0.24		0,21 (shake map non interattive.. Forse troppo bassa)		0.35			From ALA 2001: Ground motion for Port of Moin , near Limon, was estimated based on mapped intensity MMI VIII=PGA0,35g			1		708	21.0315	9.4489149	0.44928				welded			0	heavy crude	0.95	total loss of their contents due to the classical "elephant-foot" buckling of the vertical walls near the base
Costa Rica	1991	7.6	Recope Refinery, Moin	34			0.24	0.24		0,21 (shake map non interattive.. Forse troppo bassa)		0.35			From ALA 2001: Ground motion for Port of Moin , near Limon, was estimated based on mapped intensity MMI VIII=PGA0,35g			1		709	21.0315	9.4489149	0.44928				welded			0	heavy crude	0.95	total loss of their contents due to the classical "elephant-foot" buckling of the vertical walls near the base
Costa Rica	1991	7.6	Recope Refinery, Moin	34			0.24	0.24		0,21 (shake map non interattive.. Forse troppo bassa)		0.35			From ALA 2001: Ground motion for Port of Moin , near Limon, was estimated based on mapped intensity MMI VIII=PGA0,35g			1		715	29.566	12.496952	0.42268		floating		welded			0	gasoline	0.92	Floating roof collapse
Costa Rica	1991	7.6	Recope Refinery, Moin	34			0.24	0.24		0,21 (shake map non interattive.. Forse troppo bassa)		0.35			From ALA 2001: Ground motion for Port of Moin , near Limon, was estimated based on mapped intensity MMI VIII=PGA0,35g			1		716	29.566	12.496952	0.42268		floating		welded			0	gasoline	0.92	Floating roof collapse
Costa Rica	1991	7.6	Recope Refinery, Moin	34			0.24	0.24		0,21 (shake map non interattive.. Forse troppo bassa)		0.35			From ALA 2001: Ground motion for Port of Moin , near Limon, was estimated based on mapped intensity MMI VIII=PGA0,35g			1		725	17.3738	11.277737	0.64912		floating		welded			0	gasoline	0.99	Floating roof collapse
Costa Rica	1991	7.6	Recope Refinery, Moin	34			0.24	0.24		0,21 (shake map non interattive.. Forse troppo bassa)		0.35			From ALA 2001: Ground motion for Port of Moin , near Limon, was estimated based on mapped intensity MMI VIII=PGA0,35g			1		726	17.3738	11.277737	0.64912		floating		welded			0	gasoline	0.986486	Floating roof collapse
Costa Rica	1991	7.6	Recope Refinery, Moin	34			0.24	0.24		0,21 (shake map non interattive.. Forse troppo bassa)		0.35			From ALA 2001: Ground motion for Port of Moin , near Limon, was estimated based on mapped intensity MMI VIII=PGA0,35g			1		728	40.5389	11.887345	0.29323				welded			0	fuel oil	0.964103	It suffered severe damage to the roof and the tops of the walls due to sloshing of the contents. The forces due to hydrodynamic effects caused rupturing of the joint in the steel plates at the roof-wall junction
Costa Rica	1991	7.6	Recope Refinery, Moin	34			0.24	0.24		0,21 (shake map non interattive.. Forse troppo bassa)		0.35			From ALA 2001: Ground motion for Port of Moin , near Limon, was estimated based on mapped intensity MMI VIII=PGA0,35g			1		733	40.5389	11.887345	0.29323		floating		welded			0	gasoline	0.935897	Severe floating roof tilting
Costa Rica	1991	7.6	Recope Refinery, Moin	34			0.24	0.24		0,21 (shake map non interattive.. Forse troppo bassa)		0.35			From ALA 2001: Ground motion for Port of Moin , near Limon, was estimated based on mapped intensity MMI VIII=PGA0,35g			1		738	14.3258	9.4489149	0.65957				welded			0	heavy crude	0.970968	total loss of their contents due to the classical "elephant-foot" buckling of the vertical walls near the base
Costa Rica	1991	7.6	Recope Refinery, Moin	34			0.24	0.24		0,21 (shake map non interattive.. Forse troppo bassa)		0.35			From ALA 2001: Ground motion for Port of Moin , near Limon, was estimated based on mapped intensity MMI VIII=PGA0,35g			1		745	10.0585	9.4489149	0.93939				welded			0	diesel oil	0.967742	total loss of their contents due to the classical "elephant-foot" buckling of the vertical walls near the base
Costa Rica	1991	7.6	Recope Refinery, Moin	34																792	4.57206	4.5720556	1			welded			0	heavy naphta	1	Overturned tank, Explosion (non lo voglio considerare in "Modifiche 9TRIS"
Costa Rica	1991	7.6	Holanda Chem Plant	34			0.24	0.24				0.35			From ALA 2001: Ground motion for Port of Moin , near Limon, was estimated based on mapped intensity MMI VIII=PGA0,35g			1			5.53	5.53	1				welded			0			slight EFB
Costa Rica	1991	7.6	Holanda Chem Plant	34			0.24	0.24				0.35			From ALA 2001: Ground motion for Port of Moin , near Limon, was estimated based on mapped intensity MMI VIII=PGA0,35g			1			10.06	10.06	1							0			Slid 20 cm

Costa Rica	1991	7.6	Holanda Chem Plant	34			0.24	0.24				0.35			From ALA 2001: Ground motion for Port of Moin , near Limon, was estimated based on mapped intensity MMI VIII=PGA0,35g			1											0			No Damage
Costa Rica	1991	7.6	Holanda Chem Plant	34			0.24	0.24				0.35			From ALA 2001: Ground motion for Port of Moin , near Limon, was estimated based on mapped intensity MMI VIII=PGA0,35g			1											0			No Damage
Costa Rica	1991	7.6	Holanda Chem Plant	34			0.24	0.24				0.35			From ALA 2001: Ground motion for Port of Moin , near Limon, was estimated based on mapped intensity MMI VIII=PGA0,35g			1											0			No Damage
Costa Rica	1991	7.6	Holanda Chem Plant	34			0.24	0.24				0.35			From ALA 2001: Ground motion for Port of Moin , near Limon, was estimated based on mapped intensity MMI VIII=PGA0,35g			1											0			No Damage
Costa Rica	1991	7.6	Holanda Chem Plant	34			0.24	0.24				0.35			From ALA 2001: Ground motion for Port of Moin , near Limon, was estimated based on mapped intensity MMI VIII=PGA0,35g			1											0			No Damage
Costa Rica	1991	7.6	Holanda Chem Plant	34			0.24	0.24				0.35			From ALA 2001: Ground motion for Port of Moin , near Limon, was estimated based on mapped intensity MMI VIII=PGA0,35g			1											0			No Damage
Costa Rica	1991	7.6	Holanda Chem Plant	34			0.24	0.24				0.35			From ALA 2001: Ground motion for Port of Moin , near Limon, was estimated based on mapped intensity MMI VIII=PGA0,35g			1											0			No Damage
Costa Rica	1991	7.6	Holanda Chem Plant	34			0.24	0.24				0.35			From ALA 2001: Ground motion for Port of Moin , near Limon, was estimated based on mapped intensity MMI VIII=PGA0,35g			1											0			No Damage
Costa Rica	1991	7.6	Transmerquim	34			0.24	0.24				0.35			From ALA 2001: Ground motion for Port of Moin , near Limon, was estimated based on mapped intensity MMI VIII=PGA0,35g			1			8.66	8.66	1						0			EFB_ sever, no leak
Costa Rica	1991	7.6	Transmerquim	34			0.24	0.24				0.35			From ALA 2001: Ground motion for Port of Moin , near Limon, was estimated based on mapped intensity MMI VIII=PGA0,35g			1			8.66	8.66	1						0			EFB_ sever, no leak
Costa Rica	1991	7.6	Transmerquim	34			0.24	0.24				0.35			From ALA 2001: Ground motion for Port of Moin , near Limon, was estimated based on mapped intensity MMI VIII=PGA0,35g			1											0			Rocking, broken inlet/outlet pipe, loss of some contents
Costa Rica	1991	7.6	Transmerquim	34			0.24	0.24				0.35			From ALA 2001: Ground motion for Port of Moin , near Limon, was estimated based on mapped intensity MMI VIII=PGA0,35g			1											0			No Damage
Costa Rica	1991	7.6	Transmerquim	34			0.24	0.24				0.35			From ALA 2001: Ground motion for Port of Moin , near Limon, was estimated based on mapped intensity MMI VIII=PGA0,35g			1											0			No Damage
Costa Rica	1991	7.6	Transmerquim	34			0.24	0.24				0.35			From ALA 2001: Ground motion for Port of Moin , near Limon, was estimated based on mapped intensity MMI VIII=PGA0,35g			1											0			No Damage
Costa Rica	1991	7.6	Transmerquim	34			0.24	0.24				0.35			From ALA 2001: Ground motion for Port of Moin , near Limon, was estimated based on mapped intensity MMI VIII=PGA0,35g			1											0			No Damage
Costa Rica	1991	7.6	Transmerquim	34			0.24	0.24				0.35			From ALA 2001: Ground motion for Port of Moin , near Limon, was estimated based on mapped intensity MMI VIII=PGA0,35g			1											0			No Damage
Costa Rica	1991	7.6	Transmerquim	34			0.24	0.24				0.35			From ALA 2001: Ground motion for Port of Moin , near Limon, was estimated based on mapped intensity MMI VIII=PGA0,35g			1											0			No Damage
Costa Rica	1991	7.6	Transmerquim	34			0.24	0.24				0.35			From ALA 2001: Ground motion for Port of Moin , near Limon, was estimated based on mapped intensity MMI VIII=PGA0,35g			1											0			No Damage
Costa Rica	1991	7.6	Transmerquim	34			0.24	0.24				0.35			From ALA 2001: Ground motion for Port of Moin , near Limon, was estimated based on mapped intensity MMI VIII=PGA0,35g			1											0			No Damage
Costa Rica	1991	7.6	Transmerquim	34			0.24	0.24				0.35			From ALA 2001: Ground motion for Port of Moin , near Limon, was estimated based on mapped intensity MMI VIII=PGA0,35g			1											0			No Damage
Costa Rica	1991	7.6	Transmerquim	34			0.24	0.24				0.35			From ALA 2001: Ground motion for Port of Moin , near Limon, was estimated based on mapped intensity MMI VIII=PGA0,35g			1											0			No Damage
Costa Rica	1991	7.6	Transmerquim	34			0.24	0.24				0.35			From ALA 2001: Ground motion for Port of Moin , near Limon, was estimated based on mapped intensity MMI VIII=PGA0,35g			1											0			No Damage
Costa Rica	1991	7.6	Transmerquim	34			0.24	0.24				0.35			From ALA 2001: Ground motion for Port of Moin , near Limon, was estimated based on mapped intensity MMI VIII=PGA0,35g			1											0			No Damage
Costa Rica	1991	7.6	Transmerquim	34			0.24	0.24				0.35			From ALA 2001: Ground motion for Port of Moin , near Limon, was estimated based on mapped intensity MMI VIII=PGA0,35g			1											0			No Damage
Costa Rica	1991	7.6	Transmerquim	34			0.24	0.24				0.35			From ALA 2001: Ground motion for Port of Moin , near Limon, was estimated based on mapped intensity MMI VIII=PGA0,35g			1											0			No Damage
Costa Rica	1991	7.6	Transmerquim	34			0.24	0.24				0.35			From ALA 2001: Ground motion for Port of Moin , near Limon, was estimated based on mapped intensity MMI VIII=PGA0,35g			1											0			No Damage
Costa Rica	1991	7.6	Transmerquim	34			0.24	0.24				0.35			From ALA 2001: Ground motion for Port of Moin , near Limon, was estimated based on mapped intensity MMI VIII=PGA0,35g			1											0			No Damage
Costa Rica	1991	7.6	Transmerquim	34			0.24	0.24				0.35			From ALA 2001: Ground motion for Port of Moin , near Limon, was estimated based on mapped intensity MMI VIII=PGA0,35g			1											0			No Damage
Costa Rica	1991	7.6	Transmerquim	34			0.24	0.24				0.35			From ALA 2001: Ground motion for Port of Moin , near Limon, was estimated based on mapped intensity MMI VIII=PGA0,35g			1											0			No Damage
Costa Rica	1991	7.6	Transmerquim	34			0.24	0.24				0.35			From ALA 2001: Ground motion for Port of Moin , near Limon, was estimated based on mapped intensity MMI VIII=PGA0,35g			1											0			No Damage
Costa Rica	1991	7.6	Transmerquim	34			0.24	0.24				0.35			From ALA 2001: Ground motion for Port of Moin , near Limon, was estimated based on mapped intensity MMI VIII=PGA0,35g			1											0			No Damage
Costa Rica	1991	7.6	Transmerquim	34			0.24	0.24				0.35			From ALA 2001: Ground motion for Port of Moin , near Limon, was estimated based on mapped intensity MMI VIII=PGA0,35g			1											0			No Damage
Costa Rica	1991	7.6	Transmerquim	34			0.24	0.24				0.35			From ALA 2001: Ground motion for Port of Moin , near Limon, was estimated based on mapped intensity MMI VIII=PGA0,35g			1											0			No Damage
Bam	2003	6.6	Bam electrical substation	28		5 km from the fault	0.497	0,497 (Atlas: sembra sia quello piu nuovo); 0,294 (archive)		0,20-0,25					From shake map non interattiva			1					1	>=1	fixed				0	gasoline	0.95	The on-grade tank suffered severe structural damage due to ground shaking. Rigid piping connections ruptured and caused leakage of gasoline. The tank's tendency to uplift and inaccurate fabrication of the tank appurtenances were the main reasons for this failure mode. The uplift of the unanchored tank caused minor damage to the tank foundation structure. No EFB occured
Bam	2003	6.6	Bam chemical plant	27			0.413	0,413 (Atlas: sembra sia quello piu nuovo); 0,291 (archive)		0,20-0,25					From shake map non interattiva			3					1	a vista (da google map) sembrano >=1	fixed				0	oil		Though on-grade unanchored tanks were not significantly damaged, and uplift did not occur, leakage of oil took place in three out of six ongrade tanks due to sloshing (Leakage of oil from roof-to-wall junctions from sloshing)
Bam	2003	6.6	Bam chemical plant	27			0.413	0,413 (Atlas: sembra sia quello piu nuovo); 0,291 (archive)		0,20-0,25					From shake map non interattiva			3					1	a vista (da google map) sembrano >=1	fixed				0	oil		ongrade unanchored tanks were not significantly damaged, and uplift did not occur, no leakage of oil took place in these three tanks
Tokachi-oki	2003	8-8,3	West Port of Tomakomai	205			0.1	0.1		0.07					From shake map non interattiva			1		A	42.6725	22.860278	0.53571		floating					crude oil	0.89	Tank A suffered the so-called "ring fire" in which the flame was confined to the rim of the tank roof, and this fire lasted for approximately 7 h
Tokachi-oki	2003	8-8,3	West Port of Tomakomai	205			0.1	0.1		0.07					From shake map non interattiva			1		B	42.6725	22.860278	0.53571		floating					naphta	0.77	Tank B suffered sinking of the floating roof resulting in an open-top fire that lasted for 44 h. It is thought that these floating roofs sank into the storage tank as a result of damage to the roof pontoons because of large-amplitude sloshing
Tokachi-oki	2003	8-8,3	West Port of Tomakomai	205			0.1	0.1		0.07					From shake map non interattiva			1		C	49.3782	22.860278	0.46296		floating					kerosene	0.91	sinking of the floating roof. It is thought that these floating roofs sank into the storage tank as a result of damage to the roof pontoons because of large-amplitude sloshing
Tokachi-oki	2003	8-8,3	West Port of Tomakomai	205			0.1	0.1		0.07					From shake map non interattiva			1		D	49.3782	22.860278	0.46296		floating					kerosene	0.91	sinking of the floating roof. It is thought that these floating roofs sank into the storage tank as a result of damage to the roof pontoons because of large-amplitude sloshing
Tokachi-oki	2003	8-8,3	West Port of Tomakomai	205			0.1	0.1		0.07					From shake map non interattiva			1		E	49.3782	22.860278	0.46296		floating					slop	0.64	sinking of the floating roof. It is thought that these floating roofs sank into the storage tank as a result of damage to the roof pontoons because of large-amplitude sloshing
Tokachi-oki	2003	8-8,3	West Port of Tomakomai	205			0.1	0.1		0.07					From shake map non interattiva			1		F	78.0297	22.860278	0.29297		floating					crude oil	0.59	sinking of the floating roof. It is thought that these floating roofs sank into the storage tank as a result of damage to the roof pontoons because of large-amplitude sloshing
Tokachi-oki	2003	8-8,3	West Port of Tomakomai	205			0.1	0.1		0.07					From shake map non interattiva			1		G	78.0297	22.860278	0.29297		floating					crude oil	0.58	sinking of the floating roof. It is thought that these floating roofs sank into the storage tank as a result of damage to the roof pontoons because of large-amplitude sloshing
Tokachi-oki	2003	8-8,3	West Port of Tomakomai	205			0.1	0.1		0.07					From shake map non interattiva			71					0.3	<<1 Sono i molto tozzi o tozzi (google map)	fixed							No damage
Tokachi-oki	2003	8-8,3	West Port of Tomakomai	205			0.1	0.1		0.07					From shake map non interattiva			28					1	<=1 Sono i tozzi al limite (google map)	fixed							No damage
Tokachi-oki	2003	8-8,3	West Port of Tomakomai	205			0.1	0.1		0.07					From shake map non interattiva			18					1	>=1 Sono gli snelli al limite (google map)	fixed							No damage
Tokachi-oki	2003	8-8,3	West Port of Tomakomai	205			0.1	0.1		0.07					From shake map non interattiva			36					1.1	>>1 Sono gli snelli (google map)	fixed							No damage
Tokachi-oki	2003	8-8,3	West Port of Tomakomai	205			0.1	0.1		0.07					From shake map non interattiva			15					0.3	<<1 Sono i molto tozzi o tozzi (google map) [sarebbero 20 ma io ne ho tolti 5 che hanno avuto sinking of the roof]	floating							No damage
Tokachi-oki	2003	8-8,3	West Port of Tomakomai	205			0.1	0.1		0.07					From shake map non interattiva			1					1	<=1 Sono i tozzi al limite (google map)	floating							No damage
Tokachi-oki	2003	8-8,3	West Port of Tomakomai	205			0.1	0.1		0.07					From shake map non interattiva			1					1	>=1 Sono gli snelli al limite (google map)	floating							No damage
Coast of Central Perú	2007	8	Port of San Martin	55			0.34	0,34 (Atlas: sembra sia quello piu nuovo); 0,37 (archive)		0.35					From shake map non interattiva			3					0.3	<1	cone							No damage

Coast of Central Perù	2007	8	Port of San Martin	55			0.34	0,34 (Atlas: sembra sia quello piu nuovo); 0,37 (archive)		0.35					From shake map non interattiva			1					0.3	<<1	fixed	concrete base			1	water		No damage
Coast of Central Perù	2007	8	coast near Pisco	55			0.35			0.35					From shake map non interattiva			3					0.3	<1	fixed					oil		No damage
Coast of Central Perù	2007	8	coast near Pisco (Blue Pacific Oil)	55			0.4	0,40 (Atlas: sembra quello piu nuovo); 0,37 0,40 (archive)		0.35					From shake map non interattiva			6			12.0	10.1	0.84		fixed	1,5 m deep reinforced concrete raft				fish oil		No damage
Coast of Central Perù	2007	8	coast near Pisco (Blue Pacific Oil)	55			0.4	0,40 (Atlas: sembra quello piu nuovo); 0,37 0,40 (archive)		0.35					From shake map non interattiva			3			12.0	10.1	0.84		fixed					fish oil		EFB around a large extent of their perimeter. (No product was lost due to pipe or tank failure, but some had sloshed out at the top through inspection holes).
Coast of Central Perù	2007	8	coast near Pisco (Blue Pacific Oil)	55			0.4	0,40 (Atlas: sembra quello piu nuovo); 0,37 0,40 (archive)		0.35					From shake map non interattiva			1			12.0	10.1	0.84		fixed					fish oil		It showed buckling at the first strake level (1.5 m above ground). (No product was lost due to pipe or tank failure, but some had sloshed out at the top through inspection holes).
Coast of Central Perù	2007	8	coast near Pisco (Austral Fish Oil Plant)	56			0.4	0,40 (Atlas: sembra quello piu nuovo); 0,389(archive)		0.35					From shake map non interattiva			12					1.1	>1	cone fixed					fish oil		No damage
Coast of Central Perù	2007	8	coast near Pisco (Austral Fish Oil Plant)	56			0.4	0,40 (Atlas: sembra quello piu nuovo); 0,389(archive)		0.35					From shake map non interattiva			2					0.3	<1						fish oil		No damage
Coast of Central Perù	2007	8	coast near Pisco (Epesca Peru)	56			0.4	0,40 (Atlas: mi sembra quello piu nuovo); 0,384 (archive)		0.35					From shake map non interattiva			23					1.1	>1						fish oil		No damage
Coast of Central Perù	2007	8	coast near Pisco (Epesca Peru)	56			0.4	0,40 (Atlas: mi sembra quello piu nuovo); 0,384 (archive)		0.35					From shake map non interattiva			20					0.3	<1						fish oil		No damage
Coast of Central Perù	2007	8	coast near Pisco (Pluspetrol Peru)	56			0.427	0,427 (Atlas: sembra quello piu nuovo); 0,419 (archive)		0.35					From shake map non interattiva			2					0.3	<<1	floating							No damage
Coast of Central Perù	2007	8	coast near Pisco (Pluspetrol Peru)	56			0.427	0,427 (Atlas: sembra quello piu nuovo); 0,419 (archive)		0.35					From shake map non interattiva			5					0.3	<1								No damage
Coast of Central Perù	2007	8	coast near Pisco (Pluspetrol Peru)	56			0.427	0,427 (Atlas: sembra quello piu nuovo); 0,419 (archive)		0.35					From shake map non interattiva			2					1.1	>1	dome							No damage
Coast of Central Perù	2007	8	coast near Pisco (Pluspetrol Peru)	56			0.427	0,427 (Atlas: sembra quello piu nuovo); 0,419 (archive)		0.35					From shake map non interattiva			1					1.1	>1								No damage
Coast of Central Perù	2007	8	coast near Pisco (Pluspetrol Peru)	56			0.427	0,427 (Atlas: sembra quello piu nuovo); 0,419 (archive)		0.35					From shake map non interattiva			3					0.3	<1	dome							No damage
Coast of Central Perù	2007	8	coast near Pisco (Pluspetrol Peru)	56			0.427	0,427 (Atlas: sembra quello piu nuovo); 0,419 (archive)		0.35					From shake map non interattiva			3					1.1	>1	dome							No damage
Coast of Central Perù	2007	8	Storage depot (Pluspetrol Peru)	53			0.474	0,474 (Atlas: mi sembra quello piu nuovo); 0,5 (archive)		0.35					From shake map non interattiva			1					1	<=1	fixed					oil		No damage
Coast of Central Perù	2007	8	Storage depot (Pluspetrol Peru)	53			0.474	0,474 (Atlas: mi sembra quello piu nuovo); 0,5 (archive)		0.35					From shake map non interattiva			7					0.3	<1	fixed					oil		No damage
Coast of Central Perù	2007	8	Storage depot (Pluspetrol Peru)	53			0.474	0,474 (Atlas: mi sembra quello piu nuovo); 0,5 (archive)		0.35					From shake map non interattiva			5					0.3	<<1	fixed					oil		No damage
Coast of Central Perù	2007	8	Storage depot (Pluspetrol Peru)	53			0.474	0,474 (Atlas: mi sembra quello piu nuovo); 0,5 (archive)		0.35					From shake map non interattiva			1					0.3	<1	fixed					water		A water tank had buckled and split at the bottom, but this was a rusted skirt only and no product was lost. There were no signs of sideways movement.
Chile	1985	8	Concon Petroleum Refinery	70			0.24	Chile); 0,24 (Atlas Chile Valparaiso:		0.28					From shake map non interattiva	very poor clay		1		T-326 A	26	12.2	0.47		floating	sand and gravel			0	gasoline	0.9	EFB, failures of either a base plate or the weld between the wall and the base plate
Chile	1985	8	Concon Petroleum Refinery	70			0.24	Chile); 0,24 (Atlas Chile Valparaiso:		0.28					From shake map non interattiva	very poor clay		1		T-326 B	26	12.2	0.47		floating	sand and gravel			0	gasoline	0.9	EFB, failures of either a base plate or the weld between the wall and the base plate
Chile	1985	8	Concon Petroleum Refinery	70			0.24	Chile); 0,24 (Atlas Chile Valparaiso:		0.28					From shake map non interattiva	very poor clay		1		T-418 A	36.6	12.2	0.33		floating	sand and gravel			0	nafta	0.9	EFB, failures of either a base plate or the weld between the wall and the base plate
Chile	1985	8	Concon Petroleum Refinery	70			0.24	Chile); 0,24 (Atlas Chile Valparaiso:		0.28					From shake map non interattiva	very poor clay		1		T-552	22.4	12.2	0.54		floating	sand and gravel			0	solvent	0.9	EFB and break in joint bottom shell, with loss of content
Chile	1985	8	Concon Petroleum Refinery	70			0.24	Chile); 0,24 (Atlas Chile Valparaiso:		0.28					From shake map non interattiva	very poor clay		1		T-407 A	27.4	12.2	0.45		conical	sand and gravel			0	fuel oil	0.9	EFB and roof damage when their contents emptied rapidly and the relief valves were inadeguate to equilibrate the pressure. ROOF SPILLAGE
Chile	1985	8	Concon Petroleum Refinery	70			0.24	Chile); 0,24 (Atlas Chile Valparaiso:		0.28					From shake map non interattiva	very poor clay		1		T-320 A	22.4	12.2	0.54		conical	sand and gravel			0	fuel oil	0.9	EFB and roof damage when their contents emptied rapidly and the relief valves were inadeguate to equilibrate the pressure. ROOF SPILLAGE
Chile	1985	8	Concon Petroleum Refinery	70			0.24	Chile); 0,24 (Atlas Chile Valparaiso: misembra quella		0.28					From shake map non interattiva	very poor clay		1		T-4001 A	22.4	12.2	0.54		conical	sand and gravel			0	slop	0.9	EFB and roof damage when their contents emptied rapidly and the relief valves were inadeguate to equilibrate the pressure. ROOF SPILLAGE. Tilted and its roof collapsed as a result of the failure. The foundation was damaged by the oil exiting the tank
Chile	1985	8	Concon Petroleum Refinery	70			0.24	Chile); 0,24 (Atlas Chile Valparaiso:		0.28					From shake map non interattiva	very poor clay		1		T-405 A	36.6	12.2	0.33		conical	sand and gravel			0	asphalt	0.9	EFB and roof damage when their contents emptied rapidly and the relief valves were inadeguate to equilibrate the pressure. ROOF SPILLAGE
Chile	1985	8	Concon Petroleum Refinery	70			0.24	Chile); 0,24 (Atlas Chile Valparaiso:		0.28					From shake map non interattiva	very poor clay		1		T-420 A	31.8	11.6	0.36		conical	sand and gravel			0	kerosene	0.9	Slight deformation
Chile	1985	8	Concon Petroleum Refinery	70			0.24	Chile); 0,24 (Atlas Chile Valparaiso:		0.28					From shake map non interattiva	very poor clay		1		T-301 A	30.4	9.8	0.32		conical	sand and gravel			0	kerosene	0.9	Slight deformation
Chile	1985	8	Concon Petroleum Refinery	70			0.24	Chile); 0,24 (Atlas Chile Valparaiso:		0.28					From shake map non interattiva	very poor clay		1		T-422 A	44.8	12.2	0.27		conical	sand and gravel			0	kerosene	0.9	Slight deformation
Chile	1985	8	Concon Petroleum Refinery	70			0.24	Chile); 0,24 (Atlas Chile Valparaiso:		0.28					From shake map non interattiva	very poor clay		1		T-402	44.8	12.2	0.27		conical	sand and gravel			0	gasoline	0.9	No damage
Chile	1985	8	Concon Petroleum Refinery	70			0.24	Chile); 0,24 (Atlas Chile Valparaiso:		0.28					From shake map non interattiva	very poor clay		108					0.3									No damage
Chile	1985	8	Oxiquim chemical plant	50			0.23	0,286 (Atlas Chile);0,23 (Atlas Chile Valparaiso: misembra quella piu nuova)		0.28					From shake map non interattiva	(up a steep hillside) rock or shallow alluvium		10					1.1			preapared earth, most of them are located on the steep hillside			0		1	the tanks slid and the welds failed (the drain box for each of the tanks is welded to the base plate and embedded in the ground below the tank). Loss of content (all of a portion) STESSA dice: Failures were observed in welds of the plates of the shell wall; in addition, most of the tanks were filled with fluid and some lost part of its contents.
Chile	1985	8	Oxiquim chemical plant	50			0.23	Chile); 0,23 (Atlas Chile Valparaiso: misembra quella		0.28					From shake map non interattiva	(up a steep hillside) rock or shallow alluvium		1					1.1			preapared earth, most of them are located on the steep hillside					1	A fire water tank located near the top of the steep sloop slid approximately 1 - 1/2 inches and caused a pipe at its base to fail. This pipe was threaded into a flange that was bolted to the shut-off valve for the drain. The break was on the tank side of the valve, and the contents of the tank escaped.
Chile	1985	8	Oxiquim chemical plant	50			0.23	Chile); 0,23 (Atlas Chile Valparaiso:		0.28					From shake map non interattiva	alluvium at the base of a hill (poor soil)		1					1.1					stainless stell				elephant foot failure. The weld between the wall and the base failed and resulted in a leak of the liquind inside.
Chile	1985	8	Terquim Tank Farm	55			0.28	0,276 (Atlas Chile); 0,28 (Atlas Chile Valparaiso: misembra quella		0.28			0.81		From shake map non interattiva (vertical from STRESSA)			25					1.1	Dalle foto appaiono snelli, con H/D>1 ma non di molto		founded directly on sand without a concrete foundation			0			The plant generally performed well. Metal walkways connecting the tops of adjacent tanks tipically were buckled or pulled loose, indicating high relative motion. STESSA 2012 dice che: Tanks had small cracks on the weldsjoints of the shell wall with roof, so it is important to evaluate the calculation methods for free surface wave height.
Chile	1985	8	Terquim Tank Farm	55			0.28	0,276 (Atlas Chile); 0,28 (Atlas Chile Valparaiso: misembra quella piu nuova)		0.28			0.81		From shake map non interattiva (vertical from STRESSA)			1					1.1	Dalle foto appaiono snelli, con H/D>1 ma non di molto		founded directly on sand without a concrete foundation			0			One large tank containing sulfuric acid had failed and slowly leaked its contents into the ground. The tank had a small tear in the weld between the shell and the base. STESSA 2012 dice che: tanks had small cracks on the welds joints of the shell wall with roof, so it is important to evaluate the calculation methods for free surface wave height

Chile	1985	8	Tank Farm North of the Port of San Antonio	55				0,276 (Atlas Chile); 0,28 (Atlas Chile Valparaiso: misembra quella piu nuova)		0.28			0.81		From shake map non interattiva (vertical from STRESSA)	loose fill or alluvium			5		7.01049	7.0104852	1			concrete foundation			0			The site did not performe well because of severe ground failure beneath the tanks. There were very wide and deep cracks near the base of the tanks and as far as 20 feet away. The slope on which the tanks were supported apparently failed and portions of it slid into the harbor. Several of the tanks slid on their concrete foundations. None of the tanks appeared to have failed. Some of the piping at the base of the tanks may have failed as a result of the sliding and ground failures. As at Terquim, damage to the connections of steel walkways between adjacent tanks occurred due to diferential motion of the tanks. (non lo inseriscoperchè non so quanti si sono rotti)
Chile	2010	8.8	Santiago's Airport	330			0.28	0.28								soil amplification was observed (pomacita)		1			15.2402	7.1628871	0.47		fixed, supported by steel beams	concrete ring beam	welded	steel wall thickness of lower course 5 mm	0	drink water	1	The observed failure modes appeared to be tearing of the bottom course from the steel floor plate, with a nearly uniform tear vertically along one of the vertical seam welds in the lower courses. This led to collapse of the tank, with subsequent buckling and tearing of the steel. The uplifted floor plate strongly indicates that tank wall uplift occurred during the earthquake. For selfanchored at-grade steel tanks, this is the expected performance..Tank collapse was likely due to repeated wall uplifts and subsequently shells plates buckling.
Chile	2010	8.8	Santiago's Airport	330			0.28	0.28								soil amplification was observed (pomacita)		4					1	<=1			welded			fuel	0.5	No damage
Chile	2010	8.8	San Vicente International Terminal-SVIT	98			0.332	0.332		0.32		0.65	0.85		From shape file (EERI Special Earthquake Report — June 2010: at the station of Concepcion Colegio San Pedro the maximum horizontal acceleration was 0,65g and the vertical 0,58g)	liquefaction sand boils observed nearest to the roadway portion of this facility		1			3.53572	3.6576445	1.03448				welded					1	one tank was tilted approximately one degree, with liquefaction sand boils observed nearest to the roadway portion of this facility
Chile	2010	8.8	San Vicente International Terminal-SVIT	98			0.332	0.332		0.32		0.65	0.85		From shape file (EERI Special Earthquake Report — June 2010: at the station of Concepcion Colegio San Pedro the maximum horizontal acceleration was 0,65g and the vertical 0,58g)	liquefaction sand boils observed nearest to the roadway portion of this facility (ma non ha interessato questi altri tanks)		6					0.3	<1 da google map	fixed		welded					No damage
Chile	2010	8.8	San Vicente International Terminal-SVIT	98			0.332	0.332		0.32		0.65	0.85		From shape file (EERI Special Earthquake Report — June 2010: at the station of Concepcion Colegio San Pedro the maximum horizontal acceleration was 0,65g and the vertical 0,58g)	liquefaction sand boils observed nearest to the roadway portion of this facility (ma non ha interessato questi altri tanks)		3					1	<=1 da google map	fixed		welded					No damage
Chile	2010	8.8	San Vicente International Terminal-SVIT	98			0.332	0.332				0.65	0.85		EERI Special Earthquake Report — June 2010: at the station of Concepcion Colegio San Pedro the maximum horizontal acceleration was 0,65g and the vertical 0,58g	liquefaction sand boils observed nearest to the roadway portion of this facility (ma non ha interessato questi altri tanks)		2					1	>=1 da google map	fixed		welded					No damage
Chile	2010	8.8	San Vicente International Terminal-SVIT	98			0.332	0.332				0.65	0.85		EERI Special Earthquake Report — June 2010: at the station of Concepcion Colegio San Pedro the maximum horizontal acceleration was 0,65g and the vertical 0,58g	liquefaction sand boils observed nearest to the roadway portion of this facility (ma non ha interessato questi altri tanks)		2					1.1	>1 da google map	fixed		welded					No damage
Chile	2010	8.8	Wine production facilities																											wine		tank wall buckling (either EFB or diamond shape), anchorage failure, separation of the bottom of the tank from the walls and fracture of valve and fitting connections to the tank wall.
Chile	2010	8.8	Concon Refinery (Enap Aconcagua)				0.24	0.24								very poor clay		55	da google maps				0.3	<1 tozzi (da google maps)								No damage (or minor)
Chile	2010	8.8	Concon Refinery (Enap Aconcagua)				0.24	0.24								very poor clay		20	da google maps				0.3	<<1 molto tozzi (da google maps)								No damage (or minor)
Chile	2010	8.8	Concon Refinery (Enap Aconcagua)				0.24	0.24								very poor clay		9	da google maps				1	<=1 tozzi al limite (da google maps)								No damage (or minor)
Chile	2010	8.8	Concon Refinery (Enap Aconcagua)				0.24	0.24								very poor clay		3	da google maps				1	>=1 snelli al limite (da google maps)								No damage (or minor)
Chile	2010	8.8	Concon Refinery (Enap Aconcagua)				0.24	0.24								very poor clay		17	da google maps				1.1	>1 snelli (da google maps)								No damage (or minor)
Chile	2010	8.8	Bio-Bio refinery near Concepción				0.334	0.334				0.65	0.85		EERI Special Earthquake Report — June 2010: at the station of Concepcion Colegio San Pedro the maximum horizontal acceleration was 0,65g and the vertical 0,58g			59	da google maps				0.3	<1 tozzi (da google maps)								one of the two steel crude oil pipelines feeding into the refinery failed due to liquefaction and lateral spreading of beach sands.
Chile	2010	8.8	Bio-Bio refinery near Concepción				0.334	0.334				0.65	0.85		EERI Special Earthquake Report — June 2010: at the station of Concepcion Colegio San Pedro the maximum horizontal acceleration was 0,65g and the vertical 0,58g			20	da google maps				0.3	<<1 molto tozzi (da google maps)								one of the two steel crude oil pipelines feeding into the refinery failed due to liquefaction and lateral spreading of beach sands.
Tohoku	2011	9	Iwaki city along the pacific coast (port area)	200				0.328							Onahama Port observatory near the tank site recorded a PGA =1533,8 cm/s^2 (1,5g)	soil subjected to liquefaction									concrete foundation						There was damage due to liquefaction caused by short period strong ground motion. Photo 8 shows an example of a settlement of oil storage tank. The valve of the tank slightly contact to the ground, therefore the asphalt of the berm was removed in order to avoid the failure of the neck of the nozzle in the further settlement due to the future earthquakes. Furthermore, the center part of bottom plate was relatively uplifted about 50cm high owing to the lateral flow of neighboring soil of the tank, and the welding area of the bottom plate cracked and oil leaked.
Tohoku	2011	9	Iwaki city along the pacific coast (port area)	200				0.328							Onahama Port observatory near the tank site recorded a PGA =1533,8 cm/s^2 (1,5g)	soil subjected to liquefaction			da google maps				<1	tozzi (da google maps)	fixed	concrete foundation						No damage
Tohoku	2011	9	Iwaki city along the pacific coast (port area)	200				0.328							Onahama Port observatory near the tank site recorded a PGA =1533,8 cm/s^2 (1,5g)	soil subjected to liquefaction			da google maps				<=1	tozzi al limite (da google maps)	fixed	concrete foundation						No damage
Tohoku	2011	9	Iwaki city along the pacific coast (port area)	200				0.328							Onahama Port observatory near the tank site recorded a PGA =1533,8 cm/s^2 (1,5g)	soil subjected to liquefaction			da google maps				<1	tozzi (da google maps)	floating	concrete foundation						No damage
Tohoku	2011	9	Iwaki city along the pacific coast (port area)	200				0.328							Onahama Port observatory near the tank site recorded a PGA =1533,8 cm/s^2 (1,5g)	soil subjected to liquefaction			da google maps				<<1	molto tozzi (da google maps)	floating	concrete foundation						No damage
Tohoku	2011	9	Iwaki city along the pacific coast (port area)	200				0.328							Onahama Port observatory near the tank site recorded a PGA =1533,8 cm/s^2 (1,5g)	soil subjected to liquefaction			da google maps				1		fixed	concrete foundation						No damage
Tohoku	2011	9	Iwaki city along the pacific coast (port area)	200				0.328							Onahama Port observatory near the tank site recorded a PGA =1533,8 cm/s^2 (1,5g)	soil subjected to liquefaction			da google maps				>=1	snelli al limite (da google maps)	fixed	concrete foundation						No damage
Tohoku	2011	9	Iwaki city along the pacific coast (port area)	200				0.328							Onahama Port observatory near the tank site recorded a PGA =1533,8 cm/s^2 (1,5g)	soil subjected to liquefaction			da google maps				<=1	tozzi al limite (da google maps)	floating	concrete foundation						No damage
Tohoku	2011	9	Iwaki city along the pacific coast (port area)	200				0.328							Onahama Port observatory near the tank site recorded a PGA =1533,8 cm/s^2 (1,5g)	soil subjected to liquefaction			da google maps				>1	snelli (da google maps)	fixed	concrete foundation						No damage
Tohoku	2011	9	Niigata (costal area)_ Primo impianto	280				0.12								zona costiera			da google maps				<1	tozzi (da google maps)	fixed							No damage
Tohoku	2011	9	Niigata (costal area)_ Primo impianto	280				0.12								zona costiera			da google maps				<<1	molto tozzi (da google maps)	fixed							No damage
Tohoku	2011	9	Niigata (costal area)_ Primo impianto	280				0.12								zona costiera			da google maps				<1	tozzi (da google maps)	floating							Typical damage of oil storage tank was caused by liquid sloshing (excited by the long-period ground motions) was found in Niigata, such as sinking of inner floating roof, leakage of oil onto deck, deformation of gauge pole, and fracture of pontoon due to the liquid sloshing. Oil spilled onto the deck of the floating roof. Oil marks on the surface of the shell plates were found in many oil storage tanks.
Tohoku	2011	9	Niigata (costal area)_ Primo impianto	280				0.12								zona costiera			da google maps				>=1	snelli al limite (da google maps)	fixed							No damage
Tohoku	2011	9	Niigata (costal area)_ Primo impianto	280				0.12								zona costiera			da google maps				<=1	tozzi al limite (da google maps)	fixed							No damage
Tohoku	2011	9	Niigata (costal area)_ Secondo impianto-parte a sud del canale	280				0.12								zona costiera			da google maps				<<1	molto tozzi (da google maps)	floating							Typical damage of oil storage tank was caused by liquid sloshing (excited by the long-period ground motions) was found in Niigata, such as sinking of inner floating roof, leakage of oil onto deck, deformation of gauge pole, and fracture of pontoon due to the liquid sloshing. Oil spilled onto the deck of the floating roof. Oil marks on the surface of the shell plates were found in many oil storage tanks.
Tohoku	2011	9	Niigata (costal area)_ Secondo impianto-parte a sud del canale	280				0.12								zona costiera			da google maps				1		floating							Typical damage of oil storage tank was caused by liquid sloshing (excited by the long-period ground motions) was found in Niigata, such as sinking of inner floating roof, leakage of oil onto deck, deformation of gauge pole, and fracture of pontoon due to the liquid sloshing. Oil spilled onto the deck of the floating roof. Oil marks on the surface of the shell plates were found in many oil storage tanks.

Tohoku	2011	9	Niigata (costal area)_ Secondo impianto-parte a sud del canale	280				0.12								zona costiera			da google maps			<1	tozzi (da google maps)	floating							Typical damage of oil storage tank was caused by liquid sloshing (excited by the long-period ground motions) was found in Niigata, such as sinking of inner floating roof, leakage of oil onto deck, deformation of gauge pole, and fracture of pontoon due to the liquid sloshing. Oil spilled onto the deck of the floating roof. Oil marks on the surface of the shell plates were found in many oil storage tanks.
Tohoku	2011	9	Niigata (costal area)_ Secondo impianto-parte a sud del canale	280				0.12								zona costiera			da google maps			<=1	tozzi al limite (da google maps)	fixed							No damage
Tohoku	2011	9	Niigata (costal area)_ Secondo impianto-parte a sud del canale	280				0.12								zona costiera			da google maps			>1	snelli (da google maps)	fixed							No damage
Tohoku	2011	9	Niigata (costal area)_ Secondo impianto-parte a sud del canale	280				0.12								zona costiera			da google maps			<1	tozzi (da google maps)	fixed							No damage
Tohoku	2011	9	Niigata (costal area)_ Secondo impianto-parte a sud del canale	280				0.12								zona costiera			da google maps			<<1	molto tozzi (da google maps)	fixed							No damage
Tohoku	2011	9	Niigata (costal area)_ Secondo impianto-parte a sud del canale	280				0.12								zona costiera			da google maps			>=1	snelli al limite (da google maps)	fixed							No damage
Tohoku	2011	9	Niigata (costal area)_ Secondo impianto-parte a nord del canale	280				0.12								zona costiera			da google maps			<<1	molto tozzi (da google maps)	fixed							No damage
Tohoku	2011	9	Niigata (costal area)_ Secondo impianto-parte a nord del canale	280				0.12								zona costiera			da google maps			>=1	snelli al limite (da google maps)	fixed							No damage
Tohoku	2011	9	Niigata (costal area)_ Secondo impianto-parte a nord del canale	280				0.12								zona costiera			da google maps			<1	tozzi (da google maps)	fixed							No damage
Tohoku	2011	9	Niigata (costal area)_ Secondo impianto-parte a nord del canale	280				0.12								zona costiera			da google maps			>1	snelli (da google maps)	fixed							No damage
Tohoku	2011	9	Niigata (costal area)_ Secondo impianto-parte a nord del canale	280				0.12								zona costiera			da google maps			1		fixed							No damage
Tohoku	2011	9	Niigata (costal area)_ Secondo impianto-parte a nord del canale	280				0.12								zona costiera			da google maps			<<1	molto tozzi (da google maps)	floating							Typical damage of oil storage tank was caused by liquid sloshing (excited by the long-period ground motions) was found in Niigata, such as sinking of inner floating roof, leakage of oil onto deck, deformation of gauge pole, and fracture of pontoon due to the liquid sloshing. Oil spilled onto the deck of the floating roof. Oil marks on the surface of the shell plates were found in many oil storage tanks.
Tohoku	2011	9	Niigata (costal area)_ Secondo impianto-parte a nord del canale	280				0.12								zona costiera			da google maps			<=1	tozzi al limite (da google maps)	fixed							No damage
Tohoku	2011	9	Niigata (costal area)_ Secondo impianto-parte a nord del canale	280				0.12								zona costiera			da google maps			<1	tozzi (da google maps)	floating							Typical damage of oil storage tank was caused by liquid sloshing (excited by the long-period ground motions) was found in Niigata, such as sinking of inner floating roof, leakage of oil onto deck, deformation of gauge pole, and fracture of pontoon due to the liquid sloshing. Oil spilled onto the deck of the floating roof. Oil marks on the surface of the shell plates were found in many oil storage tanks.
Tohoku	2011	9	Kawasaki city	388				0.182								zona costiera			da google maps			<<1	molto tozzi (da google maps)	fixed							No damage
Tohoku	2011	9	Kawasaki city	388				0.182								zona costiera			da google maps			<<1	molto tozzi (da google maps)	floating							Tipical damage of oil storage tank caused by liquid sloshing was found mainly along the Sea of Japan and the Tokyo bay. Oil spilled on the deck of the floating roof in kawasaki city. Oil marks on the surface of the shell plates were found in many storage tanks.
Tohoku	2011	9	Kawasaki city	388				0.182								zona costiera			da google maps			<1	tozzi (da google maps)	fixed							No damage
Tohoku	2011	9	Kawasaki city	388				0.182								zona costiera			da google maps			<1	tozzi (da google maps)	floating							Tipical damage of oil storage tank caused by liquid sloshing was found mainly along the Sea of Japan and the Tokyo bay. Oil spilled on the deck of the floating roof in kawasaki city. Oil marks on the surface of the shell plates were found in many storage tanks.
Tohoku	2011	9	Kawasaki city	388				0.182								zona costiera			da google maps			<=1	tozzi al limite (da google maps)	fixed							No damage
Tohoku	2011	9	Kawasaki city	388				0.182								zona costiera			da google maps			<=1	tozzi al limite (da google maps)	floating							Tipical damage of oil storage tank caused by liquid sloshing was found mainly along the Sea of Japan and the Tokyo bay. Oil spilled on the deck of the floating roof in kawasaki city. Oil marks on the surface of the shell plates were found in many storage tanks.
Tohoku	2011	9	Kawasaki city	388				0.182								zona costiera			da google maps			1		fixed							No damage
Tohoku	2011	9	Kawasaki city	388				0.182								zona costiera			da google maps			1		floating							Tipical damage of oil storage tank caused by liquid sloshing was found mainly along the Sea of Japan and the Tokyo bay. Oil spilled on the deck of the floating roof in kawasaki city. Oil marks on the surface of the shell plates were found in many storage tanks.
Tohoku	2011	9	Kawasaki city	388				0.182								zona costiera			da google maps			>=1	snelli al limite (da google maps)	fixed							No damage
Tohoku	2011	9	Kawasaki city	388				0.182								zona costiera			da google maps			>=1	snelli al limite (da google maps)	floating							Tipical damage of oil storage tank caused by liquid sloshing was found mainly along the Sea of Japan and the Tokyo bay. Oil spilled on the deck of the floating roof in kawasaki city. Oil marks on the surface of the shell plates were found in many storage tanks.
Tohoku	2011	9	Kawasaki city	388				0.182								zona costiera			da google maps			>1	snelli (da google maps)	fixed							No damage
Tohoku	2011	9	Kawasaki city	388				0.182								zona costiera			da google maps			>1	snelli (da google maps)	floating							Tipical damage of oil storage tank caused by liquid sloshing was found mainly along the Sea of Japan and the Tokyo bay. Oil spilled on the deck of the floating roof in kawasaki city. Oil marks on the surface of the shell plates were found in many storage tanks.
Tohoku	2011	9	Kawasaki city	388				0.182								zona costiera			da google maps			<1	tozzo dalla foto sul report	floating						heavy oil	The floating roof of heavy oil tank completely sank three days after the earthquake. The cause of sinking is considered as the inadequate buoyancy by failure of the pontoons due to the liquid sloshing
Tohoku	2011	9	Sakata city	230				0,10-0,12								zona costiera			da google maps			>=1	snelli al limite (da google maps)	fixed							No damage
Tohoku	2011	9	Sakata city	230				0,10-0,12								zona costiera			da google maps			<1	tozzi (da google maps)	fixed							No damage
Tohoku	2011	9	Sakata city	230				0,10-0,12								zona costiera			da google maps			>1	snelli (da google maps)	fixed							No damage
Tohoku	2011	9	Sakata city	230				0,10-0,12								thick sediment layers more than several km			da google maps												the aluminum inner floating roof of the tank was broken completely. Photo 12 (accanto) shows one of broken float tubes of the inner floating roof. The cause of failure of the roof is considered as the large and frequent liquid sloshing, and also the situation of the inner floating roof fulfills the unsafe conditions
Tohoku	2011	9	Kashima city, parte nord	300				0.38											da google maps			<<1	molto tozzi (da google maps)	floating							No damage
Tohoku	2011	9	Kashima city, parte nord	300				0.38											da google maps			<=1	tozzi al limite (da google maps)	fixed							No damage
Tohoku	2011	9	Kashima city, parte nord	300				0.38											da google maps			>1	snelli (da google maps)	fixed							No damage
Tohoku	2011	9	Kashima city, parte sud	300				0,32-0,36											da google maps			<<1	molto tozzi (da google maps)	fixed							No damage
Tohoku	2011	9	Kashima city, parte sud	300				0,32-0,36											da google maps			<<1	molto tozzi (da google maps)	floating							No damage
Tohoku	2011	9	Kashima city, parte sud	300				0,32-0,36											da google maps			<1	tozzi (da google maps)	fixed							No damage
Tohoku	2011	9	Kashima city, parte sud	300				0,32-0,36											da google maps			<1	tozzi (da google maps)	floating							No damage
Tohoku	2011	9	Kashima city, parte sud	300				0,32-0,36											da google maps			<=1	tozzi al limite (da google maps)	fixed							No damage
Tohoku	2011	9	Kashima city, parte sud	300				0,32-0,36											da google maps			<=1	tozzi al limite (da google maps)	floating							No damage
Tohoku	2011	9	Kashima city, parte sud	300				0,32-0,36											da google maps			>=1	snelli al limite (da google maps)	fixed							No damage
Tohoku	2011	9	Kashima city, parte sud	300				0,32-0,36											da google maps			>=1	snelli al limite (da google maps)	floating							No damage
Tohoku	2011	9	Kashima city, parte sud	300				0,32-0,36											da google maps			>1	snelli (da google maps)	fixed							No damage
Tohoku	2011	9	Kashima city, parte sud	300				0,36																					oil		extraction of anchor bolts
Tohoku	2011	9	Sendai	120				0,24-1,24																					water		elephant foot bulge
Tohoku	2011	9	Sendai Refinery	115				0,84-1,08														<<1	molto tozzi (da google maps)	fixed							No Damage ,"The earthquake caused only minor spills on tank roofs"
Tohoku	2011	9	Sendai Refinery	115				0,84-1,08														<<1	molto tozzi (da google maps)	floating							No Damage ,"The earthquake caused only minor spills on tank roofs"
Tohoku	2011	9	Sendai Refinery	115				0,84-1,08														<1	tozzi (da google maps)	fixed							No Damage ,"The earthquake caused only minor spills on tank roofs"
Tohoku	2011	9	Sendai Refinery	115				0,84-1,08														<1	tozzi (da google maps)	floating							No Damage ,"The earthquake caused only minor spills on tank roofs"
Tohoku	2011	9	Sendai Refinery	115				0,84-1,08														<=1	tozzi al limite (da google maps)	fixed							No Damage ,"The earthquake caused only minor spills on tank roofs"
Tohoku	2011	9	Sendai Refinery	115				0,84-1,08														>=1	snelli al limite (da google maps)	fixed							No Damage ,"The earthquake caused only minor spills on tank roofs"
Tohoku	2011	9	Sendai Refinery	115				0,84-1,08														>1	snelli (da google maps)	fixed							No Damage ,"The earthquake caused only minor spills on tank roofs"
Napa Valley	2014	6	City of Napa	8			0.32	0.32										1		tank 1		0.3	<<1 from google maps			welded			water		No damage
Napa Valley	2014	6	City of Napa	5			0.65	0.65										1		tank 2		0.3	<<1 from google maps			welded			water		No damage
Napa Valley	2014	6	City of Napa	12			0.64	0.64										1		Montana B	20.4	11.3	0.55		corrugated iron (CGI) roof supported by redwood beams on steel columns		welded		0	water		The water sloshed with approximately 6 ft amplitude, damaging the roof. There was no buckling of the walls, but some rocking was evidenced by motion at the outtake slip joint. The tank drained immediately following the event due to a nearby pipe break
Napa Valley	2014	6	City of Napa	7.5			0.28	0.28										3		tanks 3,4,5			0.3	<<1			welded			water		No damage
Napa Valley	2014	6	City of Napa	7.5			0.28	0.28										2		tanks 6, 7			0.3	<1			welded			water		No damage
Napa Valley	2014	6	City of Napa	12			0.32	0.32										1		tank 8			0.3	<<1			welded			water		No damage
Napa Valley	2014	6	City of Napa	17			0.234	0.234										1		tank 9			0.3	<<1			welded			water		No damage
Napa Valley	2014	6	City of Napa	12			0.594	0.594										2		tank 10,11			0.3	<<1			welded			water		No damage

Napa Valley	2014	6	City of Napa (Trefethen winery)	16				0.35										3	fermentation tanks			1.1	>1	fixed		welded	stainless steel	1	wine	1	ruptured anchors, shifted 12inches, (and buckled tank wall with 75% loss of content : danno conseguente quindi non lo metto)
Napa Valley	2014	6	City of Napa (Trefethen winery)	16				0.35										36	fermentation tanks			1.1	>1	fixed		welded	stainless steel	1	wine	0	No damage
Napa Valley	2014	6	City of Napa (Trefethen winery)	16				0.35										1	fermentation tanks			1.1	>1	fixed		welded	stainless steel	1	wine		damage to the upper portion of the tank. The dents can be attributed to the catwalk banging against the tank during the earthquake; no loss of content
Napa Valley	2015	6	City of Napa (Mondavi Winery)	26.5				0.148										1	fermentation tanks			1.1	>1	fixed		welded	stainless steel	1	wine	1	damage to the upper portion of the tank. The dents can be attributed to the catwalk banging against the tank during the earthquake; no loss of content
Napa Valley	2015	6	City of Napa (Mondavi Winery)	26.5				0.148										1	fermentation tanks			1.1	>1	fixed		welded	stainless steel	1	wine	1	Pull out failure of the anchors and damage to the steel tank wall; no loss of content (in particular in this tank The seam in this tank ruptured due to buckling of the exterior wall. no loss of content)
Napa Valley	2015	6	City of Napa (Mondavi Winery)	26.5				0.148										5	fermentation tanks			1.1	>1	fixed		welded	stainless steel	1	wine	1	Pull out failure of the anchors and damage to the steel tank wall; no loss of content
Napa Valley	2015	6	City of Napa (Mondavi Winery)	26.5				0.148										2	fermentation tanks			1.1	>1	fixed		welded	stainless steel		wine	0	No damage
Napa Valley	2015	6	City of Napa (Mondavi Winery)	26.5				0.148										35	fermentation tanks			1.1	>1	fixed		welded	stainless steel		wine	0	No damage
Adak	1986	8	Fuel Pier Yard. Small craft refuel tank				0.2			0.2					ALA 2001			1			10.04	15.06	1.5					1	fuel	0.5	No damage
Adak	1986	8	Power Plant 3				0.2			0.2					ALA 2001			1			5.44	8.15	1.50					1		0.75	No damage
Adak	1986	8	Power Plant 3				0.2			0.2					ALA 2001			1			5.44	8.15	1.50					1		0.75	No damage
Chile	1985	8	Las Ventanas Power Plant				0.25			0.25					ALA 2001			1			6.08	9.12	1.5					1		0.75	No damage
Chile	1985	8	Las Ventanas Power Plant				0.25			0.25					ALA 2001			1			6.08	9.12	1.5					1		0.75	No damage
Chile	1986	8	Las Ventanas Power Plant				0.25			0.25					ALA 2001			1			6.08	9.12	1.5					1		0.75	No damage
Chile	1987	8	Las Ventanas Power Plant				0.25			0.25					ALA 2001			1			9.3	13.94	1.50					1	oil	0.75	No damage
Chile	1988	8	Las Ventanas Power Plant				0.25			0.25					ALA 2001			1			9.3	13.94	1.50					1	oil	0.75	No damage
New Zealand	1987	6.5	Caxton Paper Mill Chip				0.4			0.4					ALA 2001			1			11.31	16.96	1.50					1		0.75	No damage
New Zealand	1987	6.5	Caxton Paper Mill Hydrogen Peroxide				0.4			0.4					ALA 2001			1			2.64	3.95	1.50					1		0.75	No damage
New Zealand	1987	6.5	Caxton Paper Mill Secondary Bleach Tower				0.4			0.4					ALA 2001			1			5.44	8.15	1.50					1		0.84	No damage
New Zealand	1987	6.5	New Zealand Distillery Bulk				0.5			0.5					ALA 2001			1		Tank 2	7.48	5.61	0.75					1		0.84	No damage
New Zealand	1987	6.5	New Zealand Distillery Bulk				0.5			0.5					ALA 2001			1		Tank 5	4.59	3.44	0.75					1		0.75	No damage
New Zealand	1987	6.5	New Zealand Distillery Bulk				0.5			0.5					ALA 2001			1		Tank 6	4.59	3.44	0.75					1		0.75	No damage
New Zealand	1987	6.5	New Zealand Distillery Bulk				0.5			0.5					ALA 2001			1		Tank 7	8.77	6.58	0.75					1		0.75	No damage
New Zealand	1987	6.5	New Zealand Distillery Bulk				0.5			0.5					ALA 2001			1		Tank 9	3.32	2.49	0.75					1		0.75	No damage
New Zealand	1987	6.5	Whakatane Board Mills Pulp				0.3			0.3					ALA 2001			1			7.84	11.76	1.50					1		0.75	No damage
New Zealand	1987	6.5	Whakatane Board Mills Pulp				0.3			0.3					ALA 2001			1			7.84	11.76	1.50					1		0.75	No damage
New Zealand	1987	6.5	Whakatane Board Mills Pulp				0.3			0.3					ALA 2001			1			7.84	11.76	1.50					1		0.75	No damage
San Fernando	1971	6.61	Glendale power plant				0.28			0.28					ALA 2001			1			3.62	5.42	1.50					1	distilled water	0.75	No damage
San Fernando	1971	6.61	Glendale power plant				0.28			0.28					ALA 2001			1			3.62	5.42	1.50					1	distilled water	0.75	No damage
San Fernando	1971	6.61	Glendale power plant				0.28			0.28					ALA 2001			1			4.01	6.01	1.50					1	distilled water	0.75	No damage
San Fernando	1971	6.61	Glendale power plant				0.28			0.28					ALA 2001			1			3.62	5.42	1.50					1	fuel oil	0.75	No damage
San Fernando	1971	6.61	Pasadena Power plant				0.2			0.2					ALA 2001			1		B1 water tank	7.28	10.92	1.50					1	distilled water	0.75	No damage
San Fernando	1971	6.61	Pasadena Power plant				0.2			0.2					ALA 2001			1		B2 water tank	7.78	9.56	1.23					1	distilled water	0.89	No damage
San Fernando	1971	6.61	Pasadena Power plant				0.2			0.2					ALA 2001			1		B3 water tank	5.46	13.92	2.55					1	distilled water	0.88	No damage